Fall 12-15-2023

On the Anti-adipogenic Function of Collagen Triple Helix Repeat-containing Protein 1

Matthew E. Siviski
University of Maine, matthew.siviski@gmail.com

ON THE ANTI-ADIPOGENIC FUNCTION OF COLLAGEN TRIPLE HELIX REPEAT-CONTAINING PROTEIN 1

by

Matthew Edmund Siviski

B.S., Fordham University, 2012

A DISSERTATION

Submitted in Partial Fulfillment of the

Requirements for the Degree of

Doctor of Philosophy

(in Biomedical Science)

The Graduate School

The University of Maine

December 2023

Advisory Committee:

Igor Prudovsky, Faculty Scientist II, MaineHealth Institute for Research, Advisor
Volkhard Lindner, Faculty Scientist III, MaineHealth Institute for Research
Calvin Vary, Faculty Scientist III, MaineHealth Institute for Research
Robert Koza, Faculty Scientist II, MaineHealth Institute for Research
Ivette Emery, Program Director, MaineHealth Institute for Research
Robert Wheeler, Associate Professor, The University of Maine

ON THE ANTI-ADIPOGENIC FUNCTION OF COLLAGEN TRIPLE HELIX REPEAT-CONTAINING PROTEIN 1

By Matthew Edmund Siviski

Dissertation Advisor: Dr. Igor Prudovsky

An Abstract of the Thesis Presented
in Partial Fulfillment of the
Requirements for the
Degree of Doctor of Philosophy
(in Biomedical Science)
December 2023

ABSTRACT: Adipogenesis is regulated by the coordinated activity of adipogenic transcription factors, including PPAR-gamma (PPARG) and C/EBP alpha (CEBPA). Thus, dysregulated adipogenesis predisposes adipose tissues to adipocyte hypertrophy and hyperplasia. We have previously reported that mice possessing a homozygous null gene mutation in collagen triple helix repeat-containing protein 1 (CTHRC1) have increased adiposity compared to wildtype mice, supporting the concept that CTHRC1 regulates body composition. Herein, we investigated the anti-adipogenic activity of CTHRC1. Using 3T3-L1 preadipocytes, we showed significantly reduced adipogenic differentiation in the presence of CTHRC1 commensurate to marked suppression of *Cebpa* and *Pparg* gene expression. In addition, CTHRC1 increased the expression of the anti-adipogenic factor SOX9 (transcription factor SOX-9) and promoted its nuclear translocation. Importantly, *Sox9* gene knockdown demonstrated that the anti-adipogenic effect of CTHRC1 is dependent on SOX9 expression, while the ability of CTHRC1 to regulate SOX9 was attenuated by Rho and Rac1 signaling pathway inhibitors. Collectively, these data support that a

CTHRC1-Rho/Rac1-SOX9 signaling axis negatively regulates adipogenesis. We also report selective expression of *CTHRC1* in *PDGRFA*-expressing cell populations in human white adipose tissue, but not brown or perivascular adipose tissues. Congruently, flow cytometry analysis of mouse white adipose tissue revealed CTHRC1 expression in PDGFR-alpha^{+} stromal cells.

ACKNOWLEDGEMENTS

I am grateful for having been given the opportunity to pursue a career in basic science research. Thank you to Drs. Charles Emala, George Gallos, and Peter Yim at Columbia University for giving me that start. Your collective example set the tone of always welcoming people to the lab. I also want to thank my thesis advisory committee for your patience and support: Drs. Igor Prudovsky, Volkhard Lindner, Calvin Vary, Robert Koza, Ivette Emery, and Robert Wheeler. Thank you to Dr. Volkhard Lindner for developing CTHRC1 materials and reagents that made the research possible, and to members of the MaineHealth and UMaine communities who have helped me along the way, especially fellow students. A special thank you to Doreen Kacer and Shivangi Pande; you have made the lab fun. I am indebted to my advisor, Dr. Igor Prudovsky, whose guidance and enthusiasm kept me going when the firm reality sunk in that basic research is exceedingly difficult. It has been a worthwhile pursuit; I truly love science. Thank you, Igor.

DEDICATION

To my friends and family, who I love and cherish. To David Schaller, FF-NRP, USMC. I miss those discussions between calls at 03:00 about the perspective of it all, my friend.

TABLE OF CONTENTS

LIST OF TABLES

LIST OF FIGURES

LIST OF ABBREVIATIONS

2-mercaptoethanol (2-me)

3-isobutyl-1-methylxanthine (IBMX)

Acetyl-CoA carboxylase (ACC)

Acyl-CoA:diacylglycerol acyltransferase (DGAT)

Acylglycerolphosphate acyltransferase (AGPAT)

adipocyte mesenchymal transition (AMT)

Adipocyte triglyceride lipase (ATGL)

Angiomotins (AMOTs)

Beta–galactosidase (βgal)

Bone morphogenetic proteins (BMPs)

brown adipose tissue (BAT)

cAMP response element-binding protein (CREB)

CCAAT/enhancer-binding protein alpha (C/EBP alpha)

CCAAT/enhancer-binding protein beta (C/EBP beta)

CCAAT/enhancer-binding protein delta (C/EBP delta)

Collagen triple helix repeat (CTHR) domain

Collagen triple helix repeat-containing protein 1 (CTHRC1)

Complement C1q tumor necrosis factor-related proteins (CTRPs)

Component 1q (C1q)

CREB binding protein/E1A binding protein p300 (CBP/p300)

cyclic AMP (cAMP)

Desert hedgehog protein (DHH)

endoplasmic reticulum (ER)

enzyme-linked immunosorbent assay (ELISA)

epithelial-to-mesenchymal (EMT)

ethylenediaminetetraacetic acid (EDTA)

Fatty acid synthase (FASN)

Fatty acid-binding protein 4 (FABP4)

Filamentous actin (F-actin)

Focal adhesion kinase 1 (FAK)

Frizzled-6 (FZD6)

G protein-coupled receptor (GPCR)

GATA-binding factor 2 (GATA2)

Glycerol-3-phosphate acyltransferase (GPAT)

Glycogen synthase kinase-3 beta (GSK3B)

Hormone-sensitive lipase (HSL)

Immunoglobulin G (IgG)

Indian hedgehog protein (IHH)

inguinal white adipose tissue (iWAT)

Insulin-like growth factor 1 (IGF-1)

Insulin-like growth factor 2 (IGF-II)

Large tumor suppressor kinases (LATS)

Lysophosphatidic acid (LPA)

Map kinases (MAPK)

Mediator complex subunit 12 (MED12)

Meis homeobox 1 (MEIS1)

Microfibrillar-associated protein 5 (MFAP5)

Monoglyceride lipase (MGL)

N,N,N',N'-tetramethyl-ethylenediamine (TEMED)

NSC 23766 (N)

perivascular adipose tissue (PVAT)

Peroxisome proliferator-activated receptor gamma (PPAR-gamma)

Phosphatidic acid (PA)

Phosphodiesterase 3B (PDE3B)

Planar cell polarity (PCP)

Platelet-derived growth factor receptor alpha (PDGFR-alpha)

Preadipocyte factor 1 (PREF1)

Prostaglandin D2 (PGD2)

Protein kinase A (PKA)

Protein kinase B (AKT)

Protein patched homolog 1 (PTC1)

Protein smoothened (SMO)

PVDF (polyvinylidene difluoride)

Ras-related dexamethasone induced 1 (RASD1)

Rho-associated kinase (ROCK)

Sonic hedgehog protein (SHH)

SRY-type HMG box (SOX)

stromal vascular fraction (SVF)

Tat interactive protein-60 (TIP60)

Transcription factor SOX-9 (SOX9)

Transcription initiation factor IIB (GTF2B)

Transforming growth factor beta-1 (TGFB1)

Type 1 collagen alpha 1 (Col1a1)

Uncoupling protein-1 (UCP1)

WW domain containing E3 ubiquitin protein ligase 2 (WWP2)

Y-27632 (Y)

Yes-associated protein 1 (YAP)

SPECIFIC AIMS

Aim 1: To determine if the ability of CTHRC1 to suppress lipid accumulation in differentiating adipocytes *in vitro* is attributed to the downregulation of adipogenic gene expression.

Hypothesis: A CTHRC1-SOX9 axis of signaling negatively regulates adipogenic gene expression *in vitro*.

Aim 2: To examine the expression of CTHRC1 in the stromal vascular milieu of white adipose tissue.

Hypothesis: CTHRC1 is expressed among white adipose PDGFR-alpha^{+} stromal cells *in vivo*.

CHAPTER 1: REVIEW OF THE LITERATURE

1.1 Structure and function of adipocytes

The human body possesses integrated control mechanisms to regulate energy reserves and expenditure. Chief among them is the storage and usage of energy from sources of fat (*i.e.*, lipids). Despite the benefits that these regulatory mechanisms have played over the course of human evolution, modern lifestyle habits in developed societies, including sedentary living in addition to excessive consumption of energy-rich food, has led to a dramatic rise in obesity and obesity-related pathophysiologies including diabetes and heart disease (1-3). Accordingly, a better understanding of adipocyte structure and function, including the regulatory pathways of adipogenesis and adipose tissue formation, bolsters the basic and translational research platforms to develop improved treatments for obesity and obesity-related comorbidities. To this end, the following subsections discuss the molecular underpinnings of adipocyte formation, with a particular focus on the developmental origins of white adipocytes retained in white adipose tissues.

1.1.1 The adipocyte and adipose tissue landscape

Adipocytes, also referred to as lipocytes or fat cells, are derived from mesenchymal stem cells and are grouped into three distinct classes: white, beige, and brown adipocytes (4). Both white and beige adipocytes are derived from $PAX7^{-}$:$MYF5^{-}$ progenitor cells, while brown adipocytes are derived from $PAX7^{+}$:$MYF5^{+}$ progenitor cells (4). More recently, beige adipocyte precursor cells were shown to be distinct from white adipocyte precursor cells, thus supporting the notion that white, beige, and brown adipogenic lineages are developmentally distinct from one another

(4). White adipocytes are classically viewed as sites of lipid synthesis and catabolism in response to whole-body energy demand, while beige and brown adipocytes express uncoupling protein-1 (UCP1) that functions to dissipate stored chemical energy as heat (4). Thus, beige and brown adipocytes are thermogenic cells in that they can regulate thermogenesis (*i.e.*, heat production).

Originally, it was presumed that brown adipocytes are present only in human neonates who do not possess the thermoregulatory ability to produce body heat by shivering. However, it is now appreciated that brown adipocytes are also present in adult humans, principally within thoracic, interscapular, and perirenal brown adipose tissue depots (4). White adipocytes are more ubiquitously expressed in the adult human in comparison to brown adipocytes, and are retained in many connective tissues throughout the body as well as in distinct adipose tissues (5). Among white adipose tissues, adipocytes are embedded in vascular loose connective tissue and are typically divided into lobules by fibrous septa that carry the larger blood vessels (5, 6). As such, adipose tissue is highly vascularized commensurate to its role in metabolism as a vital source of free fatty acids which are released into the bloodstream and used by peripheral cells and tissues to generate ATP (5). Adipose tissues are found in specific subcutaneous and visceral regions throughout the body including the mesenteries and omenta, the female breast, bone marrow, the retroperitoneal region around the kidney, the retro-orbital region behind the eyeball, in the deep plantar skin of the foot, as well as among localized pads in the synovial membrane of joints. In addition to its role as an energy reserve, white adipose tissues are a vital source of thermal insulation (*e.g.*, subcutaneous adipose tissues), and also act as mechanical shock-absorbers (*e.g.*, the presence of adipose depots within the soles of the feet and joints) (5).

Individually, white adipocytes measure about 20-150 μm in diameter, and are either oval or spherical in shape, but when packed together in tissues they are polygonal (4). On the other

hand, brown adipocytes measure an average diameter of 10-25 μm and are composed of multiple lipid droplets in contrast to white adipocytes which comprise a single large lipid droplet (4). Brown adipocytes also possess more mitochondria than white adipocytes, congruent with the role of the brown adipocyte heat-producing pathway regulated by UCP1 which, localized in the inner mitochondrial membrane, disrupts the proton (*i.e.*, hydrogen ion) gradient between the mitochondrial intermembrane space and matrix thus converting the potential energy generated by the hydrogen ion gradient into thermal energy (4). Therefore, UCP1 facilitates thermogenesis and significantly attenuates the ability of brown adipocytes to generate ATP from oxidative phosphorylation (4). In contrast, beige adipocytes possess functional characteristics of both white and brown adipocytes in response to the presence or absence of thermogenic stimuli. For example, UCP1 protein expression is enhanced by cold exposure or enhanced adrenergic tone; however, in the absence of such thermogenic stimuli, beige adipocytes possess a lower basal level of UCP1 expression and can thus efficiently synthesize or catabolize lipids based on whole-body energy demands in a comparable manner to white adipocytes which are devoid of UCP1 expression (4).

Each white adipocyte contains a peripheral rim of cytoplasm surrounding a single lipid droplet composed of a phospholipid monolayer which encapsulates neutral lipid species, the vast majority of which are triacylglycerides comprised of glycerol esters of fatty acids including oleic, palmitic, and stearic acids (7). Triacylglyceride *de novo* lipogenesis encompasses the processes of free fatty acid synthesis as well as the binding of three fatty acid molecules to a glycerol backbone to form discrete triacylglyceride species (7). Within the cytoplasm, acetyl-CoA carboxylase (ACC) catalyzes the carboxylation of acetyl-CoA to produce malonyl-CoA, from which fatty acid synthase (FASN) helps orchestrate the synthesis of fatty acyl-CoA

molecules from acetyl-CoA and malonyl-CoA substrates (7). The carboxylation of acetyl-CoA is a rate-limiting determinant in fatty acid synthesis, wherein protein kinase A is an established negative regulator of malonyl-CoA production due to its inhibitory phosphorylation of acetyl-CoA carboxylase (7). The major pathway of triacylglyceride synthesis involves glycerol-3-phosphate and occurs primarily in the endoplasmic reticulum (7). Glycerol-3-phosphate is principally derived from intermediates of glycolysis and the citric acid cycle, and in the initial step of triacylglyceride synthesis, glycerol-3-phosphate acyltransferase (GPAT) catalyzes the addition of a fatty acyl-CoA molecule to glycerol-3-phosphate to produce a lysophosphatidic acid (LPA). Next, acylglycerolphosphate acyltransferase (AGPAT) catalyzes the addition of a fatty acyl-CoA molecule to LPA to form a phosphatidic acid (PA). Phosphatidic acid phosphatase (PAP) then dephosphorylates PA yielding a diacylglycerol, upon which acyl-CoA:diacylglycerol acyltransferase (DGAT) catalyzes the final addition of a fatty acyl-CoA molecule to produce a triacylglyceride species (7). Within the leaflets of the endoplasmic reticulum (ER) phospholipid bilayer, triacylglycerides and other neutral lipid species (*e.g.*, cholesterol esters) accumulate and coalesce into a nascent lipid droplet that buds from the ER and releases into the cytosol, in which the polar head groups of the droplet's phospholipid monolayer are oriented towards the cytosol. In white adipocytes, nascent lipid droplets fuse together to form a mature, unilocular lipid droplet which, itself, is also a site of localized triacylglyceride synthesis, storage, or catabolism in response to whole-body energy demand (7). Lipids derived from sources of food, so-called dietary fats, are transported throughout the body in lipoproteins which are endocytosed into cells (8). In addition to adipocytes, many other cell types can form lipid droplets (albeit much smaller in size than those that prevail in white adipocytes) and metabolize lipids (9).

Hallmarks of white adipocyte formation include the activation of genes that positively regulate lipogenesis, thus allowing adipocytes to efficiently synthesize and store neutral lipid species within lipid droplets, as well as the acquisition of cellular machinery governing the catabolism of those lipids (10). Accordingly, embedded within the phospholipid monolayer of the lipid droplet are proteins that regulate lipid metabolism, the most abundant of which is perilipin 1 which functions to "coat" the lipid droplet and thus sterically hinder cytoplasmic lipases from physically interacting with triacylglycerides and catabolizing them into constituent free fatty acids, an enzymatic process referred to as lipolysis (further discussed below). Fatty acid binding protein 4 (FABP4) is also expressed in mature adipocytes and functions as a critical lipid chaperone protein (1). However, factors that enhance lipid metabolism, including adrenergic and TNF-alpha signaling, stimulate lipolysis in part by positively regulating the phosphorylation of perilipin 1 by protein kinase A (PKA), which results in a conformational change of perilipin 1 thus permitting the maximal translocation of lipases from the cytoplasm to the surface of the lipid droplet (11). On the other hand, insulin is the predominant physiological suppressor of lipolysis due to its attenuation of PKA-dependent perilipin 1 phosphorylation (4, 12). Moreover, insulin activates AKT in a PI3K/mTOR-dependent manner, thus enhancing the activating phosphorylation of phosphodiesterase 3B (PDE3B) by AKT (13). PDE3B functions to increase AMP levels by catalyzing the hydrolysis of cyclic AMP (cAMP), which therefore decreases the activation rate of PKA by cAMP (13). Insulin has also been demonstrated to suppress lipolysis by negatively regulating the gene expression of lipases (4).

Fundamentally, lipolysis is the stepwise enzymatic process that converts triacylglycerides to glycerol plus three molecules of free fatty acids (4). Adipocyte triglyceride lipase (ATGL) catalyzes the primary cleavage of triacylglycerol to diacylglycerol, following which hormone-

sensitive lipase (HSL) serves as the major diglyceride lipase, and monoglyceride lipase (MGL) completes the lipolytic process by catalyzing the breakdown of monoacylglycerol to glycerol and a free fatty acid molecule (14). Free fatty acids are then released into the bloodstream to nourish peripheral tissues including skeletal and heart muscle cells which possess high-energy demands (5). The physiological pH of blood and the extracellular environment is slightly basic (with a normal pH tightly buffered to a range of about 7.35 to 7.45); therefore, the carboxyl group of a free fatty acid is deprotonated (*i.e.*, loss of a hydrogen ion; H^+) at physiological pH and thus negatively charged (15, 16). Free fatty acids enter cells via fatty acid transporters, as well as through a diffusion mechanism wherein the negatively charged carboxylate group of a fatty acid can acquire a proton (*i.e.*, H^+) at the outer leaflet of the plasma membrane, thus neutralizing the charge of the fatty acid and permitting its rapid diffusion across the membrane, following which the proton is released at the inner leaflet of the plasma membrane as the free fatty acid enters the cytoplasm (16). Beta oxidation of free fatty acids generates acetyl-CoA which, in turn, enters the citric acid cycle to produce NADH and FADH2 that are critical substrates used in oxidative phosphorylation to produce ATP for the cell (4).

Adipose lipid profiling reveals marked differences in lipid composition based on the anatomical location and type of adipose tissue. For example, Liaw and colleagues determined from tandem mass spectrometry analyses that mouse inguinal white adipose tissue (iWAT) and perirenal WAT differ in the prevalence of unique cardiolipin, phosphatidylserine, and phosphatidylcholine lipid species, while triglycerides of medium fatty acyl chain length significantly predominate in iWAT (17). On the other hand, triglycerides were shown to be less abundant in mouse interscapular brown adipose tissue, though they are comprised of longer fatty acyl chains than the triglyceride species present in inguinal and perirenal WAT (17). In

comparing the lipid profiles of differentiating white adipocytes *in vitro*, Liaw and colleagues also demonstrated that, congruent with white adipose tissues, white adipocytes developing in culture accumulate triglycerides, namely saturated triglyceride species, and posited that white adipocytes utilize unsaturated, longer acyl chain fatty acids to satiate their energy demands during their differentiation from white adipocyte progenitor cells to white adipocytes (17). Differentiating adipocytes further revealed significant changes in the prevalence and composition of hexosylceramides, sphingomyelins, and cholesterols (17), thus underscoring how lipid profiles reflect the unique metabolic demands of preadipocyte-to-adipocyte differentiation. As such, the regulation of white adipocyte differentiation is discussed in the following subsections.

1.1.2 Cellular origins of adipocytes

The process of adipocyte formation is defined by three discrete stages: the commitment of mesenchymal stems cells to the adipogenic lineage, mitotic clonal expansion of these early adipocyte progenitor cells, followed by terminal adipogenic differentiation of adipocyte progenitor cells to adipocytes. In a developmental context, adipocytes develop from mesenchyme (and are thus primarily mesodermal in origin), though in the cephalic region adipocytes develop from the neuroectoderm and are thus ectodermal in origin. Rodent models of adipocyte lineage tracing reveal the presence of adipose-specific markers by embryonic days 16.5-17.5 in subcutaneous regions, though visceral adipose tissues develop later and become visible by approximately postnatal day 7 (4). In assessing the developmental origins of white adipocytes, it is well-documented that mesenchymal stem cell and adipocyte progenitor cells are retained within the stromal vascular fraction (SVF) of white adipose tissues (18). The SVF, in this context, refers to a heterogeneous cell population derived from the mechanical/enzymatic

digestion of adipose tissues that includes fibroblasts, immune cells, endothelial cells, as well as cells of adipogenic lineage (19).

From adipogenic lineage tracing investigations of SVF cells derived from mouse inguinal white adipose tissue, mesenchymal stems cells define the earliest adipocyte progenitor cell population and are characterized by $PREF1^{+}$:$CD24^{+}$: PDGFR-$alpha^{-}$ expression (2). Ultimately, mesenchymal stem cells advancing in the adipogenic lineage become $PREF1^{-}$:$CD24^{-}$:PDGFR-$alpha^{+}$ adipocyte progenitor cells capable of undergoing terminal differentiation to white adipocytes (2). Refined lineage tracing investigations have further revealed that the white adipose tissue SVF contains several discrete adipocyte progenitor cell populations in both mice and humans, specific progenitor cell populations which are also referred to as preadipocytes in part based on their ability to efficiently undergo terminal adipogenic differentiation when isolated in cell culture. For example, Merrick and colleagues reported the existence of $ICAM1^{+}$ preadipocytes and $CD142^{+}$ preadipocytes derived from $DPP4^{+}$ progenitor cells (18). Congruent with the adipogenic lineage tracing investigation published by Gulyaeva and colleagues, these $DPP4^{+}$ multipotent cells were shown to be mesenchymal progenitors given their capacity for multi-lineage differentiation, including osteocyte differentiation, while both $ICAM1^{+}$ and $CD142^{+}$ committed preadipocytes revealed high levels of PDGFR-alpha and could be efficiently differentiated into white adipocytes *in vitro*. It was further appreciated in this report by Merrick and colleagues that $DPP4^{+}$ mesenchymal progenitor cells occupy the reticular interstitium, which is defined as a fluid-filled compartment composed of abundant collagen and elastin fiber networks that encases many organs including adipose tissues, while $ICAM1^{+}$ and $CD142^{+}$ preadipocytes reside in a perivascular compartment encapsulated by the reticular interstitium which also possesses a collagen-rich network of extracellular matrix (18).

Independent lineage tracing investigations employing alternative adipogenic lineage markers have further shown that adipose-derived mesenchymal stem cells are also characterized by $CD24^+$:$CD34^+$ cell surface expression and give rise to preadipocytes marked by PDGFR-$alpha^+$:PDGFR-$beta^+$ cell surface expression in mice and humans (18, 19). In mice, SCA-1 is a well-established marker of the adipogenic lineage wherein Friedman and colleagues demonstrated the identity of a $CD24^+$:$CD29^+$:$CD34^+$:$SCA\text{-}1^+$ mesenchymal stem cell population capable of proliferating and differentiating into white adipocytes *in vitro* (20). Mesenchymal stem cells also give rise to mural cells which include both vascular smooth muscle cells and pericytes (4, 18). Thus, given that adipocytes and vasculature develop in close association with one another, it has been suggested that mural cells resident to adipose tissues can undergo a phenotypic switch to become adipocyte progenitor cells capable of differentiating into adipocytes (4). In a developmental context, it is posited that during childhood and early adulthood the number of mature adipocytes in the body becomes fixed; however, it is well documented that adipocytes turn over in which old adipocytes die and new adipocytes arise owing to adipogenic differentiation. For example, among humans, as many as 8% of all subcutaneous adipocytes turn over each year (4). Expounding on *in vivo* adipogenesis in states of obesity, Rosen and Spiegelman emphasize that new adipocyte formation is not the primary driver of obesity itself, but is rather a consequence of the body's need to store excess calories due to overnutrition or diminished energy expenditure (4). Correspondingly, in the obese state, adipose tissue remodeling is characterized by both hyperplasia (increased number of adipocytes as a result of enhanced adipogenesis) and hypertrophy (increased adipocyte size attributed to lipid droplet expansion) (4). Although numerous independent reports have shown that adipocytes are derived from mesenchymal stem cells, Gavin and colleagues reported that high-fat feeding in

mice results in the scenario where stores of mesenchymal adipocyte progenitor cells can become diminished due to enhanced rates of *in vivo* adipogenesis and, in response, new adipocytes can arise from bone marrow hematopoietic stem cells (21). It is unclear whether hematopoietic stem cell-derived adipocytes are functionally aberrant regarding their insulin sensitivity and ability to synthesize/catabolize lipids, or if they otherwise contribute to pathologic remodeling of white adipose tissues. In states of metabolic or physical stress, including obesity and trauma, a process referred to as "adipocyte mesenchymal transition" (AMT) has been shown to contribute to fibrotic, pathologic remodeling of adipose tissues (22, 23). AMT is facilitated by fibrotic stimuli (mechanical stress, YAP signaling, TGFB1 signaling, etc.) where adipocytes first lose adipogenic gene expression, thus facilitating their de-differentiation to preadipocytes which are subsequently reprogrammed to multipotent mesenchymal progenitor cells capable of differentiating to myofibroblasts (*i.e.*, contractile fibroblasts that express alpha smooth muscle actin) (22, 23). Interestingly, evidence suggests AMT is a bi-directional process whereby myofibroblasts can be reverted back to adipocytes (22, 23). On the whole, the use of *in vivo* lineage tracing technologies will aid in a more complete understanding of discrete adipogenic lineages, including the cellular origins of adipocytes in various organs and tissues, as well as an enhanced comprehension of how adipogenic lineages contribute to healthy versus pathologic adipose tissue remodeling commensurate to their role in governing adipocyte formation and function. Accordingly, the following subsections provide an overview of known signaling pathways and factors that regulate the process of white adipocyte formation.

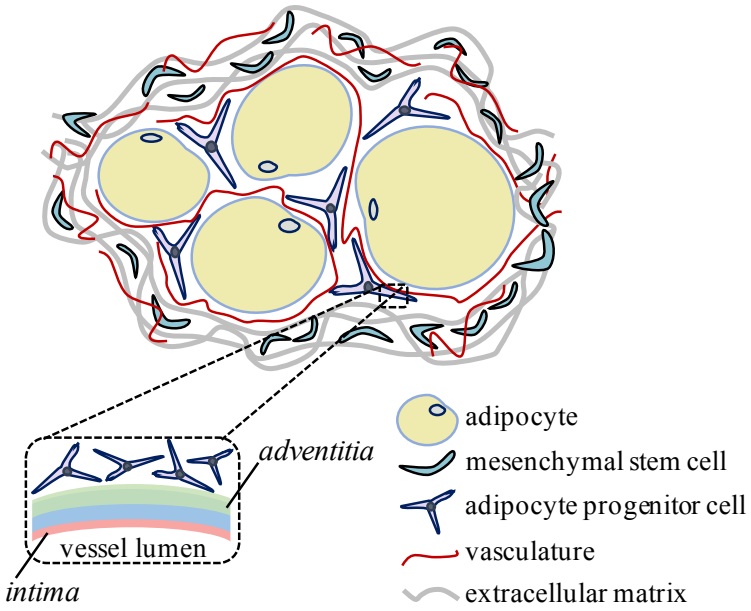

Figure 1. **Localization of adipogenic progenitors within white adipose tissues**. Adipocytes are derived from mesenchymal stem cells. Within white adipose tissues, mesenchymal stem cells reside in the reticular interstitium, which is an anatomically distinct, fluid-filled compartment possessing a collagen-rich network of extracellular matrix. Mesenchymal stem cells undergo adipogenic lineage commitment to become adipocyte progenitor cells (*i.e.*, preadipocytes), which are capable of undergoing terminal adipogenic differentiation into adipocytes. Adipocyte progenitor cells occupy the highly vascularized adipocyte compartment, which is separate from the reticular interstitium, and are positioned between adipocytes and adjacent to vascular adventitia (as also depicted in the inset). Adipocyte turnover, in which old adipocytes die and new adipocytes arise owing to the differentiation of adipocyte progenitor cells, is a key facet of maintaining insulin-responsive adipocytes within white adipose tissues.

1.1.3 Commitment of progenitor cells to the adipogenic lineage

Preceding the adipogenic differentiation of preadipocytes into adipocytes (*i*.e., adipogenesis), multipotent progenitor cells first "commit" to the adipogenic lineage and thus acquire the cellular machinery to undergo adipogenesis. Although it has been recently demonstrated that certain progenitor cells derived from hematopoietic stem cells are capable of committing to the adipogenic lineage, particularly under obesogenic conditions (21), this subsection focuses on the commitment of mesenchymal stem cells to the white adipogenic lineage.

There are several known mechanisms describing the process by which $PAX7^{-}$:$MYF5^{-}$ mesenchymal stem cells undergo white adipogenic lineage commitment. For example, bone morphogenetic protein (BMP) 2 and BMP4 both positively regulate the adipogenic lineage commitment of mesenchymal stem cells (5, 24). BMPs are members of the TGFB superfamily known to bind several bone morphogenetic protein receptors, including BMPR1 and BMPR2, which phosphorylate the R-SMADs (*e.g*., SMAD1/5/8) that, in turn, dimerize and subsequently complex with the co-SMAD, SMAD4, to undergo nuclear translocation (24). Such R-SMAD/co-SMAD heterotrimeric complexes interact with nuclear co-repressors and co-activators to regulate gene transcription (5). In the context of adipogenic lineage commitment, BMP2 and BMP4 have been shown to positively regulate cytoskeletal- and extracellular matrix-associated factors, including lysyl oxidase and translationally controlled tumor protein (TCTP), which function to disrupt the F-actin cytoskeleton and promote a more rounded cell shape (5, 25). Moreover, separate genetic knockdown of either protein-lysine 6-oxidase, TCTP, or SMAD4 attenuated mesenchymal stem cell adipogenic lineage commitment induced by BMP2 or BMP4, while overexpression of constitutively active BMP receptors promoted lineage commitment even in the absence of BMP2 or BMP4 (5). By activating the SMAD1/5/8 complexes, BMP2 and BMP4

have also been shown to enhance adipogenic gene expression in mesenchymal progenitor cells, including C/EBP beta, C/EBP alpha, and PPAR-gamma (5).

Relatedly, Bowers and Lane have demonstrated that WNT signaling acts upstream of BMP4 to enhance adipogenic lineage commitment of mesenchymal stem cells (26). WNTs are secreted glycoproteins and serve as ligands for the frizzled receptor family in conjunction with LDL-related receptor-5 or -6 (LRP5/6) coreceptors to activate canonical WNT signaling, thus promoting the nuclear localization of Catenin beta-1 (CTNB1) where it binds T-cell factor/lymphoid-enhancing factor (TCF/LEF) promoters (5, 26). In the absence of WNT signaling, CTNB1 is phosphorylated by GSK3B and embedded in a destruction complex consisting of GSK3B, axin, and adenomatous polyposis coli, whereby phospho-CTNB1 is targeted for ubiquitination and proteasomal degradation (26). The R-spondins are also known to activate WNT signaling, of which Bowers and Lane purport that R-spondin-2 and -3 stimulate canonical WNT signaling to drive BMP4 expression in mesenchymal stem cells, which thus positively regulates SMAD1/5/8 signaling to enhance adipogenic gene expression therein (5). On the other hand, Hedgehog (HH) signaling negatively regulates the adipogenic lineage commitment of mesenchymal stem cells (5, 25). HH signaling involves the activation of Protein patched homolog 1 (PTC1) receptors by Sonic hedgehog (SHH), Indian hedgehog (IHH), or Desert hedgehog (DHH), thus stimulating the G protein-coupled receptor (GPCR) homolog, Smoothened (SMO), resulting in the nuclear localization of the GLI family of transcription factors (27). Activation of HH signaling in mesenchymal stem cells has been shown to enhance the gene expression of GLI1, GLI2, and GLI3 which, in turn, suppress adipogenic gene expression and promote osteogenic lineage commitment. Congruently, mesenchymal stem cells

undergoing adipogenic lineage commitment demonstrate downregulated GLI1, GLI2, and GLI3 gene expression (5).

On the whole, the commitment of mesenchymal stem cells to the adipogenic lineage is marked by changes in gene expression as well as morphological changes to the cell, namely the disruption of the F-actin cytoskeleton and the acquisition of a round cell shape phenotype. While HH signaling and other determinants inhibit adipogenic lineage commitment, there is strong evidence to suggest that BMP2/4 signaling enhances adipogenic lineage commitment commensurate to the positive regulation of adipogenic gene expression in mesenchymal stem cells, thus giving rise to adipocyte progenitor cells which are capable of undergoing terminal adipogenic differentiation into adipocytes. The mechanisms underpinning the regulation of adipogenic gene expression in adipocyte progenitor cells is further discussed in the next subsection.

1.1.4 Terminal adipogenic differentiation

The commitment of mesenchymal stem cells to the adipogenic lineage yields adipocyte progenitor cells (*i.e.*, preadipocytes) that possess the capacity to undergo terminal adipogenic differentiation. Adipogenesis is therefore the cellular process of preadipocyte-to-adipocyte differentiation which gives rise to mature, lipid-laden white adipocytes (*Figure 2*). To date, the regulation of adipogenesis, including changes in the gene expression and cell cycle profiles of the differentiating preadipocyte, has been most extensively characterized *in vitro* with the use of transformed cell lines such as 3T3-L1 and 3T3-F442A preadipocytes, in addition to primary cells (*e.g.*, mouse embryonic fibroblasts, stromal vascular cells harvested from white adipose tissues, etc.). *In vitro* adipogenesis can be achieved over the course of about 6-10 days through a process

of chemically stimulating such adipocyte progenitor cells with insulin, IBMX (3-isobutyl-1-methylxanthine), and dexamethasone. Respectively, this chemical cocktail serves to activate insulin/insulin growth factor receptors, inhibit phosphodiesterase activity which thus enhances cAMP-PKA signaling, and positively regulate glucocorticoid pathways, the implications of which are discussed below in more detail. Glitazones, which are a class of small molecules known to stimulate PPAR-gamma transcriptional activity, are often included as part of this chemical cocktail to enhance the overall rate of adipogenesis *in vitro* (4, 5).

Preadipocytes stimulated with insulin, IBMX, and dexamethasone will initially experience cell cycle arrest for a period of about 16-20 hours, followed by reentry into the cell cycle and several rounds of mitosis (commonly referred to as mitotic clonal expansion in adipogenesis literature). Mitotic clonal expansion at this juncture of the adipogenesis program is requisite since forced inhibition of DNA replication or blocking cell cycle progression has been shown to prevent preadipocyte differentiation (5). The combined application of insulin, IBMX, and dexamethasone also serves to positively regulate the adipogenic transcription factor C/EBP beta early in the adipogenesis program. Moreover, IBMX, owing to its suppression of phosphodiesterases, enhances cAMP-PKA signaling which activates cAMP response element-binding protein (CREB). The phosphorylation of CREB by PKA thus positively regulates the transcriptional activity of CREB which increases *CEBPB* gene expression, as well as *CEBPD* gene expression, which is another adipogenic transcription factor upregulated early in the adipogenesis program (5). On the other hand, the interplay of insulin and dexamethasone functions to enhance the DNA binding activity of C/EBP beta. As elucidated by Kim and colleagues, dexamethasone increases the gene expression of the Ras family small G protein, RASD1 (Ras-related dexamethasone induced 1), which, quite intriguingly, couples insulin

growth factor 1 (IGF-1) receptor signaling to map kinase (MAPK) (28). In the presence of RASD1, insulin is thus able to stimulate an IGF-1 receptor-SHC/GRB2-MAPK axis of signaling. Active MAPK, in turn, phosphorylates threonine residue 188 of C/EBP beta (5). While the insulin receptor can also function to enhance MAPK signaling, particularly through SHC-GRB2 complex activation induced by insulin receptor substrates, the insulin receptor itself is maintained at low basal levels of expression in preadipocytes (28).

Relative to the treatment of preadipocytes with insulin, IBMX, and dexamethasone, phosphorylation of C/EBP beta by MAPK occurs approximately 4 hours following chemical stimulation (5). This can be explained on the basis that marked *RASD1* gene expression has been observed several hours after the application of dexamethasone in culture (29). 16-20 hours following chemical stimulation with insulin, IBMX, and dexamethasone, C/EBP beta phosphorylation by glycogen synthase kinase-3 beta (GSK3B) has been observed at threonine residue 179 or serine residue 184 (5). To date, this relative delay in C/EBP phosphorylation by GSK3B *in vitro* has not been addressed in the literature. GSK3B is a constitutively active kinase stemming from autophosphorylation at tyrosine residue 216 (30), while phosphorylation of GSK3B at serine residue 9 by AKT and other kinases, for example, has been shown to inhibit its kinase activity (31). Furthermore, Kim and colleagues demonstrated that, although RASD1 couples IGF-1 receptor signaling to the MAPK signaling pathway, RASD1 does not diminish the ability of insulin to activate the IGF-1 receptor or enhance PI3K/AKT effector signaling, including the phosphorylation of GSK3B at serine residue 9 (28). It is plausible that, following chemical treatment of preadipocytes with insulin, IBMX, and dexamethasone *in vitro*, GSK3B is initially inactivated and is only thus able to regain appreciable kinase activity hours following the

onset of chemical treatment, presumably when insulin-PI3K-AKT signaling has significantly subsided.

Nevertheless, dual phosphorylation at threonine residue 188 and threonine residue 179/serine residue 184 by MAPK and GSK3B, respectively, is required for C/EBP beta DNA binding activity (5, 32). Given the finding that there is a more than 12-hour lag in MAPK- versus GSK3B-induced C/EBP beta phosphorylation based on *in vitro* investigations of adipogenic signaling, phospho-C/EBP beta thus displays a high degree of protein stability. C/EBP delta is also a direct substrate of GSK3B which phosphorylates its serine residue 167 (33). The phosphorylation of both C/EBP beta and C/EBP delta induces conformational changes that promote their respective homo- and heterodimerization, and thus the acquisition of DNA binding function (5). At this juncture of the adipogenesis program, preadipocytes are still arrested in the cell cycle; however, heterochromatin centromeric satellite DNA possesses C/EBP regulatory elements thus allowing the binding of C/EBP beta and C/EBP delta which, in turn, facilitates chromatin remodeling (34), cell cycle reentry, and preadipocyte mitotic clonal expansion (5, 28). RASD1 expression has also been demonstrated to be required for the G1-S transition of the cell cycle early in the adipogenesis program (28), data which further support the essential role of C/EBP beta as both a regulator of the cell cycle and adipogenic gene expression. The genes for the adipogenic transcription factors C/EBP alpha and PPAR-gamma also possess C/EBP regulatory elements and, in this manner, C/EBP beta and C/EBP delta function to positively regulate *CEBPA* and *PPARG* gene expression (34, 35). Unlike C/EBP beta and C/EBP delta, the binding of C/EBP alpha to centromeric satellite DNA produces an antimitotic effect such that preadipocytes in the advancing stages of the adipogenesis program once again undergo cell cycle arrest (34). However, relative to the onset of preadipocyte mitotic clonal expansion, C/EBP beta

and C/EBP delta are initially unable to enhance *CEBPA* gene expression due to the inhibitory binding of SP1 (Specificity protein 1) to the C/EBP alpha gene promoter (34). Following several rounds of mitotic clonal expansion, SP1 expression is downregulated permitting significant transactivation of *CEBPA* gene expression by C/EBP beta and C/EBP delta, and thus the onset of cell cycle arrest given the antimitotic activity of C/EBP alpha (5). Moreover, when C/EBP alpha and PPAR-gamma are more appreciably expressed, it has been suggested that C/EBP alpha is principally responsible for maintaining the active gene expression of both *CEBPA* and *PPARG* via transactivation of C/EBP regulatory elements contained within the proximal promoter region of each gene (34).

As with C/EBP beta and C/EBP delta, several phosphoacceptors within C/EBP alpha are substrates for GSK3B (*e.g.*, threonine residues 222 and 226), though the functional consequences of such phosphorylation events have not been investigated (36). C/EBP alpha homodimerization (in addition to heterodimerization with C/EBP beta or C/EBP delta) lends DNA binding activity in which the activation of *PPARG* gene expression, in particular, further enhances the expression of lipogenic genes, including perilipins and fatty acid-binding protein 4 (FABP4) (5), the functions of which are discussed in greater detail in the previous section (*1.1.1 The adipocyte and adipose tissue landscape*). At this stage of the adipogenesis program, when the expression and activity of C/EBP alpha and PPAR-gamma abound, lipogenic factors are expressed at greater levels and function to equip the developing, cell cycle arrested adipocyte with the necessary cellular machinery to synthesize, store, and metabolize lipids. Based on *in vitro* methods of adipogenesis, while dexamethasone and IBMX are omitted during the later stages of the adipogenesis program, insulin is continually applied to cells at intermittent intervals (*e.g.*, every second or third day) given its ability to positively regulate *de novo* lipogenesis (5), and as

discussed in the previous section herein (*1.1.1 The adipocyte and adipose tissue landscape*). Taken together, over the span of 6-10 days in culture, preadipocytes can be differentiated into mature, lipid-laden white adipocytes.

From studies implementing *in vitro* models of adipogenesis, investigators have discerned critical aspects of the adipogenesis program, including temporal patterns of adipogenic and lipogenic gene expression, as well as the mechanisms underpinning the regulation of those genes. The gene expression choreography of adipogenesis has also been investigated *in vivo* using reporter mouse models, flow cytometry, single-cell RNA sequencing, and other methods to delineate cell populations among adipose tissues that define the adipogenic lineage (2, 18). From these investigations, mesenchymal stem cells advancing in the adipogenic lineage have been shown to acquire adipogenic gene expression, while preadipocytes more advanced in the adipogenic lineage possess significant adipogenic gene expression including *CEBPA* and *PPARG* (2, 18). While refined lineage tracing investigations are paramount for better understanding the regulation of adipogenesis *in vivo*, such corroborating adipogenic gene expression data highlight the relevance and utility of implementing *in vitro* methods to study novel aspects of adipogenic signaling in concert with animal models.

Complimentary *in vitro* and *in vivo* approaches to studying adipogenic signaling has also aided in characterizing negative regulators of adipogenesis in part by defining how these factors influence the lineage commitment of pluripotent mesenchymal stem cells (37). In addition to the adipogenic lineage, mesenchymal stem cells can undergo lineage commitment towards other cell fates including but not limited to chondrocytes, osteoblasts, endothelial cells, and myocytes (37). In this context, Kruppel-like factor 2 (KLF2) has been shown to enhance osteoblast differentiation while its inhibition of the C/EBP alpha gene promoter negatively regulates

adipogenesis (5). Moreover, while canonical WNT signaling functions to enhance the adipogenic lineage commitment of mesenchymal stem cells in addition to preadipocyte mitotic clonal expansion (thus increasing the total pool of preadipocytes available to differentiate into adipocytes), WNT10B, for example, suppresses terminal adipogenic differentiation by inhibiting *PPARG* gene expression (5) and promotes osteoblast differentiation (38). Similarly, while it has been shown that TGF-β superfamily members BMP2 and BMP4 promote mesenchymal stem cell adipogenic lineage commitment, the TGFB1 pathway inhibits adipogenic gene expression while promoting osteoblast differentiation and overall bone formation (5, 39). Furthermore, Li and colleagues have investigated the role of the zinc finger transcription factor, GATA-binding factor 2 (GATA2), among mesenchymal lineages, and revealed from the use of transgenic mouse models harboring either a mesenchymal stem cell-, adipocyte-, or osteoblast-specific deletion in *Gata2* how GATA2 positively regulates both the adipogenic and osteogenic lineage commitment of mesenchymal stem cells, yet negatively regulates adipogenesis and osteoblast differentiation (40). These data suggest that GATA2 functions to enhance the number of adipocyte and osteocyte progenitor cells within local microenvironments *in vivo*. Transcription factor SOX-9 (SOX9) has also been identified as transcriptional regulator of mesenchymal lineages. For example, SOX9 expression is required for chondrocyte formation (41), while it has also been shown to inhibit adipogenesis (2). Regarding the latter, the Sul group first identified the anti-adipogenic function of SOX9 by determining that it is a PREF1 (preadipocyte factor 1) effector protein (42). Earlier reports demonstrated that SOX9 directly inhibits adipogenic gene promoters (42), while a more recent investigation further highlighted that the direct SOX9 effector, meis homeobox 1 (MEIS1), also inhibits the gene promoters of C/EBP beta, C/EBP delta, C/EBP alpha, and PPAR-gamma (2). Moreover, Gulyaeva and colleagues showed that downregulation

of *Sox9* gene expression in mice is required for adipogenesis *in vivo*, and demonstrated that subcutaneously implanted preadipocytes bearing a null mutation in *Sox9* undergo an enhanced rate of adipogenesis *in situ* versus implanted preadipocytes possessing wildtype *Sox9* gene expression (2). Therefore, these studies highlight the physiological relevance of SOX9 in the regulation of *in vivo* adipogenesis. To this end, the ability of CTHRC1 to regulate SOX9 expression and its anti-adipogenic activity is further discussed in the proceeding sections herein.

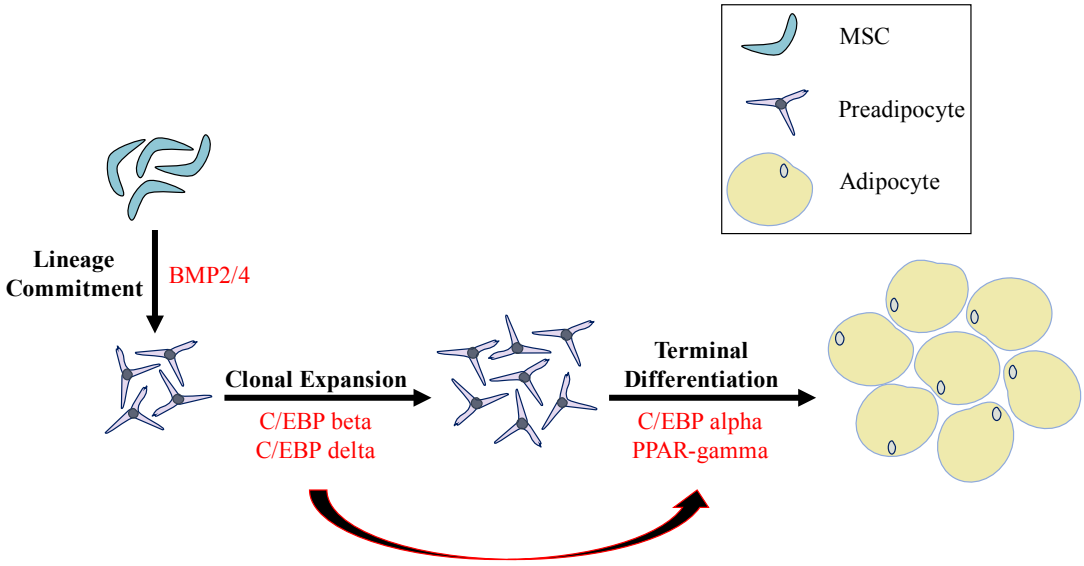

Figure 2. Transcriptional regulation of adipogenic lineage commitment and differentiation. Mesenchymal stem cells define the earliest adipocyte progenitor cell population. Bone morphogenetic proteins 2 and 4 (BMP2/4) positively regulate mesenchymal stem cell adipogenic lineage commitment by enhancing the basal expression levels of adipogenic genes including C/EBP beta and C/EBP delta. C/EBP beta and C/EBP delta promote mitotic clonal expansion of preadipocytes, and function to transactivate the expression levels of C/EBP alpha and PPAR-gamma. C/EBP alpha induces cell cycle arrest in the latter stages of the adipogenesis program

and robustly enhances the gene expression levels of PPAR-gamma which, in turn, positively regulates the gene expression of lipogenic factors that equip the developing adipocyte with the requisite machinery to synthesize, store, and metabolize lipids.

1.2 CTHRC1 structure and function

Collagen triple helix repeat-containing protein 1 (CTHRC1) is a secreted protein discovered by Dr. Volkhard Lindner and colleagues at Maine Medical Center Research Institute (currently MaineHealth Institute for Research). This introductory subsection will focus on the discovery of the *CTHRC1* gene, with an emphasis on the molecular characterization of CTHRC1, as well as established features of its biochemistry and signaling.

1.2.1 Identification of the CTHRC1 gene

The genesis of the CTHRC1 story is rooted in basic biology research focused on vascular remodeling. As conveyed in the seminal publication on CTHRC1, the recurrent clinical failure of angioplasty procedures secondary to constrictive arterial remodeling led Dr. Lindner and colleagues to investigate potential differentially expressed genes in normal versus balloon-injured arteries (43). Remarkably, in a foregone era of genetics preceding the publication of the Human Genome Project in 2001, the novel gene *CTHRC1* was discovered in the late 1990s from a balloon catheter injury model of rat carotid arteries (43). *Cthrc1* was first identified by automated DNA sequence analysis of rat subtractive hybridization cDNA libraries of normal versus balloon-injured arteries. Human *CTHRC1* was subsequently cloned using cDNA libraries generated from cultured human smooth muscle cells. In this primary report, *Cthrc1* mRNA was not detected in normal rat carotid arteries. However, significant *Cthrc1* mRNA levels were

detected 4 days and 8 days following balloon catheterization in rat (43), thus underpinning the nuanced, transient nature of *Cthrc1* gene expression that is a focus of the following section. It was further appreciated in this primary publication that CTHRC1 boasts at least 500 million years of conservation in the evolutionary record and is a highly conserved gene among vertebrate species (44). Interestingly, Leclere and colleagues later reported the existence of several *Cthrc1* paralog genes in most nonvertebrate species, and posited from phylogenetic analysis that the genesis of the *Cthrc1* gene likely occurred over 750 million years ago in the last common metazoan ancestor as a result of a novel gene fusion event of two preexisting domains: a collagen triple helix repeat (CTHR) domain and a C1q-like domain (44). To this end, the following sections will further describe the molecular and structural features of CTHRC1, as well as its gene expression trends.

1.2.2 The molecular structure of CTHRC1

In the primary publication on CTHRC1, Dr. Lindner and colleagues characterized that CTHRC1 is a secreted protein and possesses a N-terminal hydrophobic signal peptide, a short CTHR domain containing 12 GXY repeats, followed by a highly conserved C-terminal domain (*Figure 3*). When this first report was published in 2005, the C-terminal domain of CTHRC1 was not known to possess sequence homology to other protein domains based on BLAST searches of primary protein structures (43). The initial molecular characterization of CTHRC1 also suggested that it is N-glycosylated and capable of trimerization given its CTHR domain which, itself, is susceptible to collagenase digestion (43). Moreover, CTHRC1 possesses 10 cysteine residues (of which 8 cysteine residues are located in the C-terminal domain) (45). By Western blot analysis, secreted CTHRC1 was shown to run as an apparent dimer and trimer under non-

reducing chemical conditions, and as a monomer under reducing conditions at a molecular weight of approximately 28 kDa (43). Intriguingly, this seminal report further highlighted that the rat pulmonary artery smooth muscle cell line, PAC1, expresses endogenous CTHRC1, in which Western blot analysis revealed two distinct CTHRC1 fragments approximately 16 and 18 kDa in weight (46). As such, plasmin was purported to cleave a putative propeptide region thus resulting in an N-terminally truncated CTHRC1 species capable of inhibiting collagen matrix deposition (46). Recently, the presence of a propeptide within CTHRC1 was confirmed (47).

More than twenty years after the discovery of the *CTHRC1* gene, Leclere and colleagues published the first in-depth phylogenetic analysis on the evolution of *Cthrc1* genes, and therein demonstrated how the sequence evolutionary rate of *Cthrc1* markedly decreased beginning with the gnathostome lineage (*i.e.*, "jawed vertebrates") (44). Regarding the evolutionary conservation of the C-terminal domain of *Cthrc1*, in particular, and especially among the gnathostome lineage, Leclere and colleagues used three-dimensional alignment modeling softwares (*e.g.*, HHpred) and determined that the C-terminal domain possesses striking structural homology to the globular complement component 1q (C1q) superfamily domain. Congruent with the authors of the primary publication on CTHRC1, who suggested that CTHRC1 is likely not a "structural" collagen-like protein based, in part, on their observation of its transient gene expression patterns (44), Leclere and colleagues posited that the highly conserved C1q-like domain within CTHRC1 could regulate key aspects of its molecular function, while its short CTHR domain, which possesses only 12 GXY repeats, contrasts considerably to bona fide structural collagen species whose CTHR domains typically contain hundreds of GXY repeats that facilitate vast triple helical formation.

Similar to CTHRC1, Complement C1q tumor necrosis factor-related proteins (CTRPs) are secreted factors possessing a variable N-terminal domain, followed by a short CTHR domain adjoining a globular C-terminal domain (48). CTRPs exude both anti-inflammatory and insulin-sensitizing effects (48), as was shown for the adipose tissue secreted factor, adiponectin. While adiponectin possesses hormone functionality and can bind to several known cell surface receptors, it is also characterized by non-canonical endocrine function, including its ability to bind anionic phospholipid and sphingolipid species present in liposomes, low-density lipoproteins, cell membranes, and plasma (48). Critically, mutagenic deletion of its C1q-like C-terminal domain prevents adiponectin from binding lipids (48). In further evaluating the hormone-independent functions of adiponectin, Ye and colleagues contend that, by virtue of its C1q-like domain, adiponectin targets ectopic lipids (*e.g.*, low-density lipoproteins, membranous debris, etc.) within vessels and extracellular spaces and shuttles them to phagocytes (48). Itself, C1q is best characterized in innate immunity as the initiator of the classical complement cascade, and is capable of binding the Fc region of most immunoglobulin G (IgG) subclasses (48, 49). Congruently, C1q is also known to bind lipid species, including cardiolipin and phosphatidylserine, thus facilitating the opsonization of apoptotic cells and microbes (48). C1q, as well as other protein species harboring C1q-like structure, nevertheless display a diversity of functions and molecular activities. Regarding CTHRC1, it is noteworthy that its purported C1q-like C-terminal domain comprises more than half of its molecular composition (44). While future investigations are required to functionally characterize the C-terminal domain of CTHRC1, the motif is nonetheless remarkably conserved among vertebrate species. On the whole, Leclere and colleagues observed that the *Cthrc1* gene is highly conserved among vertebrates in a syntenic block that includes *Frizzled6* (*Fzd6*) (44). Intriguingly, CTHRC1 has been shown to bind the

extracellular domain of Fzd6 to drive planar cell polarity signaling (50), suggesting that the *Cthrc1-Fzd6* genomic linkage is functionally important.

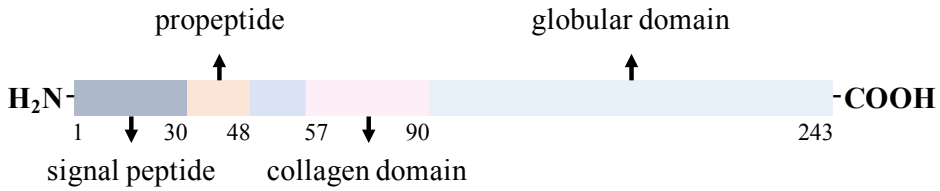

Figure 3. **Structure of collagen triple helix repeat-containing protein 1 (CTHRC1)**. Graphical illustration of the functional domains of human CTHRC1. CTHRC1 contains a proline-rich, hydrophobic N-terminal signal peptide (amino acids 1-30) which is cleaved during the transport of the nascent CTHRC1 molecule to the lumen of the endoplasmic reticulum. Recently, it was shown that CTHRC1 possesses a propeptide region (amino acids 33-48) (47). The cleavage of the propeptide results in a truncated form of CTHRC1 with enhanced biological activity (47). CTHRC1 is also comprised of a short collagen-like domain (amino acids 57-90) consisting of twelve G-X-Y repeats that enables the protein to form trimers. By Western blot analysis, secreted CTHRC1 runs principally as a homodimer and homotrimer under non-reducing chemical conditions, though higher molecular weight complexes are observed (*Figure 4B*). On the other hand, Western blot analysis under chemically reducing conditions reveals that secreted CTHRC1 runs as a monomer at an approximate molecular weight of 28 kDa (*Figure 4B*). CTHRC1 contains ten cysteine residues, eight of which are located in the globular C-terminal domain. CTHRC1 can also undergo *N*-glycosylation at asparagine 188 (a post-translational modification which has been reported to stabilize CTHRC1 and decrease its overall rate of protein turnover) (51). The C-terminal domain of CTHRC1 spans amino acids 91-243,

and is not known to share structural homology with other protein domains. However, based on 3D protein modeling, it was recently suggested that the C-terminal domain of CTHRC1 is similar in structure to the globular component 1q (C1q) superfamily domain, which includes secreted factors like adiponectin and other complement C1q tumor necrosis factor-related protein (CTRP) family members.

1.2.3 CTHRC1 expression trends

In the seminal publication on CTHRC1, Dr. Lindner and colleagues first identified that *Cthrc1* is a gene whose expression in adventitial fibroblasts and intimal smooth muscle cells of rat arteries is transiently increased following injury via balloon angioplasty (43). At the protein level, CTHRC1 was expressed post injury in the cellular compartment of arterial fibroblast and smooth muscle cells, while neither *Cthrc1* mRNA nor protein expression were detected in rat arteries prior to vascular injury. In this report, exogenous application of either BMP4 or TGFB1 to NIH3T3 mouse fibroblast cultures significantly enhanced endogenous *Cthrc1* mRNA levels *in vitro*, and the recombinant overexpression of CTHRC1 in PAC1 rat smooth muscle cells markedly decreased the mRNA expression of type 1 collagen alpha 1 (*Col1a1*) (43). Of note, in the vascular wound healing process, TGFB1 signaling positively regulates collagen synthesis and deposition which, in turn, enhances adventitial smooth muscle cell proliferation, typically resulting in luminal narrowing of the remodeling vasculature (*i.e.*, constrictive vascular remodeling) (43). In a follow-on investigation assessing the role of CTHRC1 in vascular remodeling, in which ischemic injury was induced by ligating mouse carotid arteries in wildtype versus transgenic *Cthrc1*-overexpressing mice, it was determined that transgenic mice displayed significantly decreased carotid artery intimal area, as well as markedly reduced intimal smooth

muscle cell proliferation within the injured vessel (52). It was also determined in this report that CTHRC1 significantly decreased the phosphorylation of SMAD2/3, suggesting that the effect of CTHRC1 on vascular remodeling could pertain to its negative regulation of TGFB1 signaling and corresponding reduction in the expression of fibrillar collagen species, including type 1 collagen (52). The relationship between CTHRC1 and TGFB1 signaling events is therefore dichotomous: while TGF-β signaling drives *Cthrc1* gene expression, CTHRC1 can suppress the activities of TGFB1 effector proteins, including SMAD2/3, in an apparent regulatory feedback loop (52).

The initial discovery that *Cthrc1* gene expression is transiently increased secondary to vascular injury, and is thus potentially integral in wound healing and tissue remodeling processes, next prompted several independent investigations of *Cthrc1* expression trends during embryonic and early postnatal development in mice. Durmus and colleagues first published in 2006 that *Cthrc1* is expressed in the notochord at embryonic day (E) 8.5, based on in situ hybridization analyses, and becomes expressed in somites by E9.5, as well as in the hindbrain-midbrain junction and otic placode of the developing head at this latter time point (53). At E14.5, marked *Cthrc1* mRNA expression was detected in chondrocytes and developing bone (including skull, ribs, and vertebrae), as well as in the developing kidney. Based on immunostaining, CTHRC1 protein expression was detected in the visceral endoderm at E6.5, and in the notochord and neural tube at E12.5. At E14.5, CTHRC1 protein expression was localized throughout ventricular and atrial myocardia, as well as in the skull, ribs, and vertebrae of the developing skeleton system, thus congruent with the aforementioned bone in situ hybridization data (53). Also, CTHRC1 was detected in the chondrocytes of long bones, in addition to the surrounding perichondrium and periosteum, as well as within the mineralized bone matrix of adult mice (53).

Constitutive expression of CTHRC1 in osteocytes and osteoblasts is responsible for its secretion into circulation (54), while constitutive CTHRC1 expression has also been detected by certain neurons in the brain (55).

1.2.4 The effect of CTHRC1 on signaling pathways and networks

Pioneer vascular biology investigations published in the mid 2000s highlighted the discovery of CTHRC1 and how it is markedly upregulated in vasculature following injury , where it was shown to restrict the deposition of collagen extracellular matrix by suppressing SMAD2/3 phosphorylation, which corresponded with accelerated wound healing given enhanced migration of smooth muscle cells and fibroblasts (43, 46, 52). CTHRC1 has also been shown to regulate WNT signaling in cancer (56). In adenocarcinoma, CTHRC1 enhanced the nuclear translocation of CTNB1, while in ovarian cancer, CTHRC1 promoted epithelial-to-mesenchymal (EMT) transition through the WNT/CTNB1 effector, protein snail (56). CTHRC1 secreted from osteoclasts has also been shown to drive WNT/CTNB1 signaling in osteoblasts resulting in enhanced basic fibroblast growth factor expression and the development of cancerous bone lesions (57). Additionally, it has been reported that CTNB1can bind the *CTHRC1* promoter to enhance transcription, while CTHRC1 *N*-glycosylation can stabilize CTHRC1 protein expression in oral squamous cell carcinoma (51). On the other hand, CTHRC1 overexpression in both HEK293T and gastrointestinal stromal tumor cells suppressed canonical WNT signaling but enhanced noncanonical WNT/planar cell polarity (PCP) signaling (50, 58).

CTHRC1 has been shown to interact with extracellular components of canonical and noncanonical WNT signaling (50, 59, 60). Co-immunoprecipitation studies using HEK293T cells revealed the binding of CTHRC1 to FZD3, FZD5, FZD6, ROR2, WNT3A, WNT5A, and

WNT11 (50). Unlike full-length CTHRC1, a CTHRC1 mutant lacking the C-terminal domain was unable to bind FZD6, ROR2, WNT3A, WNT5A, and WNT11 (50). In cervical, pancreatic, and urothelial cancers, CTHRC1 has also been shown to drive PCP signaling (57). In human umbilical vein endothelial cells, CTHRC1 was reported to phosphorylate ERK and JNK by activating PCP signaling (57). In both HEK293T cells and primary gastrointestinal stromal tumor cells, CTHRC1 was shown to enhance the levels of Rho-GTP and Rac1-GTP in a PCP-dependent manner (45). Interestingly, the aforementioned CTHRC1 mutant, which lacks the C-terminal domain, was unable to enhance the levels of Rho-GTP or Rac1-GTP, suggesting that the C-terminal domain of CTHRC1 functions to regulate PCP signaling (45). In models of ovarian cancer, CTHRC1 has also been shown to regulate integrin signaling and the activation of FAK1 (Focal adhesion kinase 1) thus enhancing cancer cell adhesion, migration, and invasion (45).

1.2.5 CTHRC1 regulates body composition

CTHRC1 has also been shown to regulate body composition. Stohn and colleagues determined that *Cthrc1*-null mice are characterized by significantly increased adiposity in both subcutaneous and visceral adipose tissues in comparison to age-matched wildtype mice (55). *Cthrc1*-null mice also revealed decreased lean mass and energy expenditure in comparison to wildtype organisms. Moreover, transgenic mice overexpressing human *CTHRC1* had significantly decreased adipocyte size and adiposity in relation to wildtype controls. Stohn and colleagues further demonstrated that CTHRC1 suppresses *in vitro* adipogenesis. Primary stromal vascular cells were isolated from the inguinal white adipose tissue (iWAT) of wildtype or age-matched *Cthrc1*-null mice. Upon chemical induction of adipogenic differentiation *in vitro*, stromal cells derived from *Cthrc1*-null mice had comparatively enhanced adipocyte differentiation and maturation.

These data were recapitulated using 3T3-L1 preadipocyte cells, in which adenoviral overexpression of human *CTHRC1* significantly inhibited adipogenic differentiation based on decreased levels of lipid accumulation (55). Collectively, these data support that CTHRC1 could restrict adiposity by enhancing voluntary energy expenditure and regulating adipocyte differentiation.

CHAPTER 2: MATERIALS AND METHODS

2.1 Adenoviral transduction and conditioned media preparation

3T3-L1 cells, originally from Zen-Bio (Cat. # LIP-1-L1-F), were seeded at passage 14 in 15 cm dishes (CytoOne; CC7682-3614) containing DMEM (high glucose, without sodium pyruvate; Sigma Aldrich; D5796) supplemented with 4% fetal bovine serum (v/v; Hyclone; SH30396.03), 6% bovine calf serum (v/v; Cytiva; SH30072.03), and 1x antibiotic-antimycotic solution (Gibco; 15240-062), which we refer to as full-serum DMEM. 3T3-L1 cells were grown in a 5% CO_2 atmosphere at 37˚C. Cells were transduced as described (55) with adenoviral vectors overexpressing either human *CTHRC1* or control *β–galactosidase* (*βgal*). Briefly, 8 hours following the onset of transduction, cells were washed twice with full-serum DMEM (8 mL per dish per wash), and then incubated for 15 hours in 22 mL of full-serum DMEM. Conditioned media were collected in 50 mL conical tubes and centrifuged at 450 x g for 3 minutes to pellet any detached cells, after which conditioned media supernatants were transferred to fresh 50 mL conical tubes for study and stored at 4˚C. The presence of recombinant human CTHRC1 in conditioned medium was confirmed by Western blot analysis, or by an established ELISA as described previously (55). From ELISA, we determined that the concentration of recombinant human CTHRC1 in undiluted conditioned medium is approximately 9-10 ng/mL. In this study, we evaluated the effect of human CTHRC1 conditioned medium at specific dilutions (methodology described below), corresponding to the following concentration range of recombinant human CTHRC1: 1/4 dilution (2.5 ng/mL); 1/12 dilution (800 pg/mL); 1/60 dilution (150 pg/mL).

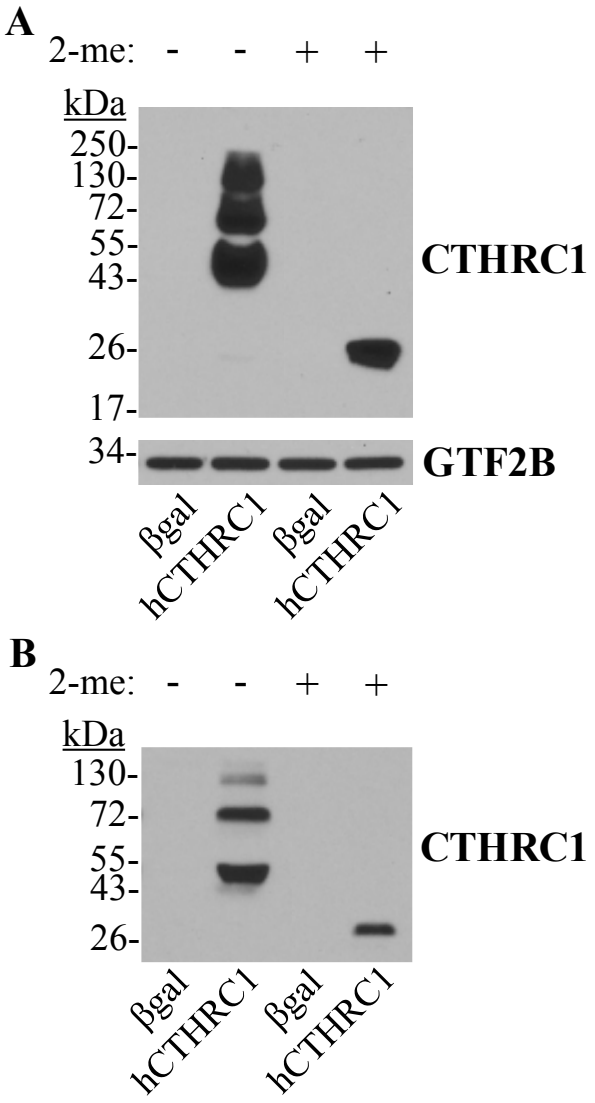

Figure 4. **Assessment of CTHRC1 by immunoblotting**. 3T3-L1 cells were transduced with adenoviral vectors overexpressing either human *CTHRC1* (hCTHRC1) or control *β–galactosidase* (βgal) for a period of 15 hours. Afterwards, conditioned media were collected, and whole-cell lysates were prepared from the transduced cells. **A**) Immunoblotting of transduced whole-cell lysates run in the absence or presence of the reducing agent 2-mercaptoethanol (2-me). GTF2B served as the loading control. **B**) Immunoblotting of conditioned media run in the absence or presence of the reducing agent 2-mercaptoethanol (2-me). The presence of

recombinant human CTHRC1 in transduced whole-cell lysates and conditioned media was probed using a rabbit monoclonal antibody raised against the C-terminus of human CTHRC1 (clone Vli55).

2.2 Exogenous application of conditioned media and adipogenic differentiation

3T3-L1 cells were grown and expanded in a sub-confluent manner in 10 cm dishes in full-serum DMEM. For study, 3T3-L1 cells were seeded at passage 11 in 24-well plates (TC24; CytoOne; CC7682-7524) at a density corresponding to 70% confluence in the presence of βgal or human CTHRC1 conditioned medium. Prior to the application of conditioned media to cells, βgal and human CTHRC1 conditioned media were first diluted in full-serum DMEM to specific final dilutions as indicated. Cells were suspended in freshly diluted conditioned media in 15 mL conical tubes and plated at a volume of 0.5 mL per TC24 well. After seeding, TC24 plates were vigorously agitated in all directions for several seconds every 30 minutes for a total period of 2 hours in order to prevent cells from clumping in the center of each well. In terms of a relative timeline, cells were seeded on Day -3, after which media were changed on a daily basis and replenished with freshly diluted βgal or human CTHRC1 conditioned medium at a volume of 0.5 mL per TC24 well. Freshly diluted βgal and human CTHRC1 conditioned media were also added on a daily basis during the six day period of chemically-stimulated adipogenesis. Beginning on Day 0, cells were treated with adipogenic differentiation induction cocktail including insulin (10 μg/mL, final; Sigma Aldrich; 19278), 3-isobutyl-1-methylxanthine (IBMX, 0.5 mM, final; Sigma Aldrich; 410957), and dexamethasone (1 μM, final; Tocris; 1126). The cocktail of insulin, IBMX, and dexamethasone was applied on Day 0, after which media were changed on Day 1 and replenished with freshly prepared insulin, IBMX, and dexamethasone. On

Day 2 and Day 4, media were changed and replenished with insulin (10 μg/mL, final). On Day 3 and Day 5, media were changed and replenished with only βgal or human CTHRC1 conditioned medium. In studies utilizing the Rac1 inhibitor, NSC 23766 (Tocris; 2161), and the Rho-associated kinase inhibitor, Y-27632 (Tocris; 1254), these reagents were freshly added on a daily basis beginning at the moment of cell seeding on Day -3. For all experiments utilizing TC24 plates, each well contained a final volume of 0.5 mL.

2.3 Assessment of YAP or SOX9 nuclear localization

3T3-L1 cells were seeded in triplicate on sterile, round 12 mm glass coverslips (Chemglass Life Sciences; CLS-1763-012) in TC24 plates in the presence of βgal or human CTHRC1 conditioned medium as described above. At the indicated timepoints, cells were fixed using 10% neutral formalin (Sigma Aldrich; F5554). Next, cells were washed twice in phosphate buffered saline (PBS) and blocked overnight at 4˚C in immunofluorescence blocking buffer consisting of PBS supplemented with 2% bovine serum albumin (w/v), 0.2% Tween 20 (v/v), 0.1% sodium azide (w/v), and 0.2% Triton X-100 (v/v). Following blocking, primary antibodies against YAP (Cell Signaling Technology; Cat. # 14074) or SOX9 (Cell Signaling Technology; Cat. # 82630) were prepared at a 1/250 dilution in immunofluorescence blocking buffer and applied to coverslips overnight at 4˚C. The next day, cells were washed twice in PBS. Alexa Fluor 546 Phalloidin (Molecular Probes; A22283) and Alexa Fluor 488 chicken anti-rabbit antibody (Invitrogen; A21441) were each prepared at a 1/250 dilution in immunofluorescence blocking buffer, to which Hoechst 33342 (4 μM; Thermo Fisher Scientific; 62249) was also added. This secondary antibody solution was applied to each coverslip for 1 hour at room temperature in darkness. Cells were then washed twice in PBS, after which each coverslip was inverted and embedded in

Vectashield Mounting Medium (Vector Laboratories, Inc.; H-1000), and secured in the center of a microscope slide (25 x 75 x 1 mm; VWR Scientific; 48312-705) with clear nail polish along the circumference of the coverslip. Confocal microscopy of the preparations was performed using the Leica SP8 microscope (Leica Microsystems) within the Histopathology and Microscopy Core Facility at MaineHealth Institute for Research.

2.4 Lentiviral-mediated RNA interference studies

Passage 9 3T3-L1 cells were seeded in two 10 cm dishes at approximately 600,000 cells per dish in full-serum DMEM. 4 hours later, upon complete cell attachment, cells were transduced with lentiviral particles overexpressing either a shRNA construct targeting *Sox9* mRNA (*i.e.*, shSOX9) or a non-targeting scrambled control shRNA construct (*i.e.*, shSCR). shSOX9 and shSCR lentiviral plasmids were a kind gift from Dr. Robert Weinberg, and were originally prepared as described (61). Briefly, the following shRNA sequences were cloned in the pLKO.1-puro lentiviral plasmid vector: shSOX9 (CTCCACCTTCACTTACATGAA); shSCR (CCTAAGGTTAAGTCGCCCTCG). shSOX9 and shSCR lentiviruses were then generated at the Viral Vector Core Facility at MaineHealth Institute for Research. Lentiviral transduction was conducted by incubating the cells for 15 hours with 8 μg/mL of polybrene (Sigma Aldrich; TR-1003-G) plus respective lentiviral particles in 10 mL of full-serum DMEM. Following lentiviral transduction, cells were washed twice in full-serum DMEM, and then treated with 10 mL of full-serum DMEM supplemented with puromycin (2 μg/mL, final; Gibco; A11138-03). After that, shSOX9 and shSCR lentivirally transduced cells were expanded in the continued presence of puromycin in a sub-confluent manner. For study, shSOX9 and shSCR cells were seeded in TC24 plates in the presence of βgal or human CTHRC1 conditioned medium as described above.

2.5 Oil Red O staining

In TC24 plates, medium was aspirated and wells were washed with serum-free DMEM and fixed with 10% neutral formalin overnight at room temperature. Formalin was then aspirated and wells were washed with 60% 2-propanol. Oil Red O (Sigma Aldrich; 1320-06-5) solution was prepared as previously described (55), and applied at a volume of 250 µL per well. Plates were incubated on a rotator at room temperature for 15 min, and then washed twice with distilled water. Oil Red O was eluted with 100% 2-propanol (250 µL per well), and plates were then incubated by rotation at room temperature for 15 min. 200 µL of eluate was added to one well of a clear, round-bottom 96-well plate (BRAND*plates*; 781840). Oil Red O absorbance was then measured at 520 nm using a FlexStation 3 plate reader (Molecular Devices) set to room temperature. Per 96-well plate, four wells were loaded with 200 µL of 100% 2-propanol to account for absorbance background. Oil Red O absorbance data were normalized by subtracting the average absorbance value of 2-propanol from the raw absorbance data.

2.6 Western blotting

Whole-cell lysates were prepared from cells treated with conditioned media and grown in TC24 plates, as described above, by first washing cells with PBS and then scraping each well in 50 µL of protein lysis buffer (ITSI Biosciences; K-0045-50). Per experimental group, protein lysates were pooled from six TC24 wells into a 1.5 mL microcentrifuge tube and immediately flash frozen on dry ice. Subsequently, lysates were thawed on ice, briefly vortexed, and their relative protein concentrations determined by absorbance spectroscopy using Coomassie Brilliant Blue (Thermo Scientific; 23236) measured at a 595 nm wavelength. 250 µL of lysate was transferred to a fresh 1.5 mL microcentrifuge tube and re-suspended with 83 µL of 4x Laemmli Sample

Buffer supplemented with 10% 2-mercaptoethanol. Samples were boiled at 100˚C for 5 minutes, and loaded at a volume of 20 µL per lane in 12% polyacrylamide gels at equalized protein concentrations alongside a broad range protein standard (New England BioLabs; P7719S). 12% polyacrylamide gels were prepared as follows. A glass 1.5 mm spacer plate (Bio-Rad; 1653312) was assembled with a short plate (Bio-Rad; 1653308) using a gel caster apparatus (Bio-Rad; 1653303). Next, 7.5 mL of running gel was prepared per cast and allowed to fully polymerize underneath a thin layer of sec-butanol (Sigma Aldrich; 78-92-2). The following running gel constituent concentrations and percentages are final; double distilled water was used as the diluent: 12% acrylamide (prepared from stock 30% Acrylamide/Bis Solution 29:1; Bio-Rad; 1610156), 0.38 M Tris (prepared from a 1.5 M stock solution at pH 8.8; Sigma Aldrich; 77-86-1), 0.1% sodium dodecyl sulfate (Roche; 151-21-3), 0.1% ammonium persulfate (Sigma Aldrich; A3678), and 0.04% TEMED (N,N,N',N'-tetramethyl-ethylenediamine; Sigma Aldrich; 110-18-9). Upon running gel polymerization, sec-butanol was rinsed off using cold tap water, after which 3 mL of stacking gel was added to the cast along with a 1.5 mm 10 hole gel making comb (Bio-Rad; 1653359). The following stacking gel constituent concentrations and percentages are final; double distilled water was used as the diluent: 5% acrylamide (prepared from stock 30% Acrylamide/Bis Solution 29:1), 0.125 M Tris (prepared from a 1.0 M stock solution at pH 6.8), 0.1% sodium dodecyl sulfate, 0.1% ammonium persulfate, and 0.1% TEMED. Upon polymerization, 12% polyacrylamide gels were assembled in a Mini-PROTEAN 3 Cell (Bio-Rad; 165-3301) according to the manufacturer's instructions, and run at 100 volts (Power Pac 200, Bio-Rad; 25501) for 2 hours in approximately 500 mL of running buffer comprised of 25 mM Tris, 76 mM sodium dodecyl sulfate, and 959 mM glycine (Sigma Aldrich; 56-40-6). Gels were subjected to a wet transfer for 3 hours at 50 volts according to the manufacturer's

instructions (Hoefer; TE62) using PVDF transfer membrane (polyvinylidene difluoride; Thermo Scientific; 88518) in a transfer buffer solution comprised of 25 mM Tris, 192 mM glycine, and 20% methanol (v/v; VWR Chemicals; BDH1135). PVDF blots were then blocked in Tris-buffered saline with Tween 20 (TBST; Cell Signaling Technology; 9997) supplemented with 5% powdered, non-fat milk (w/v) for 2 hours at room temperature or overnight at 4˚C. Blots were then briefly washed with TBST, and incubated with primary antibody overnight by rotation at 4˚C. Primary antibodies were prepared in a TBST solution supplemented with 2% bovine serum albumin and 0.1% sodium azide. Following overnight incubation, the primary antibody solution was removed, and blots were washed with TBST in triplicate (5 minutes per wash). Secondary antibodies were prepared to a final dilution of 1/5000 in TBST supplemented with 5% powdered, non-fat milk (w/v), after which blots were incubated for 1 hour at room temperature. Following incubation with secondary antibodies, blots were washed with TBST in triplicate (5 minutes per wash). Chemiluminescent solution (ProSignal Pico; Prometheus; 20-300B) was applied to the blot for 1 minute after which autoradiography film (Thomas Scientific; 1141J52) was exposed at various intervals under red light and developed using a SRX-101A manufactured by Konica Minolta. The following rabbit primary antibodies were purchased from Cell Signaling Technology: C/EBP beta (Cat. # 3087), C/EBP delta (Cat. # 2318), C/EBP alpha (Cat. # 8178), PPAR-gamma (Cat. # 2435), FABP4 (Cat. # 2120), SOX9 (Cat. # 82630), and GTF2B (Cat. # 4149), CHOP (Cat. # 5554), Beta-Actin (Cat. # 4970), and SPARC (Cat. # 8725). Mouse monoclonal antibody (clone Vli19C07 and clone Vli10G07) raised against the N-terminus of human CTHRC1, as well as rabbit monoclonal antibody (clone Vli55) raised against the C-terminus of CTHRC1, were produced in-house: further product information is available on the MaineHealth Institute for Research website. The following HRP-conjugated secondary

antibodies were purchased from Cell Signaling Technology: horse anti-mouse (Cat. # 7076); goat anti-rabbit (Cat. # 7074). Densitometry was performed using ImageJ (National Institutes of Health) by normalizing the intensity of a given protein band relative to the intensity of its respective loading control (as indicated).

2.7 RT-qPCR

RNA was prepared from cell culture by first washing cells with PBS at 0.5 mL per well, and then scraping each well in 50 µL of TRIzol Reagent (Ambion; 15596018). Per experimental group, TRIzol cell lysate preparations were pooled from six TC24 wells into a 1.5 mL microcentrifuge tube and immediately flash frozen on dry ice and then stored at -70˚C. On the day of RNA isolation, 250 µL of each TRIzol cell lysate preparation was added to a fresh 1.5 mL microcentrifuge tube containing an additional volume of 750 µL of TRIzol, briefly vortexed, and allowed to sit for 5 minutes at room temperature. For studies involving the isolation of RNA from mouse inguinal white adipose tissue, frozen adipose tissue was pulverized in liquid nitrogen using a mortar and pestle, and then re-suspended in 1 mL of TRIzol and allowed to sit for 5 minutes at room temperature with intermittent vortexing. In all cases, 100 µL of stock 1-bromo-3-chloropropane (Sigma Aldrich; B9673) was then added to the 1 mL volume of TRIzol/lysed cells. Each tube was briefly vortexed and allowed to sit for 5 minutes at room temperature, followed by a 15 minute centrifugation at 12,000 x g at 4˚C. 350 µL of the upper aqueous layer was then transferred to a fresh 1.5 mL microcentrifuge tube containing 350 µL of 70% ethanol (Sigma Aldrich; E7023) and mixed thoroughly by briefly vortexing. This 700 µL volume was transferred to a Zymo-Spin IIICG Column included in the *Quick*-RNA Miniprep Kit (Zymo Research; R1055), and RNA was subsequently isolated following the kit manufacturer's

instructions. The RNA concentration per sample was measured using a NanoDrop 2000c spectrophotometer (Thermo Fisher Scientific; ND2000CLAPTOP), and 500 ng of cDNA was then generated in 0.2 mL PCR tubes (USA Scientific; 1402-4300) following the manufacturer's instructions (Reverse Transcription Supermix for RT-qPCR; Bio-Rad; 1708841) using a GeneAmp PCR System 9700 (AB Applied Biosystems; 4303481H). cDNA was loaded at 5.7 ng per well in a 96-well qPCR plate (USA Scientific; 1402-8900) in triplicate per sample. Respective forward and reverse cDNA primer pairs (see below) were loaded in each well at a final concentration of 839 nM. The 20 µL final reaction volume per well contained AzuraQuant Green (Azura Genomics; 2024-07) which was diluted following the manufacturer's instructions. qPCR reactions were thermally cycled according to the AzuraQuant Green manufacturer's instructions using a 96-well CFX Connect 96 (Bio-Rad; 1855201). 5'-to-3' forward (F) and reverse (R) primer sequences were used to detect the following target mouse genes:

Sox9 (F: CACACGTCAAGCGACCCATGAA ; R: TCTTCTCGCTCTCGTTCAGCAG),

Gtf2b (F: ATGGCGGACAGAATCAACCTCC ; R: ACAAGCAGAGGCTATCGCGTCA),

Cthrc1 (F: CCTGGACCCCAAACTATAAGCA ; R: AGCCACTGAACAGAACTCGC),

Cebpb (F: CAACCTGGAGACGCAGCACAAG ; R: GCTTGAACAAGTTCCGCAGGGT),

Cebpd (F: CGAGAACGAGAAGCTGCATCAG ; R: CCCAAAGAAACTAGCGATTCGG),

Cebpa (F: GCAAAGCCAAGAAGTCGGTGGA ; R: CCTTCTGTTGCGTCTCCACGTT),

Pparg (F: GTACTGTCGGTTTCAGAAGTGCC ; R: ATCTCCGCCAACAGCTTCTCCT),

Fabp4 (F: GCTGCAGCCTTTCTCACC ; R: CACTTTCCTTGTGGCAAAGC).

Actb (F: CATTGCTGACAGGATGCAGAAGG; R: TGCTGGAAGGTGGACAGTGAGG)

Fn1 (F: CCCTATCTCTGATACCGTTGTCC ; R: TGCCGCAACTACTGTGATTCGG)

Col1a1 (F: CCTCAGGGTATTGCTGGACAAC ; R: CAGAAGGACCTTGTTTGCCAGG)

Igf2 (F: CTTCAGTTTGTCTGTTCGGACCG; R: GTGGCACAGTATGTCTCCAGGA)

2.8 Co-culture

Passage 11 3T3-L1 cells were grown in 22 mL of full-serum DMEM to 100% confluence in 15 cm dishes and then transduced with adenoviral vectors overexpressing either human *CTHRC1* or control *β–galactosidase* as described above. In parallel, non-transduced 3T3-L1 cells at passage 11 were grown in 10 mL of full-serum DMEM in a 10 cm dish. Upon reaching approximately 70% confluence in the 10 cm dish, non-transduced cells were incubated for 30 min in a 2 μM solution of CellTracker Deep Red (Thermo Fisher Scientific; C34565) prepared in serum-free DMEM according to the manufacturer's instructions. Following incubation, CellTracker-labelled cells were treated with 0.25% Trypsin-EDTA. At the moment CellTracker-labelled cells were trypsinized, adenovirally transduced cells had been washed and incubated in full-serum DMEM by this point for 18 hours. As such, transduced cells in 15 cm dishes were trypsinized. In 15 mL conical tubes, two co-cultures were then prepared: 1) CellTracker-labelled 3T3-L1 cells plus adenovirally transduced 3T3-L1 cells overexpressing βgal; 2) CellTracker-labelled 3T3-L1 cells plus adenovirally transduced 3T3-L1 cells overexpressing human CTHRC1. In each 15 mL conical tube, CellTracker-labelled cells and transduced cells were added at equal ratios, mixed by inversion, and added to a 6-well plate at approximately 750,000 cells in a 2 mL volume of full-serum DMEM per well. Prior to cell seeding, sterilized thickness 1 glass coverslips (22 x 22 mm; Corning; 2845-22) were placed in each well of the 6-well plate. The βgal co-culture and CTHRC1 co-culture were each seeded on glass coverslips in triplicate. The day after cell seeding, old medium was removed and replenished with full-serum DMEM (2 mL per well). The

next day (Day 0), co-cultures were treated with insulin, IBMX, and dexamethasone (as described above) prepared in full-serum DMEM (2 mL per well). On Day 1, old medium was removed, and insulin, IBMX, and dexamethasone freshly prepared in full-serum DMEM were added. On Day 2, old medium was removed, and insulin freshly prepared in full-serum DMEM was added. On Day 3, old medium was removed, and full-serum DMEM was added. On Day 4, cells were protected from light and fixed using 10% neutral formalin for 1 hour at room temperature at a volume of 2 mL formalin per well. Next, cells were washed twice in PBS and blocked overnight at 4˚C in darkness using immunofluorescence blocking buffer (2 mL per well). Following blocking, Hoechst 33342 (4 µM, final), Bodipy 493/503 (5 µM, final; Invitrogen; D3922), and Alexa Fluor 546 Phalloidin (1/100 final dilution) were prepared in immunofluorescence blocking buffer and applied to each coverslip at 40 µL per well for 1 hour at room temperature in darkness, wherein each coverslip was fully covered with parafilm. The parafilm was then removed and cells were then washed twice in PBS, after which each coverslip was inverted and embedded in Vectashield Mounting Medium, and secured on a microscope slide with clear nail polish along the perimeter of the coverslip. Confocal microscopy of the preparations was performed using the Leica SP8 microscope (Leica Microsystems) at the Histopathology and Microscopy Core Facility at MaineHealth Institute for Research.

2.9 Assessment of the F-actin cytoskeleton

Passage 11 3T3-L1 cells were seeded on sterilized thickness 1 glass coverslips (22 x 22 mm) in a 6-well plate at approximately 250,000 cells in a 2 mL volume of full-serum DMEM per well. Cells reached confluence several days later and were then transduced in triplicate with adenoviral vectors overexpressing either human *CTHRC1* or control *β–galactosidase* as

described above. Two days after adenoviral transduction, cells were fixed for 1 hour at room temperature using 10% neutral formalin at a volume of 2 mL formalin per well. Next, cells were washed twice in PBS (2 mL per well) and blocked overnight at 4˚C in darkness using immunofluorescence blocking buffer (2 mL per well). Following blocking, Hoechst 33342 (4 μM, final) and Alexa Fluor 546 Phalloidin (1/100 final dilution) were prepared in immunofluorescence blocking buffer and applied to each coverslip at 40 μL per well for 1 hour at room temperature in darkness, wherein each coverslip was fully covered with parafilm. The parafilm was then removed and cells were washed twice in PBS (2 mL per well), after which each coverslip was inverted and embedded in Vectashield Mounting Medium and secured in the center of a microscope slide with clear nail polish along the perimeter of the coverslip. Confocal microscopy of the preparations was performed using the Leica SP8 microscope (Leica Microsystems) following the manufacturer's instructions at the Histopathology and Microscopy Core Facility at MaineHealth Institute for Research.

2.10 Mice

All protocols involving animals were approved by the Institutional Animal Care and Use Committee at MaineHealth Institute for Research (protocol number 2105) and were in compliance with all applicable regulations and guidelines, including the National Institutes of Health Guide for Care and Use of Laboratory Animals. *Cthrc1*-null mice with global, homozygous inactivation of the collagen triple helix repeat-containing 1 gene have been previously described (62). Wildtype and *Cthrc1*-null C57BL/6 mice were kindly provided by Dr. Volkhard Lindner.

2.11 Isolation of stromal vascular fraction cells

Inguinal white adipose tissue was surgically removed (both left and right lobes) per mouse, minced with a sterile razor blade in a 6 cm petri dish (VWR; 25384-060), and then transferred to a 15 mL conical tube and digested with collagenase D (1.5 units/ml; Roche; 59983422) and dispase II (2.4 units/ml; Sigma Aldrich; D4693) in 2.5 mL of DMEM/F12 (Corning; 10-092-CV) containing 0.8% bovine serum albumin at 37˚C with agitation for 45 minutes. Dissociated cells were passed through a 100 μm strainer (VWR North American; 76327-102) into a 50 mL conical tube and centrifuged at 450 x g for 3 minutes. The supernatant was then aspirated, and SVF cells were collected in 1 mL of a PBS solution supplemented with 0.5% bovine serum albumin and 2 mM EDTA (ethylenediaminetetraacetic acid; Sigma Aldrich; E9884), which we refer to as FACS buffer.

2.12 Multi-parameter flow cytometry

SVF cells were treated with 1 mL of ACK lysis buffer (ThermoFisher Scientific; A1049201) for 5 min at room temperature in a 15 mL conical tube, after which 10 mL of FACS buffer was added, and cells were centrifuged for 3 min at 450 x g. The supernatant was aspirated, and the cell pellet was re-suspended in 100 μL of DPBS (Corning; 21-031-CV) plus 100 μL of VioBlue viability stain (ThermoFisher Scientific; L3495) according to the manufacturer's instructions, and transferred to a FACS tube (Falcon; 352054). Cells were light protected and incubated for 25 min at room temperature. 1 mL of DPBS was added, and cells were centrifuged for 3 min at 450 x g. The supernatant was aspirated and cells were re-suspended in 100 μL of a Fc blocking solution for 10 min at 4˚C, which was initially prepared by adding 25 μL of stock TruStain FcX (BioLegend; 101320) to 225 μL FACS buffer. 250 μL of FACS buffer was then added, and cells

were distributed to three FACS tubes at a volume of 100 µL/tube. Next, 100 µL of FACS buffer was added to each tube supplemented with or without the following antibody panels – panel 1: no antibodies; panels 2-3: $CD24^{FITC}$ (BioLegend; 101816; clone M1/69), $PDGFR\text{-}alpha^{PeCy7}$ (BioLegend; 135912; clone APA5), $CD31^{PacificBlue}$ (BioLegend; 102422; clone 390), $CD45^{PacificBlue}$ (BioLegend; 103126; clone 30-F11), and $TER119^{PacificBlue}$ (BioLegend; 116232). Cells were incubated for 30 min at 4˚C, after which FACS buffer was added at 1.5 mL/tube, followed by centrifugation for 3 min at 450 x g and supernatant aspiration. Cells were incubated in fixation/permeabilization buffer (BD Biosciences; 554714) for 40 minutes at room temperature, followed by washing with permeabilization solution (BD Biosciences; 554714) at 1 mL/tube, centrifugation for 4 min at 450 x g, and supernatant aspiration. Next, 200 µL of permeabilization solution was added to each tube supplemented with or without the following antibody panels – panels 1/2: no antibodies; panel 3: $CTHRC1^{APC}$ (produced in-house, clone Vli08G09). Cells were incubated for 30 min at 4˚C, after which permeabilization solution was added at 2 mL/tube, followed by centrifugation for 4 min at 450 x g and supernatant aspiration. Cells were re-suspended in FACS buffer at 250 µL/tube. Panels were sequentially analyzed using the MACSQUANT Analyzer (Miltenyi Biotec) following the manufacturer's instructions at the Flow Cytometry Core Facility at MaineHealth Institute for Research.

2.13 RNA sequencing

Human PVAT tissue isolation, library preparation, sequencing, and analytical methodologies were conducted by Angueira and colleagues (63). Filtered feature barcode matrices were retrieved from the Gene Expression Omnibus. Previously published (64) deep neck BAT single-nucleus RNA-seq filtered feature barcode matrices were retrieved from the European

Bioinformatics Institute and reanalyzed. Single-cell RNA sequencing was conducted on human subcutaneous adipose tissue (18) and filtered feature barcode matrices were retrieved from the Gene Expression Omnibus.

Seurat objects were constructed for each tissue sample (n=18) using Seurat v4.1.1 (65). Data were filtered based on number of unique features, percent.mt, and doublets were removed using Scrublet v1.0. Filtered objects were integrated together using the library harmony v0.1.1. Data were log normalized with a scale.factor of 10000, using the Seurat function NormalizeData. For use in clustering, an assay was added in which the normalized data were scaled to fit a distribution with a variance of 1 and a mean of 0 using the ScaleData function. The variables percent.mt, nFeature_RNA, and the S and G2M cell cycle scores, determined through the CellCycleScoring, were regressed out to limit effects on clustering. A principal component analysis was performed using the Seurat function RunPCA over features which were identified as highly variable through use of the previously ran FindVariableFeatures function. Dimensionality reduction was accomplished using the FindNeighbors, FindClusters, and RunUMAP functions with the dims and resolution parameters set to 60 and 0.6, respectively. The DimPlot, FeaturePlot, and VlnPlot functions were utilized to visualize the clusters and marker genes. Manual cluster identification was executed using the FindAllMarkers function, while automatic cluster identification was supplementally performed using the ScType v1.0 package. Immune cells were removed based on PTPRC and MRC1 expression. To save plots, ggsave function from ggplot2 v3.3.6 was utilized (66).

2.14 Data availability

Human PVAT single-nucleus RNA sequencing filtered feature barcode matrices were retrieved from Gene Expression Omnibus data repository under accession GSE164528 (63). Human deep-neck BAT single-nucleus RNA sequencing filtered feature barcode matrices were retrieved from the European Bioinformatics Institute under accession E-MTAB-8564. (63). Filtered feature barcode matrices from single-cell RNA sequencing of human subcutaneous adipose tissue were retrieved from the Gene Expression Omnibus under accession GSE128890 (18).

2.15 Statistical analysis

Paired Student t-test was used to compare the mean values of two conditions. In addition, two-way analysis of variance (listed in *Table B.1*) was used to compare the "vehicle" group to the "N+Y" group presented in *Figure 14A*. All data in this report are presented as the mean ± SEM (standard error of the mean).

CHAPTER 3: CTHRC1 NEGATIVELY REGULATES ADIPOGENESIS *IN VITRO*

3.1 Paracrine CTHRC1 suppresses lipid accumulation in differentiating adipocytes

We have reported that adenoviral overexpression of human CTHRC1 significantly inhibits chemically-induced 3T3-L1 mouse cell adipogenic differentiation (55). Herein, we assessed whether CTHRC1 might possess paracrine function by conducting an adipogenic differentiation co-culture experiment. Briefly, 3T3-L1 cells were transduced with adenoviral vectors overexpressing either human *CTHRC1* or control *β–galactosidase* (*βgal*). In parallel, non-transduced 3T3-L1 cells were fluorescently labelled with CellTracker. Two co-cultures were then seeded: 1) non-transduced 3T3-L1 cells plus transduced 3T3-L1 cells overexpressing βgal; 2) non-transduced 3T3-L1 cells plus transduced 3T3-L1 cells overexpressing human CTHRC1 (hCTHRC1). Relative to the βgal co-culture, the percentage of non-transduced cells positively stained with the neutral lipid dye, BODIPY, was significantly lower in the CTHRC1 co-culture after four days of chemically-induced adipogenic differentiation (*Figure 5A-C*). These data support that secreted CTHRC1 suppresses lipid accumulation in differentiating adipocytes.

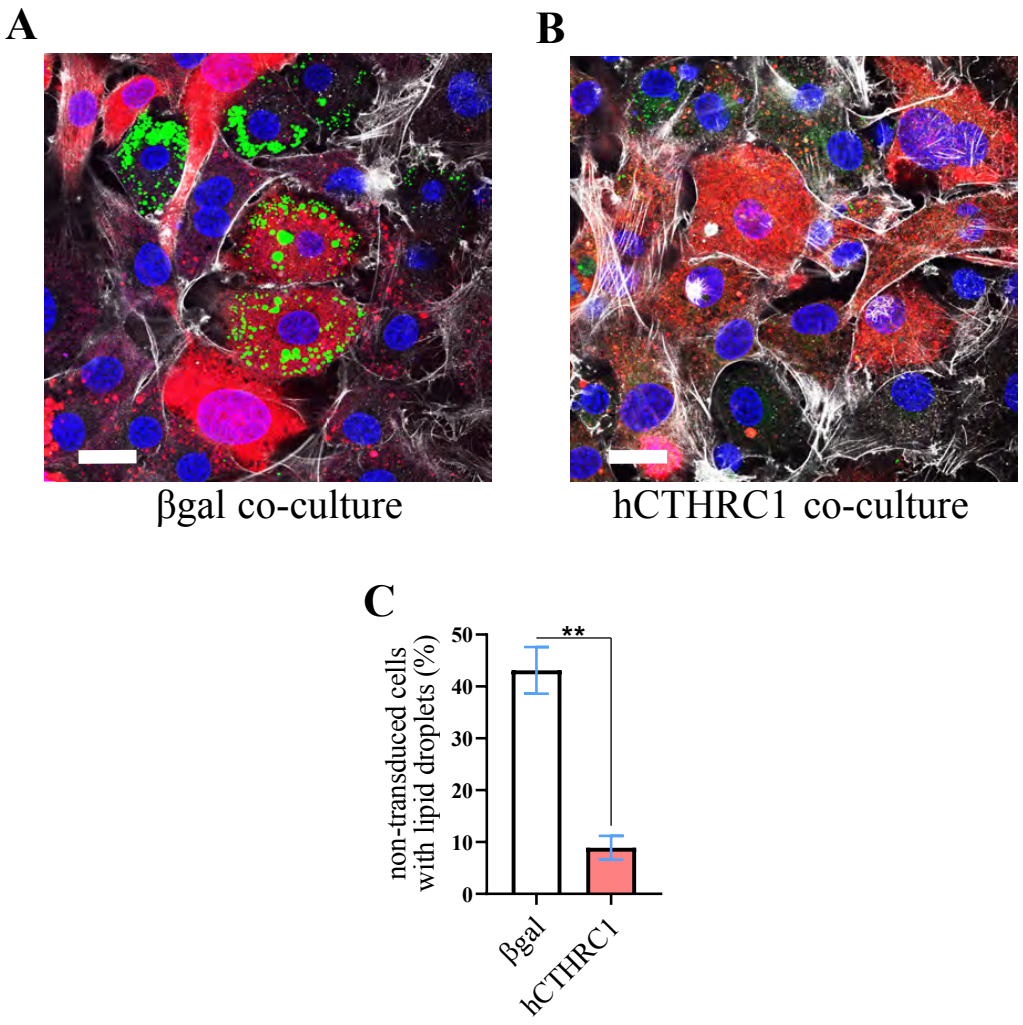

Figure 5. **CTHRC1 suppresses lipid accumulation *in vitro* in a paracrine-dependent manner**. **A**,**B**) Representative confocal microscopy images of non-transduced 3T3-L1 cells labelled with CellTracker Deep Red (red) that were co-cultured with unlabeled 3T3-L1 cells adenovirally transduced with control *β–galactosidase* (**A**) or human C*THRC1* (**B**). Each co-culture group was subjected to chemically-induced adipogenic differentiation for four days, and then stained with the neutral lipid dye, Bodipy (green). Nuclei were stained with Hoechst (blue), and the F-actin cytoskeleton was stained with Alexa Fluor 546 Phalloidin (white). The width of the white rectangle (lower left-hand corner) denotes the scale: 10 μm. **C**) Quantification of

CellTracker-labelled cells stained with Bodipy per co-culture. 10 separate fields were analyzed per co-culture per experiment (n=3; ** p≤0.01).

3.2 Exogenously applied CTHRC1 suppresses lipid accumulation in differentiating adipocytes

We next investigated the regulation of lipid accumulation relative to the application of exogenous hCTHRC1. For these studies, we exploited the feature that CTHRC1 is a secreted factor, and thus prepared conditioned media from 3T3-L1 cells transduced with adenoviral vectors expressing either human *CTHRC1* or control *βgal*, which we refer to as hCTHRC1 or βgal conditioned medium, respectively. Despite divergence in the amino acid composition of the N-terminal signal peptide and the adjacent pro-peptide regions, mouse and human CTHRC1 otherwise share nearly identical sequence homology, differing in a single amino acid within the C-terminal domain. In 3T3-L1 cells, endogenous mouse CTHRC1 was not detected at the mRNA or protein levels (data not shown). The presence of recombinant human CTHRC1 in conditioned medium was confirmed by an established ELISA or by Western blot analysis (*Figure 6A*). For these adipogenesis experiments, 3T3-L1 cells were seeded on Day -3 in the presence of either βgal or hCTHRC1 conditioned medium, and the chemical induction of adipogenic differentiation commenced on Day 0. Cells were chemically stimulated for a total period of six days in the continued presence of βgal or hCTHRC1 conditioned medium, and then stained with the neutral lipid dye, Oil Red O (*Figure 6B*,*C*). Based on absorbance spectroscopy measuring the relative concentration of eluted Oil Red O, we observed that 3T3-L1 cells treated with hCTHRC1 conditioned medium had significantly lower lipid content in comparison to cells

treated with βgal conditioned medium control (*Figure 6B*,*C*). These data support that hCTHRC1 conditioned medium suppresses lipid accumulation in differentiating adipocytes.

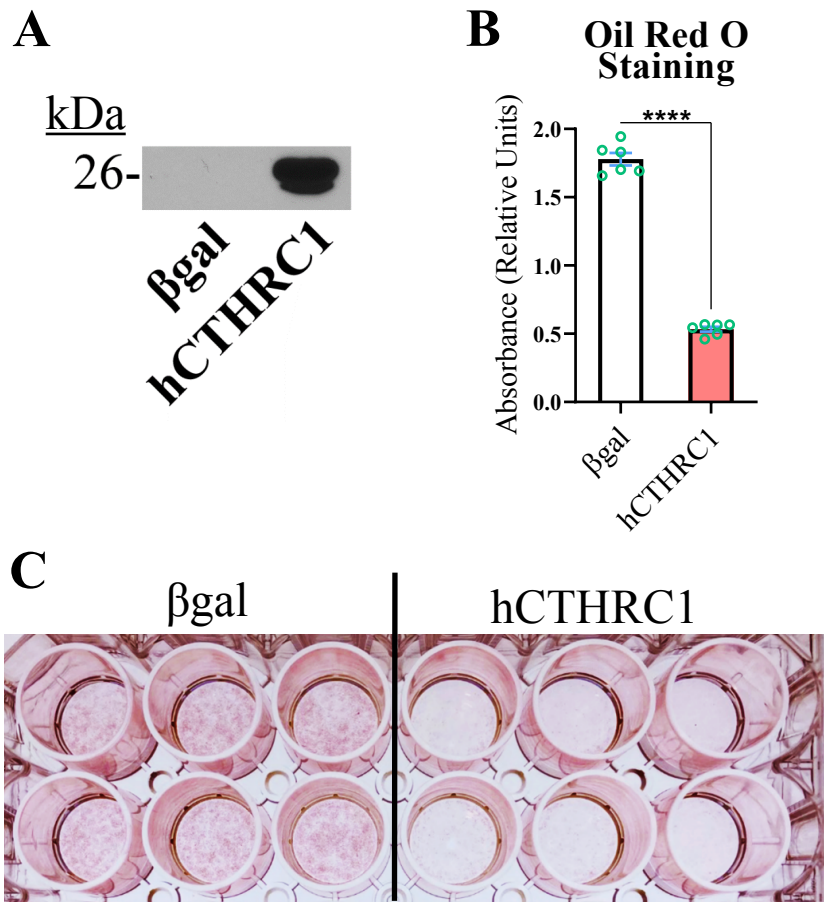

Figure 6. **Exogenously applied CTHRC1 suppresses lipid accumulation *in vitro*.**

A) Western blot analysis of hCTHRC1 protein expressed in hCTHRC1 conditioned medium but not βgal conditioned medium. **B**,**C**) Representative Oil Red O quantification data. 3T3-L1 cells were seeded on Day -3 with βgal or hCTHRC1 conditioned medium at a 1/4 dilution, and then chemically stimulated to undergo adipogenic differentiation for a total period of 6 days. Cells were formalin fixed on Day 6 and stained with Oil Red O, which was then eluted and its

concentration determined by absorbance spectroscopy (**B**) (n=3; **** p≤0.0001). Per experiment, 3T3-L1 cells were plated in one 24-well plate in which 6 wells were treated with either βgal or hCTHRC1 conditioned medium. **C**) Representative image of Oil Red O staining: left) cells treated with βgal conditioned medium; right) cells treated with hCTHRC1 conditioned medium.

3.3 CTHRC1 negatively regulates adipogenic gene expression

Given that the exogenous application of hCTHRC1 conditioned medium decreased lipid accumulation in 3T3-L1 cells following induction of adipogenic differentiation (*Figure 6B*), we next assessed the effect of hCTHRC1 conditioned medium on adipogenic gene expression. As before, 3T3-L1 cells were seeded on Day -3 in the presence of either βgal or hCTHRC1 conditioned medium, and then chemically stimulated to undergo adipogenesis beginning on Day 0. Whole-cell lysates were collected on Days 0, 2, and 6 for qPCR analyses. Samples collected on Day 0 were undifferentiated controls. Consistent with literature detailing the temporal expression patterns of both adipogenic and lipogenic genes during the course of adipogenic differentiation (Guo et al., 2015), elevated *Cebpb* and *Cebpd* gene expression on Day 2 preceded significant induction of *Cebpa, Pparg*, and *Fabp4* gene expression on Day 6 (*Figure 7A-E*). Of note, cells treated with hCTHRC1 conditioned medium displayed significantly decreased C*ebpd* gene expression on Day 0 (*Figure 7B*), as well as marked decrease of C*ebpa*, P*parg*, and F*abp4* gene expression on Day 6 (*Figure 7C-E*). Taken together, the ability of hCTHRC1 conditioned medium to suppress lipid accumulation is commensurate to its inhibition of adipogenic gene expression, thus supporting the hypothesis that CTHRC1 is a negative regulator of preadipocyte-to-adipocyte differentiation.

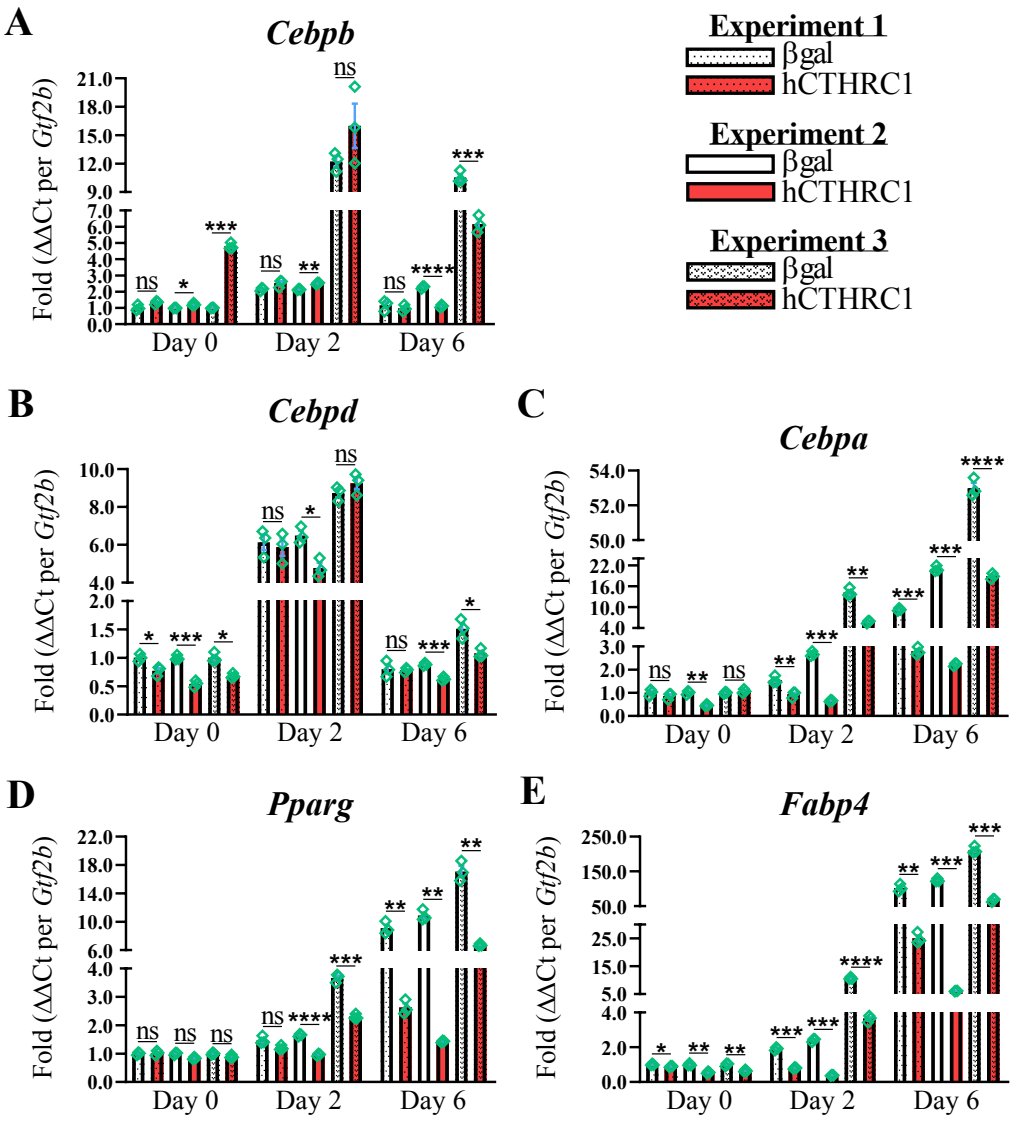

Figure 7. **Exogenously applied hCTHRC1 conditioned medium inhibits adipogenic gene expression *in vitro***. **A-E**) hCTHRC1 conditioned medium applied to 3T3-L1 cells before and during the course of chemically-stimulated adipogenic differentiation negatively regulates the mRNA expression of adipogenic and lipogenic factors as demonstrated by qPCR analyses. 3T3-L1 cells were seeded on Day -3 with either βgal or hCTHRC1 conditioned medium at a 1/4 dilution, after which whole-cell lysates were collected on Day 0, 2, or 6 relative to the chemical induction of adipogenic differentiation. **A-E**) qPCR fold expression differences in specific

mRNA transcript levels relative to housekeeping *Gtf2b* expression levels from three independent experiments (n=3; * p≤0.05, ** p≤0.01, *** p≤0.001, **** p≤0.0001).

3.4 CTHRC1 negatively regulates adipogenic transcription factor protein expression

Given data supporting that CTHRC1 negatively regulates adipogenic gene expression, we next assessed the effect of hCTHRC1 conditioned medium on the protein expression levels of adipogenic transcription factors. As before, 3T3-L1 cells were seeded on Day -3 in the presence of either βgal or hCTHRC1 conditioned medium, and then chemically stimulated to undergo adipogenesis beginning on Day 0. Whole-cell lysates were collected on Days 0, 2, and 6 for Western blot analyses. Samples collected on Day 0 were undifferentiated controls. Consistent with literature detailing the temporal expression patterns of both adipogenic and lipogenic genes during the course of adipogenic differentiation (35), these temporal adipogenic gene expression trends were recapitulated at the protein level (*Figure 8A-F*), in which C/EBP beta and C/EBP delta protein expression were highest on Day 2, while C/EBP alpha, PPAR-gamma, and FABP4 each displayed maximal protein expression levels on Day 6. C/EBP alpha, PPAR-gamma, and FABP4 protein expression levels, in particular, were also significantly reduced on Day 6 in cells treated with hCTHRC1 conditioned medium (*Figure 8D-F*). Taken together, the ability of hCTHRC1 conditioned medium to suppress lipid accumulation is commensurate to its inhibition of adipogenic transcription factor protein expression, thus supporting the hypothesis that CTHRC1 is a negative regulator of preadipocyte-to-adipocyte differentiation.

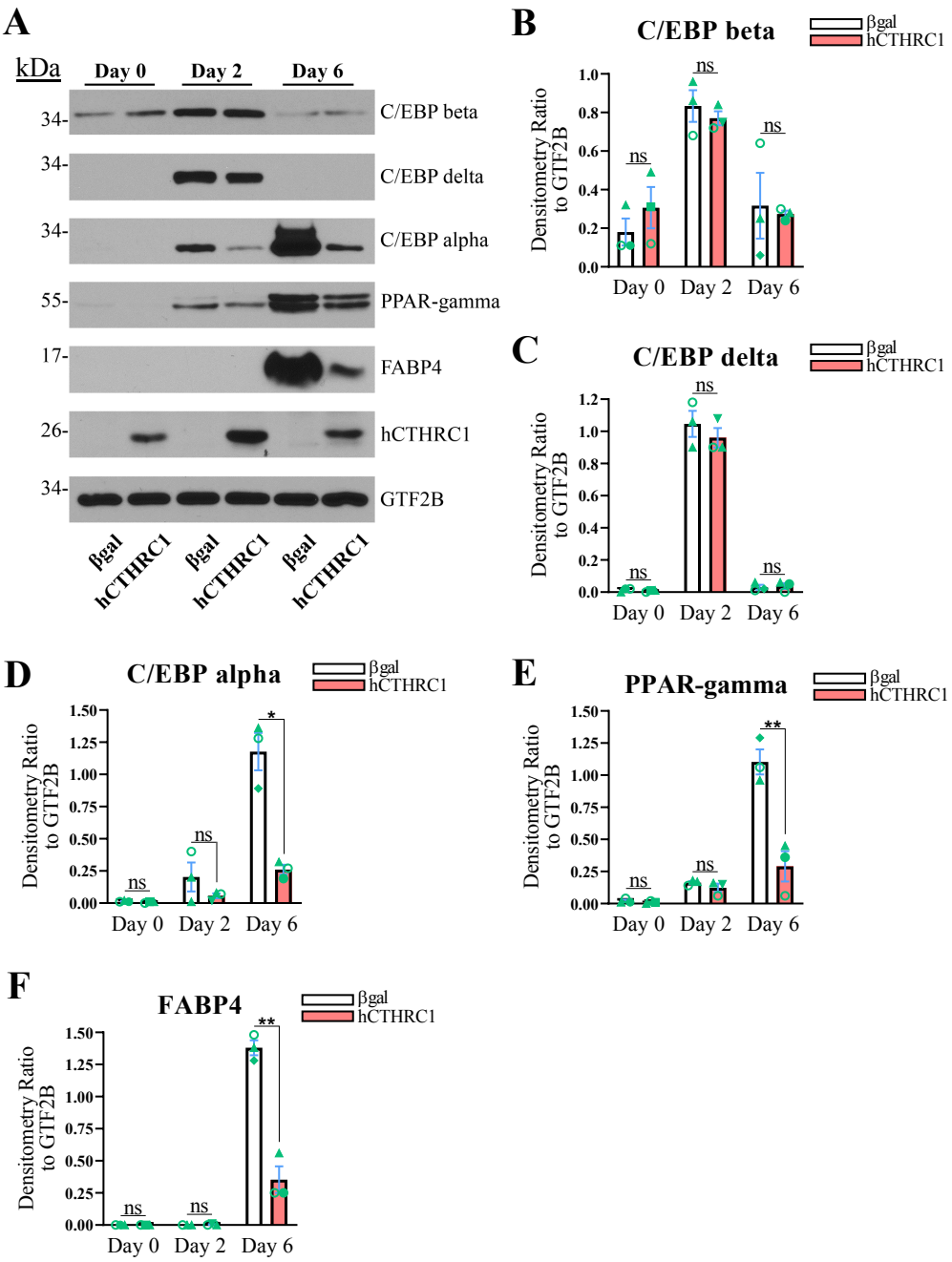

Figure 8. **Exogenously applied hCTHRC1 conditioned medium inhibits adipogenic transcription factor protein expression *in vitro*. A-F**) hCTHRC1 conditioned medium applied to 3T3-L1 cells before and during the course of chemically-stimulated adipogenic differentiation negatively regulates the protein expression of adipogenic and lipogenic factors as demonstrated

by Western blot analyses. 3T3-L1 cells were seeded on Day -3 with either βgal or hCTHRC1 conditioned medium at a 1/4 dilution, after which whole-cell lysates were collected on Day 0, 2, or 6 relative to the chemical induction of adipogenic differentiation. **A**) Representative Western blots. **B**-**F**) Average protein fold change densitometry values relative to housekeeping GTF2B protein expression levels from three independent experiments (n=3; * $p \leq 0.05$, ** $p \leq 0.01$).

3.5 CTHRC1 enhances both the gene and protein expression of SOX9

Given evidence in support of the anti-adipogenic function of CTHRC1 (*Figures 4-7*), we next focused on potential CTHRC1 effector proteins with demonstrated anti-adipogenic activity. It was recently shown that a subpopulation of activated fibroblasts in heart tissues co-express high levels of CTHRC1 and SOX9 following myocardial infarction (67). SOX9 is a well-established transcription factor with marked anti-adipogenic function (2). When we assessed if CTHRC1 regulates *Sox9* gene expression in 3T3-L1 cells, we found that cells treated with hCTHRC1 conditioned medium expressed increased SOX9 at both the mRNA (*Figure 9A*) and protein (*Figure 9B*,C) levels in comparison to cells treated with βgal conditioned medium. These data support that hCTHRC1 conditioned medium positively regulates SOX9 mRNA and protein expression levels in preadipocytes.

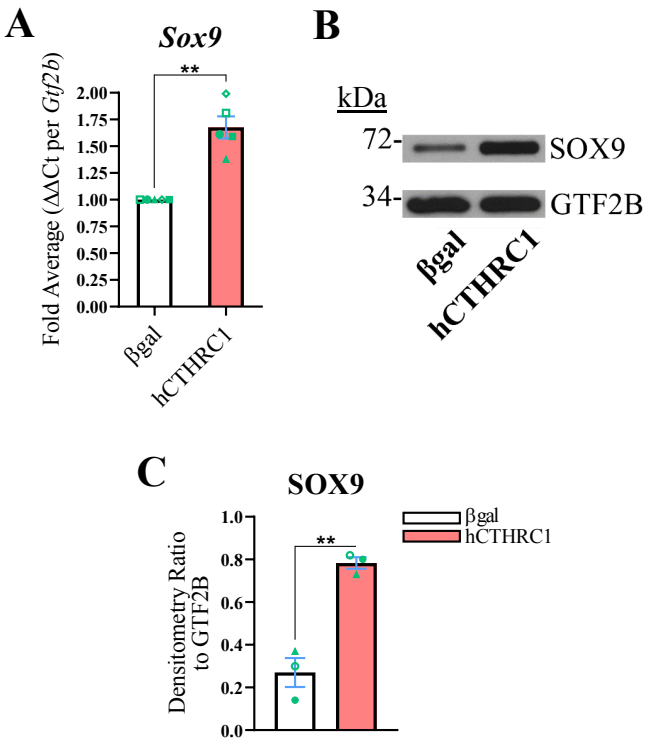

Figure 9. **Exogenously applied hCTHRC1 conditioned medium enhances *Sox9* gene expression *in vitro***. **A-C**) 3T3-L1 cells were seeded on Day -3 with either βgal or hCTHRC1 conditioned medium at a 1/4 dilution. Whole-cell lysates were collected on Day 0 in order to determine SOX9 expression by qPCR (**A**) and Western blot (**B**) analyses. **A**) Average fold expression differences in *Sox9* mRNA levels relative to housekeeping *Gtf2b* gene expression levels from five independent experiments (n=5; ** p≤0.01). **C**) Average SOX9 protein fold change densitometry values relative to housekeeping GTF2B protein expression levels from three independent experiments (n=3; ** p≤0.01).

3.6 CTHRC1 enhances SOX9 nuclear translocation

SOX9 is a transcriptional regulator known to translocate to the nucleus and thus suppress the activity of adipogenic gene promoters (42). Given data supporting that CTHRC1 enhances *Sox9*

gene expression in 3T3-L1 preadipocytes (*Figure 9*), we next assessed the effect of CTHRC1 on SOX9 nuclear translocation. As before, 3T3-L1 cells were seeded on Day -3 with either βgal or hCTHRC1 conditioned medium at a 1/4 dilution, and then subjected to four days of chemically-stimulated adipogenic differentiation. Confocal microscopy analysis of SOX9 nuclear translocation in 3T3-L1 cells revealed that application of hCTHRC1 conditioned medium significantly enhanced SOX9 nuclear localization on Day 0 in comparison to cells treated with βgal conditioned medium (*Figure 10A*,*B*). Moreover, enhanced SOX9 nuclear translocation was also observed on Day 4 of chemically-stimulated adipogenic differentiation in 3T3-L1 cells treated with hCTHRC1 conditioned medium but not in cells treated with βgal conditioned medium (*Figure 10C*,*D*). These data support that hCTHRC1 conditioned medium enhances the basal levels of SOX9 nuclear translocation in preadipocytes, and also functions to preserve the expression levels of SOX9 in the nucleus when preadipocytes are chemically stimulated to undergo adipogenic differentiation *in vitro*.

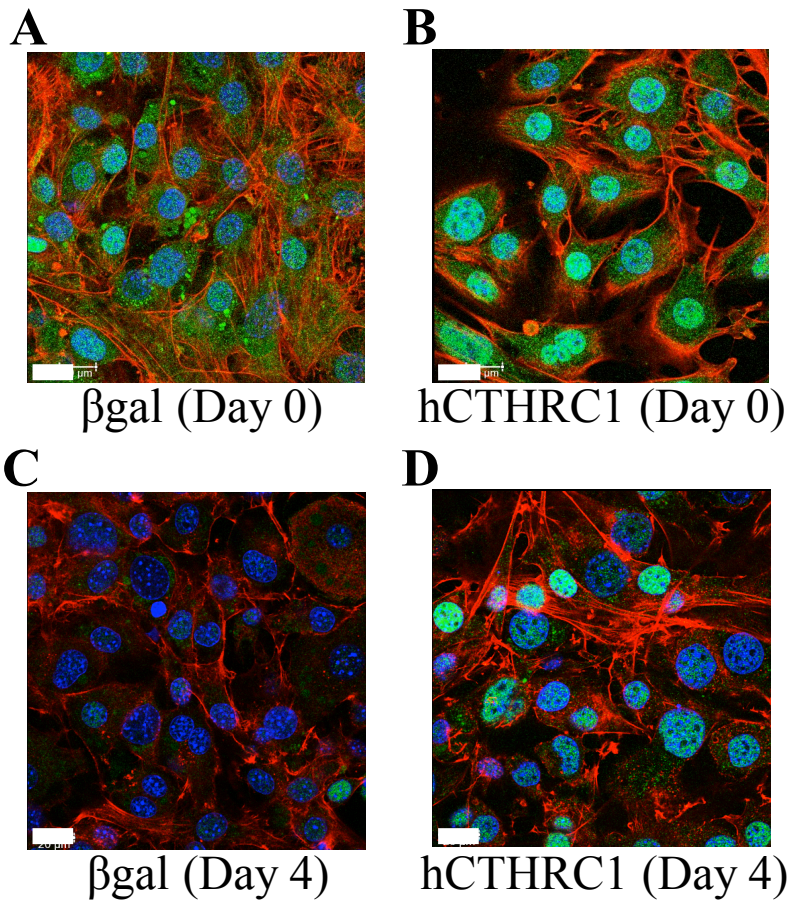

Figure 10. **Exogenously applied hCTHRC1 conditioned medium enhances SOX9 nuclear translocation *in vitro***. 3T3-L1 cells were seeded on Day -3 with either βgal or hCTHRC1 conditioned medium at a 1/4 dilution, after which cells were formalin fixed on either Day 0 or Day 4 relative to the chemical induction of adipogenic differentiation. **A**,**B**) Representative confocal microscopy images of SOX9 protein localization on Day 0 in 3T3-L1 cells treated with either βgal conditioned medium (**A**) or hCTHRC1 conditioned medium (**B**). **C**,**D**) Representative confocal microscopy images of SOX9 protein localization on Day 4 of adipogenic differentiation in 3T3-L1 cells treated with either βgal conditioned medium (**C**) or hCTHRC1 conditioned

medium (**D**). Nuclei (blue); SOX9 (green); F-actin/Alexa Fluor 546 Phalloidin (red). The length of the white rectangle (lower left-hand corner) denotes the scale: 20 μm.

3.7 Assessing the anti-adipogenic activity of hCTHRC1 conditioned medium at various dilutions

Based on Oil Red O analyses, we next sought to determine an effective dilution range in which application of hCTHRC1 conditioned medium significantly decreases the degree of lipid accumulation in differentiating 3T3-L1 preadipocytes. Thus, 3T3-L1 cells were seeded on Day -3 with either βgal or hCTHRC1 conditioned medium at the following dilutions followed by six days of chemically stimulated adipogenic differentiation: 1/4, 1/8, 1/12, 1/16, 1/20, 1/24, or 1/32. Notably, each dilution of hCTHRC1 conditioned medium significantly suppressed overall lipid accumulation in comparison to respective βgal conditioned medium controls (*Figure 11*). From ELISA, we determined that the concentration of recombinant human CTHRC1 in undiluted conditioned medium is approximately 9-10 ng/mL, which corresponds as follows to each dilution of hCTHRC1 conditioned medium: 1/4 dilution (2.5 ng/mL), 1/8 dilution (1.25 ng/mL), 1/12 dilution (800 pg/mL), 1/16 dilution (600 pg/mL), 1/20 dilution (480 pg/mL), 1/24 dilution (400 pg/mL), 1/32 dilution (300 pg/mL). Congruent with Stohn and colleagues who extrapolated that the physiological range of CTHRC1 in circulation in mice is expressed on the order of pg/mL concentrations (62), these data provide evidence in support of the hypothesis that secreted hCTHRC1 still possesses anti-adipogenic activity when exogenously applied at concentrations below 2.5 ng/mL to preadipocytes.

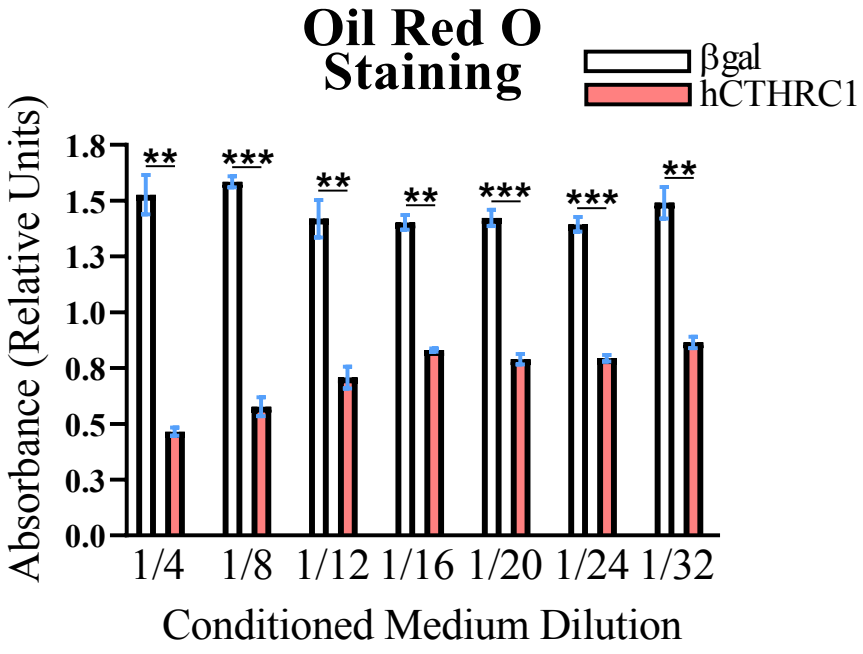

Figure 11. **Assessment of the anti-adipogenic effect of hCTHRC1 conditioned medium at various dilutions *in vitro***. Representative Oil Red O quantification data. 3T3-L1 cells were seeded on Day -3 with βgal or hCTHRC1 conditioned medium at the following dilutions: 1/4, 1/8, 1/12, 1/16, 1/20, 1/24, or 1/32. Cells were seeded in a 24-well plate corresponding to three wells per each conditioned medium dilution, and then chemically stimulated to undergo adipogenic differentiation beginning on Day 0. Cells were formalin fixed on Day 6 and stained with Oil Red O, which was then eluted and its concentration determined by absorbance spectroscopy (** $p \leq 0.01$, *** $p \leq 0.001$).

3.8 SOX9 protein expression is critical for the anti-adipogenic activity of CTHRC1

Based on data supporting that CTHRC1 increases *Sox9* gene expression as well as SOX9 protein nuclear translocation in preadipocytes (*Figures 8*,*9*), we next queried if SOX9 protein expression

is required for the anti-adipogenic activity of CTHRC1. As such, we implemented a RNA interference (RNAi) strategy to knockdown *Sox9* gene expression in 3T3-L1 cells. Briefly, 3T3-L1 cells were transduced with lentiviral vectors overexpressing either a shRNA construct against mouse *Sox9* mRNA (*i.e.*, shSOX9), or a non-targeting, scrambled control shRNA construct (*i.e.*, shSCR). Puromycin was then used to select transduced shSOX9 and shSCR cells. It is well documented that when primary adipocyte progenitor cells or transformed cell lines, including 3T3-L1 cells, are extensively passaged or become confluent during passaging, the cells lose their ability to efficiently differentiate into adipocytes *in vitro* (68, 69). Accordingly, we did not implement single-cell cloning strategies following lentiviral transduction, and instead propagated all puromycin-selected shSCR and shSOX9 cells in a sub-confluent manner prior to study. On this basis, we posited that the degree of *Sox9* gene knockdown was variable among shSOX9 cells. Given that hCTHRC1 conditioned medium significantly enhanced *Sox9* mRNA expression (*Figure 9A*), we further rationalized that higher concentrations of hCTHRC1 conditioned medium could "outcompete" the constitutively expressed shRNA construct targeting *Sox9* mRNA, particularly in shSOX9 cells with less efficient lentiviral transduction, and thus negate overall *Sox9* gene knockdown. On this basis, and also in consideration of data supporting that hCTHRC1 conditioned medium possesses marked anti-adipogenic activity even when exogenously applied to 3T3-L1 cells at a 1/32 dilution (*i.e.*, at an approximate 300 pg/mL concentration of secreted recombinant hCTHRC1), we opted to assay βgal and hCTHRC1 conditioned media at a dilution of 1/60 (*i.e.*, at an approximate 150 pg/mL concentration of secreted recombinant hCTHRC1) for the RNAi adipogenic differentiation studies. Based on Oil Red O absorbance spectroscopy data, and relative to βgal conditioned medium control, application of hCTHRC1 conditioned medium significantly decreased 3T3-L1 adipogenic

differentiation in shSCR cells but not shSOX9 cells (*Figure 12A*). Furthermore, based on the quantification of SOX9 protein expression levels, in comparison to the application of βgal conditioned medium, hCTHRC1 conditioned medium significantly enhanced SOX9 levels in shSCR cells but not in shSOX9 cells, the latter displaying significant knockdown of SOX9 protein expression levels (*Figure 12B*,*C*). Thus, these data provide evidence in support of the hypothesis that SOX9 protein expression is critical for the anti-adipogenic activity of hCTHRC1 conditioned medium.

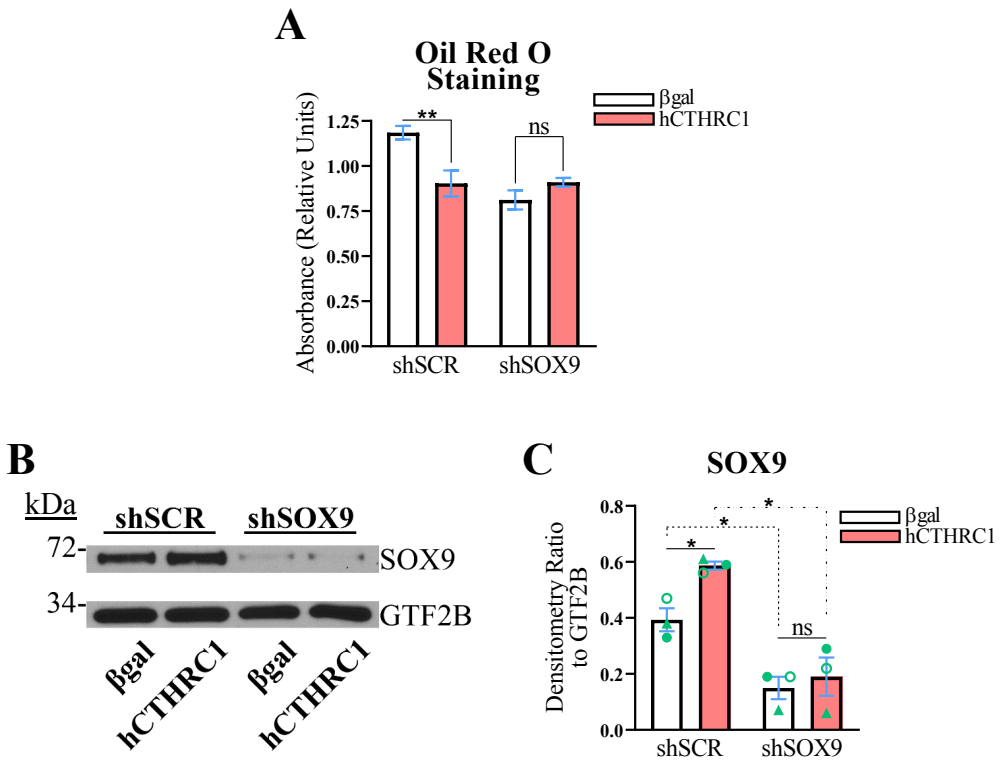

Figure 12. **SOX9 expression is indispensable to anti-adipogenic CTHRC1 signaling *in vitro*.** **A-C**) 3T3-L1 cells were lentivirally transduced with either a shRNA construct targeting *Sox9* mRNA (*i.e.*, shSOX9), or a non-targeting scrambled control shRNA construct (*i.e.*, shSCR). The resultant shSOX9 and shSCR cells were seeded on Day -3 with βgal or hCTHRC1 conditioned

medium at a dilution of 1/60. Whole-cell lysates were collected from cohorts of shSOX9 and shSCR cells on Day 0 to assess SOX9 protein expression levels by Western blot analysis (**B**,**C**), while the other cohorts were chemically stimulated to undergo adipogenic differentiation for a total period of 6 days (**A**). **A**) Representative Oil Red O quantification data. shSOX9 and shSCR cells were formalin fixed on Day 6 and stained with Oil Red O, which was then eluted and its concentration determined by absorbance spectroscopy. Per experiment, shSOX9 and shSCR cells were plated in 24-well plates in which 6 wells each were treated with βgal or hCTHRC1 conditioned medium at a dilution of 1/60 (n=3; ** $p \leq 0.01$). **C**) Average SOX9 protein fold change densitometry values relative to housekeeping GTF2B protein expression levels from three independent experiments (n=3; * $p \leq 0.05$).

3.9 Higher-concentrated hCTHRC1 conditioned medium negates RNAi-mediated *Sox9* gene knockdown

Based on results of the RNAi adipogenic differentiation studies when assaying conditioned media at a 1/60 dilution, which thus support that SOX9 expression is indispensable to the anti-adipogenic activity of CTHRC1, we also assessed the adipogenic effect of conditioned media when applied to shSOX9 and shSCR cells at a higher-concentrated 1/12 dilution. While the application of hCTHRC1 conditioned medium at the 1/60 dilution significantly decreased 3T3-L1 adipogenic differentiation in shSCR cells but not shSOX9 cells, the application of hCTHRC1 conditioned medium at the 1/12 dilution exerted a significant anti-adipogenic effect when applied to both shSCR cells and shSOX9 cells (*Figure 13A*,*B*). Importantly, when assessing the concentration-dependent effect of hCTHRC1 conditioned medium on SOX9 expression, SOX9 protein expression levels did not statistically differ in shSCR cells versus shSOX9 cells when

hCTHRC1 conditioned medium was applied at the 1/12 dilution (*Figure 13C*). In contrast, application of hCTHRC1 conditioned medium at the 1/60 dilution revealed that shSOX9 cells expressed significantly decreased SOX9 protein expression levels in comparison to shSCR cells (*Figure 13C*). Given that we did not implement single-cell cloning strategies following lentiviral transduction, these SOX9 protein expression data can plausibly be attributed to the heterogeneous degree of *Sox9* gene knockdown among the population of shSOX9 cells, such that higher-concentrated hCTHRC1 conditioned medium can negate overall *Sox9* gene knockdown in shSOX9 cells. Critically, when hCTHRC1 conditioned medium was applied at the 1/60 dilution to shSOX9 cells, its application was not able to significantly enhance SOX9 protein expression or suppress adipogenic differentiation relative to the application of βgal conditioned medium control (*Figure 12A-C*). Based on our RNAi experimental strategy, these SOX9 protein expression data further suggest that hCTHRC1 conditioned medium is unable to impede overall *Sox9* gene knockdown in shSOX9 cells when the concentration of recombinant human CTHRC1 therein is below 800 pg/mL at an approximate range of 150 pg/mL.

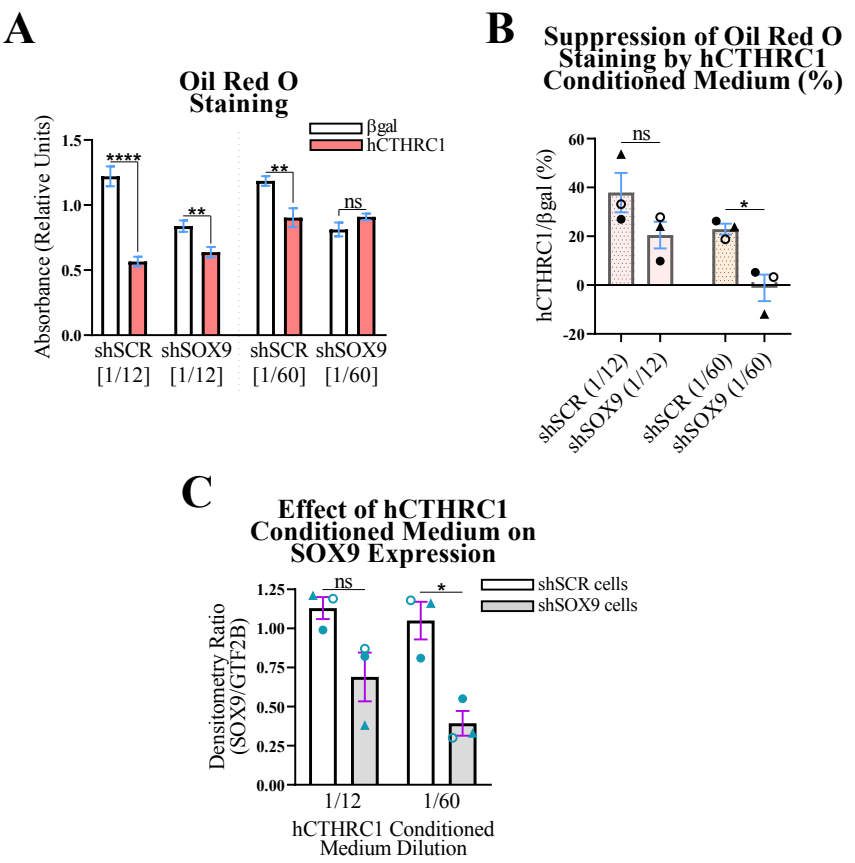

Figure 13. **Higher-concentrated hCTHRC1 conditioned medium negates *Sox9* gene knockdown in 3T3-L1 cells**. **A-C**) 3T3-L1 cells were lentivirally transduced with either a shRNA construct targeting *Sox9* mRNA (*i.e.*, shSOX9), or a non-targeting scrambled control shRNA construct (*i.e.*, shSCR). The resultant shSOX9 and shSCR cells were seeded on Day -3 with βgal or hCTHRC1 conditioned medium at dilutions of either 1/12 or 1/60. Whole-cell lysates were collected from cohorts of shSOX9 and shSCR cells on Day 0 to assess SOX9 protein expression levels by Western blot analysis (**C**), while the other cohorts were chemically stimulated to undergo adipogenic differentiation for a total period of 6 days (**A**,**B**). **A**) Representative Oil Red O quantification data. shSOX9 and shSCR cells were formalin fixed on Day 6 and stained with Oil Red O, which was then eluted and its concentration determined by

absorbance spectroscopy. Per experiment, shSOX9 and shSCR cells were plated in 24-well plates in which 6 wells each were treated with βgal or hCTHRC1 conditioned medium at dilutions of either 1/12 or 1/60 (n=3; ** p≤0.01, **** p≤0.0001). **B**) Graphical representation quantifying that hCTHRC1 conditioned medium loses its anti-adipogenic effect when applied to shSOX9 cells at a 1/60 dilution (displayed as average percent reduction in Oil Red O staining relative to the application of hCTHRC1 conditioned medium). In contrast, the anti-adipogenic effect of hCTHRC1 conditioned medium at a 1/12 dilution is not statistically different when applied to either shSOX9 or shSCR cells. Data reflect the averages from three independent experiments (n=3; * p≤0.05). **C**) SOX9 protein fold change densitometry values relative to housekeeping GTF2B protein expression levels quantifying the concentration-related effect of hCTHRC1 conditioned medium on SOX9 levels in both shSOX9 and shSCR cells (n=3; * p≤0.05)

3.10 CTHRC1-induced SOX9 nuclear translocation is positively regulated in a Rho/Rac1-dependent manner

Given data in support of the hypothesis that the anti-adipogenic activity of CTHRC1 is regulated by SOX9 (*Figures 11*,*12*), and in further consideration that the anti-adipogenic function of SOX9 is predicated on its nuclear translocation and direct inhibition of adipogenic gene promoters (2), we next investigated specific facets of CTHRC1 signaling that might regulate SOX9 nuclear translocation. Hironaka and colleagues recently reported that the actin binding protein, drebrin, stabilizes the F-actin cytoskeleton in myofibroblasts which, in turn, enhances the nuclear translocation of SOX9 (70). Moreover, disruption of actin stress fibers in adipocyte progenitor cells has been shown to enhance their adipogenic differentiation (71), and we have observed that

CTHRC1 overexpression enhances the F-actin cytoskeleton in 3T3-L1 cells (*Figure A.1*). Because Rho-like GTPases are also well characterized regulators of the actin cytoskeleton, and other investigations have demonstrated that CTHRC1 overexpression significantly increases the levels of both Rho-GTP and Rac1-GTP (50, 72), we hypothesized that Rho and Rac1 signaling positively regulate CTHRC1-mediated SOX9 nuclear translocation. To address this hypothesis, 3T3-L1 cells were seeded in the presence of βgal or hCTHRC1 conditioned medium at a 1/60 dilution, with or without the combined treatment of NSC 23766 ("N") and Y-27632 ("Y"). NSC 23766 is a well-defined Rac1 activation-specific inhibitor (73), while Y-27632 is a potent inhibitor of the direct Rho effector, Rho-associated kinase (ROCK) (74). Significantly, the combined application of N (10 μM, final) and Y (15 μM, final) attenuated SOX9 nuclear translocation caused by treatment with hCTHRC1 conditioned medium (*Figure 14A-D*). Quantification of SOX9-positive nuclei further revealed that the combined application of N and Y reduced SOX9 nuclear translocation to the same basal levels in 3T3-L1 cells despite treatment with either βgal or hCTHRC1 conditioned medium (*Figure 14E*). Therefore, these data support that Rho and Rac1 signaling positively regulate SOX9 nuclear translocation induced by hCTHRC1 conditioned medium.

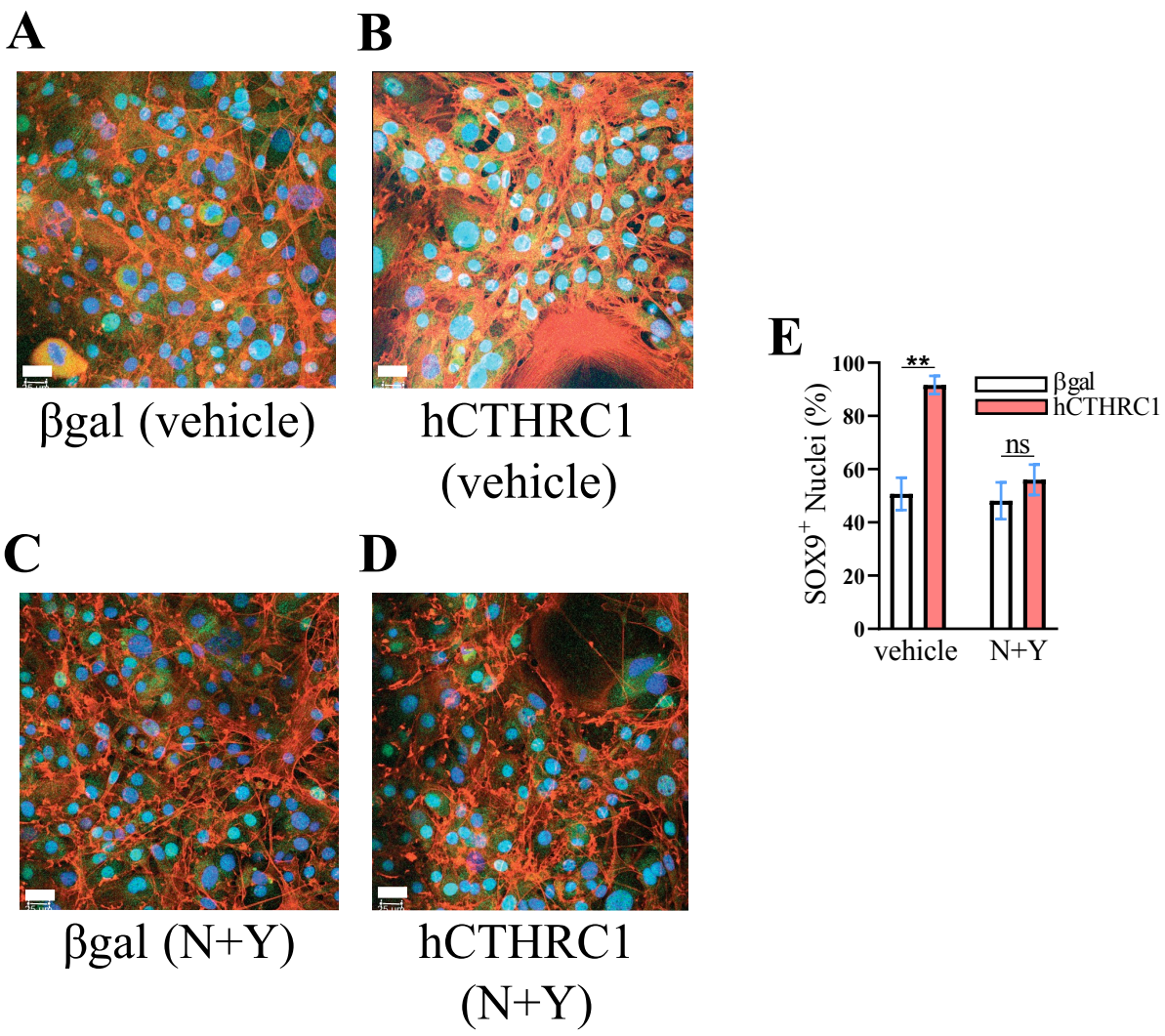

Figure 14. **CTHRC1 increases SOX9 nuclear localization in a Rho/Rac1-dependent manner *in vitro***. **A-E**) 3T3-L1 cells were seeded on Day -3 with βgal or hCTHRC1 conditioned medium at a 1/60 dilution in the absence or presence of the combined application of NSC 23766 (N; 10 μM) and Y-27632 (Y; 15 μM). N (NSC 23766) is a well-defined Rac1 activation-specific inhibitor, and Y (NSC 23766) is a potent inhibitor of the direct Rho effector, Rho-associated kinase. **A-D**) Representative confocal microscopy images of SOX9 protein localization on Day 0 in 3T3-L1 cells treated with either βgal conditioned medium (**A**,**C**) or hCTHRC1 conditioned

medium (**B**,**D**) in the absence (**A**,**B**) or presence (**C**,**D**) of the combined application of N (10 μM) and Y (15 μM): nuclei (blue); SOX9 (green); F-actin/Alexa Fluor 546 Phalloidin (red). The length of the white rectangle (lower left-hand corner) denotes the scale: 25 μm. **E**) Quantification of $SOX9^+$ nuclei based on 10 separate fields per experiment (n=3; ** $p \leq 0.01$).

3.11 Rho and Rac1 signaling positively regulate anti-adipogenic CTHRC1 activity

Given data supporting that CTHRC1 increases SOX9 nuclear localization in a Rho/Rac1-dependent manner, we next investigated whether the combined chemical inhibition of Rac1 and Rho signaling pathways with N (NSC 23766) and Y (NSC 23766), respectively, negates the anti-adipogenic effect produced by hCTHRC1 conditioned medium. As before, we applied βgal and hCTHRC1 conditioned media at dilutions of 1/60, in which 3T3-L1 cells were treated with or without N and Y. However, the combined application of N and Y at final concentrations of 10 μM and 15 μM, respectively, resulted in significant detachment of cells several days after the onset of chemically stimulated adipogenic differentiation (data not shown). Therefore, we reduced the final concentrations of N and Y to 3 μM and 5 μM, respectively, and repeated the adipogenic differentiation experiments. Based on Oil Red O absorbance spectroscopy data, in three out of four experiments, hCTHRC1 conditioned medium produced a significant anti-adipogenic effect when applied in the presence of N and Y (*Figure 15A*). However, when quantifying the percent suppression of Oil Red O staining relative to the application of hCTHRC1 conditioned medium, the application of N and Y significantly reduced the anti-adipogenic effect of hCTHRC1 conditioned medium (*Figure 15B*). This result was further corroborated based on two-way analysis of variance (*Table B.1*), which indicated that hCTHRC1 conditioned medium produced a statistically greater anti-adipogenic effect when N and Y were

omitted. In correlating these Oil Red O data relative to SOX9 protein expression levels, it is noteworthy that, in direct comparison to cells treated with βgal conditioned medium, application of hCTHRC1 conditioned medium with or without the combined presence of N and Y (3 μM and 5 μM, respectively) significantly increased SOX9 protein expression levels (*Figure 15C*,*D*). Critically, however, in assessing the effect of hCTHRC1 conditioned medium on SOX9 expression, the application of N and Y significantly reduced SOX9 protein expression levels in comparison to vehicle control (*Figure 15D*). Thus, the data presented here support the notion that the anti-adipogenic effect of hCTHRC1 conditioned medium is dependent on the positive regulation of Rho and Rac1 signaling.

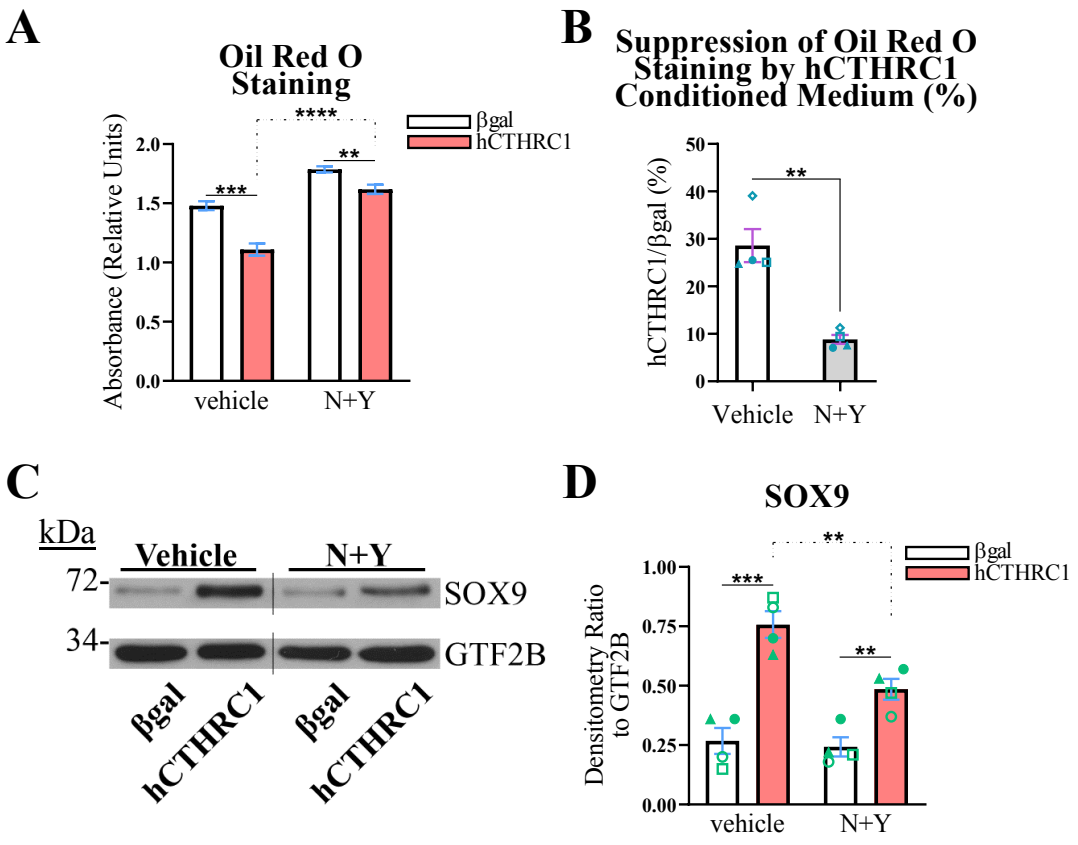

Figure 15. **Rho and Rac1 signaling mediate the SOX9-dependent anti-adipogenic function of CTHRC1 *in vitro***. **A-D**) 3T3-L1 cells were seeded on Day -3 with βgal or hCTHRC1 conditioned medium at a dilution of 1/60, in the absence or presence of the combined application of NSC 23766 (N; 3 μM) and Y-27632 (Y; 5 μM) (N+Y). N (NSC 23766) is a well-defined Rac1 activation-specific inhibitor, and Y (Y-27632) is a potent inhibitor of the direct Rho effector, Rho-associated kinase. Whole-cell lysates were collected from cohorts of cells on Day 0 to assess SOX9 protein expression levels by Western blot analysis (**C**,**D**), while the other cohorts were chemically stimulated to undergo adipogenic differentiation for a total period of 6 days (**A**,**B**). **A**) Representative Oil Red O quantification data. 3T3-L1 cells were formalin fixed on Day 6 and stained with Oil Red O, which was then eluted and its concentration determined by absorbance spectroscopy. Per experiment, 3T3-L1 cells were plated in 24-well plates in which 6

wells each were treated with βgal or hCTHRC1 conditioned medium at a dilution of 1/60, in the presence or absence of N+Y (n=4; ** p≤0.01, *** p≤0.001, **** p≤0.0001). **B**) Graphical representation quantifying that hCTHRC1 conditioned medium has a significantly diminished anti-adipogenic effect when applied in the presence of N+Y (displayed as average percent reduction in Oil Red O staining relative to the application of hCTHRC1 conditioned medium). Data reflect the averages from four independent experiments (n=4; ** p≤0.01). **C**) Representative Western blot image where the vertical line denotes the splice junction within both SOX9 and GTF2B immunoblots. **D**) Average SOX9 protein fold change densitometry values relative to housekeeping GTF2B protein expression levels from four independent experiments (n=4; ** p≤0.01, *** p≤0.001).

3.12 Individually suppressing either Rho or Rac1 signaling is not sufficient to negate anti-adipogenic CTHRC1 activity

Given data supporting that the anti-adipogenic effect of hCTHRC1 conditioned medium is dependent on the positive regulation of Rho and Rac1 signaling, we also assessed whether the independent chemical inhibition of Rac1 and Rho signaling pathways with N (NSC 23766) and Y (NSC 23766), respectively, could negate anti-adipogenic CTHRC1 activity. As such, we applied βgal and hCTHRC1 conditioned media at dilutions of 1/60, in which 3T3-L1 cells were treated with or without N, Y, or the combination of N and Y. Unlike the combined application of N and Y, the individual treatment of 3T3-L1 cells with either N or Y was not sufficient to significantly downregulate the anti-adipogenic effect of hCTHRC1 conditioned medium when comparing the results of three independent Oil Red O experiments (*Figure 16A*). Congruently, unlike the combined application of N and Y, the individual treatment of 3T3-L1 cells with either

N or Y was not able to attenuate the increase in SOX9 protein expression levels produced by hCTHRC1 conditioned medium (*Figure 16B*). Therefore, these results suggest that both Rho and Rac1 signaling are integral components with respect to the ability of hCTHRC1 conditioned medium to positively regulate SOX9 protein expression, as well as to negatively regulate *in vitro* adipogenesis.

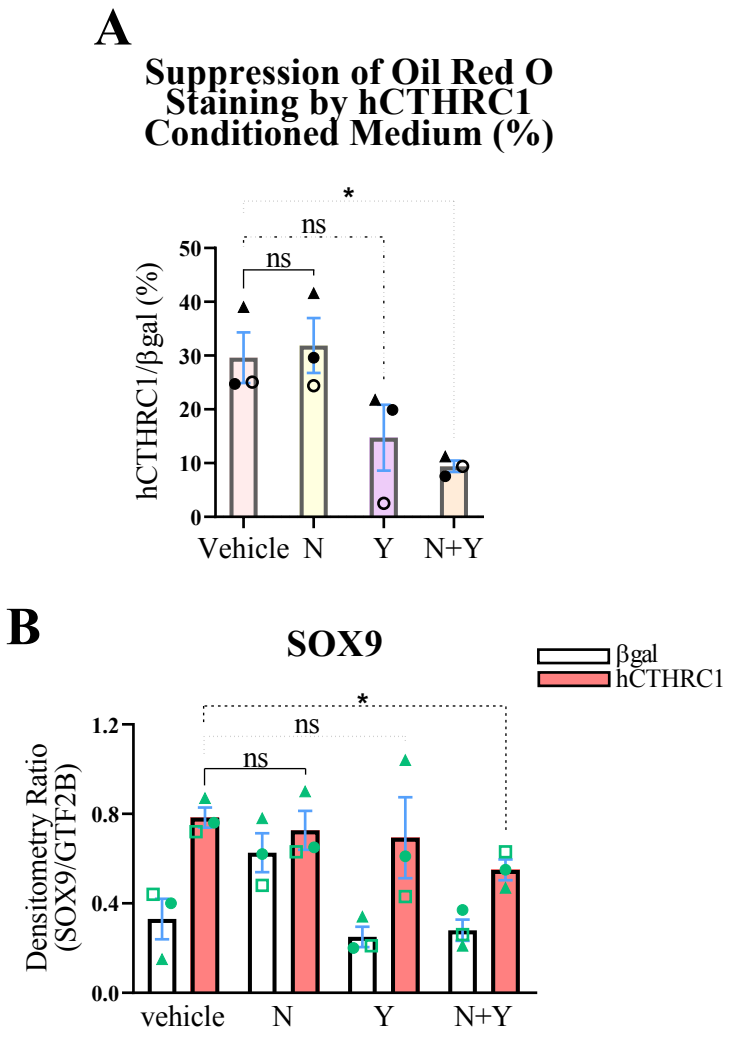

Figure 16. **Individually suppressing Rho or Rac1 signaling pathways does not significantly downregulate SOX9 protein expression or the anti-adipogenic effect of CTHRC1 *in vitro*.** **A**,**B**) 3T3-L1 cells were seeded on Day -3 with βgal or hCTHRC1 conditioned medium at a dilution of 1/60, in the absence or presence of NSC 23766 (N; 3 μM), Y-27632 (Y; 5 μM), or the combined application of N (3 μM) and Y (5 μM) (N+Y). N (NSC 23766) is a well-defined Rac1 activation-specific inhibitor, and Y (Y-27632) is a potent inhibitor of the direct Rho effector, Rho-associated kinase. Whole-cell lysates were collected from cohorts of cells on Day 0 to assess SOX9 protein expression levels by Western blot analysis (**B**), while the other cohorts were chemically stimulated to undergo adipogenic differentiation for a total period of 6 days (**A**). **A**) Graphical representation quantifying that hCTHRC1 conditioned medium has a significantly diminished anti-adipogenic effect when applied in the presence of N+Y, but not when applied in the individual presence of N or Y (displayed as average percent reduction in Oil Red O staining relative to the application of hCTHRC1 conditioned medium). 3T3-L1 cells were formalin fixed on Day 6 and stained with Oil Red O, which was then eluted and its concentration determined by absorbance spectroscopy. Per experiment, 3T3-L1 cells were plated in 24-well plates in which 6 wells each were treated with βgal or hCTHRC1 conditioned medium at a dilution of 1/60, in the presence or absence of N, Y, or N+Y. Data reflect the averages from three independent experiments (n=3; * $p \leq 0.05$). **B**) Average SOX9 protein fold change densitometry values relative to housekeeping GTF2B protein expression levels from three independent experiments (n=3; * $p \leq 0.05$).

3.13 CTHRC1 enhances YAP nuclear translocation

Based on our data supporting that Rho and Rac1 signaling positively regulates the anti-adipogenic activity of CTHRC1, we next queried the literature to determine other potential CTHRC1 effector proteins with established anti-adipogenic function. Thus, the transcriptional regulator, yes-associated protein 1 (YAP), became a factor of interest given that it is known to inhibit 3T3-L1 adipogenic differentiation (75), while Rho and Rac1 signaling have been further shown to positively regulate YAP nuclear translocation (76). On this basis, we assessed the effect of hCTHRC1 conditioned medium on YAP nuclear translocation. 3T3-L1 cells were seeded on Day -3 with either βgal or hCTHRC1 conditioned medium at a 1/4 dilution, and then subjected to four days of chemically stimulated adipogenic differentiation. Confocal microscopy analysis of YAP nuclear translocation in 3T3-L1 cells revealed that application of hCTHRC1 conditioned medium significantly enhanced YAP nuclear localization on Day 0 in comparison to cells treated with βgal conditioned medium (*Figure 17A*,*B*). Moreover, enhanced YAP nuclear translocation was also observed on Day 4 of chemically stimulated adipogenic differentiation in 3T3-L1 cells treated with hCTHRC1 conditioned medium but not in cells treated with βgal conditioned medium (*Figure 17C*,*D*). These data support that hCTHRC1 conditioned medium enhances the basal levels of YAP nuclear translocation in preadipocytes, and also functions to preserve the expression levels of YAP in the nucleus when preadipocytes are chemically stimulated to undergo adipogenic differentiation *in vitro*.

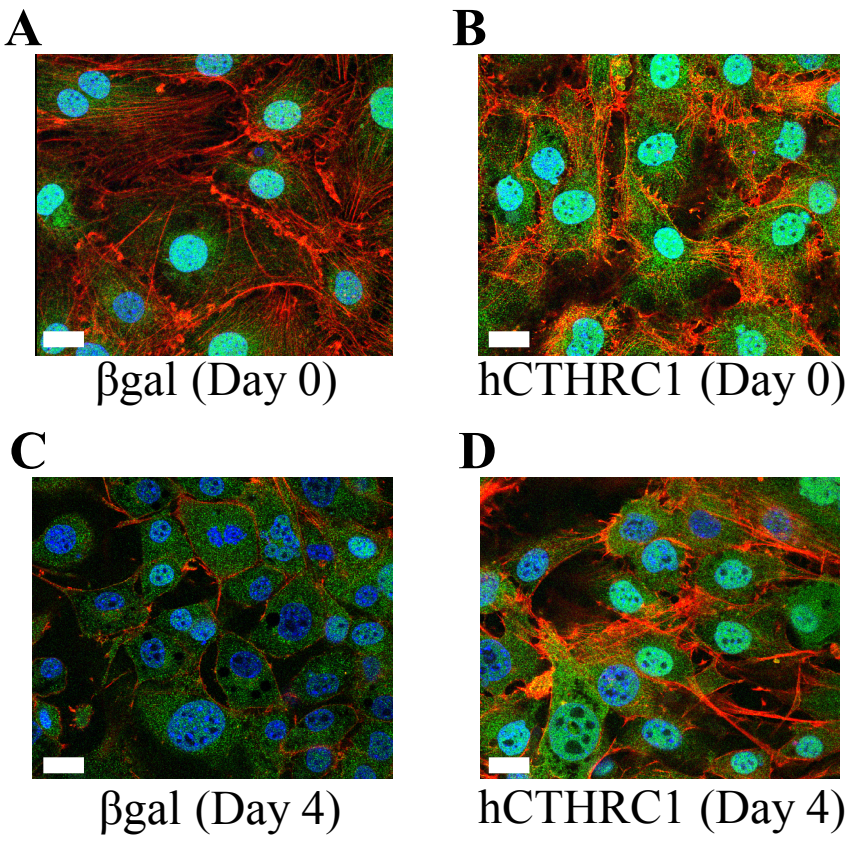

Figure 17. **Exogenously applied hCTHRC1 conditioned medium enhances YAP nuclear translocation *in vitro***. 3T3-L1 cells were seeded on Day -3 with either βgal or hCTHRC1 conditioned medium at a 1/4 dilution, after which cells were formalin fixed on either Day 0 or Day 4 relative to the chemical induction of adipogenic differentiation. **A**,**B**) Representative confocal microscopy images of YAP protein localization on Day 0 in 3T3-L1 cells treated with either βgal conditioned medium (**A**) or hCTHRC1 conditioned medium (**B**). **C**,**D**) Representative confocal microscopy images of YAP protein localization on Day 4 of adipogenic differentiation in 3T3-L1 cells treated with either βgal conditioned medium (**C**) or hCTHRC1 conditioned medium (**D**). Nuclei (blue); YAP (green); F-actin/Alexa Fluor 546 Phalloidin (red). The length of the white rectangle (lower left-hand corner) denotes the scale: 20 μm.

3.14 CTHRC1-induced YAP nuclear translocation is positively regulated in a Rho/Rac1-dependent manner

Given that Rho/Rac1 signaling have been shown to positively regulate YAP nuclear translocation (76), we next investigated whether the combined chemical inhibition of Rac1 and Rho signaling pathways with N (NSC 23766) and Y (NSC 23766), respectively, negates the ability of hCTHRC1 conditioned medium to regule YAP nuclear translocation. As before, we applied βgal and hCTHRC1 conditioned media at dilutions of 1/60, in which 3T3-L1 cells were treated with or without N and Y. Moreover, the combined application of N and Y attenuated YAP nuclear translocation caused by treatment with hCTHRC1 conditioned medium (*Figure 18A-D*). Therefore, these data support that Rho and Rac1 signaling positively regulate YAP nuclear translocation induced by hCTHRC1 conditioned medium.

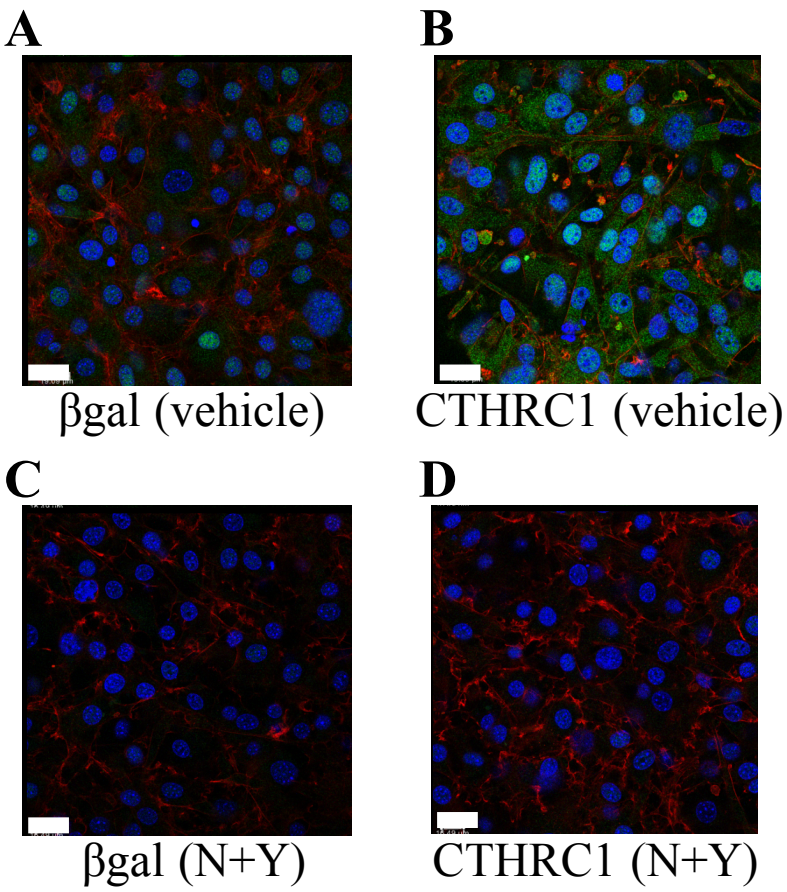

Figure 18. **CTHRC1 induces YAP nuclear localization in a Rho/Rac1-dependent manner *in vitro***. 3T3-L1 cells were seeded on Day -3 with βgal or hCTHRC1 conditioned medium at a 1/60 dilution in the absence or presence of the combined application of NSC 23766 (N; 10 μM) and Y-27632 (Y; 15 μM) (N+Y). N (NSC 23766) is a well-defined Rac1 activation-specific inhibitor, and Y (Y-27632) is a potent inhibitor of the direct Rho effector, Rho-associated kinase. **A**-**D**) Representative confocal microscopy images of YAP protein localization on Day 0 in 3T3-L1 cells treated with either βgal conditioned medium (**A**,**C**) or hCTHRC1 conditioned medium (**B**,**D**) in the absence (**A**,**B**) or presence (**C**,**D**) of the combined application of N and Y (N+Y): nuclei (blue); SOX9 (green); F-actin/Alexa Fluor 546 Phalloidin (red). The length of the white rectangle (lower left-hand corner) denotes the scale: 20 μm.

3.15 Discussion of Chapter 3

Our data highlight the anti-adipogenic function of CTHRC1, demonstrating its ability to negatively regulate adipogenic transcription factor gene expression at both the mRNA and protein levels. In this context, CTHRC1 also positively regulated *Sox9* gene expression and the nuclear localization of SOX9 protein. Congruent with the anti-adipogenic function of SOX9, wherein SOX9 silences adipogenic genes by binding to their promoter regions in an inhibitory manner (2, 42), CTHRC1 preserved SOX9 nuclear localization even after the chemical stimulation of adipogenic differentiation *in vitro*. This spatiotemporal observation supports that SOX9 nuclear translocation is a critical element of anti-adipogenic CTHRC1 signaling. We also identified the contribution of Rho-like GTPase signaling to the regulation of anti-adipogenic CTHRC1 function. Specifically, we observed that the combined suppression of Rho and Rac1 signaling attenuates the ability of CTHRC1 to enhance SOX9 protein expression as well as SOX9 nuclear localization, thus resulting in a significant reduction of anti-adipogenic CTHRC1 activity.

We further defined that SOX9 protein expression is indispensable to CTHRC1 anti-adipogenic activity based on adipogenic differentiation studies that implemented RNAi-mediated *Sox9* gene knockdown in 3T3-L1 cells. The 3T3-L1 cell line, which constitutes the most extensively investigated *in vitro* model of adipogenesis (77), has been shown to display a diminished capacity to differentiate into adipocytes if extensively passaged or reaches confluence during passaging (68, 69). For this reason, as part of our RNAi-based studies, we did not implement single-cell cloning strategies following lentiviral transduction and puromycin selection of shSCR and shSOX9 cells. Despite extensively optimizing our lentiviral transduction methods, including the applied concentration of lentiviral particles for each vector, in addition to

refining the duration of transduction preceding puromycin selection, we consistently observed that more shSCR cells survived puromycin selection than shSOX9 cells. Thus, at the moment shSCR and shSOX9 cells were seeded for study, shSOX9 cells were at a slightly higher passage than shSCR cells. This is reflected in our Oil Red O absorbance spectroscopy data revealing that shSCR cells underwent an overall higher degree of adipogenic differentiation than shSOX9 cells. However, from these RNAi adipogenic differentiation studies, it was consistently observed that the anti-adipogenic effect of hCTHRC1 conditioned medium is dependent on SOX9 protein expression levels. In addition, chemical suppression of Rho and Rac1 signaling pathways not only enhanced the adipogenic differentiation of 3T3-L1 cells despite concomitant treatment with hCTHRC1 conditioned medium, but also significantly attenuated the ability of hCTHRC1 conditioned medium to enhance SOX9 protein expression. These results are congruent with Gulyaeva and colleagues who demonstrated that *Sox9*-deficient, primary mouse adipocyte progenitor cells underwent increased adipogenic differentiation *in vitro* in comparison to *Sox9*-wildtype adipocyte progenitor cells (2), thus supporting the overall correlation between enhanced adipogenesis and decreased SOX9 expression. Collectively, these data support that a CTHRC1-Rho/Rac1-SOX9 signaling axis negatively regulates adipogenesis.

Application of hCTHRC1 conditioned medium to 3T3-L1 cells, as well as adenovirus-mediated overexpression of human *CTHRC1* in 3T3-L1 cells, enhanced the F-actin cytoskeleton. As mesenchymal stem cells commit to the adipogenic lineage thus becoming adipocyte progenitor cells (*i.e.*, preadipocytes) capable of undergoing adipogenic differentiation into mature adipocytes, downregulation of Rho-like GTPase signaling disrupts the F-actin cytoskeleton during the advancement of the adipogenesis program resulting in lipid-laden adipocytes with a rounded cell shape (78). The F-actin cytoskeleton is also regulated

concomitantly with Hippo-dependent or -independent signaling (79), which further mediates the nuclear translocation of YAP. In the case of Hippo-dependent signaling, YAP is sequestered in the cytoplasm given its association with adhesion molecules (*e.g.*, cadherins) (79). In this context, cadherins also function to positively regulate the phosphorylation of large tumor suppressor kinases (LATS) which, in turn, phosphorylate angiomotins (AMOTs) resulting in their dissociation from the actin cytoskeleton where they can also sequester YAP in the cytoplasm (79). Depolymerization of the F-actin cytoskeleton further results in the dissociation of AMOTs from the actin cytoskeleton and their sequestration of cytoplasmic YAP (76). On the other hand, activation of receptor tyrosine kinases and G(q) protein-coupled receptors functions to inhibit LATS phosphorylation thus stimulating YAP nuclear translocation (76). Hippo-independent regulation of YAP pertains to how the cell responds to the tension of the extracellular matrix such that a stiff mechanical environment enhances the formation of F-actin stress fibers that associate with focal adhesions to promote YAP nuclear translocation (80). Thus, common to both Hippo-dependent and -independent signaling is the architecture of the robust F-actin cytoskeleton in promoting the shuttling of cytoplasmic YAP to the nucleus.

As with SOX9, application of hCTHRC1 conditioned medium to 3T3-L1 cells preserved YAP nuclear localization even after the chemical stimulation of adipogenic differentiation *in vitro*. Once translocated to the nucleus, YAP interacts with its cognate DNA-binding partners, the TEA domain (TEAD) proteins, to regulate gene transcription (76). Relatedly, YAP is a known transcriptional activator of *SOX9* gene expression (81). Therefore, while our data support that Rho and Rac1 signaling enhance the nuclear localization of both YAP and SOX9, future investigations will be required to confirm whether YAP is situated directly within the CTHRC1-

SOX9 axis, where it could function to positively regulate *SOX9* gene expression and thus augment anti-adipogenic CTHRC1 signaling.

Further investigations are also required to discern the mechanism by which CTHRC1 enhances SOX9 nuclear translocation. Posttranslational modifications are known to modify SOX9 function, in which the phosphorylation of SOX9 at serine residue 181 has been shown to enhance SOX9 nuclear translocation and DNA binding activity (82). While it is conceivable that the phosphorylation of SOX9 at serine 181 could augment the overall anti-adipogenic function of SOX9, this has yet to be addressed in the literature. In addition, serine 181 of SOX9 has been identified as a direct substrate for multiple kinases including Rho-associated kinase (82) and AKT (83). With respect to the activities of these kinases, Y-27632 directly inhibits the kinase function of Rho-associated kinase, while the inhibition of Rac1 activity with NSC 23766 could potentially suppress AKT signaling based on literature situating Rac1-GTP (*i.e.*, "active" Rac1) upstream of the PI3K-AKT pathway (84). In this manner, it is plausible that the chemical suppression of Rho and Rac1 signaling pathways with Y-27632 and NSC 23766, respectively, could inhibit SOX9 phosphorylation thus downregulating overall SOX9 nuclear translocation. Finally, based on a report by Feng and colleagues, it is noteworthy that G(q) protein-coupled receptor signaling activates Rac1 and Rho via the guanine nucleotide-binding protein alpha-q (GNAQ)-regulated guanine nucleotide exchange factor, TRIO (76). This report further established that a GNAQ-Rho/Rac1 axis of signaling functions to enhance YAP nuclear translocation (76). Therefore, we suggest that the nuclear translocation of both YAP and SOX9 could be cohesively regulated by a CTHRC1-Rho/Rac1 axis of signaling.

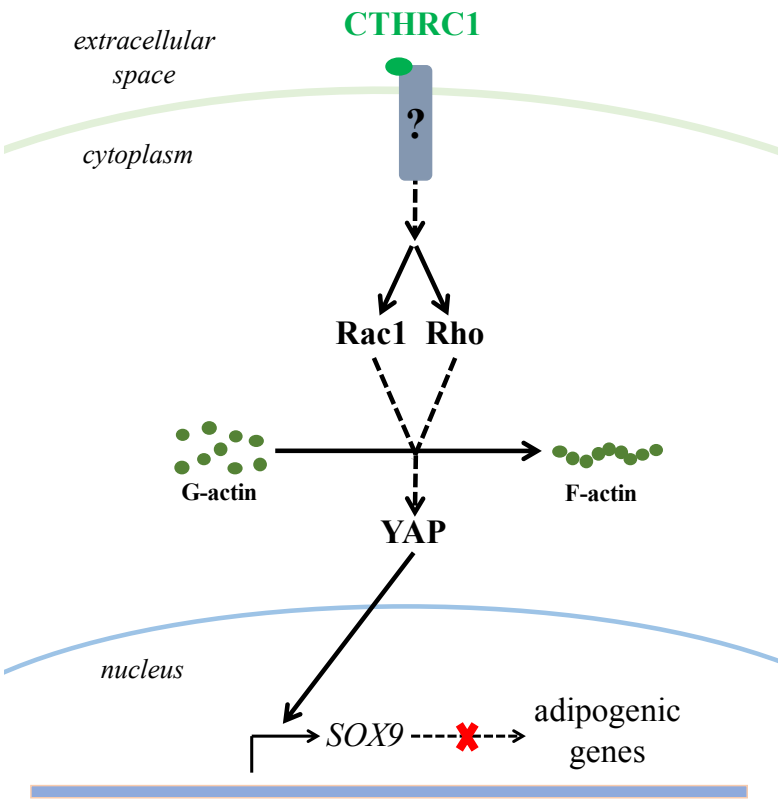

Figure 19. **Proposed model of a CTHRC1-Rho/Rac1-YAP-SOX9 axis of signaling**. Our data support the hypothesis that the anti-adipogenic effect of CTHRC1 is positively regulated by SOX9. We provided further evidence supporting that Rho and Rac1 signaling mediates the CTHRC1-SOX9 axis, in which the combined chemical inhibition of Rho and Rac1 signaling pathways downregulates the anti-adipogenic effect of CTHRC1 and its ability to enhance both SOX9 protein expression and SOX9 nuclear translocation. YAP is a transcriptional regulator with demonstrated anti-adipogenic function, and it has also been shown to enhance *SOX9* gene expression. As with SOX9, YAP nuclear localization induced by hCTHRC1 conditioned medium is also suppressed commensurate to the chemical inhibition of Rho and Rac1 signaling. We suggest that YAP could be situated directly within the CTHRC1-SOX9 axis, where it could function to enhance *SOX9* gene expression and thus positively regulate the overall anti-

adipogenic activity of CTHRC1. CTHRC1 also enhances the F-actin cytoskeleton. We further suggest that CTHRC1 positively regulates Rho/Rac1 signaling to maintain a robust F-actin cytoskeleton that promotes the shuttling of YAP and SOX9 to the nucleus.

CHAPTER 4: CTHRC1 IS EXPRESSED IN PDGFR-ALPHA^{+} STROMAL CELLS OF ADIPOSE

4.1 *Cthrc1* gene expression in subcutaneous white adipose tissue decreases during postnatal development

We have previously reported that stromal vascular fraction (SVF) cells harvested from mouse inguinal white adipose tissue (iWAT) express detectable *Cthrc1* mRNA levels (55), while it has been further demonstrated from transcriptomic analysis of C57BL/6 mice that *Cthrc1* gene expression in iWAT decreases during early postnatal development (*Figure 20A*). Congruently, we observed a marked decrease in *Cthrc1* gene expression in the iWAT isolated from 3-month-old mice versus 7-day-old mice (*Figure 20B*). Taken together, these data suggest that *Cthrc1* gene expression in mouse iWAT is downregulated throughout postnatal development.

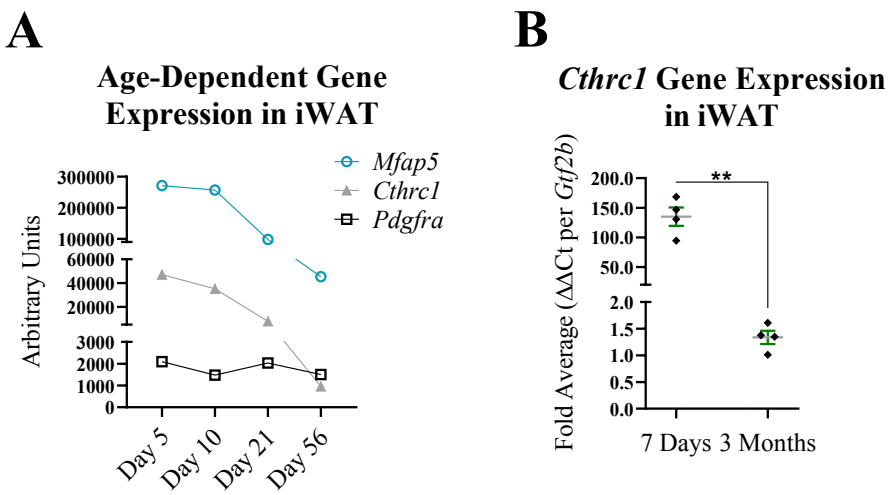

Figure 20. **Postnatal decrease of *Cthrc1* gene expression in mouse subcutaneous adipose tissue**. **A**) *Cthrc1*, *Mfap5*, and *Pdgfra* mRNA expression levels in inguinal white adipose tissue

(iWAT) during postnatal development. Koza and colleagues (3) conducted microarray analyses of RNA isolated from the iWAT of C57BL/6 male mice aged 5, 10, 21, and 56 days, in which *Cthrc1* and *Mfap5* gene expression were shown to decrease in iWAT during early postnatal development. **B**) qPCR analysis of *Cthrc1* gene expression in iWAT isolated from 7-day-old and 3-month-old C57BL/6 male mice. Data were normalized to housekeeping *Gtf2b* expression levels, and are presented as the average fold value per mouse (n=4; ** $p \leq 0.01$).

4.2 Wildtype and *Cthrc1*-null juvenile mice display differential *Sox9* gene expression in subcutaneous white adipose tissue

On the basis that *Cthrc1* gene expression in mouse inguinal white adipose tissue (iWAT) decreases throughout postnatal development (*Figure 20*), we next proceeded to analyze *Sox9* gene expression in the iWAT isolated from 7-day-old wildtype and *Cthrc1*-null C57BL/6 littermate mice, and observed significantly higher *Sox9* gene expression levels among the iWAT derived from wildtype pups (*Figure 21*). These data provide evidence in support of correlative *Cthrc1* and *Sox9* gene expression patterns within mouse subcutaneous white adipose tissue.

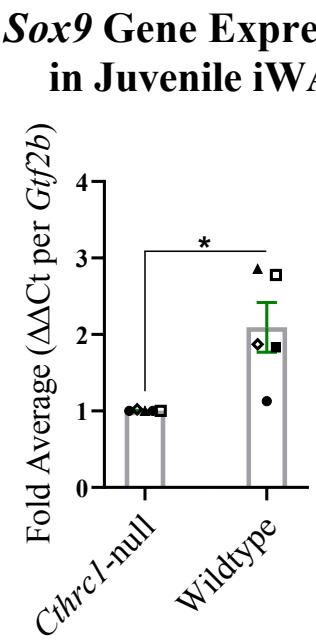

Figure 21. ***Cthrc1*-null mice display decreased *Sox9* gene expression in subcutaneous adipose tissue**. qPCR analysis of *Sox9* gene expression in iWAT isolated from 7-day-old wildtype and *Cthrc1*-null C57BL/6 littermate mice that were derived from heterozygous breeding pairs (three litters in total). Data were normalized to housekeeping *Gtf2b* expression levels, and are presented as the average fold value per mouse (n=5; * $p \leq 0.05$).

4.3 CTHRC1 is expressed among PDGFR-alpha$^+$ stromal cells in subcutaneous white adipose tissue

Next, we conducted multi-parameter flow cytometry (*Figure 22A-H*) to assess CTHRC1 protein expression among SVF cells harvested from the iWAT of juvenile C57BL/6 mice (5-day-old pups). Following the strategy of Gulyaeva and colleagues (2), SVF cells that expressed either TER119 (erythroid cells), CD31 (endothelial cells), or CD45 (immune cells) were excluded from the multi-parameter analysis that assessed CTHRC1 expression chiefly among CD24$^+$ or

PDGFR-alpha^{+} SVF cells. Accordingly, CTHRC1 was detected in PDGFR-alpha^{+} SVF cells (*Figure 22F*), with negligible CTHRC1 expression detected in CD24^{+} SVF cells (*Figure 22G*). Among PDGFR-alpha^{+} SVF cells, we also identified a subpopulation(s) of YAP^{+}:CTHRC1^{+} cells (*Figure 22H*). Intriguingly, all CTHRC1^{+} SVF cells were shown to express YAP (*Figure 22H*). As with PDGFR-alpha^{+} SVF cells, not all YAP^{+} SVF cells expressed CTHRC1; however, our findings nevertheless reveal the existence of PDGFR-alpha^{+}:YAP^{+}:CTHRC1^{+} stromal cells expressed in mouse subcutaneous white adipose tissue.

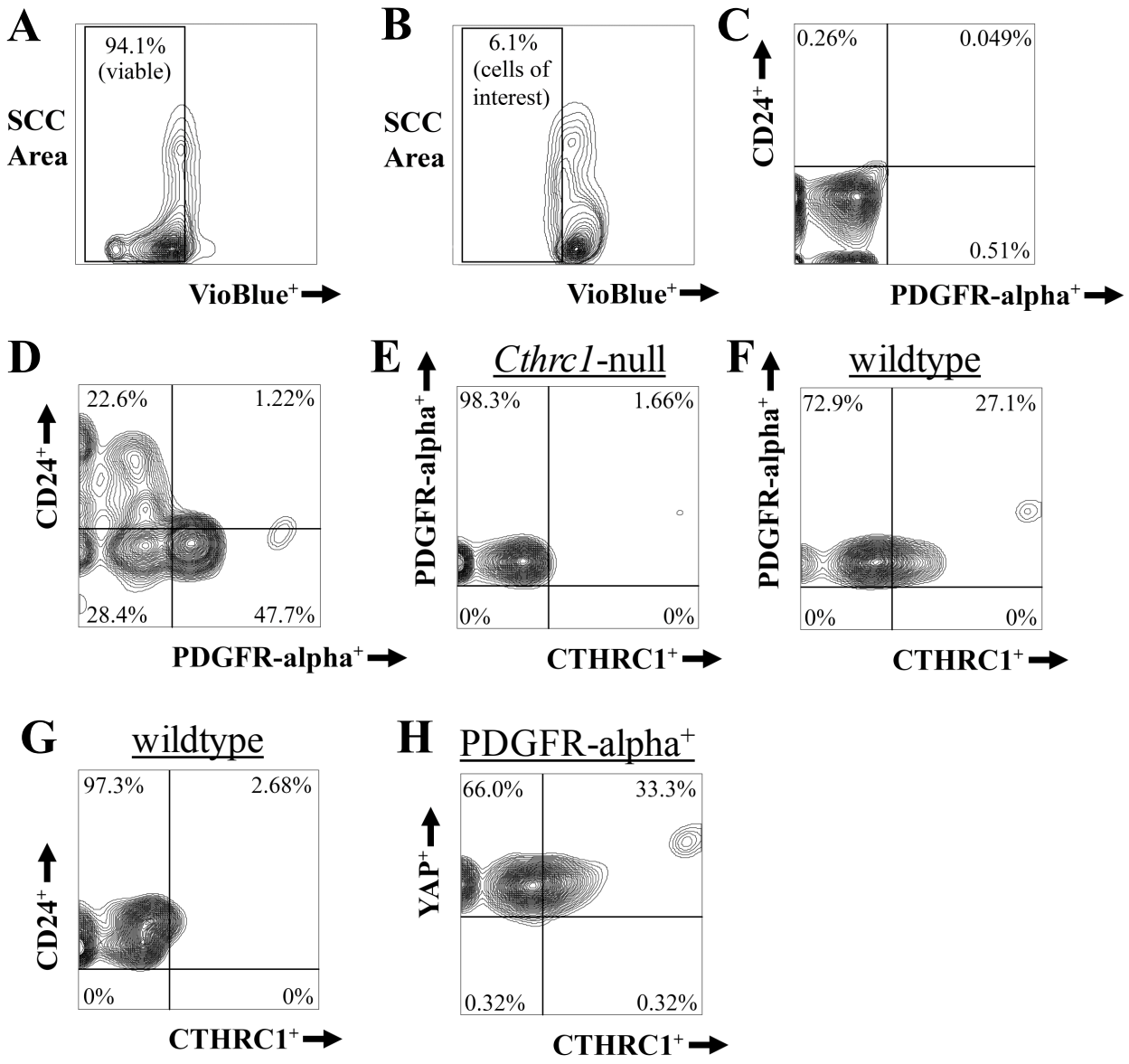

Figure 22. **PDGFR-alpha$^+$ stromal cells express CTHRC1 *in vivo***. **A-H**) Representative multi-parameter workflow, displayed in the form of contour plots, assessing endogenous CTHRC1 protein expression in CD24$^+$ versus PDGFR-alpha$^+$ stromal vascular fraction (SVF) cells. SVF cells were harvested from the iWAT of 5-day-old wildtype and *Cthrc1*-null C57BL/6 mice. SVF cells from three mice were pooled together per genotype (n=4). Dead SVF cells, in addition to SVF cells of erythroid lineage (TER119$^+$), CD31$^+$ endothelial cells, and CD45$^+$

immune cells (*i.e.*, lineage-negative cells), were omitted from the multi-parameter FACS analysis. **A**,**B**) VioBlue-treated SVF cells stained without (**A**) or with (**B**) lineage-negative markers. Side scatter (SCC) area. **C**,**D**) Live SVF cells treated without (**C**) or with (**D**) antibodies against CD24 and PDGFR-alpha. **E**) No detectable CTHRC1 expression in PDGFR-alpha$^+$ SVF cells derived from *Cthrc1*-null mice. **F**) Detectable CTHRC1 expression in certain PDGFR-alpha$^+$ SVF cells derived from age-matched wildtype mice. **G**) Negligible expression of CTHRC1 in CD24$^+$ SVF cells derived from age-matched wildtype mice. **H**) PDGFR-alpha$^+$:CTHRC1$^+$ stromal cells express YAP.

4.4 *PDGFRA*$^+$:*MFAP5*$^+$ cells express *CTHRC1* and *SOX9* in human subcutaneous white adipose tissue

Next, we evaluated *CTHRC1* gene expression in adult human subcutaneous white adipose tissues, brown adipose tissue (BAT), and perivascular adipose tissue (PVAT). Based on available single-nuclei or single-cell RNA sequencing databases, we observed significant *CTHRC1* expression in human subcutaneous white adipose tissues, principally among cells expressing high mRNA levels of *PDGFRA* and *MFAP5* (microfibrillar-associated protein 5) (*i.e.*, *PDGFRA*$^+$:*MFAP5*$^+$ cell populations) (*Figure 23A-D*). While *CTHRC1* expression in subcutaneous white adipose tissues did not differ in lean versus obese human subjects, it was not significantly detectable in human BAT or PVAT (*Figure 23C*). Furthermore, *SOX9* mirrored the gene expression patterns of *CTHRC1*, albeit expressed at lower levels, and was most abundantly expressed in human subcutaneous white adipose tissues among *PDGFRA*$^+$:*MFAP5*$^+$ cell populations (*Figure 23D*). Therefore, the analysis of *PDGFRA*$^+$:*MFAP5*$^+$ stromal cells in human

subcutaneous white adipose tissues demonstrated a positive correlation between patterns of *CTHRC1* and *SOX9* gene expression.

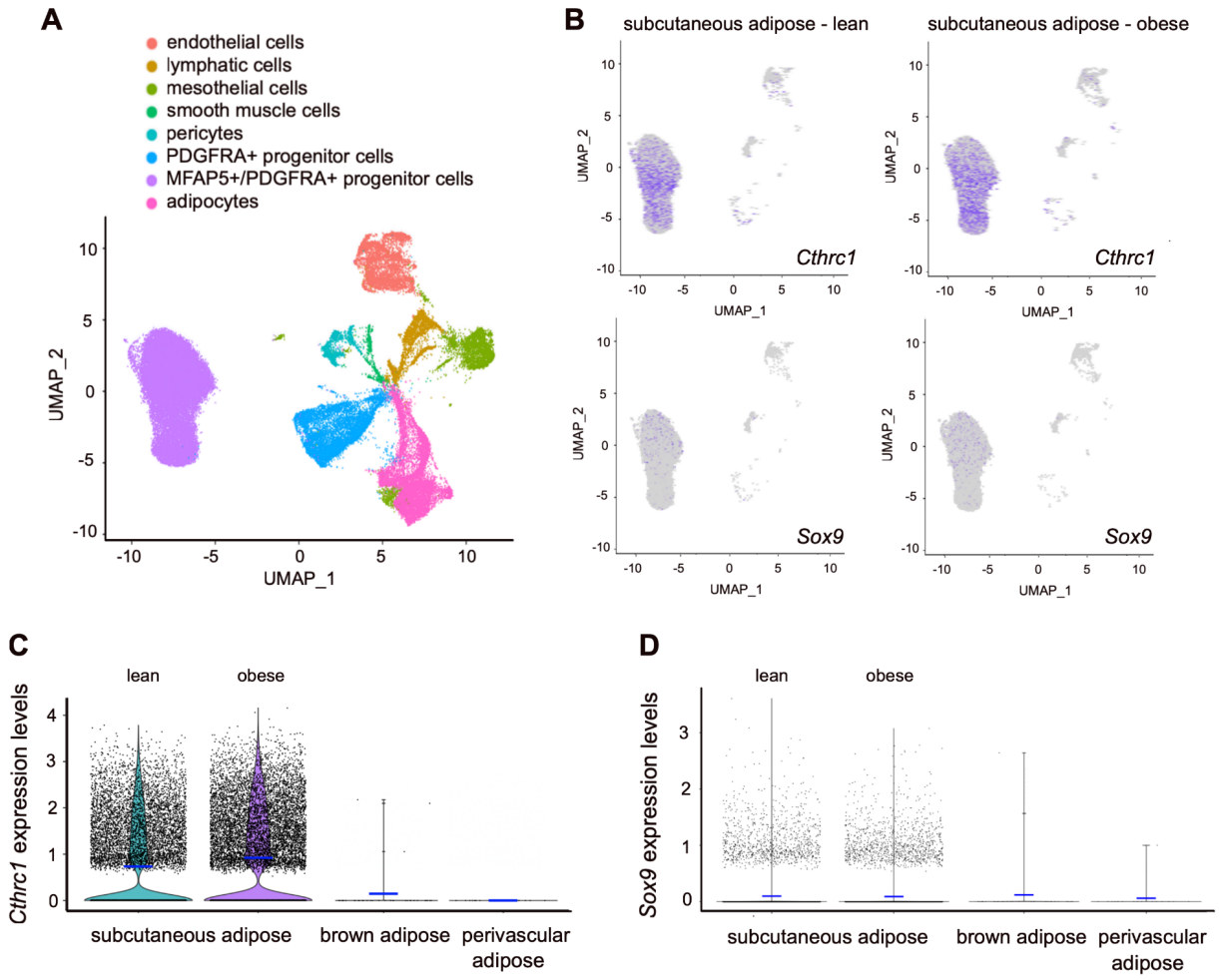

Figure 23. Identification of *CTHRC1* and *SOX9* gene expression in *PDGFRA*$^{+}$:*MFAP5*$^{+}$ enriched cell populations in human subcutaneous white adipose tissue. A) Harmonized UMAP projection of perivascular adipose and brown adipose single-nuclei RNA sequencing, as well as subcutaneous white adipose single-cell RNA sequencing, from lean and obese human donors. Data were filtered based on number of unique features and percent.mt. Doublets were

removed using Scrublet. **B**) UMAP projection displaying *CTHRC1* and *SOX9* expression as indicated by purple coloration. *CTHRC1* expression is observed in *PDGFRA*$^{+}$:*MFAP5*$^{+}$ cell populations in subcutaneous white adipose from both lean and obese human donors. *SOX9* mirrors *CTHRC1* gene expression patterns, though is expressed at lower levels. **C**,**D**) ViolinPlots displaying the distribution of *CTHRC1* (**C**) and *SOX9* (**D**) expression among *PDGFRA*$^{+}$:*MFAP5*$^{+}$ cells in human perivascular, brown, and subcutaneous white adipose tissues. Mean expression is displayed by a blue horizontal bar. In comparing subcutaneous white adipose from lean versus obese human donors, there was no significant difference in the expression levels of *CTHRC1* or *SOX9*.

4.5 Discussion of Chapter 4

The results of multi-parameter flow cytometry analysis identified a novel PDGFR-alpha^{+}:CTHRC1^{+} stromal cell population retained within inguinal white adipose tissue (iWAT). During early postnatal development, adipose tissue compartments are significantly expanding due to two central factors: (i) adipocyte progenitor cells are actively recruited to differentiate into adipocytes, and (ii) there is a simultaneous increase in adipocyte hypertrophy (85). From lineage tracing investigations of stromal vascular fraction (SVF) cells in iWAT, mesenchymal stems cells define the earliest adipocyte progenitor cell population and are characterized by PREF1^{+}:CD24^{+}:PDGFR-alpha^{-} expression (2). Ultimately, mesenchymal stem cells advancing in the adipogenic lineage become PREF1^{-}:CD24^{-}:PDGFR-alpha^{+} preadipocytes capable of undergoing terminal differentiation to white adipocytes (Gulyaeva et al., 2018). Our finding that CTHRC1 is expressed among CD24^{-}:PDGFR-alpha^{+} stromal cells in mouse iWAT could

therefore suggest that CTHRC1 is expressed in the adipogenic lineage among a population of preadipocytes.

In a recent study focused on the gene expression profiles of human adipose tissue-derived SVF cells, *CTHRC1* mRNA levels were significantly enhanced following the chemical induction of adipogenic differentiation of these SVF cells *in vitro* (86). However, *CTHRC1* mRNA expression was upregulated in a SVF subpopulation that did not terminally differentiate into mature adipocytes and was chiefly characterized by high expression levels of extracellular matrix genes (86). Relatedly, to identify cells expressing *CTHRC1* in human adipose tissues we queried single-cell and single-nuclei transcriptomic data, and report herein selective expression of *CTHRC1* in *PDGFRA*$^{+}$:*MFAP5*$^{+}$ gene-rich cell populations in subcutaneous white adipose tissues, but not within BAT or PVAT. *CTHRC1* and *SOX9* displayed correlative gene expression patterns among these *PDGFRA*$^{+}$:*MFAP5*$^{+}$ cells, which supports the hypothesis that CTHRC1 could function *in vivo* to positively regulate *SOX9* gene expression within white adipose tissues. Moreover, Vaittinen and colleagues found that MFAP5 localizes in the extracellular matrix of human abdominal subcutaneous adipose tissue (87). Using an *in vitro* model of human adipogenic differentiation, it was also reported that *MFAP5* mRNA is expressed maximally in preadipocytes and minimally in adipocytes (87), data which are congruent with a recent investigation demonstrating that MFAP5 suppresses 3T3-L1 cell adipogenic differentiation (88). Although MFAP5 has been characterized as a secreted protein associated with microfibrils within the extracellular matrix (87), Zhang and colleagues reported an intracellular functionality in its suppression of adipogenesis given that MFAP5 was shown to both bind to and inhibit the expression of SND1 (Staphylococcal nuclease and tudor domain-containing 1), which is a well-established co-activator of PPAR-gamma (88). Intriguingly, similar to the gene expression

profile of *Cthrc1* in mouse iWAT, *Mfap5* mRNA levels also decrease during early postnatal development, suggesting that downregulation of both *Cthrc1* and *Mfap5* gene expression could be required for terminal differentiation of preadipocytes *in vivo*. Importantly, in directly comparing the degree of *Sox9* gene expression among iWAT derived from wildtype and *Cthrc1*-null juvenile littermate mice, *Sox9* mRNA levels were significantly enhanced in wildtype mice. These data further present the possibility that CTHRC1 could function as a regulator of SOX9 *in vivo*.

MFAP5 expression has also been reported in various fibroblast populations, including cancer-associated fibroblasts (89). Similarly, although PDGFR-alpha is expressed in preadipocytes (2), it is a known marker of stromal fibroblast populations that are separate from the adipogenic lineage (90). Regarding stromal cells resident to white adipose tissues, Marcelin and colleagues found that PDGFR-alpha^{+}:CD9^{high} stromal populations possess a myofibroblastic phenotype. Notably, *Cthrc1* mRNA expression significantly correlated with this PDGFR-alpha^{+} sub-population robustly expressing CD9 protein (91). Correspondingly, *Mfap5* gene expression was enhanced in this PDGFR-alpha^{+}:CD9^{high} stromal cell population (91). *Cthrc1* mRNA expression has also been detected in cardiac fibroblasts (67, 70). In one report, both *Cthrc1* and *Sox9* gene expression were significantly upregulated in a subpopulation of activated, pro-fibrotic fibroblasts following myocardial infarction in mice (67). More recently, Hironaka and colleagues demonstrated using mouse cardiac myofibroblasts that the actin binding protein, drebrin, stabilizes the F-actin cytoskeleton, increases *Cthrc1* gene expression, and promotes the nuclear translocation of SOX9 protein (70). Therefore, this corroborating investigation suggests that F-actin stability, in relation to SOX9 localization within the nucleus, comprise core elements of CTHRC1-related signaling. Among white adipose tissues, our data present the possibility that

CTHRC1 could be expressed in the adipogenic lineage among a population of preadipocytes. On the other hand, CTHRC1 may also be expressed in adipose PDGFR-alpha^{+} stromal fibroblasts, from where it could be secreted in order to tightly regulate the differentiation of adipocyte progenitor cells therein. Accordingly, refined lineage tracing experiments will be essential in order to elucidate the expression of CTHRC1 among discrete fibroblastic and/or adipocyte progenitor cell populations of adipose tissues. In that connection, using mice we also demonstrated that all CTHRC1^{+} stromal cells within subcutaneous white adipose tissue express YAP. While these data suggest coregulation of the *CTHRC1* and *YAP* genes *in vivo*, it is plausible that CTHRC1 is a positive regulator of *YAP* gene expression (or vice versa) among specific populations of adipose tissue stromal cells. Our novel identification of PDGFR-alpha^{+}:YAP^{+}:CTHRC1^{+} stromal cells could thus aid future investigations seeking to define the lineage identify and function of these CTHRC1^{+} stromal cells *in vivo*.

Adipose tissue hypertrophy and hyperplasia are well defined characteristics of obesity, in which obese individuals are at a greater risk of developing diabetes, metabolic syndrome, and other related comorbidities (1). In the obese state, there are multiple lines of evidence supporting that adipocytes can become insulin resistant (6). In the lean state, adipocyte turnover, in which old adipocytes are degraded and new adipocytes arise owing to adipogenic differentiation, has also been demonstrated to be an essential facet of maintaining insulin-responsive adipocytes (92). Thus, future investigations will be critical in order to fully define the molecular mechanism by which CTHRC1 suppresses adipogenic signaling, and how CTHRC1 could be therapeutically targeted to finely regulate the rate at which new, insulin-responsive adipocytes are formed, while altogether preventing precocious adipogenesis *in vivo*.

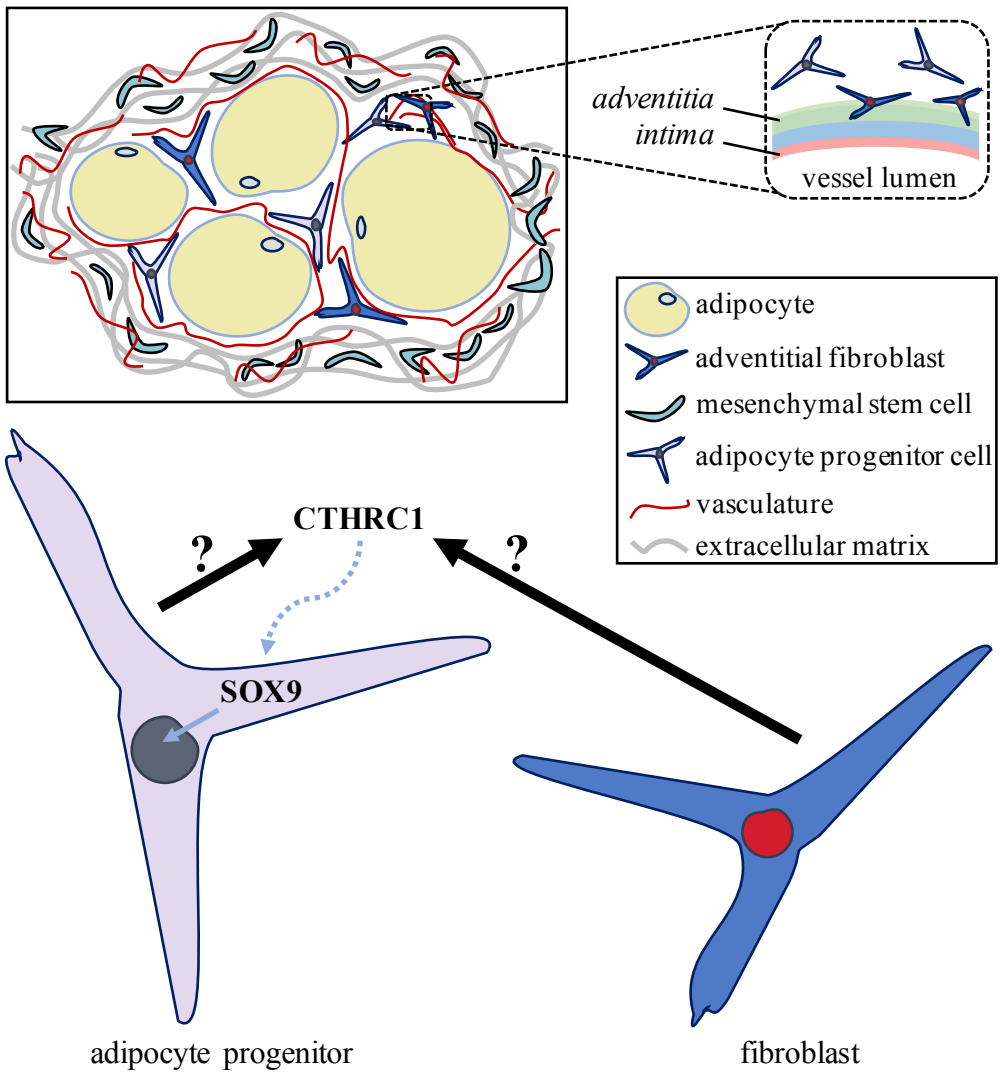

Figure 24. **Conceptualizing the CTHRC1-SOX9 axis within white adipose tissues**. Graphical illustration addressing the question of whether CTHRC1 is expressed and secreted from adipocyte progenitor cells and/or fibroblasts within white adipose tissues. As with adipocyte progenitor cells, fibroblast cells are also present in the adipocyte compartment, though mostly within the vascular adventitia. We report herein the presence of CTHRC1 in PDGFR-alpha^{+} stromal cells derived from mouse subcutaneous white adipose tissue, and also report the selective expression of *CTHRC1* mRNA within a *PDGFRA*$^{+}$:*MFAP5*$^{+}$ gene-rich cell population retained

in human subcutaneous white adipose tissue. Adipocyte progenitor cells and fibroblasts both express PDGFR-alpha and MFAP5; therefore, our investigation highlights the possibility that CTHRC1 could be expressed within adipogenic and/or fibroblastic lineages among white adipose tissues. Both scenarios support that CTHRC1, owing to its secretion from such PDGFR-alpha^{+} stromal cells, could suppress the local differentiation of adipocyte progenitor cells through its putative anti-adipogenic effector protein, SOX9. If CTHRC1 is expressed among adipocyte progenitor cells, this could further suggest that the CTHRC1-SOX9 axis functions in a feedforward manner to negatively regulate adipogenesis *in vivo*. Additional questions arise from the observation that *Cthrc1* gene expression in mouse subcutaneous white adipose tissue markedly decreases during early postnatal development (*Figure 20*). Is this trend recapitulated during human development? If so, is *CTHRC1* gene expression regulated at low levels in human white adipose tissues? Commensurate to adipocyte turnover in adult white adipose tissues, is *CTHRC1* gene expression transiently activated as a means to limit the degree of new adipocyte formation therein? Finally, does the CTHRC1-SOX9 axis function to prevent precocious adipogenesis *in vivo*, thus regulating the formation of insulin-responsive white adipocytes which promote the metabolic fitness of adipose tissues that cater to whole-body energy demands?

CHAPTER 5: PERSPECTIVES ON SOX9

Our data support the hypothesis that CTHRC1 is a positive regulator of SOX9. For example, our *in vitro* results demonstrate that CTHRC1 enhances *Sox9* gene expression and positively regulates SOX9 nuclear translocation. In the context of adipogenesis, the expression of SOX9 within the nucleus is paramount to its anti-adipogenic function given that it inhibits adipogenic gene promoters (2). Our *in vivo* data provide further evidence supporting that CTHRC1 regulates SOX9 gene expression. Moreover, in one study directly comparing juvenile wildtype and C*thrc1*-null littermate mice, *Sox9* gene expression was significantly higher in the inguinal white adipose tissue of wildtype mice. From RNA sequencing, we also observed correlative gene expression patterns between *CTHRC1* and *SOX9* in *PDGFRA*$^{+}$:*MFAP5*$^{+}$ cell populations retained in human subcutaneous white adipose tissues. Given our *in vitro* data supporting that SOX9 is a critical regulator of anti-adipogenic CTHRC1 activity, we further posit that a CTHRC1-SOX9 axis of signaling functions to regulate adipogenesis *in vivo*.

SOX9 is a member of the SRY-type HMG box (SOX) family of transcription factors which are characterized by a high mobility group (HMG) box DNA-binding domain, and is further part of the SOXE subgroup including SOX8 and SOX10 which share collective structural homology (93). SOX9 possesses a consensus DNA-binding motif (AGAACAATGG), while the HMG domain of SOX9 facilitates its sequence-specific DNA binding (94). The dimerization domain (DIM) of SOX9 is situated near the N-terminus and is adjacent to the HMG domain (93). The DIM domain of SOX9 promotes homodimerization, as well as heretodimerization with other SOXE subgroup members (95). In certain contexts, SOX9 dimerization is required for its DNA binding and transcriptional activity, including the activation of cartilage-specific genes (95).

Additionally, SOX9 possesses two transactivation domains: the transactivation domain located in the middle (TAM), and the transactivation domain at the C-terminus (TAC) (93). TAM and TAC domains enhance the transcriptional activity of SOX9 by engaging transcriptional co-activators. For example, the TAC domain has been shown to interact directly with mediator complex subunit 12 (MED12), CREB binding protein/E1A binding protein p300 (CBP/p300), WW domain containing E3 ubiquitin protein ligase 2 (WWP2), and Tat interactive protein-60 (TIP60) (93, 96). Relative to established anti-adipogenic gene targets of SOX9 as discussed in the previous section (*1.1.4 Terminal adipogenic differentiation*), Gulyaeva and colleagues reported the finding that SOX9 transcriptionally activates *Meis1*, and further demonstrated that MEIS1 suppresses adipogenesis by directly inhibiting the gene promoters of C/EBP alpha, C/EBP beta, C/EBP delta, and PPAR-gamma (2). SOX9 is referred to as the master regulator of chondrogenesis and drives the chondrogenic lineage commitment of mesenchymal stem cells (93). Thus, the potent, redundant anti-adipogenic function of the SOX9-MEIS1 axis further underscores the important role SOX9 plays in the regulation of mesenchymal lineages. Future investigations are necessary to elucidate if CTHRC1 can promote the expression of MEIS1 either in a SOX9-depedent or -independent manner, and whether CTHRC1 also functions to enhance the transcriptional activity of SOX9 by regulating its DNA binding, dimerization, or transactivation domains. In addition, it further remains to be determined whether CTHRC1 regulates SOX9 posttranslational modifications, its RNA-binding functions (a unique manner in which SOX9 regulates protein translation of certain target genes), or the activity of SOX9 as an identified pioneer factor capable of regulating chromatin accessibility and the epigenome (93, 97, 98).

In various cellular contexts, SOX9 gene expression has been shown to be positively regulated by multiple signaling factors including prostaglandin D2 (PGD2), hedgehog, fibroblast growth factor (FGF), non-canonical WNT, BMP, and TGFB1 (93, 97). As discussed in the previous section (*3.15 Discussion of Chapter 3*), YAP is also a known transcriptional activator of SOX9 (97). Thinking in terms beyond the scope of the proposed CTHRC1-YAP-SOX9 signaling axis suggested herein, for example, BMP and TGFB1 both positively regulate CTHRC1 and SOX9 gene expression (45, 97). However, the relationship between CTHRC1 and TGFB1 is dichotomous in that, while TGFB1 is known to enhance CTHRC1 expression, CTHRC1 can act as a negative regulator of TGFB1 signaling (45, 52). It is plausible that, in certain contexts, CTHRC1 could downregulate TGFB1 signaling thus suppressing SOX9 expression. While SOX9 is known to inhibit terminal adipogenic differentiation, Gulyaeva and colleagues also placed SOX9 directly in the adipogenic lineage within adipose, revealing that *Sox9* gene expression is expressed maximally in mesenchymal stem cells and to a lesser degree in PDGRF-alpha^{+} preadipocytes (93). Therefore, these data support the finding that SOX9 is a negative regulator of mesenchymal stem cell adipogenic lineage commitment as well as preadipocyte-to-adipocyte differentiation. While the link between TGFB1 and SOX9 signaling has not yet been functionally established in the adipose tissue biology/adipogenesis fields, it is thought provoking to speculate that CTHRC1 could, at times, context-dependently suppress TGFB1/SOX9 signaling to promote the adipogenic lineage commitment of mesenchymal stem cells. This effect would thus increase the available pool of preadipocytes capable of differentiating into adipocytes. Commensurate to the metabolic needs of adipose tissues to maintain their supply of insulin-responsive adipocytes, CTHRC1 could theoretically regulate a “healthy” degree of adipocyte turnover *in vivo* by reengaging SOX9 signaling at this juncture to prevent precocious

adipogenesis. This speculative point further addresses the need to determine how CTHRC1 influences the adipogenic lineage at large, particularly with respect to the regulation of multiple signaling pathways and networks that choreograph the formation of mature adipocytes from mesenchymal progenitor cells.

CHAPTER 6: CONSOLIDATED DISCUSSION, PITFALLS, SUCCESSES, AND FUTURE EXPERIMENTAL DIRECTIONS

This final chapter is composed principally in a narrative form and addressed to those who might inherit this body of work and seek to expand the knowledge of how CTHRC1 contributes to the field of adipose tissue biology research. In this section, I outline the trajectory of my experimental reasonings and findings. Perhaps most important, I also explain my experimental failures and shortcomings, and offer my opinion on how research devoted to anti-adipogenic CTHRC1 signaling could be advanced.

The publication by our group, "Cthrc1 controls adipose tissue formation, body composition, and physical activity" (55), established the correlation between high CTHRC1 expression levels and reduced lipid accumulation in differentiating adipocytes *in vitro*, thus paving the way for me to investigate if CTHRC1 regulates adipogenic gene expression. Prior to my work optimizing and utilizing human CTHRC1 conditioned medium (discussed below), I relied on adenovirus to overexpress human CTHRC1 in preadipocyte cell lines (*e.g.*, 3T3-L1 cells). As illustrated in *Figure C.1.*, adenoviral-mediated hCTHRC1 overexpression in 3T3-L1 cells significantly decreased *Cebpb*, *Cebpd*, *Cebpa*, and *Pparg* gene expression levels. Intriguingly, in two out of three conditioned medium experiments, 3T3-L1 cells treated with hCTHRC1 conditioned medium showed significantly increased *Cebpb* mRNA levels on Day 0, while *Cebpd* mRNA levels on Day 0 were downregulated by application of hCTHRC1 conditioned medium in all three experiments (*Figure 7*). These collective data suggest that there are differences in the regulation of *Cebpb* gene expression in an experimental model system where hCTHRC1 is more constitutively expressed (*i.e.*, adenoviral transduction) versus methods

where hCTHRC1 conditioned medium is applied once daily. Regarding the latter, it would also be important to discern the relative activity of hCTHRC1 conditioned medium. For example, relative to a single application of hCTHRC1 conditioned medium to 3T3-L1 cells or other cell types, when is *Sox9* gene expression maximally expressed? How long does it take for SOX9 to maximally translocate to the nucleus? Better understanding such spatiotemporal dynamics could be a critical determinant in optimizing future experiments to further address the putative CTHRC1-SOX9 signaling axis. Since SOX9 is known to directly bind to the proximal promoter regions of *Cebpb* and *Cebpd* in an inhibitory manner (2), why does adenoviral overexpression of hCTHRC1 in 3T3-L1 cells, or the daily application of hCTHRC1 conditioned medium to 3T3-L1 cells, both result in marked downregulation of *Cebpd* gene expression on Day 0, while *Cebpb* mRNA levels display differential patterns of expression when comparing the qPCR results based on these two discrete *in vitro* methods of introducing hCTHRC1 to 3T3-L1 cells? In this respect, I think one important future direction would be to assess if adenoviral-mediated hCTHRC1 overexpression or the application of hCTHRC1 conditioned medium regulates the binding of SOX9 to adipogenic genes including *Cebpb*, *Cebpd*, *Cebpa*, and *Pparg*. These chromatin immunoprecipitation (ChIP) efforts could also be accompanied by sequencing (*i.e.*, ChIP-Seq) to determine the broader landscape of how CTHRC1 might regulate SOX9-DNA interactions. Such data could be fundamentally important to the understanding of how adipogenesis is regulated in states of health versus obesity. If CTHRC1 regulates the binding of SOX9 to specific DNA enhancer regions or regulatory elements in states of health to control adipogenesis and adipocyte turnover within adipose tissues, for example, might certain obesogenic phenotypes be attributed to mutations that hinder or prevent CTHRC1-mediated SOX9 DNA binding? My collective body of thesis work supports the hypothesis that CTHRC1 positively regulates multiple facets of

SOX9 signaling including its gene expression levels and protein nuclear translocation, and assessing whether CTHRC1 also regulates SOX9 DNA binding activity would be a logical step forward.

Given the finding that adenoviral-mediated hCTHRC1 overexpression in 3T3-L1 cells suppresses adipogenic gene expression (*Figure C.1.*) in the early stages of my Ph.D. studies, I next investigated whether this anti-adipogenic effect is potentially regulated by C/EBP-homologous protein (CHOP). CHOP is an anti-adipogenic factor that prevents C/EBP beta, C/EBP delta, and C/EBP alpha DNA binding as a result of forming heterodimers with these adipogenic transcription factors (99, 100). Consequently, CHOP protein expression has also been shown to be downregulated early in the adipogenesis program *in vitro* (99). We happened to possess a monoclonal antibody against CHOP, and I designed an experiment in which whole-cell lysates were prepared from adenovirally transduced 3T3-L1 cells on Day 0 and Day 2 relative to the onset of chemically induced adipogenic differentiation. Interestingly, we observed in a reproducible manner that CHOP protein expression is increased on Day 2 in 3T3-L1 cells overexpressing hCTHRC1 (*Figure D.1.*). I next investigated the effect of adenoviral-mediated hCTHRC1 overexpression on *Chop* mRNA levels in 3T3-L1 cells at multiple timepoints during the course of adipogenic differentiation. Paradoxically, these qPCR data revealed that hCTHRC1 overexpression significantly decreased *Chop* gene expression in 3T3-L1 cells (*Figure D.1.*). However, because we consistently observed that CHOP protein expression was increased on Day 2 of adipogenic differentiation in 3T3-L1 cells overexpressing hCTHRC1, we developed a RNAi strategy to investigate whether *Chop* mRNA knockdown affects the ability of hCTHRC1 overexpression to suppress 3T3-L1 cell adipogenic differentiation. I spent considerable time and effort investigating the *Chop* knockdown efficiency of multiple shRNA constructs, and learned

the hard way that 3T3-L1 cells are exceedingly difficult to directly transfect with retroviral plasmid vectors. I observed that nucleofection strategies augment 3T3-L1 cell transfection efficiency in comparison to lipofectamine-based procedures; however, in hindsight, I made the critical mistake of using single-cell cloning strategies to propagate puromycin-selected 3T3-L1 cells, which resulted in populations of transfected cells with meager abilities to differentiate into adipocytes in culture (data not shown). To further avoid the pitfalls of these *Chop* knockdown experiments using 3T3-L1 cells, we next acquired age-matched wildtype and *Chop*-null C57BL/6 male mice from which I harvested stromal vascular cells from inguinal white adipose tissue. These primary stromal cells were transduced with control or hCTHRC1-expressing adenovirus, and then subjected to chemically stimulated adipogenic differentiation (*Figure D.1.*) supporting that CHOP does not regulate the ability of hCTHRC1 overexpression to suppress adipogenesis *in vitro*. Using 3T3-L1 cells, I later observed that application of hCTHRC1 conditioned medium markedly suppressed CHOP protein expression on Day 0 and Day 2 relative to the onset of chemically stimulated adipogenic differentiation (*Figure D.1.*). Since CHOP protein expression has been shown to be induced by endoplasmic reticulum (ER) stress (101), it is plausible that increased CHOP protein levels observed on Day 2 of adipogenic differentiation in 3T3-L1 cells overexpressing hCTHRC1 (*Figure D.1.*) was an artifact of ER stress primarily attributable to a high degree of adenoviral-mediated hCTHRC1 synthesis and ER processing.

The co-culture data presented in *Figure 5* support the hypothesis that CTHRC1 could exert its anti-adipogenic effects in a paracrine manner, and so I next started to develop the methodology of applying secreted CTHRC1 to cells in the form of the conditioned medium. The choice to focus on conditioned medium was attributed to the limitation that we did not possess a reliable form of recombinant human CTHRC1 (though recently, colleagues of Dr. Lindner at

Boehringer Ingelheim have produced recombinant CTHRC1 with demonstrated pro-glycolytic activity in cultured endothelial cells, and it remains to be determined if it also possesses anti-adipogenic activity). During the early stages of my work with conditioned medium, I would let secreted CTHRC1 accumulate in cell culture medium for a period of 4 days. When I applied this "4-days-old" hCTHRC1 conditioned medium to confluent 3T3-L1 cells, for example, I was not able to observe evidence for the binding of hCTHRC1 based on Western blotting (data not shown). This included studies in which 3T3-L1 cells were incubated with hCTHRC1 conditioned medium on ice in the presence of a chemical crosslinker (data not shown). I then took a shot in the dark and decided to first apply 4-days-old hCTHRC1 conditioned medium to 3T3-L1 cells before they reached 100% confluence. While application of 4-days-old hCTHRC1 conditioned medium did not produce an anti-adipogenic effect when 3T3-L1 cells were chemically stimulated to undergo adipogenic differentiation, I did observe evidence for the putative binding of hCTHRC1 to these cells comparable to the Western blot data presented in *Figure 8*. Out of curiosity, on several occasions after collecting 4-days-old hCTHRC1 conditioned medium from 3T3-L1 cells that had been transduced with hCTHRC1-expressing adenovirus, I replenished the cell culture dishes with full-serum DMEM and observed for how long the cells would survive. Interestingly, after about 10 days, 3T3-L1 cells that had been transduced with hCTHRC1-expressing adenovirus began to undergo spontaneous adipogenic differentiation, unlike control transduced cells, based on the observation that some 3T3-L1 cells started to accumulate lipid droplets (data not shown). This led me to speculate that CTHRC1 might also enhance the expression of a pro-adipogenic secreted factor that, when expressed above a certain threshold, could nullify the anti-adipogenic effect of CTHRC1 itself (a hypothesized negative feedback loop of sorts). Based on this theory, I started collecting hCTHRC1 conditioned medium at earlier

intervals, and observed that some "batches" of hCTHRC1 conditioned medium collected 2 days after adenoviral transduction would produce an anti-adipogenic effect, while 1-day-old hCTHRC1 conditioned medium produced a consistent anti-adipogenic effect based on Oil Red O staining (*Figure E.1.*), though the percent reduction in Oil Red O staining compared to 3T3-L1 cells treated with βgal conditioned medium was variable – some iterations (*i.e.*, "batches") of 1-day-old hCTHRC1 conditioned medium produced a 15% reduction in Oil Red O staining, while others yielded a 40% reduction (data not shown). In hopes of addressing mechanistic elements as part of my thesis work (*e.g.*, Rho/Rac1 and SOX9 signaling), I knew I needed to produce hCTHRC1 conditioned medium that produced a consistent anti-adipogenic effect from "batch" to "batch," and ultimately found that hCTHRC1 conditioned medium collected 15 hours following the 8-hour adenoviral transduction window of 3T3-L1 cells produced such an effect. As discussed above, while it is certainly plausible that CTHRC1 could enhance the expression of a pro-adipogenic secreted factor that, when expressed above a specific threshold level in conditioned medium, could counteract the anti-adipogenic activity of CTHRC1 (see below for the discussion on immunodepletion), I also speculate that secreted CTHRC1 could become misfolded if it accumulates at too high of a level in conditioned medium. *Figure 4* demonstrates that CTHRC1 present in 15-hours-old hCTHRC1 conditioned medium runs on a Western blot principally as a dimer and trimer under nonreducing conditions, and as a monomer in the presence of the disulfide bond reducing agent, 2-mercaptoethanol. CTHRC1 possesses 10 cysteine residues and, while it is purely conjecture, if secreted CTHRC1 accumulates in conditioned medium above a certain threshold, might it become misfolded or aggregated due to indiscriminate disulfide bonding? Using a similar logic, might secreted CTHRC1 require chaperone proteins to maintain its proper folding and biological activity? If secreted CTHRC1

reaches a certain concentration in conditioned medium (or along its journey in the secretory pathway), could the endogenous supply of CTHRC1 chaperone proteins become exhausted thus resulting in misfolded, inactive secreted CTHRC1? While it is not yet fully understood, 15-hours-old hCTHRC1 conditioned medium nevertheless displays robust, reproducible anti-adipogenic activity.

Molecular investigations of how CTHRC1 interacts with cell surface receptors and other proteins has not been the focus of my thesis research. However, in my investigation of the putative CTHRC1-SOX9 signaling axis, I have stumbled upon certain observations that potentially relate to how CTHRC1 signals through cell surface receptors. As discussed at greater length in the Chapter 3 Discussion (*3.15*), G(q) protein-coupled receptor signaling has been shown to activate both Rho and Rac1 (76). More specifically, activation of Rho and Rac1 was shown to be mediated by the guanine nucleotide exchange factor, TRIO, which is directly activated by guanine nucleotide-binding protein alpha-q (76). From private discussion with Dr. Evi Kostenis at the University of Bonn, who is a world leader in G protein-coupled receptor signaling, Dr. Kostenis gifted me the selective inhibitor of guanine nucleotide-binding protein alpha-q that was synthesized in her laboratory, FR900359 (102). Intriguingly, application of FR900359 (FR) to 3T3-L1 cells negated the anti-adipogenic effect produced by hCTHRC1 conditioned medium and its ability to enhance SOX9 protein expression levels (*Figure F.1.*). While this work is preliminary and requires the scrutiny of greater quantitation and reproducibility, it is thought provoking to hypothesize that CTHRC1 could regulate G protein-coupled receptor signaling. In thinking further outside the box, I hypothesize that CTHRC1 could signal through the class of adhesion G protein-coupled receptors which are known to bind extracellular matrix or neighboring cell-surface ligands (103). If the hCTHRC1 Western blot

data presented in *Figure 8* are indeed evidence of bona fide CTHRC1 binding, as opposed to a phenomenological artifact of the cell culture materials or methods, then the methodology is fully in place to investigate CTHRC1 binding partners by immunoprecipitation of whole-cell lysate and follow-on mass spectrometry analysis. By extension, immunoprecipitation and subsequent mass spectrometry analysis of hCTHRC1 in 15-hours-old hCTHRC1 conditioned medium could discern whether secreted CTHRC1 binds to other secretome proteins/factors. As far as additional mechanistic insights regarding the anti-adipogenic activity of 15-hours-old hCTHRC1 conditioned medium, application of verteporfin (VP) to 3T3-L1 cells also negated the anti-adipogenic effect of hCTHRC1 conditioned medium while lowering overall levels of adipogenic differentiation based on Oil Red O staining (*Figure G.1.*). VP is an inhibitor of YAP transcriptional activity (104) and could serve as an important tool to help determine whether YAP is a transcriptional activator of *SOX9* gene expression as it pertains to the putative CTHRC1-SOX9 axis of signaling.

Perhaps most critical to the future use and investigation of 15-hours-old hCTHRC1 conditioned medium is to decisively determine whether hCTHRC1 is directly mediating the anti-adipogenic effect produced by this conditioned medium when it is applied to preadipocytes in culture. Fortunately, the methods are almost in place to address this question once and for all. I have observed that streptococcal bacteria-derived Protein G binds hCTHRC1, and have further observed that bovine sera impede the overall efficiency of hCTHRC1 immunoprecipitation (data not shown). From recent ELISA data which confirm the successful removal of hCTHRC1 from conditioned medium (*Figure H.1.*), this promising result was obtained from a series of refinement and optimization. First, 15-hours-old hCTHRC1 conditioned medium was diluted eight times in serum-free DMEM to dilute the overall concentration of bovine sera. Second, anti-

CTHRC1 monoclonal antibody clone Vli13E09 was pre-conjugated to Protein A Sepharose beads prior to conditioned medium incubation. Unfortunately, based on Oil Red O staining (*Figure H.1.*), these data suggest that hCTHRC1 present in hCTHRC1 conditioned medium incubated with control naïve IgG-conjugated Protein A Sepharose is becoming inactivated. One thought is that, given our immunoprecipitation regimen of incubating condition medium with conjugated Protein A Sepharose beads by overnight rotation at 4°C, hCTHRC1 could be aggregating as an artifact of the excessive mechanical rotation. Efforts to confirm the presence of hCTHRC1 aggregate complexes by native (*i.e.*, non-denaturing) immunoblotting were inconclusive (data not shown). If there is any merit to this hypothesis regarding hCTHRC1 aggregation, I am in favor of using a conjugated Protein A Sepharose column such that hCTHRC1 in conditioned medium could be immunoprecipitated by gravity or low speed centrifugation in order to avoid prolonged mechanical rotation strategies. On the other hand, if the results of future immunoprecipitation optimization efforts suggest that Protein A is somehow directly inactivating hCTHRC1, hCTHRC1 could likely be immunoprecipitated using biotinylated Vli13E09 conjugated to a streptavidin column or beads. Alternatively, a neutralizing anti-CTHRC1 antibody could be investigated, developed, or procured. If it is determined that secreted hCTHRC1 does not possess direct anti-adipogenic function, this would support the interesting conclusion that a secreted CTHRC1 effector protein(s) positively mediates the anti-adipogenic activity of 15-hours-old hCTHRC1 conditioned medium, thus warranting deeper investigation into the CTHRC1-regulated secretome to identify such anti-adipogenic secreted factors that enhance SOX9 signaling.

Going back several years to a fortuitous discussion with Dr. Rob Koza, it was determined that *Cthrc1* gene expression levels in mouse inguinal white adipose tissue markedly decline

during postnatal development (*Figure 20A*). I later recapitulated these array data based on qPCR analysis (*Figure 20B*). During early postnatal development, in particular, the adipose tissue compartment is rapidly expanding due to enhanced adipocyte hypertrophy and hyperplasia (85). If CTHRC1 is conclusively determined to be an anti-adipogenic factor, why is its gene expression in mouse inguinal white adipose tissue expressed at high levels during the period of postnatal development when significant adipogenesis is occurring *in vivo*? One approach to address this question would be to determine when CTHRC1 mRNA levels are expressed maximally in the developing adipose of mice. Mouse inguinal white adipose tissue, like other subcutaneous and visceral adipose depots, develops from the mesenchyme and is primarily mesodermal in origin (4). During embryonic development, the earliest recognizable structure resembling an adipose tissue is a cluster of vasculature called a "primitive organ" (4), while PPAR-gamma expression is detectable in mice by embryonic day 14.5 (preceding the development of characteristic adipose tissues) (105). Hypothetically, the observation that *Cthrc1* gene expression in mouse inguinal white adipose tissue decreases more than 100-fold during the period from postnatal day 7 to 3 months of age (*Figure 20A*) could pale in comparison to changes in *Cthrc1* gene expression in the mesenchyme throughout embryonic adipose tissue development. Though speculative, it is plausible that *Cthrc1* gene expression in the mesenchyme of mice on embryonic day 10 versus *Cthrc1* gene expression in nascent adipose tissue on postnatal day 1, for example, could decrease more than 1000-fold. This would suggest that significant downregulation of *Cthrc1* gene expression is requisite for the advancement of perinatal adipose tissue development. Harvesting embryonic mesenchyme and the developing adipose at various timepoints during perinatal and very early postnatal development (*e.g.*, postnatal days 1-3) would provide an excellent platform for RNA sequencing to discern the gene

expression profile of CTHRC1 and other factors throughout the entire course of adipose tissue development *in vivo*. Similarly, implementation of the *Pref1* reporter mouse model characterized by Gulyaeva and colleagues (2) could inform whether CTHRC1 is expressed in $PREF1^{+}$ mesenchymal stem cells within the adipogenic lineage. It is also important to reanalyze the RNA sequencing data of human subcutaneous adipose tissues in which *CTHRC1* and *SOX9* gene expression both clustered in adipose stromal cells expressing high levels of *PDGFRA* and *MFAP5* (*Figure 23*). Fundamentally, are CTHRC1 and SOX9 expressed in the same stromal cell populations of adipose?

The finding that adult *Cthrc1*-null mice are characterized by enhanced adiposity in comparison to age-matched wildtype mice (55) could support that, in a developmental context, CTHRC1 functions to restrict adipogenesis during the perinatal and early postnatal periods of development, thus limiting the overall number of preadipocytes that differentiate into adipocytes. If so, such precocious adipogenesis in *Cthrc1*-null mice during embryonic and early postnatal development could predispose these mutant mice to hyperplastic and hypertrophic adipose tissue phenotypes in adulthood. Feeding adult wildtype and *Cthrc1*-null mice a high-fat diet could further exacerbate those differences in adiposity. Therefore, it is an open question whether CTHRC1 expression is enhanced commensurate to high-fat feeding and functions to restrict diet-induced obesity. It should also be noted that a global, homozygous null mutation in *Sox9* in mice is embryonically lethal (106). The implementation of postnatal *Sox9* gene deletion to assess evidence in support of the putative CTHRC1-SOX9 signaling axis *in vivo* could be achieved using mice with floxed *Sox9* alleles (107). For example, these floxed mice could be crossed with *Cthrc1*-null mice and then challenged with high-fat feeding to determine whether null mutations

in both *Sox9* and *Cthrc1* exacerbate diet-induced obesity, or otherwise promote hyperplastic/hypertrophic adipose phenotypes in mice fed a standard chow diet.

I will conclude this chapter by offering some final perspectives on how readily available data and experimental resources could aid the advancement of CTHRC1 research in the field of adipose tissue biology. Like *Cthrc1* (*Figure 20A*), many genes expressed in mouse inguinal white adipose tissue are characterized by decreasing levels of expression during early postnatal development, including *Pref1*, *Igf2* (Insulin-like growth factor II), and *Fn1* (Fibronectin) (3). In connection to SOX9 signaling, the cleaved extracellular domain of PREF1 has been shown to bind fibronectin in the extracellular matrix thus stabilizing fibronectin-integrin receptor interactions which positively regulate *SOX9* gene expression (42). Application of hCTHRC1 conditioned medium to 3T3-L1 cells produced a variable effect on PREF1 expression at the mRNA and protein levels during the course of chemically stimulated adipogenic differentiation (*Figure I.1.*). Regardless, by Western blot analysis, it would be important to determine whether application of hCTHRC1 conditioned medium enhances the enzymatic cleavage of PREF1. The extracellular domain of PREF1 is cleaved by disintegrin and metalloproteinase domain-containing protein 17 (ADAM17) (42). In addition, several small molecules are known to inhibit the enzymatic activity of ADAM17, including TAPI 1 (108), which could be useful in the investigation of whether hCTHRC1 conditioned medium enhances PREF1 cleavage via the activity of ADAM17. I have also shown that hCTHRC1 conditioned medium enhances *Fn1* gene expression and decreases *Col1a1* gene expression in 3T3-L1 cells (*Figure J.1.*). LeClair and colleagues also showed that overexpression of CTHRC1 decreased type 1 collagen protein expression levels in smooth muscle cells (52). These collective data support the notion that CTHRC1 regulates the collagen extracellular matrix. It is well documented that an abundance of

collagen fibers in the extracellular matrix promote a "rigid," mechanically tense matrix that can cause adipocyte hypertrophy and insulin resistance (4). Therefore, it would also be important to determine whether CTHRC1 promotes collagen extracellular matrix remodeling in adipose tissues. Finally, I showed that hCTHRC1 conditioned medium enhances *Igf2* gene expression in 3T3-L1 cells (*Figure J.1.*). IGF-II has been shown to preserve the stemness and renewal of adipose-derived stromal cells (109) and promote glucose metabolism (110). To this end, questions arise regarding the effect of CTHRC1 on the regulation of the secretome, and whether factors including IGF-II contribute to the boarder scope of CTHRC1 signaling *in vivo*.

In conclusion, the investigation of the CTHRC1-regulated secretome is an important step forward in determining how CTHRC1 exudes its anti-adipogenic effect and whether its biological activity is mediated by potential binding partners in the extracellular milieu. In a preliminary assessment of the CTHRC1-regulated secretome, 3T3-L1 cells were transduced with control or hCTHRC1-expressing adenovirus, after which conditioned media were collected 2, 4, or 8 days thereafter. The presence of hCTHRC1 in 2-, 4-, and 8-days-old hCTHRC1 conditioned media was confirmed by ELISA (data not shown), and conditioned media were then subjected to proteomic analysis by mass spectrometry (*Table L.1.*). Although hCTHRC1 was not detected by mass spectrometry analysis, the secretome analysis did show, for example, that secreted protein acidic and rich in cysteine (SPARC) had increasing fold expression values in hCTHRC1 conditioned medium (*Table L.1.*). In comparison to control βgal conditioned media, SPARC registered a nearly 4-fold increase in 2-days-old hCTHRC1 conditioned medium, a 28-fold increase in 4-days-old hCTHRC1 conditioned medium (though this did not reach statistical significance, and these data are not shown), and a greater than 150-fold increase in 8-days-old hCTHRC1 conditioned medium. Intriguingly, by Western blot analysis, SPARC was expressed

at the same levels in βgal and hCTHRC1 conditioned media (*Figure K.1.*). Also, treatment of 3T3-L1 cells with hCTHRC1 conditioned medium did not enhance *Sparc* mRNA expression levels (*Figure K.1.*). Taken together, I hypothesize that the results of the preliminary secretome analysis can be explained on the basis that SPARC binds to secreted hCTHRC1, and potentially masks the ability of hCTHRC1 to be detected by mass spectrometry. SPARC is known to regulate extracellular matrix-integrin interactions (111) and, while wholly speculative, if SPARC is a binding partner of secreted CTHRC1, how might this interaction regulate the ability of CTHRC1 to signal through cell surface receptors? Does SPARC potentially inhibit CTHRC1 activity, thus explaining why 4-days-old hCTHRC1 conditioned medium, for example, did not produce an anti-adipogenic effect when applied to 3T3-L1 cells (*Figure E.1.*)? By extension of this logic, might 15-hours-old hCTHRC1 conditioned medium exude significant anti-adipogenic activity on the basis that SPARC does not appreciably accumulate in conditioned medium during this window of time (*Figure K.1.*)?

Collectively, these are just some of the questions that can be gleaned from the body of my thesis research; questions which I hope you find helpful and potentially thought provoking. Also included for your reference are quantitative proteomic data based on adenovirally transduced 3T3-L1 cells overexpressing hCTHRC1 (*Table M.1.*). The table reflects statistically significant differentially expressed proteins, and is organized such that control transduced 3T3-L1 cells (βgal) are normalized to hCTHRC1-overexpressing 3T3-L1 cells (*Table M.1.*). That said, I want to personally welcome you to this field. Please do not hesitate to contact me should you have any questions. Also, please keep me informed on your research progress, and good luck! I look forward to your future correspondence. For your reference, below is a summation of future directions that I think are necessary and important to pursue:

- Removal of hCTHRC1 from conditioned medium (is hCTHRC1 a direct negative regulator of adipogenic signaling?)

- Assessment of whether recombinant CTHRC1 produced at Boehringer Ingelheim possesses anti-adipogenic activity

- Are CTHRC1 and SOX9 expressed in the same stromal cell populations of adipose?

- Does CTHRC1 regulate SOX9 posttranslational modifications and DNA binding activity?

- RNA sequencing of white adipose tissue during perinatal and very early postnatal development. Therein, how does the CTHRC1 gene expression profile change?

- Evaluation of the CTHRC1-regulated secretome, proteome, and phospho-proteome

REFERENCES

1. Berger E, Geloen A. FABP4 Controls Fat Mass Expandability (Adipocyte Size and Number) through Inhibition of CD36/SR-B2 Signalling. Int J Mol Sci. 2023;24(2).

2. Gulyaeva O, Nguyen H, Sambeat A, Heydari K, Sul HS. Sox9-Meis1 Inactivation Is Required for Adipogenesis, Advancing Pref-1(+) to PDGFRalpha(+) Cells. Cell Rep. 2018;25(4):1002-17 e4.

3. Koza RA, Nikonova L, Hogan J, Rim JS, Mendoza T, Faulk C, et al. Changes in gene expression foreshadow diet-induced obesity in genetically identical mice. PLoS Genet. 2006;2(5):e81.

4. Rosen ED, Spiegelman BM. What we talk about when we talk about fat. Cell. 2014;156(1-2):20-44.

5. Tang QQ, Lane MD. Adipogenesis: from stem cell to adipocyte. Annu Rev Biochem. 2012;81:715-36.

6. van Kruijsdijk RC, van der Wall E, Visseren FL. Obesity and cancer: the role of dysfunctional adipose tissue. Cancer Epidemiol Biomarkers Prev. 2009;18(10):2569-78.

7. Grabner GF, Xie H, Schweiger M, Zechner R. Lipolysis: cellular mechanisms for lipid mobilization from fat stores. Nat Metab. 2021;3(11):1445-65.

8. Nussbaumerova B, Rosolova H. Obesity and Dyslipidemia. Curr Atheroscler Rep. 2023.

9. van Herpen NA, Schrauwen-Hinderling VB. Lipid accumulation in non-adipose tissue and lipotoxicity. Physiol Behav. 2008;94(2):231-41.

10. Lefterova MI, Haakonsson AK, Lazar MA, Mandrup S. PPARgamma and the global map of adipogenesis and beyond. Trends Endocrinol Metab. 2014;25(6):293-302.

11. Keenan SN, De Nardo W, Lou J, Schittenhelm RB, Montgomery MK, Granneman JG, et al. Perilipin 5 S155 phosphorylation by PKA is required for the control of hepatic lipid metabolism and glycemic control. J Lipid Res. 2021;62:100016.

12. Kersten S. Mechanisms of nutritional and hormonal regulation of lipogenesis. EMBO Rep. 2001;2(4):282-6.

13. DiPilato LM, Ahmad F, Harms M, Seale P, Manganiello V, Birnbaum MJ. The Role of PDE3B Phosphorylation in the Inhibition of Lipolysis by Insulin. Mol Cell Biol. 2015;35(16):2752-60.

14. Tardelli M. Monoacylglycerol lipase reprograms lipid precursors signaling in liver disease. World J Gastroenterol. 2020;26(25):3577-85.

15. Bruno MJ, Rusinova R, Gleason NJ, Koeppe RE, 2nd, Andersen OS. Interactions of drugs and amphiphiles with membranes: modulation of lipid bilayer elastic properties by changes in acyl chain unsaturation and protonation. Faraday Discuss. 2013;161:461-80; discussion 563-89.

16. Pashkovskaya AA, Vazdar M, Zimmermann L, Jovanovic O, Pohl P, Pohl EE. Mechanism of Long-Chain Free Fatty Acid Protonation at the Membrane-Water Interface. Biophys J. 2018;114(9):2142-51.

17. Liaw L, Prudovsky I, Koza RA, Anunciado-Koza RV, Siviski ME, Lindner V, et al. Lipid Profiling of In Vitro Cell Models of Adipogenic Differentiation: Relationships With Mouse Adipose Tissues. J Cell Biochem. 2016;117(9):2182-93.

18. Merrick D, Sakers A, Irgebay Z, Okada C, Calvert C, Morley MP, et al. Identification of a mesenchymal progenitor cell hierarchy in adipose tissue. Science. 2019;364(6438).

19. Iwayama T, Steele C, Yao L, Dozmorov MG, Karamichos D, Wren JD, Olson LE. PDGFRalpha signaling drives adipose tissue fibrosis by targeting progenitor cell plasticity. Genes Dev. 2015;29(11):1106-19.

20. Rodeheffer MS, Birsoy K, Friedman JM. Identification of white adipocyte progenitor cells in vivo. Cell. 2008;135(2):240-9.

21. Gavin KM, Sullivan TM, Maltzahn JK, Rahkola JT, Acosta AS, Kohrt WM, et al. Hematopoietic stem cells produce intermediate lineage adipocyte progenitors that simultaneously express both myeloid and mesenchymal lineage markers in adipose tissue. Adipocyte. 2021;10(1):394-407.

22. Zhu Q, Zhu Y, Hepler C, Zhang Q, Park J, Gliniak C, et al. Adipocyte mesenchymal transition contributes to mammary tumor progression. Cell Rep. 2022;40(11):111362.

23. Marangoni RG, Korman B, Varga J. Adipocytic Progenitor Cells Give Rise to Pathogenic Myofibroblasts: Adipocyte-to-Mesenchymal Transition and Its Emerging Role in Fibrosis in Multiple Organs. Curr Rheumatol Rep. 2020;22(11):79.

24. Modica S, Wolfrum C. The dual role of BMP4 in adipogenesis and metabolism. Adipocyte. 2017;6(2):141-6.

25. Ahmad B, Serpell CJ, Fong IL, Wong EH. Molecular Mechanisms of Adipogenesis: The Anti-adipogenic Role of AMP-Activated Protein Kinase. Front Mol Biosci. 2020;7:76.

26. Bowers RR, Lane MD. Wnt signaling and adipocyte lineage commitment. Cell Cycle. 2008;7(9):1191-6.

27. Briscoe J, Therond PP. The mechanisms of Hedgehog signalling and its roles in development and disease. Nat Rev Mol Cell Biol. 2013;14(7):416-29.

28. Cha JY, Kim HJ, Yu JH, Xu J, Kim D, Paul BD, et al. Dexras1 mediates glucocorticoid-associated adipogenesis and diet-induced obesity. Proc Natl Acad Sci U S A. 2013;110(51):20575-80.

29. Kemppainen RJ, Behrend EN. Dexamethasone rapidly induces a novel ras superfamily member-related gene in AtT-20 cells. J Biol Chem. 1998;273(6):3129-31.

30. Lochhead PA, Kinstrie R, Sibbet G, Rawjee T, Morrice N, Cleghon V. A chaperone-dependent GSK3beta transitional intermediate mediates activation-loop autophosphorylation. Mol Cell. 2006;24(4):627-33.

31. Thornton TM, Pedraza-Alva G, Deng B, Wood CD, Aronshtam A, Clements JL, et al. Phosphorylation by p38 MAPK as an alternative pathway for GSK3beta inactivation. Science. 2008;320(5876):667-70.

32. Kim JW, Tang QQ, Li X, Lane MD. Effect of phosphorylation and S-S bond-induced dimerization on DNA binding and transcriptional activation by C/EBPbeta. Proc Natl Acad Sci U S A. 2007;104(6):1800-4.

33. Scott LM, Civin CI, Rorth P, Friedman AD. A novel temporal expression pattern of three C/EBP family members in differentiating myelomonocytic cells. Blood. 1992;80(7):1725-35.

34. Tang QQ, Lane MD. Activation and centromeric localization of CCAAT/enhancer-binding proteins during the mitotic clonal expansion of adipocyte differentiation. Genes Dev. 1999;13(17):2231-41.

35. Guo L, Li X, Tang QQ. Transcriptional regulation of adipocyte differentiation: a central role for CCAAT/enhancer-binding protein (C/EBP) beta. J Biol Chem. 2015;290(2):755-61.

36. Ross SE, Erickson RL, Hemati N, MacDougald OA. Glycogen synthase kinase 3 is an insulin-regulated C/EBPalpha kinase. Mol Cell Biol. 1999;19(12):8433-41.

37. Nellinger S, Kluger PJ. How Mechanical and Physicochemical Material Characteristics Influence Adipose-Derived Stem Cell Fate. International Journal of Molecular Sciences. 2023;24(4).

38. Perkins RS, Singh R, Abell AN, Krum SA, Miranda-Carboni GA. The role of WNT10B in physiology and disease: A 10-year update. Front Cell Dev Biol. 2023;11:1120365.

39. Chen G, Deng C, Li Y-P. TGF-β and BMP Signaling in Osteoblast Differentiation and Bone Formation. International Journal of Biological Sciences. 2012;8(2):272-88.

40. Wan Y, Salminen M, Zuo H, Huynh H, Li X. Gata2 Is a Rheostat for Mesenchymal Stem Cell Fate in Male Mice. Endocrinology. 2016;157(3):1021-8.

41. Lefebvre V, Dvir-Ginzberg M. SOX9 and the many facets of its regulation in the chondrocyte lineage. Connective Tissue Research. 2016;58(1):2-14.

42. Wang Y, Sul HS. Pref-1 regulates mesenchymal cell commitment and differentiation through Sox9. Cell Metab. 2009;9(3):287-302.

43. Pyagay P, Heroult M, Wang Q, Lehnert W, Belden J, Liaw L, et al. Collagen triple helix repeat containing 1, a novel secreted protein in injured and diseased arteries, inhibits collagen expression and promotes cell migration. Circ Res. 2005;96(2):261-8.

44. Leclere L, Nir TS, Bazarsky M, Braitbard M, Schneidman-Duhovny D, Gat U. Dynamic Evolution of the Cthrc1 Genes, a Newly Defined Collagen-Like Family. Genome Biol Evol. 2020;12(2):3957-70.

45. Mei D, Zhu Y, Zhang L, Wei W. The Role of CTHRC1 in Regulation of Multiple Signaling and Tumor Progression and Metastasis. Mediators Inflamm. 2020;2020:9578701.

46. Leclair RJ, Wang Q, Benson MA, Prudovsky I, Lindner V. Intracellular localization of Cthrc1 characterizes differentiated smooth muscle. Arterioscler Thromb Vasc Biol. 2008;28(7):1332-8.

47. Toomey BH, Mitrovic SA, Lindner-Liaw M, Leon Vazquez RG, Kacer D, Ryzhov S, et al. Activated CTHRC1 promotes glycolysis in endothelial cells: Implications for metabolism and angiogenesis. Vascul Pharmacol. 2023;153:107246.

48. Peterson JM, Wei Z, Wong GW. C1q/TNF-related protein-3 (CTRP3), a novel adipokine that regulates hepatic glucose output. J Biol Chem. 2010;285(51):39691-701.

49. Gaboriaud C, Frachet P, Thielens NM, Arlaud GJ. The Human C1q Globular Domain: Structure and Recognition of Non-Immune Self Ligands. Frontiers in Immunology. 2012;2.

50. Yamamoto S, Nishimura O, Misaki K, Nishita M, Minami Y, Yonemura S, et al. Cthrc1 selectively activates the planar cell polarity pathway of Wnt signaling by stabilizing the Wnt-receptor complex. Dev Cell. 2008;15(1):23-36.

51. Liu G, Sengupta PK, Jamal B, Yang HY, Bouchie MP, Lindner V, et al. N-glycosylation induces the CTHRC1 protein and drives oral cancer cell migration. J Biol Chem. 2013;288(28):20217-27.

52. LeClair RJ, Durmus T, Wang Q, Pyagay P, Terzic A, Lindner V. Cthrc1 is a novel inhibitor of transforming growth factor-beta signaling and neointimal lesion formation. Circ Res. 2007;100(6):826-33.

53. Durmus T, LeClair RJ, Park KS, Terzic A, Yoon JK, Lindner V. Expression analysis of the novel gene collagen triple helix repeat containing-1 (Cthrc1). Gene Expr Patterns. 2006;6(8):935-40.

54. Jin YR, Stohn JP, Wang Q, Nagano K, Baron R, Bouxsein ML, et al. Inhibition of osteoclast differentiation and collagen antibody-induced arthritis by CTHRC1. Bone. 2017;97:153-67.

55. Stohn JP, Wang Q, Siviski ME, Kennedy K, Jin YR, Kacer D, et al. Cthrc1 controls adipose tissue formation, body composition, and physical activity. Obesity (Silver Spring). 2015;23(8):1633-42.

56. Jiang N, Cui Y, Liu J, Zhu X, Wu H, Yang Z, Ke Z. Multidimensional Roles of Collagen Triple Helix Repeat Containing 1 (CTHRC1) in Malignant Cancers. J Cancer. 2016;7(15):2213-20.

57. Myngbay A, Manarbek L, Ludbrook S, Kunz J. The Role of Collagen Triple Helix Repeat-Containing 1 Protein (CTHRC1) in Rheumatoid Arthritis. Int J Mol Sci. 2021;22(5).

58. Lv Y, Zhang L, Ma J, Fei X, Xu K, Lin J. CTHRC1 overexpression promotes ectopic endometrial stromal cell proliferation, migration and invasion via activation of the Wnt/beta-catenin pathway. Reprod Biomed Online. 2020;40(1):26-32.

59. Yang XM, You HY, Li Q, Ma H, Wang YH, Zhang YL, et al. CTHRC1 promotes human colorectal cancer cell proliferation and invasiveness by activating Wnt/PCP signaling. Int J Clin Exp Pathol. 2015;8(10):12793-801.

60. Matsuoka K, Kohara Y, Naoe Y, Watanabe A, Ito M, Ikeda K, Takeshita S. WAIF1 Is a Cell-Surface CTHRC1 Binding Protein Coupling Bone Resorption and Formation. J Bone Miner Res. 2018;33(8):1500-12.

61. Guo W, Keckesova Z, Donaher JL, Shibue T, Tischler V, Reinhardt F, et al. Slug and Sox9 cooperatively determine the mammary stem cell state. Cell. 2012;148(5):1015-28.

62. Stohn JP, Perreault NG, Wang Q, Liaw L, Lindner V. Cthrc1, a novel circulating hormone regulating metabolism. PLoS One. 2012;7(10):e47142.

63. Angueira AR, Sakers AP, Holman CD, Cheng L, Arbocco MN, Shamsi F, et al. Defining the lineage of thermogenic perivascular adipose tissue. Nat Metab. 2021;3(4):469-84.

64. Sun W, Dong H, Balaz M, Slyper M, Drokhlyansky E, Colleluori G, et al. snRNA-seq reveals a subpopulation of adipocytes that regulates thermogenesis. Nature. 2020;587(7832):98-102.

65. Hao Y, Hao S, Andersen-Nissen E, Mauck WM, 3rd, Zheng S, Butler A, et al. Integrated analysis of multimodal single-cell data. Cell. 2021;184(13):3573-87 e29.

66. Villanueva RAM, Chen ZJ. ggplot2: Elegant Graphics for Data Analysis (2nd ed.). Measurement: Interdisciplinary Research and Perspectives. 2019;17(3):160-7.

67. Ruiz-Villalba A, Romero JP, Hernandez SC, Vilas-Zornoza A, Fortelny N, Castro-Labrador L, et al. Single-Cell RNA Sequencing Analysis Reveals a Crucial Role for CTHRC1 (Collagen Triple Helix Repeat Containing 1) Cardiac Fibroblasts After Myocardial Infarction. Circulation. 2020;142(19):1831-47.

68. Zhao X, Hu H, Wang C, Bai L, Wang Y, Wang W, Wang J. A comparison of methods for effective differentiation of the frozen-thawed 3T3-L1 cells. Anal Biochem. 2019;568:57-64.

69. Wolins NE, Quaynor BK, Skinner JR, Tzekov A, Park C, Choi K, Bickel PE. OP9 mouse stromal cells rapidly differentiate into adipocytes: characterization of a useful new model of adipogenesis. J Lipid Res. 2006;47(2):450-60.

70. Hironaka T, Takizawa N, Yamauchi Y, Horii Y, Nakaya M. The well-developed actin cytoskeleton and Cthrc1 expression by actin-binding protein drebrin in myofibroblasts promote cardiac and hepatic fibrosis. J Biol Chem. 2023;299(3):102934.

71. Hansson B, Moren B, Fryklund C, Vliex L, Wasserstrom S, Albinsson S, et al. Adipose cell size changes are associated with a drastic actin remodeling. Sci Rep. 2019;9(1):12941.

72. Ma MZ, Zhuang C, Yang XM, Zhang ZZ, Ma H, Zhang WM, et al. CTHRC1 acts as a prognostic factor and promotes invasiveness of gastrointestinal stromal tumors by activating Wnt/PCP-Rho signaling. Neoplasia. 2014;16(3):265-78, 78 e1-13.

73. Gao Y, Dickerson JB, Guo F, Zheng J, Zheng Y. Rational design and characterization of a Rac GTPase-specific small molecule inhibitor. Proc Natl Acad Sci U S A. 2004;101(20):7618-23.

74. Narumiya S, Ishizaki T, Uehata M. Use and properties of ROCK-specific inhibitor Y-27632. Methods Enzymol. 2000;325:273-84.

75. Lorthongpanich C, Thumanu K, Tangkiettrakul K, Jiamvoraphong N, Laowtammathron C, Damkham N, et al. YAP as a key regulator of adipo-osteogenic differentiation in human MSCs. Stem Cell Res Ther. 2019;10(1):402.

76. Feng X, Degese MS, Iglesias-Bartolome R, Vaque JP, Molinolo AA, Rodrigues M, et al. Hippo-independent activation of YAP by the GNAQ uveal melanoma oncogene through a trio-regulated rho GTPase signaling circuitry. Cancer Cell. 2014;25(6):831-45.

77. Mubtasim N, Gollahon L. Characterizing 3T3-L1 MBX Adipocyte Cell Differentiation Maintained with Fatty Acids as an In Vitro Model to Study the Effects of Obesity. Life (Basel). 2023;13(8).

78. Audano M, Pedretti S, Ligorio S, Gualdrini F, Polletti S, Russo M, et al. Zc3h10 regulates adipogenesis by controlling translation and F-actin/mitochondria interaction. J Cell Biol. 2021;220(3).

79. Anton IM, Wandosell F. WIP, YAP/TAZ and Actin Connections Orchestrate Development and Transformation in the Central Nervous System. Front Cell Dev Biol. 2021;9:673986.

80. Seo J, Kim J. Regulation of Hippo signaling by actin remodeling. BMB Rep. 2018;51(3):151-6.

81. Liu Y, Zhuo S, Zhou Y, Ma L, Sun Z, Wu X, et al. Yap-Sox9 signaling determines hepatocyte plasticity and lineage-specific hepatocarcinogenesis. J Hepatol. 2022;76(3):652-64.

82. Haudenschild DR, Chen J, Pang N, Lotz MK, D'Lima DD. Rho kinase-dependent activation of SOX9 in chondrocytes. Arthritis Rheum. 2010;62(1):191-200.

83. Al-Zahrani KN, Abou-Hamad J, Pascoal J, Labreche C, Garland B, Sabourin LA. AKT-mediated phosphorylation of Sox9 induces Sox10 transcription in a murine model of HER2-positive breast cancer. Breast Cancer Res. 2021;23(1):55.

84. Yang Y, Du J, Hu Z, Liu J, Tian Y, Zhu Y, et al. Activation of Rac1-PI3K/Akt is required for epidermal growth factor-induced PAK1 activation and cell migration in MDA-MB-231 breast cancer cells. J Biomed Res. 2011;25(4):237-45.

85. Bruder J, Fromme T. Global Adipose Tissue Remodeling During the First Month of Postnatal Life in Mice. Front Endocrinol (Lausanne). 2022;13:849877.

86. Yang Loureiro Z, Joyce S, DeSouza T, Solivan-Rivera J, Desai A, Skritakis P, et al. Wnt signaling preserves progenitor cell multipotency during adipose tissue development. Nat Metab. 2023;5(6):1014-28.

87. Vaittinen M, Kolehmainen M, Ryden M, Eskelinen M, Wabitsch M, Pihlajamaki J, et al. MFAP5 is related to obesity-associated adipose tissue and extracellular matrix remodeling and inflammation. Obesity (Silver Spring). 2015;23(7):1371-8.

88. Zhang T, Li H, Sun S, Zhou W, Zhang T, Yu Y, et al. Microfibrillar-associated protein 5 suppresses adipogenesis by inhibiting essential coactivator of PPARgamma. Sci Rep. 2023;13(1):5589.

89. Wang Y, Wang R, Li B, Huang Z, Zhao S, Chen S, et al. Cancer-associated fibroblasts in the invasive tumour front promote the metastasis of oral squamous cell carcinoma through MFAP5 upregulation. Gene. 2023;876:147504.

90. Muhl L, Genové G, Leptidis S, Liu J, He L, Mocci G, et al. Single-cell analysis uncovers fibroblast heterogeneity and criteria for fibroblast and mural cell identification and discrimination. Nature Communications. 2020;11(1).

91. Marcelin G, Ferreira A, Liu Y, Atlan M, Aron-Wisnewsky J, Pelloux V, et al. A PDGFRalpha-Mediated Switch toward CD9(high) Adipocyte Progenitors Controls Obesity-Induced Adipose Tissue Fibrosis. Cell Metab. 2017;25(3):673-85.

92. Lowe CE, O'Rahilly S, Rochford JJ. Adipogenesis at a glance. J Cell Sci. 2011;124(Pt 16):2681-6.

93. Ming Z, Vining B, Bagheri-Fam S, Harley V. SOX9 in organogenesis: shared and unique transcriptional functions. Cell Mol Life Sci. 2022;79(10):522.

94. Mertin S, McDowall SG, Harley VR. The DNA-binding specificity of SOX9 and other SOX proteins. Nucleic Acids Res. 1999;27(5):1359-64.

95. Huang YH, Jankowski A, Cheah KS, Prabhakar S, Jauch R. SOXE transcription factors form selective dimers on non-compact DNA motifs through multifaceted interactions between dimerization and high-mobility group domains. Sci Rep. 2015;5:10398.

96. Hattori T, Coustry F, Stephens S, Eberspaecher H, Takigawa M, Yasuda H, de Crombrugghe B. Transcriptional regulation of chondrogenesis by coactivator Tip60 via chromatin association with Sox9 and Sox5. Nucleic Acids Res. 2008;36(9):3011-24.

97. Lefebvre V, Angelozzi M, Haseeb A. SOX9 in cartilage development and disease. Curr Opin Cell Biol. 2019;61:39-47.

98. Balsalobre A, Drouin J. Pioneer factors as master regulators of the epigenome and cell fate. Nat Rev Mol Cell Biol. 2022;23(7):449-64.

99. Tang QQ, Lane MD. Role of C/EBP homologous protein (CHOP-10) in the programmed activation of CCAAT/enhancer-binding protein-beta during adipogenesis. Proc Natl Acad Sci U S A. 2000;97(23):12446-50.

100. Horndasch M, Lienkamp S, Springer E, Schmitt A, Pavenstadt H, Walz G, Gloy J. The C/EBP homologous protein CHOP (GADD153) is an inhibitor of Wnt/TCF signals. Oncogene. 2006;25(24):3397-407.

101. Oyadomari S, Mori M. Roles of CHOP/GADD153 in endoplasmic reticulum stress. Cell Death Differ. 2004;11(4):381-9.

102. Schrage R, Schmitz AL, Gaffal E, Annala S, Kehraus S, Wenzel D, et al. The experimental power of FR900359 to study Gq-regulated biological processes. Nat Commun. 2015;6:10156.

103. Stoveken HM, Hajduczok AG, Xu L, Tall GG. Adhesion G protein-coupled receptors are activated by exposure of a cryptic tethered agonist. Proc Natl Acad Sci U S A. 2015;112(19):6194-9.

104. Feng J, Gou J, Jia J, Yi T, Cui T, Li Z. Verteporfin, a suppressor of YAP-TEAD complex, presents promising antitumor properties on ovarian cancer. Onco Targets Ther. 2016;9:5371-81.

105. Berry DC, Stenesen D, Zeve D, Graff JM. The developmental origins of adipose tissue. Development. 2013;140(19):3939-49.

106. Akiyama H, Chaboissier MC, Martin JF, Schedl A, de Crombrugghe B. The transcription factor Sox9 has essential roles in successive steps of the chondrocyte differentiation pathway and is required for expression of Sox5 and Sox6. Genes Dev. 2002;16(21):2813-28.

107. Barrionuevo F, Bagheri-Fam S, Klattig J, Kist R, Taketo MM, Englert C, Scherer G. Homozygous inactivation of Sox9 causes complete XY sex reversal in mice. Biol Reprod. 2006;74(1):195-201.

108. Sommer C, Schmidt C, George A, Toyka KV. A metalloprotease-inhibitor reduces pain associated behavior in mice with experimental neuropathy. Neurosci Lett. 1997;237(1):45-8.

109. Wang C, Li X, Dang H, Liu P, Zhang BO, Xu F. Insulin-like growth factor 2 regulates the proliferation and differentiation of rat adipose-derived stromal cells via IGF-1R and IR. Cytotherapy. 2019;21(6):619-30.

110. Uchimura T, Hollander JM, Nakamura DS, Liu Z, Rosen CJ, Georgakoudi I, Zeng L. An essential role for IGF2 in cartilage development and glucose metabolism during postnatal long bone growth. Development. 2017;144(19):3533-46.

111. Arnold SA, Brekken RA. SPARC: a matricellular regulator of tumorigenesis. J Cell Commun Signal. 2009;3(3-4):255-73.

APPENDICES

APPENDIX A: CTHRC1 regulates the F-actin cytoskeleton

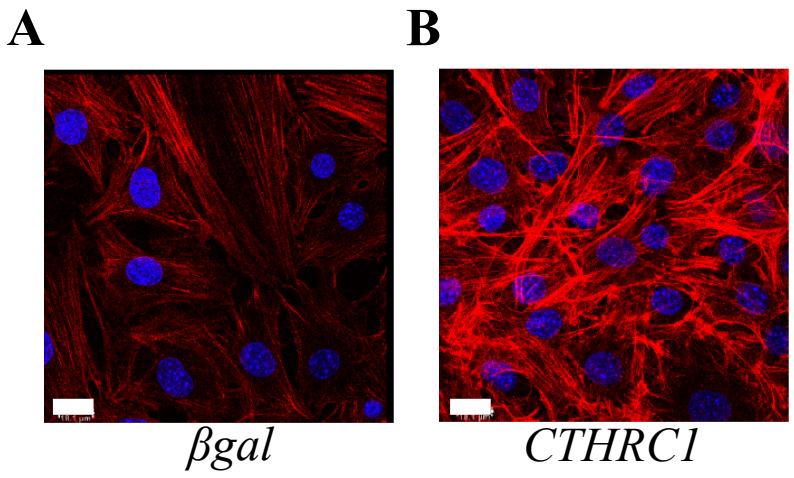

Figure A.1. CTHRC1 enhances the F-actin cytoskeleton. Representative confocal microscopy images of the enhanced F-actin cytoskeleton in cells overexpressing human CTHRC1. 3T3-L1 cells were transduced with adenoviral vectors overexpressing either control *β–galactosidase* (**A**) or human *CTHRC1* (**B**). Two days following the onset of adenoviral transduction, cells were formalin fixed and treated with Hoechst nuclear stain (blue) or Alexa Fluor 546 Phalloidin (red). The length of the white rectangle (lower left-hand corner) denotes the scale: 20 μm. (n=4).

APPENDIX B: Two-way ANOVA data

Experiment Identifier	Sum of Squares	Mean Square	F value	Significance (P-value)
A	0.0202	0.0202	6.492	0.0215
B	0.0436	0.0436	5.779	0.0272
C	0.0844	0.0844	27.231	<0.0001
D	0.0342	0.0342	7.757	0.0114

Table B.1. Two-way ANOVA. Two-way analysis of variance (ANOVA) table displaying the significance of the interaction term between the "vehicle" and "N+Y" groups graphically displayed in *Figure 14A*. The significant interaction term in four independent experiments strongly supports the hypothesis that the anti-adipogenic effect of hCTHRC1 conditioned medium is diminished in a statistically significant manner when specific Rho-like GTPase chemical inhibitors are applied (*i.e.*, N and Y). N (NSC 23766) is a well-defined Rac1 activation-specific inhibitor (73), and Y (Y-27632) is a potent inhibitor of the direct Rho effector, Rho-associated kinase (74).

APPENDIX C: CTHRC1 overexpression inhibits adipogenic gene expression

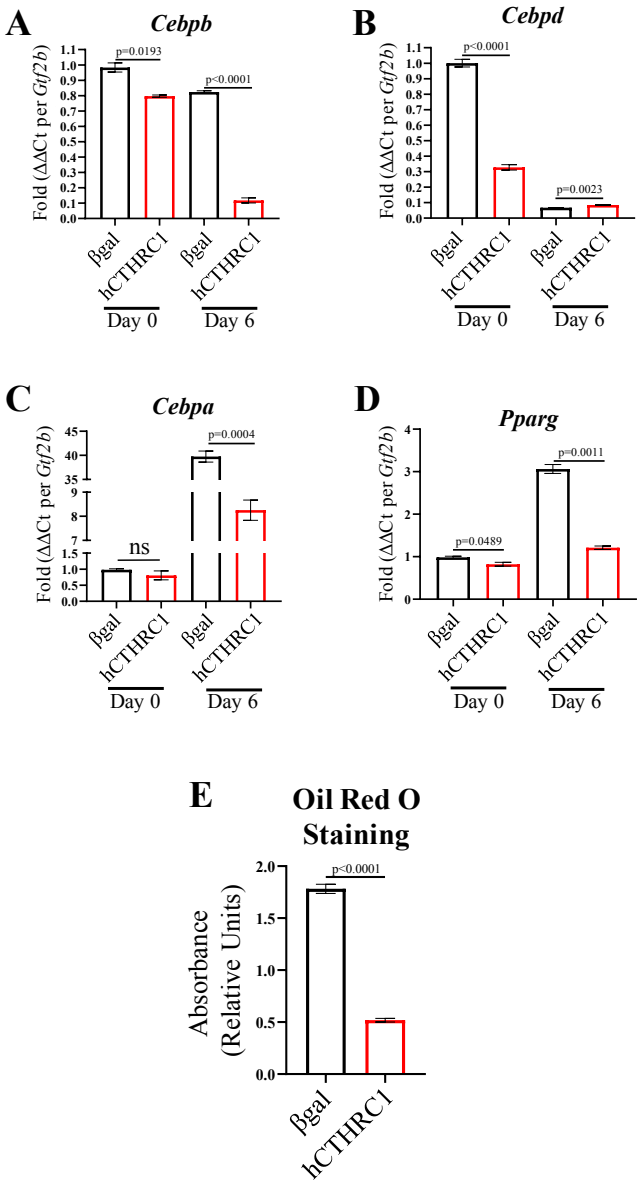

Figure C.1. Adenoviral overexpression of hCTHRC1 suppress lipid accumulation and adipogenic gene expression in differentiating adipocytes. 3T3-L1 cells were transduced with adenoviral vectors overexpressing either control *β–galactosidase* (βgal) or human *CTHRC1* (hCTHRC1). Two days following the onset of adenoviral transduction, whole-cell lysates were

collected for qPCR analyses (**A**-**D**), while other cohorts were chemically stimulated to undergo adipogenic differentiation for a total period of 6 days (**E**). **A**-**D**) Representative qPCR fold expression differences in specific mRNA transcript levels relative to housekeeping *Gtf2b* expression levels (n=3). **E**) Representative Oil Red O quantification data determined by absorbance spectroscopy (n=3).

APPENDIX D: Assessing the role of CHOP expression

relative to the anti-adipogenic effect of CTHRC1 overexpression

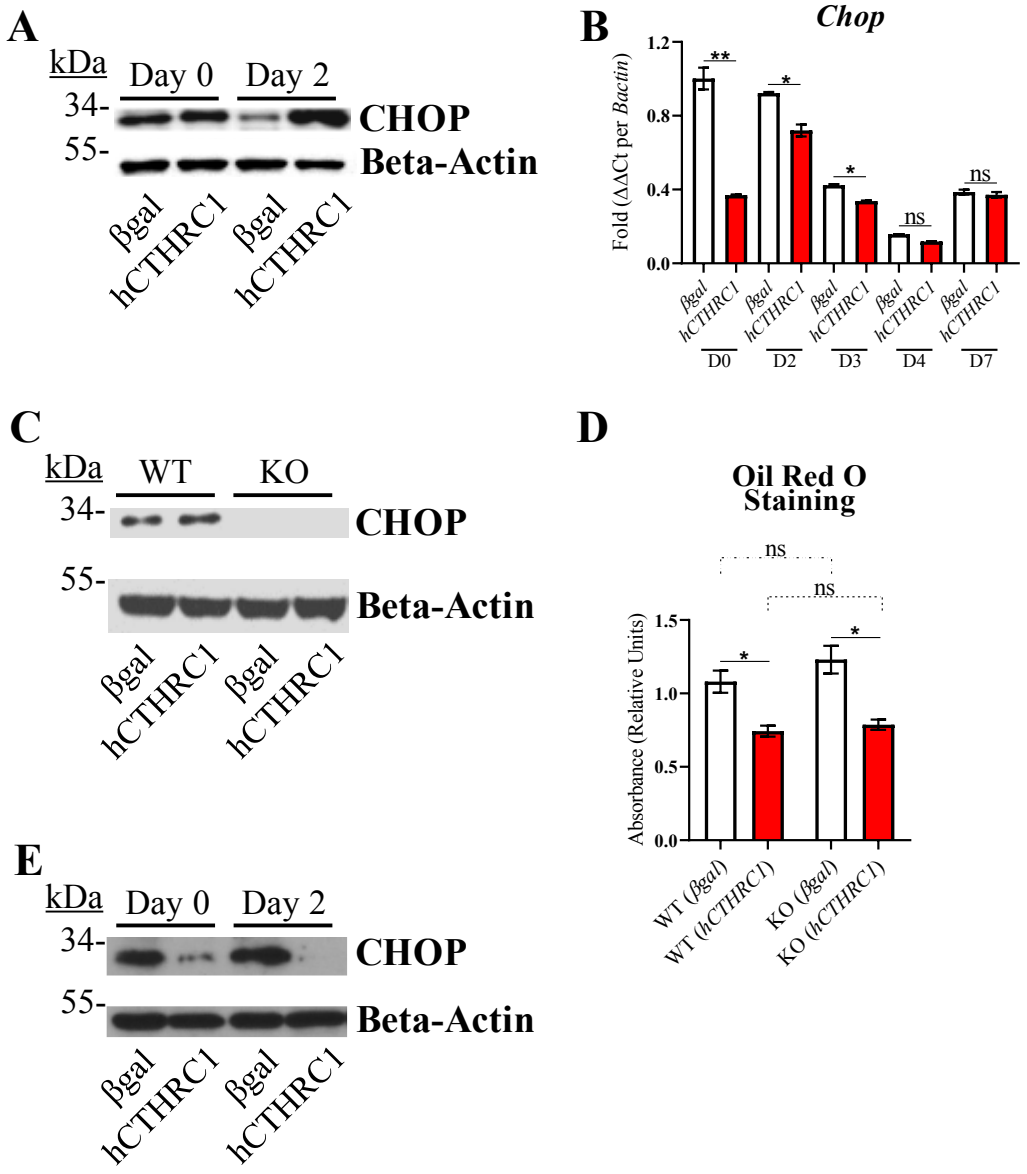

Figure D.1. Assessing the anti-adipogenic effect of CTHRC1 overexpression in preadipocytes relative to CHOP expression levels. **A**) 3T3-L1 cells were transduced with adenoviral vectors overexpressing either control *β–galactosidase* (βgal) or human *CTHRC1*

(hCTHRC1). Two days following the onset of adenoviral transduction (*i.e.*, Day 0), whole-cell lysates were collected while other cohorts of cells were chemically stimulated to undergo adipogenic differentiation in which whole-cell lysates were collected on Day 2 relative to chemical induction. Representative Western blot of CHOP protein expression. Beta-actin served as the loading control (n=3). **B**) 3T3-L1 cells were transduced with adenoviral vectors overexpressing either control *β–galactosidase* (βgal) or human *CTHRC1* (hCTHRC1). Two days following the onset of adenoviral transduction [*i.e.*, Day 0 (D0)], whole-cell lysates were collected while other cohorts of cells were chemically stimulated to undergo adipogenic differentiation in which whole-cell lysates were collected on Day 2 (D2), Day 3 (D3), Day 4 (D4), and Day 7 (D7) relative to chemical induction. Representative qPCR fold expression differences in CHOP mRNA levels relative to housekeeping Beta-actin expression levels (n=3; * $p \leq 0.05$, ** $p \leq 0.01$). **C**,**D**) Stromal vascular fraction cells were isolated from the inguinal white adipose tissue of 12-week-old wildtype (WT) and *Chop*-null (KO) C57BL/6 male mice and subjected to chemically stimulated adipogenic differentiation for seven days. **C**) Representative Western blot of CHOP protein expression. Beta-actin served as the loading control (n=2). **D**) Representative Oil Red O quantification data determined by absorbance spectroscopy (n=2; * $p \leq 0.05$). **E**) 3T3-L1 cells were seeded on Day -3 with either βgal or hCTHRC1 conditioned medium at a 1/4 dilution, after which whole-cell lysates were collected on Day 0 for Western blot analysis of CHOP protein expression. Beta-actin served as the loading control (n=2).

APPENDIX E: Determining the anti-adipogenic effect of human CTHRC1 conditioned media

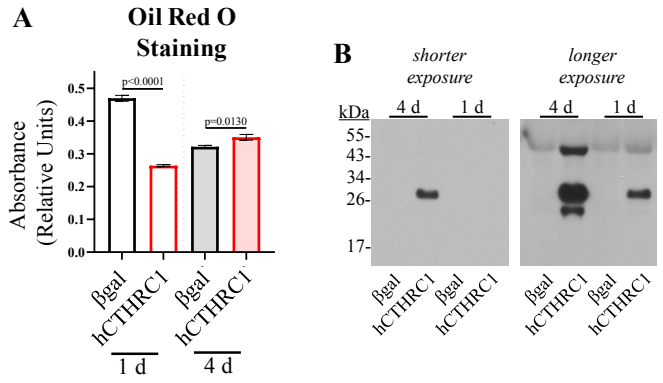

Figure E.1. Determining the anti-adipogenic effect of human CTHRC1 conditioned media. **A**,**B**) 3T3-L1 cells were transduced in duplicate with adenoviral vectors overexpressing either control *β–galactosidase* (βgal) or human *CTHRC1* (hCTHRC1) for 8 hours using serum-free DMEM. Cells were then washed and replenished with DMEM containing serum. 24 hours (*i.e.*, 1 d) or 4 days (*i.e.*, 4 d) thereafter, conditioned media were collected. **A**) Representative Oil Red O quantification data from independent experiments delineated by the dashed vertical line. In separate experiments, 3T3-L1 cells were seeded on Day -3 with βgal or hCTHRC1 conditioned medium (1-day-old or 4-days-old), and then chemically stimulated to undergo adipogenic differentiation for a total period of 6 days. Cells were formalin fixed on Day 6 and stained with Oil Red O, which was then eluted and its concentration determined by absorbance spectroscopy. The Oil Red O data reflect the trends of more than three independent experiments. **B**) Immunoblotting of respective conditioned media chemically reduced with 2-mercaptoethanol. The presence of recombinant human CTHRC1 in conditioned media was probed using a rabbit monoclonal antibody raised against the C-terminus of human CTHRC1 (clone Vli55).

APPENDIX F: Assessing the role of guanine nucleotide-binding protein alpha-q in the regulation of anti-adipogenic CTHRC1 signaling

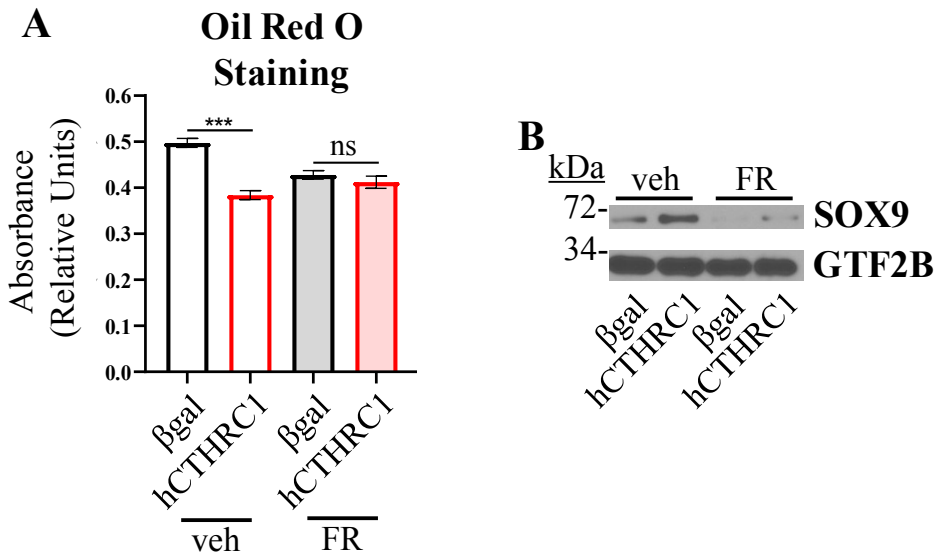

Figure F.1. Evidence for the role of guanine nucleotide-binding protein alpha-q in the positive regulation of anti-adipogenic CTHRC1 signaling. **A**,**B**) 3T3-L1 cells were seeded on Day -3 with βgal or hCTHRC1 conditioned medium in the absence or presence of FR900359 (FR), a chemical inhibitor of guanine nucleotide-binding protein alpha-q activity (102), then chemically stimulated on Day 0 to undergo adipogenic differentiation for a total period of 6 days. Cells were formalin fixed on Day 6 and stained with Oil Red O, which was then eluted and its concentration determined by absorbance spectroscopy (n=2; *** $p \leq 0.001$). (**A**). FR (1 μM, final) or vehicle (veh; 0.1% DMSO) were freshly added each day of the experiment. **B**) Immunoblotting of whole-cell lysates collected on Day 0 for SOX9 protein expression levels. GTF2B served as the loading control (n=2).

APPENDIX G: Verteporfin nullifies anti-adipogenic CTHRC1 activity

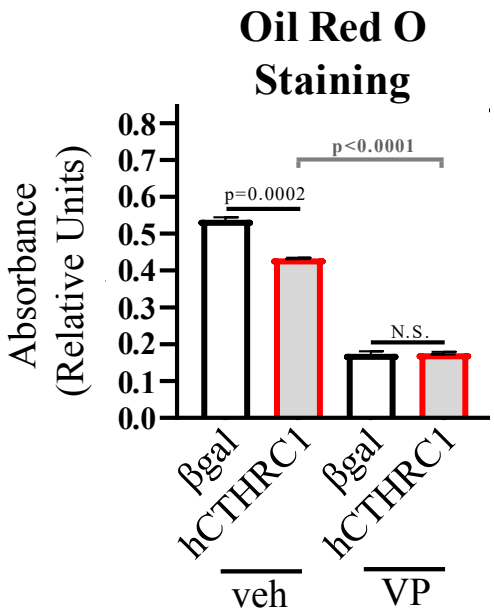

Figure G.1. Verteporfin suppresses adipogenic differentiation and nullifies anti-adipogenic CTHRC1 activity. 3T3-L1 cells were seeded on Day -3 with βgal or hCTHRC1 conditioned medium in the absence or presence of verteporfin (VP), a chemical inhibitor of YAP transcriptional activity (104), then chemically stimulated on Day 0 to undergo adipogenic differentiation for a total period of 6 days. Cells were formalin fixed on Day 6 and stained with Oil Red O, which was then eluted and its concentration determined by absorbance spectroscopy (n=2). VP (5 μM, final) or vehicle (veh; 0.1% DMSO) were freshly added each day of the experiment.

APPENDIX H: Immunodepletion of hCTHRC1 conditioned medium

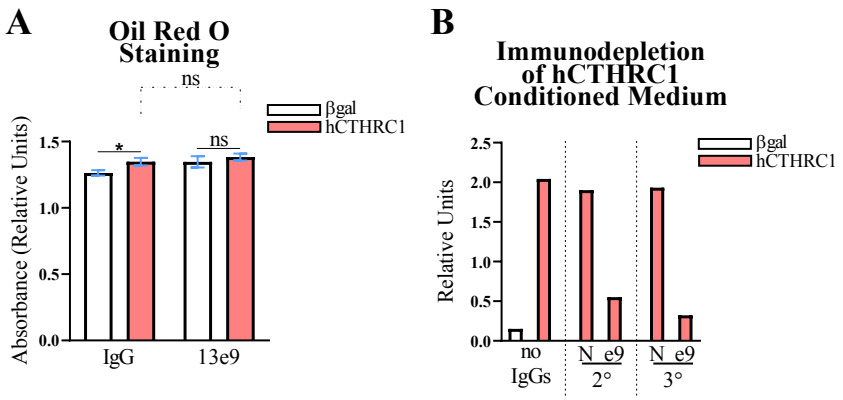

Figure H.1. Immunodepletion of hCTHRC1 conditioned medium. βgal and hCTHRC1 conditioned medium were treated by overnight rotation with Protein A-Sepharose conjugated with either naïve mouse IgG (IgG) or mouse anti-CTHRC1 IgG clone Vli13E09 (13e9). Following overnight rotation, Protein A-Sepharose was pelleted by centrifugation and the supernatant was transferred to a fresh 15 mL conical tube. Three rounds of immunodepletion were conducted in total, following which 3T3-L1 cells were seeded on Day -3 with respective conditioned media and chemically stimulated to undergo adipogenic differentiation for a total period of 6 days. Respective conditioned media were applied fresh daily. Cells were formalin fixed on Day 6 and stained with Oil Red O, which was then eluted and its concentration determined by absorbance spectroscopy (**A**) (* $p \leq 0.05$). **B**) Enzyme-linked immunosorbent assay (ELISA) data measuring the relative concentration of recombinant human CTHRC1 in conditioned media. Left panel: βgal and hCTHRC1 conditioned medium not treated with IgG/13e9-conjugated Protein A-Sepharose (no IgGs). Middle panel: hCTHRC1 conditioned medium after two rounds (2°) of immunodepletion using either naïve IgG-conjugated Protein A-Sepharose (N) or 13e9-conjugated Protein A-Sepharose (e9). Right panel: hCTHRC1 conditioned medium after three rounds (3°) of immunodepletion using either naïve IgG-conjugated Protein A-Sepharose (N) or 13e9-conjugated Protein A-Sepharose (e9).

APPENDIX I: The effect of hCTHRC1 conditioned medium on PREF1 expression levels

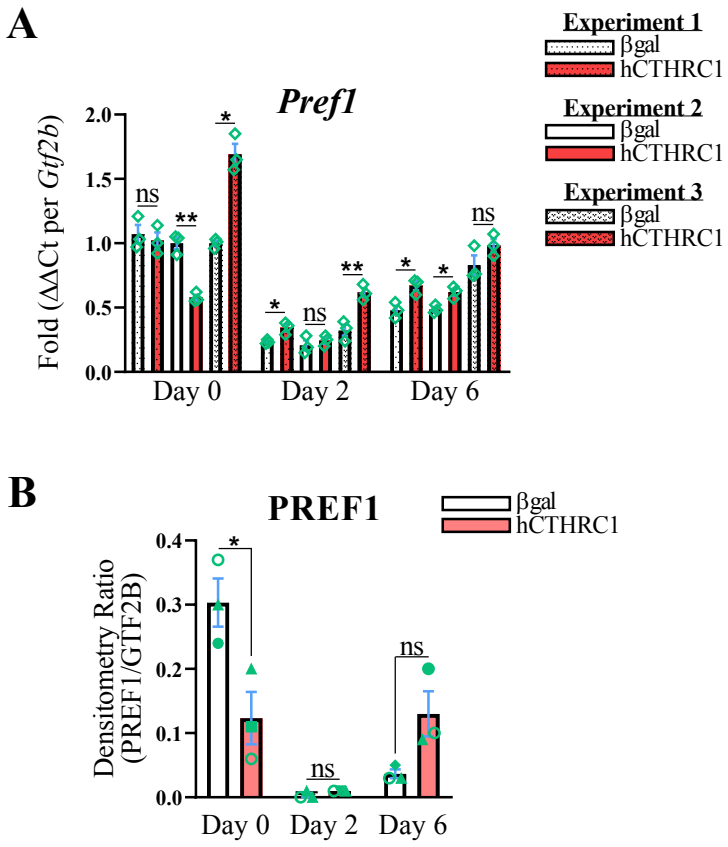

Figure I.1. Determining the effect of hCTHRC1 conditioned medium on PREF1 expression levels. 3T3-L1 cells were seeded on Day -3 with either βgal or hCTHRC1 conditioned medium at a 1/4 dilution, after which whole-cell lysates were collected on Day 0 and subjected to qPCR (**A**) or Western blot (**B**) analyses. **A**) qPCR fold expression differences in *Pref1* mRNA levels relative to housekeeping *Gtf2b* expression levels from three independent experiments (n=3; * $p \leq 0.05$, ** $p \leq 0.01$). **B**) Average PREF1 protein fold change densitometry values relative to housekeeping GTF2B protein expression levels from three independent experiments (n=3; * $p \leq 0.05$).

APPENDIX J: The effect of hCTHRC1 conditioned medium on *Igf2*, *Fn1*, and *Col1a1* gene expression levels

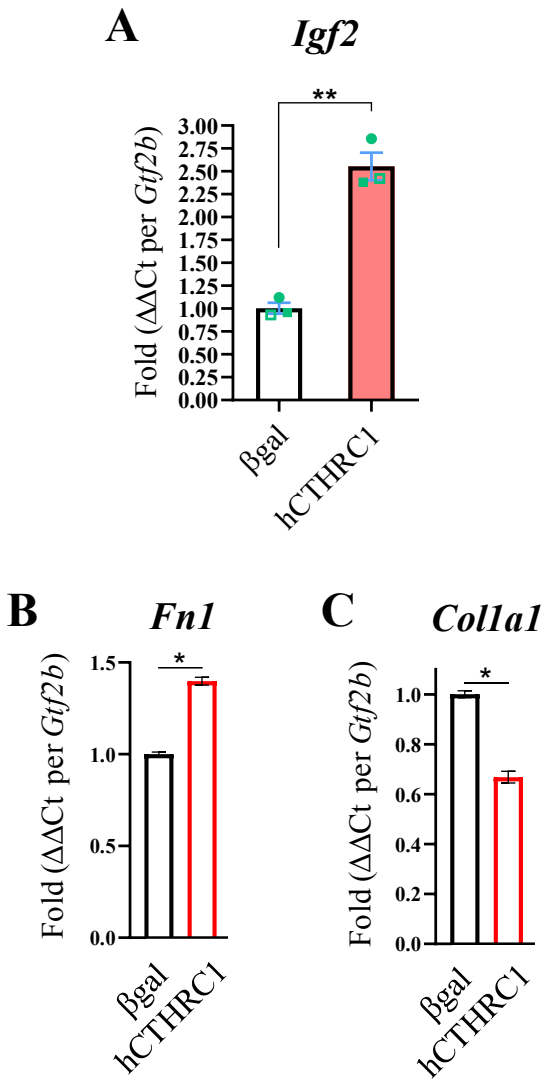

Figure J.1. Assessing the effect of hCTHRC1 conditioned medium on *Igf2*, *Fn1*, and *Col1a1* gene expression levels. 3T3-L1 cells were seeded on Day -3 with either βgal or hCTHRC1 conditioned medium at a 1/4 dilution, after which whole-cell lysates were collected on Day 0 and subjected to qPCR analyses to measure specific target genes. **A**) Representative qPCR fold

expression differences in *Igf2* mRNA levels relative to housekeeping *Gtf2b* expression levels (n=2; ** p≤0.01). **B**) Representative qPCR fold expression differences in *Fn1* mRNA levels relative to housekeeping *Gtf2b* expression levels (n=2; * p≤0.05). **C**) Representative qPCR fold expression differences in *Col1a1* mRNA levels relative to housekeeping *Gtf2b* expression levels (n=2; * p≤0.05).

APPENDIX K: The effect of hCTHRC1 conditioned medium on SPARC expression levels

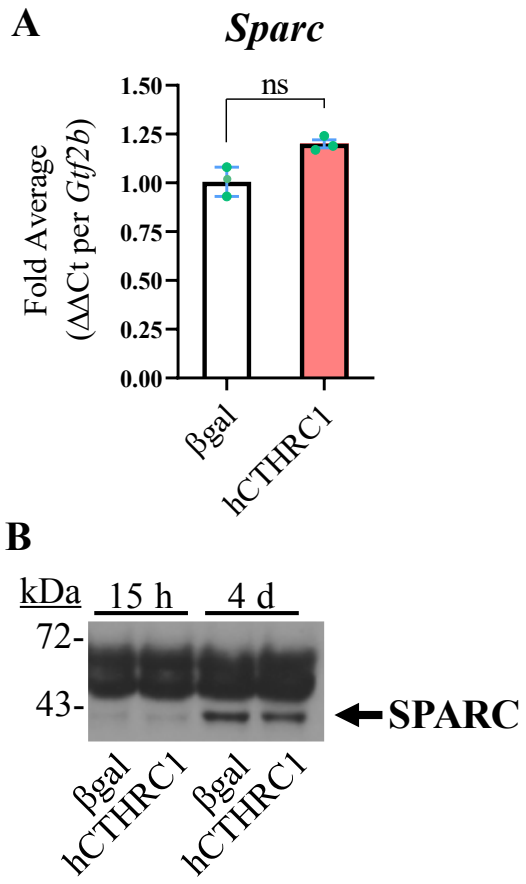

Figure K.1. Assessing the effect of hCTHRC1 conditioned medium on *Sparc* gene expression levels and determining the relative levels of SPARC protein in hCTHRC1 conditioned medium. **A**) 3T3-L1 cells were seeded on Day -3 with either βgal or hCTHRC1 conditioned medium at a 1/4 dilution, after which whole-cell lysates were collected on Day 0. Representative qPCR fold expression differences in *Sparc* mRNA levels relative to housekeeping *Gtf2b* expression levels (n=1). **B**) 3T3-L1 cells were transduced in duplicate with adenoviral vectors overexpressing either control *β–galactosidase* (βgal) or human *CTHRC1*

(hCTHRC1) for 8 hours using serum-free DMEM. Cells were then washed and replenished with DMEM containing serum. 15 hours (*i.e.*, 15 h) or 4 days (*i.e.*, 4 d) thereafter, conditioned media were collected. Immunoblotting of respective conditioned media chemically reduced with 2-mercaptoethanol. The relative levels of SPARC protein in respective conditioned media were determined by immunoblotting (n=1).

APPENDIX L: Assessing the CTHRC1-regulated secretome

Table L.1. Assessing the CTHRC1-regulated secretome. In a preliminary assessment of the hCTHRC1-regulated secretome, 3T3-L1 cells were transduced with control (βgal) or hCTHRC1-expressing adenovirus, after which conditioned media were collected 2, 4, or 8 days thereafter. The presence of hCTHRC1 in 2-, 4-, and 8-days-old hCTHRC1 conditioned media was confirmed by ELISA (data not shown), and conditioned media were then subjected to proteomic analysis by mass spectrometry. The table indicates the day on which βgal and hCTHRC1 conditioned media were collected (Day Collected column) and statistically significant differentially expressed proteins (Group column) when normalizing the hCTHRC1 conditioned medium secretome to the βgal conditioned medium secretome at each timepoint.

Day Collected	Group	Fold Change
Day 2	Myomesin-3 OS=Mus musculus OX=10090 GN=Myom3 PE=1 SV=1	5.521
Day 2	Talin-1 OS=Mus musculus OX=10090 GN=Tln1 PE=1 SV=2	11.610
Day 2	Ig kappa chain V-V region MOPC 21 OS=Mus musculus OX=10090 PE=1 SV=1	4.621
Day 2	SPARC OS=Mus musculus OX=10090 GN=Sparc PE=1 SV=1	3.856
Day 2	Leukotriene A-4 hydrolase OS=Mus musculus OX=10090 GN=Lta4h PE=1 SV=4	2.650
Day 2	Adenylate cyclase type 6 OS=Mus musculus OX=10090 GN=Adcy6 PE=1 SV=1	6.644
Day 2	Protein CIP2A OS=Mus musculus OX=10090 GN=Cip2a PE=1 SV=3	4.951

Table L.1. continued

Day 2	Ras-related protein Rab-5A OS=Mus musculus OX=10090 GN=Rab5a PE=1 SV=1	5.119
Day 2	SRC kinase signaling inhibitor 1 OS=Mus musculus OX=10090 GN=Srcin1 PE=1 SV=2	13.833
Day 2	Beta-2-syntrophin OS=Mus musculus OX=10090 GN=Sntb2 PE=1 SV=2	5.605
Day 2	Dual specificity mitogen-activated protein kinase kinase 5 OS=Mus musculus OX=10090 GN=Map2k5 PE=1 SV=1	3.258
Day 2	Heparin cofactor 2 OS=Mus musculus OX=10090 GN=Serpind1 PE=1 SV=1	3.446
Day 2	Complement C4-B OS=Mus musculus OX=10090 GN=C4b PE=1 SV=3	3.428
Day 4	Plasma protease C1 inhibitor OS=Mus musculus OX=10090 GN=Serping1 PE=1 SV=3	0.058
Day 4	Fructose-bisphosphate aldolase A OS=Mus musculus OX=10090 GN=Aldoa PE=1 SV=2	0.057
Day 4	Coagulation factor V OS=Mus musculus OX=10090 GN=F5 PE=1 SV=1	0.111
Day 4	Tubulin alpha-8 chain OS=Mus musculus OX=10090 GN=Tuba8 PE=1 SV=1	2.177
Day 4	Procollagen C-endopeptidase enhancer 1 OS=Mus musculus OX=10090 GN=Pcolce PE=1 SV=2	0.049
Day 4	Alpha-amylase 1 OS=Mus musculus OX=10090 GN=Amy1 PE=1 SV=2	0.064
Day 4	SRC kinase signaling inhibitor 1 OS=Mus musculus OX=10090 GN=Srcin1 PE=1 SV=2	3.964
Day 4	Galectin-3-binding protein OS=Mus musculus OX=10090 GN=Lgals3bp PE=1 SV=1	6.386
Day 4	Elongator complex protein 3 OS=Mus musculus OX=10090 GN=Elp3 PE=1 SV=1	0.004
Day 4	Afamin OS=Mus musculus OX=10090 GN=Afm PE=1 SV=2	0.099

Table L.1. continued

Day 4	Myristoylated alanine-rich C-kinase substrate OS=Mus musculus OX=10090 GN=Marcks PE=1 SV=2	0.188
Day 4	Elongator complex protein 4 OS=Mus musculus OX=10090 GN=Elp4 PE=1 SV=2	0.007
Day 4	Fibulin-2 OS=Mus musculus OX=10090 GN=Fbln2 PE=1 SV=2	0.248
Day 4	Inter-alpha-trypsin inhibitor heavy chain H2 OS=Mus musculus OX=10090 GN=Itih2 PE=1 SV=1	0.025
Day 4	Kininogen-1 OS=Mus musculus OX=10090 GN=Kng1 PE=1 SV=1	0.013
Day 4	Pregnancy zone protein OS=Mus musculus OX=10090 GN=Pzp PE=1 SV=3	0.680
Day 4	Hemoglobin subunit beta-1 OS=Mus musculus OX=10090 GN=Hbb-b1 PE=1 SV=2	0.037
Day 4	Beta-2-syntrophin OS=Mus musculus OX=10090 GN=Sntb2 PE=1 SV=2	0.056
Day 4	Xaa-Pro dipeptidase OS=Mus musculus OX=10090 GN=Pepd PE=1 SV=3	0.025
Day 4	Lactotransferrin OS=Mus musculus OX=10090 GN=Ltf PE=1 SV=4	6.922
Day 4	Hemoglobin subunit epsilon-Y2 OS=Mus musculus OX=10090 GN=Hbb-y PE=1 SV=2	0.115
Day 4	Collagen alpha-1(I) chain OS=Mus musculus OX=10090 GN=Col1a1 PE=1 SV=4	0.220
Day 4	Membrane primary amine oxidase OS=Mus musculus OX=10090 GN=Aoc3 PE=1 SV=3	0.111
Day 4	Ceruloplasmin OS=Mus musculus OX=10090 GN=Cp PE=1 SV=2	0.112
Day 4	Follistatin-related protein 1 OS=Mus musculus OX=10090 GN=Fstl1 PE=1 SV=2	0.233
Day 4	Antithrombin-III OS=Mus musculus OX=10090 GN=Serpinc1 PE=1 SV=1	0.025
Day 4	Complement C3 OS=Mus musculus OX=10090 GN=C3 PE=1 SV=3	0.060

Table L.1. continued

Day 4	Plasminogen activator inhibitor 1 OS=Mus musculus OX=10090 GN=Serpine1 PE=1 SV=1	8.181
Day 4	Hemoglobin subunit alpha OS=Mus musculus OX=10090 GN=Hba PE=1 SV=2	0.065
Day 4	Prenylcysteine oxidase-like OS=Mus musculus OX=10090 GN=Pcyox1l PE=1 SV=1	2.257
Day 4	Talin-1 OS=Mus musculus OX=10090 GN=Tln1 PE=1 SV=2	3.962
Day 4	Collagen alpha-2(I) chain OS=Mus musculus OX=10090 GN=Col1a2 PE=1 SV=2	0.069
Day 4	Dual specificity mitogen-activated protein kinase kinase 5 OS=Mus musculus OX=10090 GN=Map2k5 PE=1 SV=1	0.012
Day 4	Fibronectin OS=Mus musculus OX=10090 GN=Fn1 PE=1 SV=4	0.063
Day 4	Retinoic acid early-inducible protein 1-beta OS=Mus musculus OX=10090 GN=Raet1b PE=1 SV=1	32.241
Day 4	Vimentin OS=Mus musculus OX=10090 GN=Vim PE=1 SV=3	0.312
Day 4	Histone H2B type 2-E OS=Mus musculus OX=10090 GN=H2bc21 PE=1 SV=3	2.207
Day 4	Protein HEATR9 OS=Mus musculus OX=10090 GN=Heatr9 PE=4 SV=1	0.002
Day 4	Pigment epithelium-derived factor OS=Mus musculus OX=10090 GN=Serpinf1 PE=1 SV=2	1.894
Day 4	Pyruvate kinase PKM OS=Mus musculus OX=10090 GN=Pkm PE=1 SV=4	0.301
Day 4	Thioredoxin domain-containing protein 15 OS=Mus musculus OX=10090 GN=Txndc15 PE=1 SV=1	0.389
Day 4	CTD small phosphatase-like protein 2 OS=Mus musculus OX=10090 GN=Ctdspl2 PE=1 SV=1	0.017
Day 4	Protein-lysine 6-oxidase OS=Mus musculus OX=10090 GN=Lox PE=1 SV=1	0.250

Table L.1. continued

Day 4	TBC domain-containing protein kinase-like protein OS=Mus musculus OX=10090 GN=Tbck PE=1 SV=1	0.212
Day 4	Beta-1,4-galactosyltransferase 1 OS=Mus musculus OX=10090 GN=B4galt1 PE=1 SV=1	1.835
Day 4	Kin of IRRE-like protein 2 OS=Mus musculus OX=10090 GN=Kirrel2 PE=1 SV=1	8.391
Day 4	Apolipoprotein A-I OS=Mus musculus OX=10090 GN=Apoa1 PE=1 SV=2	0.032
Day 4	Complement C5 OS=Mus musculus OX=10090 GN=C5 PE=1 SV=2	0.180
Day 4	Synaptonemal complex protein 1 OS=Mus musculus OX=10090 GN=Sycp1 PE=1 SV=2	0.127
Day 4	Zinc finger protein 382 OS=Mus musculus OX=10090 GN=Znf382 PE=1 SV=1	0.611
Day 4	Prothrombin OS=Mus musculus OX=10090 GN=F2 PE=1 SV=1	0.327
Day 4	Cadherin-5 OS=Mus musculus OX=10090 GN=Cdh5 PE=1 SV=2	0.269
Day 4	Serotransferrin OS=Mus musculus OX=10090 GN=Tf PE=1 SV=1	0.255
Day 8	Beta-1,4-galactosyltransferase 1 OS=Mus musculus OX=10090 GN=B4galt1 PE=1 SV=1	4.497
Day 8	Inter-alpha-trypsin inhibitor heavy chain H2 OS=Mus musculus OX=10090 GN=Itih2 PE=1 SV=1	0.070
Day 8	Phospholipid transfer protein OS=Mus musculus OX=10090 GN=Pltp PE=1 SV=1	5.330
Day 8	SPARC OS=Mus musculus OX=10090 GN=Sparc PE=1 SV=1	152.565
Day 8	Talin-1 OS=Mus musculus OX=10090 GN=Tln1 PE=1 SV=2	29.506
Day 8	Fructose-bisphosphate aldolase B OS=Mus musculus OX=10090 GN=Aldob PE=1 SV=3	1.748
Day 8	Kin of IRRE-like protein 2 OS=Mus musculus OX=10090 GN=Kirrel2 PE=1 SV=1	12.855
Day 8	Lumican OS=Mus musculus OX=10090 GN=Lum PE=1 SV=2	7.384

Table L.1. continued

Day 8	Protein HEATR9 OS=Mus musculus OX=10090 GN=Heatr9 PE=4 SV=1	0.012
Day 8	Lactotransferrin OS=Mus musculus OX=10090 GN=Ltf PE=1 SV=4	11.748
Day 8	CDK-activating kinase assembly factor MAT1 OS=Mus musculus OX=10090 GN=Mnat1 PE=1 SV=2	128.175
Day 8	Pigment epithelium-derived factor OS=Mus musculus OX=10090 GN=Serpinf1 PE=1 SV=2	4.373
Day 8	Kininogen-1 OS=Mus musculus OX=10090 GN=Kng1 PE=1 SV=1	0.049
Day 8	Keratin, type II cytoskeletal 75 OS=Mus musculus OX=10090 GN=Krt75 PE=1 SV=1	4.970
Day 8	Plasminogen OS=Mus musculus OX=10090 GN=Plg PE=1 SV=3	0.129
Day 8	Nidogen-2 OS=Mus musculus OX=10090 GN=Nid2 PE=1 SV=2	5.859
Day 8	Dual specificity mitogen-activated protein kinase kinase 5 OS=Mus musculus OX=10090 GN=Map2k5 PE=1 SV=1	0.039
Day 8	Threonine--tRNA ligase, mitochondrial OS=Mus musculus OX=10090 GN=Tars2 PE=1 SV=1	20.761
Day 8	Probable arginine--tRNA ligase, mitochondrial OS=Mus musculus OX=10090 GN=Rars2 PE=1 SV=1	3.837
Day 8	Coagulation factor V OS=Mus musculus OX=10090 GN=F5 PE=1 SV=1	0.264
Day 8	Procollagen C-endopeptidase enhancer 1 OS=Mus musculus OX=10090 GN=Pcolce PE=1 SV=2	0.062
Day 8	DDB1- and CUL4-associated factor 1 OS=Mus musculus OX=10090 GN=Dcaf1 PE=1 SV=4	5.119
Day 8	Prosaposin OS=Mus musculus OX=10090 GN=Psap PE=1 SV=2	5.371
Day 8	Retinoic acid early-inducible protein 1-beta OS=Mus musculus OX=10090 GN=Raet1b PE=1 SV=1	214.155
Day 8	Diacylglycerol kinase theta OS=Mus musculus OX=10090 GN=Dgkq PE=1 SV=1	17.326

Table L.1. continued

Day 8	Vinculin OS=Mus musculus OX=10090 GN=Vcl PE=1 SV=4	1.712
Day 8	N-acetylmuramoyl-L-alanine amidase OS=Mus musculus OX=10090 GN=Pglyrp2 PE=1 SV=1	3.684
Day 8	Heparin cofactor 2 OS=Mus musculus OX=10090 GN=Serpind1 PE=1 SV=1	4.794
Day 8	Fibulin-2 OS=Mus musculus OX=10090 GN=Fbln2 PE=1 SV=2	0.315
Day 8	Plasminogen activator inhibitor 1 OS=Mus musculus OX=10090 GN=Serpine1 PE=1 SV=1	34.171
Day 8	Histone-lysine N-methyltransferase 2D OS=Mus musculus OX=10090 GN=Kmt2d PE=1 SV=2	0.210
Day 8	Adenylate cyclase type 6 OS=Mus musculus OX=10090 GN=Adcy6 PE=1 SV=1	27.409
Day 8	SRC kinase signaling inhibitor 1 OS=Mus musculus OX=10090 GN=Srcin1 PE=1 SV=2	8.292
Day 8	Protein CIP2A OS=Mus musculus OX=10090 GN=Cip2a PE=1 SV=3	0.385
Day 8	Serum amyloid A-3 protein OS=Mus musculus OX=10090 GN=Saa3 PE=1 SV=1	7.612
Day 8	Tubulin alpha-8 chain OS=Mus musculus OX=10090 GN=Tuba8 PE=1 SV=1	5.128
Day 8	Beta-2-microglobulin OS=Mus musculus OX=10090 GN=B2m PE=1 SV=2	2.894
Day 8	Complement C3 OS=Mus musculus OX=10090 GN=C3 PE=1 SV=3	0.018
Day 8	Antithrombin-III OS=Mus musculus OX=10090 GN=Serpinc1 PE=1 SV=1	0.047
Day 8	Histone H2B type 2-E OS=Mus musculus OX=10090 GN=H2bc21 PE=1 SV=3	7.453
Day 8	Histone H2AX OS=Mus musculus OX=10090 GN=H2ax PE=1 SV=2	2.713
Day 8	Fibulin-1 OS=Mus musculus OX=10090 GN=Fbln1 PE=1 SV=2	3.625
Day 8	Vimentin OS=Mus musculus OX=10090 GN=Vim PE=1 SV=3	0.505

Table L.1. continued

Day 8	Protein FAM117A OS=Mus musculus OX=10090 GN=Fam117a PE=1 SV=1	5.112
Day 8	Leukotriene A-4 hydrolase OS=Mus musculus OX=10090 GN=Lta4h PE=1 SV=4	5.746
Day 8	Inter-alpha-trypsin inhibitor heavy chain H3 OS=Mus musculus OX=10090 GN=Itih3 PE=1 SV=3	4.959
Day 8	Prenylcysteine oxidase-like OS=Mus musculus OX=10090 GN=Pcyox1l PE=1 SV=1	5.631
Day 8	Alpha-2-macroglobulin-P OS=Mus musculus OX=10090 GN=A2m PE=2 SV=2	0.204
Day 8	Collagen alpha-1(IV) chain OS=Mus musculus OX=10090 GN=Col4a1 PE=1 SV=4	2.439
Day 8	Complement C4-B OS=Mus musculus OX=10090 GN=C4b PE=1 SV=3	2.827
Day 8	Galectin-3-binding protein OS=Mus musculus OX=10090 GN=Lgals3bp PE=1 SV=1	9.467
Day 8	Complement C1r-B subcomponent OS=Mus musculus OX=10090 GN=C1rb PE=2 SV=1	4.051
Day 8	Collagen alpha-2(I) chain OS=Mus musculus OX=10090 GN=Col1a2 PE=1 SV=2	0.121
Day 8	Alpha-2-HS-glycoprotein OS=Mus musculus OX=10090 GN=Ahsg PE=1 SV=1	2.657
Day 8	Hemoglobin subunit beta-1 OS=Mus musculus OX=10090 GN=Hbb-b1 PE=1 SV=2	0.242
Day 8	Albumin OS=Mus musculus OX=10090 GN=Alb PE=1 SV=3	1.761
Day 8	Afamin OS=Mus musculus OX=10090 GN=Afm PE=1 SV=2	0.341
Day 8	Hemoglobin subunit alpha OS=Mus musculus OX=10090 GN=Hba PE=1 SV=2	0.158
Day 8	Neural cell adhesion molecule 1 OS=Mus musculus OX=10090 GN=Ncam1 PE=1 SV=3	0.456

Table L.1. continued

Day 8	Xaa-Pro dipeptidase OS=Mus musculus OX=10090 GN=Pepd PE=1 SV=3	0.060
Day 8	26S proteasome regulatory subunit 6A OS=Mus musculus OX=10090 GN=Psmc3 PE=1 SV=2	2.621
Day 8	Fibronectin OS=Mus musculus OX=10090 GN=Fn1 PE=1 SV=4	0.192
Day 8	Serotransferrin OS=Mus musculus OX=10090 GN=Tf PE=1 SV=1	1.610
Day 8	Myristoylated alanine-rich C-kinase substrate OS=Mus musculus OX=10090 GN=Marcks PE=1 SV=2	0.459
Day 8	Collagen alpha-1(VI) chain OS=Mus musculus OX=10090 GN=Col6a1 PE=1 SV=1	4.063
Day 8	Collagen alpha-1(I) chain OS=Mus musculus OX=10090 GN=Col1a1 PE=1 SV=4	0.731
Day 8	Ig kappa chain V-V region MOPC 21 OS=Mus musculus OX=10090 PE=1 SV=1	1.954
Day 8	Vitamin D-binding protein OS=Mus musculus OX=10090 GN=Gc PE=1 SV=2	4.860
Day 8	Collagen alpha-2(VI) chain OS=Mus musculus OX=10090 GN=Col6a2 PE=1 SV=3	4.059
Day 8	Centrosomal protein of 55 kDa OS=Mus musculus OX=10090 GN=Cep55 PE=1 SV=2	8.324
Day 8	Ras-related protein Rab-5A OS=Mus musculus OX=10090 GN=Rab5a PE=1 SV=1	5.782

APPENDIX M: The effect of CTHRC1 overexpression on the proteome

Table M.1. The effect of CTHRC1 overexpression on the proteome. 3T3-L1 cells were transduced with control (βgal) or hCTHRC1-expressing adenovirus. Whole-cell lysates were collected two days thereafter and subjected to proteomic analysis by mass spectrometry. The table indicates statistically significant differentially expressed proteins (Group column) when normalizing the βgal group to the hCTHRC1 group.

Group	Fold Change	Log (Fold Change)
UMP-CMP kinase 2, mitochondrial OS=Mus musculus OX=10090 GN=Cmpk2 PE=1 SV=2	0.299	-0.525
Interferon-induced protein with tetratricopeptide repeats 1 OS=Mus musculus OX=10090 GN=Ifit1 PE=1 SV=2	0.364	-0.438
H-2 class I histocompatibility antigen, L-D alpha chain OS=Mus musculus OX=10090 GN=H2-L PE=1 SV=2	0.423	-0.374
Ubiquitin-like protein ISG15 OS=Mus musculus OX=10090 GN=Isg15 PE=1 SV=4	0.393	-0.406
Collagen triple helix repeat-containing protein 1 OS=Mus musculus OX=10090 GN=Cthrc1 PE=2 SV=2	0.089	-1.052
Inter-alpha-trypsin inhibitor heavy chain H3 OS=Mus musculus OX=10090 GN=Itih3 PE=1 SV=3	1.995	0.300
H-2 class I histocompatibility antigen, K-W28 alpha chain OS=Mus musculus OX=10090 GN=H2-K1 PE=1 SV=2	0.501	-0.300
Isocitrate dehydrogenase [NADP], mitochondrial OS=Mus musculus OX=10090 GN=Idh2 PE=1 SV=3	1.263	0.101
Antigen peptide transporter 1 OS=Mus musculus OX=10090 GN=Tap1 PE=1 SV=3	0.404	-0.393

Table M.1. continued

Zinc finger protein 706 OS=Mus musculus OX=10090 GN=Znf706 PE=1 SV=1	0.603	-0.219
Asparagine--tRNA ligase, cytoplasmic OS=Mus musculus OX=10090 GN=Nars PE=1 SV=2	0.668	-0.175
Cysteine--tRNA ligase, cytoplasmic OS=Mus musculus OX=10090 GN=Cars PE=1 SV=2	0.764	-0.117
Interferon-activable protein 204 OS=Mus musculus OX=10090 GN=Ifi204 PE=1 SV=1	0.695	-0.158
Thrombospondin-2 OS=Mus musculus OX=10090 GN=Thbs2 PE=1 SV=2	1.854	0.268
ER membrane protein complex subunit 7 OS=Mus musculus OX=10090 GN=Emc7 PE=1 SV=1	1.447	0.160
Dermatopontin OS=Mus musculus OX=10090 GN=Dpt PE=1 SV=1	1.855	0.268
Transcription factor E2F4 OS=Mus musculus OX=10090 GN=E2f4 PE=1 SV=1	4.111	0.614
Serine/arginine-rich splicing factor 7 OS=Mus musculus OX=10090 GN=Srsf7 PE=1 SV=1	0.696	-0.157
Macrophage migration inhibitory factor OS=Mus musculus OX=10090 GN=Mif PE=1 SV=2	0.641	-0.193
Microtubule-associated protein RP/EB family member 2 OS=Mus musculus OX=10090 GN=Mapre2 PE=1 SV=1	0.653	-0.185
Acyl-coenzyme A thioesterase 2, mitochondrial OS=Mus musculus OX=10090 GN=Acot2 PE=1 SV=2	0.756	-0.122
Cytosolic phospholipase A2 OS=Mus musculus OX=10090 GN=Pla2g4a PE=1 SV=1	0.668	-0.175
Glutathione peroxidase 1 OS=Mus musculus OX=10090 GN=Gpx1 PE=1 SV=2	0.644	-0.191
Immunity-related GTPase family M protein 1 OS=Mus musculus OX=10090 GN=Irgm1 PE=1 SV=1	0.611	-0.214
Proteasome subunit beta type-8 OS=Mus musculus OX=10090 GN=Psmb8 PE=1 SV=2	0.454	-0.343

Table M.1. continued

Alanine aminotransferase 2 OS=Mus musculus OX=10090 GN=Gpt2 PE=1 SV=1	0.647	-0.189
Myosin regulatory light polypeptide 9 OS=Mus musculus OX=10090 GN=Myl9 PE=1 SV=3	0.634	-0.198
Alpha-2-macroglobulin-P OS=Mus musculus OX=10090 GN=A2m PE=2 SV=2	1.727	0.237
Lipoprotein lipase OS=Mus musculus OX=10090 GN=Lpl PE=1 SV=3	1.725	0.237
Translocation protein SEC62 OS=Mus musculus OX=10090 GN=Sec62 PE=1 SV=1	0.474	-0.324
Protein-lysine 6-oxidase OS=Mus musculus OX=10090 GN=Lox PE=1 SV=1	1.498	0.176
D-3-phosphoglycerate dehydrogenase OS=Mus musculus OX=10090 GN=Phgdh PE=1 SV=3	0.860	-0.066
Aminopeptidase N OS=Mus musculus OX=10090 GN=Anpep PE=1 SV=4	1.538	0.187
60S ribosomal protein L35a OS=Mus musculus OX=10090 GN=Rpl35a PE=1 SV=2	0.789	-0.103
Protein FAM136A OS=Mus musculus OX=10090 GN=Fam136a PE=1 SV=1	2.907	0.463
Large neutral amino acids transporter small subunit 1 OS=Mus musculus OX=10090 GN=Slc7a5 PE=1 SV=2	0.735	-0.134
Myoferlin OS=Mus musculus OX=10090 GN=Myof PE=1 SV=2	1.342	0.128
Integral membrane protein 2B OS=Mus musculus OX=10090 GN=Itm2b PE=1 SV=1	1.695	0.229
Cysteine and glycine-rich protein 1 OS=Mus musculus OX=10090 GN=Csrp1 PE=1 SV=3	0.692	-0.160
5'-AMP-activated protein kinase catalytic subunit alpha-1 OS=Mus musculus OX=10090 GN=Prkaa1 PE=1 SV=2	0.636	-0.196
ATP synthase subunit e, mitochondrial OS=Mus musculus OX=10090 GN=Atp5me PE=1 SV=2	1.459	0.164

Table M.1. continued

Pregnancy zone protein OS=Mus musculus OX=10090 GN=Pzp PE=1 SV=3	2.257	0.353
Periostin OS=Mus musculus OX=10090 GN=Postn PE=1 SV=2	1.484	0.171
Interferon-activable protein 202 OS=Mus musculus OX=10090 GN=Ifi202 PE=1 SV=3	0.595	-0.225
Protein delta homolog 1 OS=Mus musculus OX=10090 GN=Dlk1 PE=1 SV=1	1.703	0.231
Acetyl-CoA acetyltransferase, mitochondrial OS=Mus musculus OX=10090 GN=Acat1 PE=1 SV=1	1.171	0.068
ERO1-like protein alpha OS=Mus musculus OX=10090 GN=Ero1a PE=1 SV=2	0.544	-0.264
Serine hydroxymethyltransferase, mitochondrial OS=Mus musculus OX=10090 GN=Shmt2 PE=1 SV=1	0.733	-0.135
Signal peptidase complex subunit 1 OS=Mus musculus OX=10090 GN=Spcs1 PE=2 SV=3	0.453	-0.344
E3 ubiquitin-protein ligase RNF213 OS=Mus musculus OX=10090 GN=Rnf213 PE=1 SV=2	0.627	-0.203
Dipeptidase 1 OS=Mus musculus OX=10090 GN=Dpep1 PE=1 SV=2	1.538	0.187
60S acidic ribosomal protein P1 OS=Mus musculus OX=10090 GN=Rplp1 PE=1 SV=1	3.410	0.533
DnaJ homolog subfamily A member 2 OS=Mus musculus OX=10090 GN=Dnaja2 PE=1 SV=1	1.248	0.096
Glycogen phosphorylase, brain form OS=Mus musculus OX=10090 GN=Pygb PE=1 SV=3	1.230	0.090
Up-regulated during skeletal muscle growth protein 5 OS=Mus musculus OX=10090 GN=Atp5md PE=1 SV=1	0.590	-0.229
Polycystin-2 OS=Mus musculus OX=10090 GN=Pkd2 PE=1 SV=2	1.256	0.099
Protein S100-A13 OS=Mus musculus OX=10090 GN=S100a13 PE=1 SV=1	1.562	0.194

Table M.1. continued

RNA-binding protein FUS OS=Mus musculus OX=10090 GN=Fus PE=1 SV=1	0.843	-0.074
Carnitine O-palmitoyltransferase 2, mitochondrial OS=Mus musculus OX=10090 GN=Cpt2 PE=1 SV=2	0.588	-0.230
Glia-derived nexin OS=Mus musculus OX=10090 GN=Serpine2 PE=1 SV=2	1.987	0.298
Protein tweety homolog 3 OS=Mus musculus OX=10090 GN=Ttyh3 PE=1 SV=1	1.635	0.214
BH3-interacting domain death agonist OS=Mus musculus OX=10090 GN=Bid PE=1 SV=2	0.679	-0.168
Inorganic pyrophosphatase OS=Mus musculus OX=10090 GN=Ppa1 PE=1 SV=1	0.741	-0.130
Lysosome-associated membrane glycoprotein 1 OS=Mus musculus OX=10090 GN=Lamp1 PE=1 SV=2	1.199	0.079
Growth arrest-specific protein 6 OS=Mus musculus OX=10090 GN=Gas6 PE=2 SV=2	1.982	0.297
Cytochrome b-c1 complex subunit 9 OS=Mus musculus OX=10090 GN=Uqcr10 PE=1 SV=1	0.543	-0.266
Cytochrome c oxidase assembly factor 6 homolog OS=Mus musculus OX=10090 GN=Coa6 PE=1 SV=1	1.733	0.239
Membrane-associated progesterone receptor component 2 OS=Mus musculus OX=10090 GN=Pgrmc2 PE=1 SV=2	0.666	-0.176
SPARC OS=Mus musculus OX=10090 GN=Sparc PE=1 SV=1	1.407	0.148
Phosphoserine phosphatase OS=Mus musculus OX=10090 GN=Psph PE=1 SV=1	0.585	-0.233
Glycosylated lysosomal membrane protein OS=Mus musculus OX=10090 GN=Glmp PE=1 SV=1	2.394	0.379
Cofilin-1 OS=Mus musculus OX=10090 GN=Cfl1 PE=1 SV=3	0.868	-0.061
Interleukin enhancer-binding factor 3 OS=Mus musculus OX=10090 GN=Ilf3 PE=1 SV=2	0.795	-0.100

Table M.1. continued

Protein canopy homolog 2 OS=Mus musculus OX=10090 GN=Cnpy2 PE=1 SV=1	1.376	0.139
Lactadherin OS=Mus musculus OX=10090 GN=Mfge8 PE=1 SV=3	1.727	0.237
Poly [ADP-ribose] polymerase 9 OS=Mus musculus OX=10090 GN=Parp9 PE=1 SV=2	0.566	-0.247
Ankycorbin OS=Mus musculus OX=10090 GN=Rai14 PE=1 SV=1	0.918	-0.037
H/ACA ribonucleoprotein complex subunit DKC1 OS=Mus musculus OX=10090 GN=Dkc1 PE=1 SV=4	0.716	-0.145
Delta-aminolevulinic acid dehydratase OS=Mus musculus OX=10090 GN=Alad PE=1 SV=1	0.859	-0.066
High mobility group protein B1 OS=Mus musculus OX=10090 GN=Hmgb1 PE=1 SV=2	0.584	-0.233
Amyloid-beta A4 protein OS=Mus musculus OX=10090 GN=App PE=1 SV=3	1.367	0.136
Neudesin OS=Mus musculus OX=10090 GN=Nenf PE=1 SV=1	1.195	0.077
Medium-chain specific acyl-CoA dehydrogenase, mitochondrial OS=Mus musculus OX=10090 GN=Acadm PE=1 SV=1	1.289	0.110
Annexin A4 OS=Mus musculus OX=10090 GN=Anxa4 PE=1 SV=4	0.909	-0.042
Proteasome subunit beta type-9 OS=Mus musculus OX=10090 GN=Psmb9 PE=1 SV=1	0.232	-0.634
Transgelin OS=Mus musculus OX=10090 GN=Tagln PE=1 SV=3	0.863	-0.064
Annexin A1 OS=Mus musculus OX=10090 GN=Anxa1 PE=1 SV=2	0.839	-0.076
6-phosphogluconolactonase OS=Mus musculus OX=10090 GN=Pgls PE=1 SV=1	0.767	-0.115
L-lactate dehydrogenase A chain OS=Mus musculus OX=10090 GN=Ldha PE=1 SV=3	0.862	-0.065
E3 ubiquitin-protein ligase UBR4 OS=Mus musculus OX=10090 GN=Ubr4 PE=1 SV=1	0.862	-0.064

Table M.1. continued

Cytochrome b5 OS=Mus musculus OX=10090 GN=Cyb5a PE=1 SV=2	1.301	0.114
Serpin H1 OS=Mus musculus OX=10090 GN=Serpinh1 PE=1 SV=3	1.200	0.079
NAD kinase 2, mitochondrial OS=Mus musculus OX=10090 GN=Nadk2 PE=1 SV=2	0.468	-0.329
Signal transducer and activator of transcription 1 OS=Mus musculus OX=10090 GN=Stat1 PE=1 SV=1	0.663	-0.179
Hypoxanthine-guanine phosphoribosyltransferase OS=Mus musculus OX=10090 GN=Hprt1 PE=1 SV=3	0.794	-0.100
CUGBP Elav-like family member 2 OS=Mus musculus OX=10090 GN=Celf2 PE=1 SV=1	0.447	-0.350
Ras-related protein Rab-9A OS=Mus musculus OX=10090 GN=Rab9a PE=1 SV=1	1.275	0.106
E3 ubiquitin-protein ligase RNF114 OS=Mus musculus OX=10090 GN=Rnf114 PE=1 SV=2	0.808	-0.093
Major vault protein OS=Mus musculus OX=10090 GN=Mvp PE=1 SV=4	1.389	0.143
Neutral alpha-glucosidase AB OS=Mus musculus OX=10090 GN=Ganab PE=1 SV=1	0.873	-0.059
Coiled-coil domain-containing protein 91 OS=Mus musculus OX=10090 GN=Ccdc91 PE=1 SV=2	1.221	0.087
UTP--glucose-1-phosphate uridylyltransferase OS=Mus musculus OX=10090 GN=Ugp2 PE=1 SV=3	0.887	-0.052
Thrombospondin-1 OS=Mus musculus OX=10090 GN=Thbs1 PE=1 SV=1	1.477	0.169
Aspartate aminotransferase, mitochondrial OS=Mus musculus OX=10090 GN=Got2 PE=1 SV=1	0.832	-0.080
Murinoglobulin-1 OS=Mus musculus OX=10090 GN=Mug1 PE=1 SV=3	1.651	0.218
Peptidyl-prolyl cis-trans isomerase FKBP10 OS=Mus musculus OX=10090 GN=Fkbp10 PE=1 SV=2	0.777	-0.110

Table M.1. continued

Myristoylated alanine-rich C-kinase substrate OS=Mus musculus OX=10090 GN=Marcks PE=1 SV=2	1.352	0.131
Alpha-galactosidase A OS=Mus musculus OX=10090 GN=Gla PE=1 SV=1	0.860	-0.066
Sec1 family domain-containing protein 1 OS=Mus musculus OX=10090 GN=Scfd1 PE=1 SV=1	1.291	0.111
Succinyl-CoA:3-ketoacid coenzyme A transferase 1, mitochondrial OS=Mus musculus OX=10090 GN=Oxct1 PE=1 SV=1	1.397	0.145
Emerin OS=Mus musculus OX=10090 GN=Emd PE=1 SV=1	0.813	-0.090
COP9 signalosome complex subunit 1 OS=Mus musculus OX=10090 GN=Gps1 PE=1 SV=1	1.282	0.108
ATP-dependent RNA helicase A OS=Mus musculus OX=10090 GN=Dhx9 PE=1 SV=2	0.692	-0.160
Serum albumin OS=Mus musculus OX=10090 GN=Alb PE=1 SV=3	0.682	-0.166
RNA-binding protein NOB1 OS=Mus musculus OX=10090 GN=Nob1 PE=1 SV=1	0.571	-0.243
Mannosyl-oligosaccharide glucosidase OS=Mus musculus OX=10090 GN=Mogs PE=1 SV=1	1.793	0.254
60S ribosomal protein L4 OS=Mus musculus OX=10090 GN=Rpl4 PE=1 SV=3	0.904	-0.044
Splicing regulatory glutamine/lysine-rich protein 1 OS=Mus musculus OX=10090 GN=Srek1 PE=2 SV=1	0.350	-0.456
Vacuolar protein sorting-associated protein 4B OS=Mus musculus OX=10090 GN=Vps4b PE=1 SV=2	0.850	-0.071
Glycylpeptide N-tetradecanoyltransferase 1 OS=Mus musculus OX=10090 GN=Nmt1 PE=1 SV=1	0.792	-0.101
Protein disulfide-isomerase A5 OS=Mus musculus OX=10090 GN=Pdia5 PE=1 SV=1	1.420	0.152
Antithrombin-III OS=Mus musculus OX=10090 GN=Serpinc1 PE=1 SV=1	1.944	0.289

Table M.1. continued

Ras-related protein Rab-11B OS=Mus musculus OX=10090 GN=Rab11b PE=1 SV=3	1.139	0.057
Endoplasmic reticulum chaperone BiP OS=Mus musculus OX=10090 GN=Hspa5 PE=1 SV=3	0.833	-0.079
26S proteasome non-ATPase regulatory subunit 6 OS=Mus musculus OX=10090 GN=Psmd6 PE=1 SV=1	0.680	-0.168
Host cell factor 1 OS=Mus musculus OX=10090 GN=Hcfc1 PE=1 SV=2	1.993	0.299
GDP-mannose 4,6 dehydratase OS=Mus musculus OX=10090 GN=Gmds PE=1 SV=1	1.176	0.070
Serine/threonine-protein phosphatase 2A 55 kDa regulatory subunit B alpha isoform OS=Mus musculus OX=10090 GN=Ppp2r2a PE=1 SV=1	0.869	-0.061
Ran-specific GTPase-activating protein OS=Mus musculus OX=10090 GN=Ranbp1 PE=1 SV=2	0.721	-0.142
Collagen alpha-1(XVIII) chain OS=Mus musculus OX=10090 GN=Col18a1 PE=1 SV=4	0.779	-0.109
DNA topoisomerase 2-beta OS=Mus musculus OX=10090 GN=Top2b PE=1 SV=2	0.808	-0.093
S-phase kinase-associated protein 1 OS=Mus musculus OX=10090 GN=Skp1 PE=1 SV=3	1.431	0.156
Enoyl-CoA hydratase, mitochondrial OS=Mus musculus OX=10090 GN=Echs1 PE=1 SV=1	1.181	0.072
Eukaryotic translation initiation factor 3 subunit K OS=Mus musculus OX=10090 GN=Eif3k PE=1 SV=1	0.728	-0.138
Heterogeneous nuclear ribonucleoprotein L OS=Mus musculus OX=10090 GN=Hnrnpl PE=1 SV=2	1.504	0.177
Prolyl 3-hydroxylase 1 OS=Mus musculus OX=10090 GN=P3h1 PE=1 SV=2	1.512	0.180
Electron transfer flavoprotein subunit alpha, mitochondrial OS=Mus musculus OX=10090 GN=Etfa PE=1 SV=2	1.403	0.147

Table M.1. continued

Interferon-induced 35 kDa protein homolog OS=Mus musculus OX=10090 GN=Ifi35 PE=1 SV=3	0.719	-0.143
Collagen alpha-1(XII) chain OS=Mus musculus OX=10090 GN=Col12a1 PE=2 SV=3	1.182	0.073
DNA topoisomerase 1 OS=Mus musculus OX=10090 GN=Top1 PE=1 SV=2	0.765	-0.116
Translin OS=Mus musculus OX=10090 GN=Tsn PE=1 SV=1	0.768	-0.115
Hepatocyte growth factor-regulated tyrosine kinase substrate OS=Mus musculus OX=10090 GN=Hgs PE=1 SV=2	0.690	-0.161
60S ribosomal protein L36a OS=Mus musculus OX=10090 GN=Rpl36a PE=3 SV=2	0.775	-0.111
Pyridoxal-dependent decarboxylase domain-containing protein 1 OS=Mus musculus OX=10090 GN=Pdxdc1 PE=1 SV=2	0.752	-0.124
Alpha-adducin OS=Mus musculus OX=10090 GN=Add1 PE=1 SV=2	1.227	0.089
Tropomyosin beta chain OS=Mus musculus OX=10090 GN=Tpm2 PE=1 SV=1	0.797	-0.099
UPF0505 protein C16orf62 homolog OS=Mus musculus OX=10090 PE=1 SV=2	1.747	0.242
Synaptopodin OS=Mus musculus OX=10090 GN=Synpo PE=1 SV=2	0.768	-0.114
Phosphatidylethanolamine-binding protein 1 OS=Mus musculus OX=10090 GN=Pebp1 PE=1 SV=3	1.330	0.124
Glutathione reductase, mitochondrial OS=Mus musculus OX=10090 GN=Gsr PE=1 SV=3	0.847	-0.072
Apoptosis inhibitor 5 OS=Mus musculus OX=10090 GN=Api5 PE=1 SV=2	0.833	-0.079
Putative hydroxypyruvate isomerase OS=Mus musculus OX=10090 GN=Hyi PE=1 SV=2	1.430	0.155
NudC domain-containing protein 1 OS=Mus musculus OX=10090 GN=Nudcd1 PE=1 SV=2	0.749	-0.126

Table M.1. continued

Phosphoserine aminotransferase OS=Mus musculus OX=10090 GN=Psat1 PE=1 SV=1	0.678	-0.169
Metalloreductase STEAP3 OS=Mus musculus OX=10090 GN=Steap3 PE=1 SV=1	1.308	0.117
Eukaryotic translation initiation factor 5A-1 OS=Mus musculus OX=10090 GN=Eif5a PE=1 SV=2	1.179	0.072
Thioredoxin-dependent peroxide reductase, mitochondrial OS=Mus musculus OX=10090 GN=Prdx3 PE=1 SV=1	1.122	0.050
Microtubule-associated proteins 1A/1B light chain 3A OS=Mus musculus OX=10090 GN=Map1lc3a PE=1 SV=1	1.306	0.116
DnaJ homolog subfamily C member 9 OS=Mus musculus OX=10090 GN=Dnajc9 PE=1 SV=2	0.609	-0.215
Endophilin-B1 OS=Mus musculus OX=10090 GN=Sh3glb1 PE=1 SV=1	0.819	-0.087
Eukaryotic translation initiation factor 4E OS=Mus musculus OX=10090 GN=Eif4e PE=1 SV=1	0.864	-0.064
Heterogeneous nuclear ribonucleoprotein H OS=Mus musculus OX=10090 GN=Hnrnph1 PE=1 SV=3	0.825	-0.083
Importin subunit alpha-1 OS=Mus musculus OX=10090 GN=Kpna2 PE=1 SV=2	0.683	-0.165
Protein RCC2 OS=Mus musculus OX=10090 GN=Rcc2 PE=1 SV=1	0.823	-0.084
Caprin-1 OS=Mus musculus OX=10090 GN=Caprin1 PE=1 SV=2	0.910	-0.041
Apolipoprotein A-I OS=Mus musculus OX=10090 GN=Apoa1 PE=1 SV=2	0.718	-0.144
26S proteasome non-ATPase regulatory subunit 9 OS=Mus musculus OX=10090 GN=Psmd9 PE=1 SV=1	0.928	-0.033
Asporin OS=Mus musculus OX=10090 GN=Aspn PE=1 SV=1	1.501	0.176
Splicing factor 3B subunit 6 OS=Mus musculus OX=10090 GN=Sf3b6 PE=1 SV=1	0.466	-0.331

Table M.1. continued

SWI/SNF-related matrix-associated actin-dependent regulator of chromatin subfamily A member 5 OS=Mus musculus OX=10090 GN=Smarca5 PE=1 SV=1	0.703	-0.153
Exportin-T OS=Mus musculus OX=10090 GN=Xpot PE=1 SV=3	0.739	-0.131
Dynein light chain Tctex-type 1 OS=Mus musculus OX=10090 GN=Dynlt1 PE=1 SV=1	0.677	-0.169
Eukaryotic translation initiation factor 4 gamma 2 OS=Mus musculus OX=10090 GN=Eif4g2 PE=1 SV=2	0.786	-0.104
Eukaryotic translation initiation factor 3 subunit F OS=Mus musculus OX=10090 GN=Eif3f PE=1 SV=2	0.896	-0.048
Sorting nexin-9 OS=Mus musculus OX=10090 GN=Snx9 PE=1 SV=1	1.309	0.117
NSFL1 cofactor p47 OS=Mus musculus OX=10090 GN=Nsfl1c PE=1 SV=1	0.911	-0.041
Ras-related protein Rab-35 OS=Mus musculus OX=10090 GN=Rab35 PE=1 SV=1	3.790	0.579
Estradiol 17-beta-dehydrogenase 11 OS=Mus musculus OX=10090 GN=Hsd17b11 PE=1 SV=1	1.400	0.146
Keratin, type I cytoskeletal 17 OS=Mus musculus OX=10090 GN=Krt17 PE=1 SV=3	2.291	0.360
RNA 3'-terminal phosphate cyclase OS=Mus musculus OX=10090 GN=RtcA PE=1 SV=2	0.851	-0.070
Anthrax toxin receptor 2 OS=Mus musculus OX=10090 GN=Antxr2 PE=1 SV=1	1.325	0.122
Alpha-aminoadipic semialdehyde dehydrogenase OS=Mus musculus OX=10090 GN=Aldh7a1 PE=1 SV=4	1.551	0.191
Proteasome subunit beta type-1 OS=Mus musculus OX=10090 GN=Psmb1 PE=1 SV=1	0.862	-0.065
DnaJ homolog subfamily C member 25 OS=Mus musculus OX=10090 GN=Dnajc25 PE=1 SV=1	1.201	0.080

Table M.1. continued

Transitional endoplasmic reticulum ATPase OS=Mus musculus OX=10090 GN=Vcp PE=1 SV=4	1.149	0.060
Calcium-activated chloride channel regulator 3A-1 OS=Mus musculus OX=10090 GN=Clca3a1 PE=1 SV=1	0.758	-0.121
AP-2 complex subunit sigma OS=Mus musculus OX=10090 GN=Ap2s1 PE=1 SV=1	1.284	0.109
Glutathione S-transferase omega-1 OS=Mus musculus OX=10090 GN=Gsto1 PE=1 SV=2	0.722	-0.141
Integrin-linked protein kinase OS=Mus musculus OX=10090 GN=Ilk PE=1 SV=2	1.293	0.112
Copine-1 OS=Mus musculus OX=10090 GN=Cpne1 PE=1 SV=1	2.047	0.311
Protein PML OS=Mus musculus OX=10090 GN=Pml PE=1 SV=3	0.585	-0.233
Eukaryotic translation initiation factor 3 subunit A OS=Mus musculus OX=10090 GN=Eif3a PE=1 SV=5	0.908	-0.042
ATP-binding cassette sub-family E member 1 OS=Mus musculus OX=10090 GN=Abce1 PE=1 SV=1	0.888	-0.052
RNA binding motif protein, X-linked-like-1 OS=Mus musculus OX=10090 GN=Rbmxl1 PE=2 SV=1	0.872	-0.059
Target of Myb protein 1 OS=Mus musculus OX=10090 GN=Tom1 PE=1 SV=1	1.189	0.075
UPF0160 protein MYG1, mitochondrial OS=Mus musculus OX=10090 GN=Myg1 PE=1 SV=1	0.797	-0.098
CAP-Gly domain-containing linker protein 1 OS=Mus musculus OX=10090 GN=Clip1 PE=1 SV=1	1.323	0.122
Ubiquitin domain-containing protein UBFD1 OS=Mus musculus OX=10090 GN=Ubfd1 PE=1 SV=2	0.812	-0.090
Serpin B8 OS=Mus musculus OX=10090 GN=Serpinb8 PE=1 SV=2	1.924	0.284
Epididymis-specific alpha-mannosidase OS=Mus musculus OX=10090 GN=Man2b2 PE=1 SV=2	1.510	0.179

Table M.1. continued

FACT complex subunit SSRP1 OS=Mus musculus OX=10090 GN=Ssrp1 PE=1 SV=2	0.766	-0.116
S-methyl-5'-thioadenosine phosphorylase OS=Mus musculus OX=10090 GN=Mtap PE=1 SV=1	0.843	-0.074
Sodium/myo-inositol cotransporter OS=Mus musculus OX=10090 GN=Slc5a3 PE=1 SV=2	1.203	0.080
Far upstream element-binding protein 1 OS=Mus musculus OX=10090 GN=Fubp1 PE=1 SV=1	0.873	-0.059
Bifunctional purine biosynthesis protein PURH OS=Mus musculus OX=10090 GN=Atic PE=1 SV=2	0.851	-0.070
Lysosomal acid phosphatase OS=Mus musculus OX=10090 GN=Acp2 PE=1 SV=2	1.417	0.151
GTP-binding nuclear protein Ran OS=Mus musculus OX=10090 GN=Ran PE=1 SV=3	0.868	-0.061
Glutamine--fructose-6-phosphate aminotransferase [isomerizing] 1 OS=Mus musculus OX=10090 GN=Gfpt1 PE=1 SV=3	0.890	-0.051
Drebrin-like protein OS=Mus musculus OX=10090 GN=Dbnl PE=1 SV=2	1.861	0.270
Calponin-3 OS=Mus musculus OX=10090 GN=Cnn3 PE=1 SV=1	0.873	-0.059
Voltage-dependent anion-selective channel protein 3 OS=Mus musculus OX=10090 GN=Vdac3 PE=1 SV=1	1.337	0.126
Interferon-induced, double-stranded RNA-activated protein kinase OS=Mus musculus OX=10090 GN=Eif2ak2 PE=1 SV=2	0.676	-0.170
Mannose-1-phosphate guanyltransferase alpha OS=Mus musculus OX=10090 GN=Gmppa PE=1 SV=1	1.262	0.101
Aminoacyl tRNA synthase complex-interacting multifunctional protein 2 OS=Mus musculus OX=10090 GN=Aimp2 PE=1 SV=2	1.195	0.077
Tropomyosin alpha-1 chain OS=Mus musculus OX=10090 GN=Tpm1 PE=1 SV=1	0.865	-0.063
Protein FRG1 OS=Mus musculus OX=10090 GN=Frg1 PE=1 SV=2	0.810	-0.091

Table M.1. continued

Glucosamine 6-phosphate N-acetyltransferase OS=Mus musculus OX=10090 GN=Gnpnat1 PE=1 SV=1	0.787	-0.104
Inosine-5'-monophosphate dehydrogenase 2 OS=Mus musculus OX=10090 GN=Impdh2 PE=1 SV=2	1.324	0.122
Transmembrane emp24 domain-containing protein 1 OS=Mus musculus OX=10090 GN=Tmed1 PE=1 SV=1	5.490	0.740
Collagen alpha-2(V) chain OS=Mus musculus OX=10090 GN=Col5a2 PE=1 SV=1	1.308	0.117
NEDD8-activating enzyme E1 catalytic subunit OS=Mus musculus OX=10090 GN=Uba3 PE=1 SV=2	0.887	-0.052
Vacuolar protein sorting-associated protein 29 OS=Mus musculus OX=10090 GN=Vps29 PE=1 SV=1	1.470	0.167
Arginine--tRNA ligase, cytoplasmic OS=Mus musculus OX=10090 GN=Rars PE=1 SV=2	0.797	-0.099
Keratin, type I cytoskeletal 10 OS=Mus musculus OX=10090 GN=Krt10 PE=1 SV=3	2.118	0.326
rRNA 2'-O-methyltransferase fibrillarin OS=Mus musculus OX=10090 GN=Fbl PE=1 SV=2	0.710	-0.148
Tensin-3 OS=Mus musculus OX=10090 GN=Tns3 PE=1 SV=1	1.116	0.048
Tudor-interacting repair regulator protein OS=Mus musculus OX=10090 GN=Nudt16l1 PE=1 SV=2	1.103	0.042
Fatty acid-binding protein 5 OS=Mus musculus OX=10090 GN=Fabp5 PE=1 SV=3	0.758	-0.121
COP9 signalosome complex subunit 5 OS=Mus musculus OX=10090 GN=Cops5 PE=1 SV=3	1.166	0.067
Beta-2-microglobulin OS=Mus musculus OX=10090 GN=B2m PE=1 SV=2	0.299	-0.525
26S proteasome regulatory subunit 6A OS=Mus musculus OX=10090 GN=Psmc3 PE=1 SV=2	1.320	0.120
CXADR-like membrane protein OS=Mus musculus OX=10090 GN=Clmp PE=1 SV=1	1.389	0.143

Table M.1. continued

Thrombomodulin OS=Mus musculus OX=10090 GN=Thbd PE=1 SV=1	1.382	0.140
Dehydrogenase/reductase SDR family member 4 OS=Mus musculus OX=10090 GN=Dhrs4 PE=1 SV=3	1.849	0.267
Phospholemman OS=Mus musculus OX=10090 GN=Fxyd1 PE=1 SV=1	1.844	0.266
Kinesin-like protein KIF3B OS=Mus musculus OX=10090 GN=Kif3b PE=1 SV=1	2.293	0.360
Insulin-like growth factor-binding protein 7 OS=Mus musculus OX=10090 GN=Igfbp7 PE=1 SV=3	1.242	0.094
Cleavage and polyadenylation specificity factor subunit 7 OS=Mus musculus OX=10090 GN=Cpsf7 PE=1 SV=2	1.906	0.280
Gamma-interferon-inducible lysosomal thiol reductase OS=Mus musculus OX=10090 GN=Ifi30 PE=1 SV=3	1.300	0.114
Complement C4-B OS=Mus musculus OX=10090 GN=C4b PE=1 SV=3	2.764	0.442
Disabled homolog 2 OS=Mus musculus OX=10090 GN=Dab2 PE=1 SV=2	1.321	0.121
Importin subunit alpha-3 OS=Mus musculus OX=10090 GN=Kpna4 PE=1 SV=1	0.320	-0.495
Microtubule-associated protein RP/EB family member 1 OS=Mus musculus OX=10090 GN=Mapre1 PE=1 SV=3	1.235	0.092
Glucose-6-phosphate isomerase OS=Mus musculus OX=10090 GN=Gpi PE=1 SV=4	0.575	-0.240
Transcription elongation regulator 1 OS=Mus musculus OX=10090 GN=Tcerg1 PE=1 SV=2	0.859	-0.066
Heterogeneous nuclear ribonucleoprotein U OS=Mus musculus OX=10090 GN=Hnrnpu PE=1 SV=1	0.904	-0.044
Thioredoxin domain-containing protein 5 OS=Mus musculus OX=10090 GN=Txndc5 PE=1 SV=2	1.146	0.059

Table M.1. continued

Interleukin enhancer-binding factor 2 OS=Mus musculus OX=10090 GN=Ilf2 PE=1 SV=1	0.760	-0.119
Neutral amino acid transporter B(0) OS=Mus musculus OX=10090 GN=Slc1a5 PE=1 SV=2	1.190	0.075
3-hydroxyisobutyrate dehydrogenase, mitochondrial OS=Mus musculus OX=10090 GN=Hibadh PE=1 SV=1	1.366	0.135
Receptor-interacting serine/threonine-protein kinase 3 OS=Mus musculus OX=10090 GN=Ripk3 PE=1 SV=2	0.613	-0.212
Perilipin-3 OS=Mus musculus OX=10090 GN=Plin3 PE=1 SV=1	1.111	0.046
Proteasome subunit beta type-6 OS=Mus musculus OX=10090 GN=Psmb6 PE=1 SV=3	1.348	0.130
Elongation factor 1-beta OS=Mus musculus OX=10090 GN=Eef1b PE=1 SV=5	0.832	-0.080
Small nuclear ribonucleoprotein Sm D3 OS=Mus musculus OX=10090 GN=Snrpd3 PE=1 SV=1	0.887	-0.052
Mannose-P-dolichol utilization defect 1 protein OS=Mus musculus OX=10090 GN=Mpdu1 PE=1 SV=1	4.625	0.665
High mobility group nucleosome-binding domain-containing protein 3 OS=Mus musculus OX=10090 GN=Hmgn3 PE=1 SV=1	1.313	0.118
Septin-2 OS=Mus musculus OX=10090 GN=Sept2 PE=1 SV=2	0.926	-0.033
mRNA export factor OS=Mus musculus OX=10090 GN=Rae1 PE=1 SV=1	0.768	-0.115
Prohibitin OS=Mus musculus OX=10090 GN=Phb PE=1 SV=1	1.364	0.135
SH3 domain-binding glutamic acid-rich-like protein 3 OS=Mus musculus OX=10090 GN=Sh3bgrl3 PE=1 SV=1	0.653	-0.185
Delta-1-pyrroline-5-carboxylate synthase OS=Mus musculus OX=10090 GN=Aldh18a1 PE=1 SV=2	0.860	-0.066
Guanine nucleotide exchange factor MSS4 OS=Mus musculus OX=10090 GN=Rabif PE=1 SV=1	0.249	-0.603
Cathepsin L1 OS=Mus musculus OX=10090 GN=Ctsl PE=1 SV=2	1.781	0.251

Table M.1. continued

Dynactin subunit 1 OS=Mus musculus OX=10090 GN=Dctn1 PE=1 SV=3	1.169	0.068
G patch domain-containing protein 1 OS=Mus musculus OX=10090 GN=Gpatch1 PE=2 SV=1	1.840	0.265
Striatin OS=Mus musculus OX=10090 GN=Strn PE=1 SV=2	1.814	0.259
Cytosolic Fe-S cluster assembly factor NUBP2 OS=Mus musculus OX=10090 GN=Nubp2 PE=1 SV=1	0.761	-0.119
Polyglutamine-binding protein 1 OS=Mus musculus OX=10090 GN=Pqbp1 PE=1 SV=1	0.751	-0.124
Toll-interacting protein OS=Mus musculus OX=10090 GN=Tollip PE=1 SV=1	1.168	0.067
cAMP-dependent protein kinase type II-alpha regulatory subunit OS=Mus musculus OX=10090 GN=Prkar2a PE=1 SV=2	1.293	0.112
Coatomer subunit delta OS=Mus musculus OX=10090 GN=Arcn1 PE=1 SV=2	1.117	0.048
Nuclear pore complex protein Nup93 OS=Mus musculus OX=10090 GN=Nup93 PE=1 SV=1	0.754	-0.122
60S ribosomal protein L28 OS=Mus musculus OX=10090 GN=Rpl28 PE=1 SV=2	0.743	-0.129
Secretory carrier-associated membrane protein 3 OS=Mus musculus OX=10090 GN=Scamp3 PE=1 SV=3	1.226	0.088
Serine/threonine-protein kinase Nek7 OS=Mus musculus OX=10090 GN=Nek7 PE=1 SV=1	1.262	0.101
Aldehyde dehydrogenase family 3 member B1 OS=Mus musculus OX=10090 GN=Aldh3b1 PE=1 SV=1	1.409	0.149
Biglycan OS=Mus musculus OX=10090 GN=Bgn PE=1 SV=1	1.239	0.093
Cytoskeleton-associated protein 4 OS=Mus musculus OX=10090 GN=Ckap4 PE=1 SV=2	1.198	0.079
NGFI-A-binding protein 2 OS=Mus musculus OX=10090 GN=Nab2 PE=1 SV=2	0.906	-0.043

Table M.1. continued

High mobility group protein B2 OS=Mus musculus OX=10090 GN=Hmgb2 PE=1 SV=3	0.578	-0.238
BolA-like protein 1 OS=Mus musculus OX=10090 GN=Bola1 PE=1 SV=1	0.387	-0.413
Aspartate--tRNA ligase, cytoplasmic OS=Mus musculus OX=10090 GN=Dars PE=1 SV=2	0.893	-0.049
Actin, aortic smooth muscle OS=Mus musculus OX=10090 GN=Acta2 PE=1 SV=1	0.547	-0.262
Septin-5 OS=Mus musculus OX=10090 GN=Sept5 PE=1 SV=2	1.079	0.033
Alcohol dehydrogenase class 4 mu/sigma chain OS=Mus musculus OX=10090 GN=Adh7 PE=2 SV=2	1.927	0.285
40S ribosomal protein S8 OS=Mus musculus OX=10090 GN=Rps8 PE=1 SV=2	0.903	-0.044
Deoxynucleoside triphosphate triphosphohydrolase SAMHD1 OS=Mus musculus OX=10090 GN=Samhd1 PE=1 SV=3	0.797	-0.098
Ubiquitin-conjugating enzyme E2 G1 OS=Mus musculus OX=10090 GN=Ube2g1 PE=1 SV=3	0.462	-0.335
Integrin-linked kinase-associated serine/threonine phosphatase 2C OS=Mus musculus OX=10090 GN=Ilkap PE=1 SV=1	0.647	-0.189
Actin, cytoplasmic 1 OS=Mus musculus OX=10090 GN=Actb PE=1 SV=1	1.838	0.264
Ornithine aminotransferase, mitochondrial OS=Mus musculus OX=10090 GN=Oat PE=1 SV=1	1.262	0.101
Pleiotrophin OS=Mus musculus OX=10090 GN=Ptn PE=1 SV=1	1.403	0.147
Protein Niban OS=Mus musculus OX=10090 GN=Fam129a PE=1 SV=2	0.535	-0.271
Unconventional myosin-Ib OS=Mus musculus OX=10090 GN=Myo1b PE=1 SV=3	0.873	-0.059
Gremlin-1 OS=Mus musculus OX=10090 GN=Grem1 PE=2 SV=1	1.772	0.249

Table M.1. continued

Apolipoprotein B-100 OS=Mus musculus OX=10090 GN=Apob PE=1 SV=1	1.207	0.082
Scavenger receptor class F member 2 OS=Mus musculus OX=10090 GN=Scarf2 PE=1 SV=1	1.313	0.118
A-kinase anchor protein 12 OS=Mus musculus OX=10090 GN=Akap12 PE=1 SV=1	1.355	0.132
U5 small nuclear ribonucleoprotein 40 kDa protein OS=Mus musculus OX=10090 GN=Snrnp40 PE=1 SV=1	0.831	-0.080
Keratin, type II cuticular Hb5 OS=Mus musculus OX=10090 GN=Krt85 PE=1 SV=2	9.139	0.961
Serine/threonine-protein phosphatase 2B catalytic subunit beta isoform OS=Mus musculus OX=10090 GN=Ppp3cb PE=1 SV=2	1.503	0.177
Stress-induced-phosphoprotein 1 OS=Mus musculus OX=10090 GN=Stip1 PE=1 SV=1	1.277	0.106
NmrA-like family domain-containing protein 1 OS=Mus musculus OX=10090 GN=Nmral1 PE=1 SV=1	0.796	-0.099
DNA excision repair protein ERCC-6-like OS=Mus musculus OX=10090 GN=Ercc6l PE=1 SV=1	2.267	0.355
Cadherin-11 OS=Mus musculus OX=10090 GN=Cdh11 PE=1 SV=1	1.094	0.039
Heat shock protein HSP 90-alpha OS=Mus musculus OX=10090 GN=Hsp90aa1 PE=1 SV=4	0.769	-0.114
Malate dehydrogenase, mitochondrial OS=Mus musculus OX=10090 GN=Mdh2 PE=1 SV=3	1.150	0.061
Hexokinase-2 OS=Mus musculus OX=10090 GN=Hk2 PE=1 SV=1	0.752	-0.124
SH3 domain-binding protein 1 OS=Mus musculus OX=10090 GN=Sh3bp1 PE=1 SV=3	0.825	-0.084
NADH dehydrogenase [ubiquinone] 1 beta subcomplex subunit 10 OS=Mus musculus OX=10090 GN=Ndufb10 PE=1 SV=3	0.724	-0.140
Type 1 phosphatidylinositol 4,5-bisphosphate 4-phosphatase OS=Mus musculus OX=10090 GN=Pip4p1 PE=1 SV=1	1.726	0.237

Table M.1. continued

Adenylosuccinate lyase OS=Mus musculus OX=10090 GN=Adsl PE=1 SV=2	0.867	-0.062
Syntaxin-binding protein 3 OS=Mus musculus OX=10090 GN=Stxbp3 PE=1 SV=1	0.885	-0.053
Retention time calibration protein	0.928	-0.033
Mitogen-activated protein kinase kinase kinase kinase 4 OS=Mus musculus OX=10090 GN=Map4k4 PE=1 SV=1	1.157	0.063
Triokinase/FMN cyclase OS=Mus musculus OX=10090 GN=Tkfc PE=1 SV=1	1.190	0.076
STIP1 homology and U box-containing protein 1 OS=Mus musculus OX=10090 GN=Stub1 PE=1 SV=1	0.811	-0.091
Prohibitin-2 OS=Mus musculus OX=10090 GN=Phb2 PE=1 SV=1	0.826	-0.083
Keratin, type I cytoskeletal 16 OS=Mus musculus OX=10090 GN=Krt16 PE=1 SV=3	2.713	0.433
Lysosomal alpha-glucosidase OS=Mus musculus OX=10090 GN=Gaa PE=1 SV=2	1.138	0.056
SUMO-activating enzyme subunit 2 OS=Mus musculus OX=10090 GN=Uba2 PE=1 SV=1	1.457	0.163
Signal transducer and activator of transcription 3 OS=Mus musculus OX=10090 GN=Stat3 PE=1 SV=2	0.853	-0.069
Acyl carrier protein, mitochondrial OS=Mus musculus OX=10090 GN=Ndufab1 PE=1 SV=1	0.548	-0.261
Asparagine synthetase [glutamine-hydrolyzing] OS=Mus musculus OX=10090 GN=Asns PE=1 SV=3	0.765	-0.117
Ester hydrolase C11orf54 homolog OS=Mus musculus OX=10090 PE=1 SV=1	0.928	-0.032
Translocation protein SEC63 homolog OS=Mus musculus OX=10090 GN=Sec63 PE=1 SV=4	0.649	-0.188
Matrix Gla protein OS=Mus musculus OX=10090 GN=Mgp PE=3 SV=1	1.441	0.159

Table M.1. continued

Heat shock protein beta-8 OS=Mus musculus OX=10090 GN=Hspb8 PE=1 SV=1	1.664	0.221
40S ribosomal protein S2 OS=Mus musculus OX=10090 GN=Rps2 PE=1 SV=3	0.899	-0.046
Thimet oligopeptidase OS=Mus musculus OX=10090 GN=Thop1 PE=1 SV=1	0.785	-0.105
Mixed lineage kinase domain-like protein OS=Mus musculus OX=10090 GN=Mlkl PE=1 SV=1	0.536	-0.271
Prostacyclin synthase OS=Mus musculus OX=10090 GN=Ptgis PE=1 SV=1	1.267	0.103
AMP deaminase 2 OS=Mus musculus OX=10090 GN=Ampd2 PE=1 SV=1	0.731	-0.136
60S ribosomal protein L22 OS=Mus musculus OX=10090 GN=Rpl22 PE=1 SV=2	0.873	-0.059
Ribosyldihydronicotinamide dehydrogenase [quinone] OS=Mus musculus OX=10090 GN=Nqo2 PE=1 SV=3	0.822	-0.085
Sorting nexin-2 OS=Mus musculus OX=10090 GN=Snx2 PE=1 SV=2	0.786	-0.105
Ras suppressor protein 1 OS=Mus musculus OX=10090 GN=Rsu1 PE=1 SV=3	0.648	-0.188
NADH dehydrogenase [ubiquinone] 1 alpha subcomplex subunit 10, mitochondrial OS=Mus musculus OX=10090 GN=Ndufa10 PE=1 SV=1	0.806	-0.094
Protein MAK16 homolog OS=Mus musculus OX=10090 GN=Mak16 PE=1 SV=1	0.556	-0.255
X-ray repair cross-complementing protein 6 OS=Mus musculus OX=10090 GN=Xrcc6 PE=1 SV=5	0.809	-0.092
Nucleolar GTP-binding protein 1 OS=Mus musculus OX=10090 GN=Gtpbp4 PE=1 SV=3	0.854	-0.068
Sorcin OS=Mus musculus OX=10090 GN=Sri PE=1 SV=1	1.164	0.066

Table M.1. continued

Spectrin beta chain, non-erythrocytic 1 OS=Mus musculus OX=10090 GN=Sptbn1 PE=1 SV=2	1.214	0.084
Bax inhibitor 1 OS=Mus musculus OX=10090 GN=Tmbim6 PE=1 SV=1	0.223	-0.652
Protein canopy homolog 4 OS=Mus musculus OX=10090 GN=Cnpy4 PE=1 SV=1	1.700	0.231
Sulfide:quinone oxidoreductase, mitochondrial OS=Mus musculus OX=10090 GN=Sqor PE=1 SV=3	0.831	-0.080
AP-1 complex subunit gamma-1 OS=Mus musculus OX=10090 GN=Ap1g1 PE=1 SV=3	0.842	-0.075
Eukaryotic translation initiation factor 5 OS=Mus musculus OX=10090 GN=Eif5 PE=1 SV=1	0.859	-0.066
Integral membrane protein 2C OS=Mus musculus OX=10090 GN=Itm2c PE=1 SV=2	1.764	0.246
Craniofacial development protein 1 OS=Mus musculus OX=10090 GN=Cfdp1 PE=1 SV=1	0.876	-0.058
Reticulocalbin-1 OS=Mus musculus OX=10090 GN=Rcn1 PE=1 SV=1	1.100	0.041
Adenylate kinase isoenzyme 1 OS=Mus musculus OX=10090 GN=Ak1 PE=1 SV=1	1.146	0.059
Eukaryotic initiation factor 4A-II OS=Mus musculus OX=10090 GN=Eif4a2 PE=1 SV=2	0.847	-0.072
Eukaryotic translation initiation factor 3 subunit B OS=Mus musculus OX=10090 GN=Eif3b PE=1 SV=1	0.817	-0.088
Splicing factor 3B subunit 1 OS=Mus musculus OX=10090 GN=Sf3b1 PE=1 SV=1	0.833	-0.079
Derlin-1 OS=Mus musculus OX=10090 GN=Derl1 PE=1 SV=1	3.152	0.499
Ferritin light chain 1 OS=Mus musculus OX=10090 GN=Ftl1 PE=1 SV=2	1.844	0.266
Cystatin-B OS=Mus musculus OX=10090 GN=Cstb PE=1 SV=1	0.841	-0.075

Table M.1. continued

Catenin beta-1 OS=Mus musculus OX=10090 GN=Ctnnb1 PE=1 SV=1	1.305	0.115
Ras-related protein R-Ras2 OS=Mus musculus OX=10090 GN=Rras2 PE=1 SV=1	1.583	0.200
CUGBP Elav-like family member 1 OS=Mus musculus OX=10090 GN=Celf1 PE=1 SV=2	0.347	-0.460
Receptor of activated protein C kinase 1 OS=Mus musculus OX=10090 GN=Rack1 PE=1 SV=3	0.882	-0.055
Ras-related protein Rab-2A OS=Mus musculus OX=10090 GN=Rab2a PE=1 SV=1	1.460	0.164
Transmembrane protein 119 OS=Mus musculus OX=10090 GN=Tmem119 PE=1 SV=1	1.405	0.148
Phosphatidylinositol transfer protein beta isoform OS=Mus musculus OX=10090 GN=Pitpnb PE=1 SV=2	1.216	0.085
60S ribosomal protein L6 OS=Mus musculus OX=10090 GN=Rpl6 PE=1 SV=3	0.901	-0.045
Matrix metalloproteinase-14 OS=Mus musculus OX=10090 GN=Mmp14 PE=2 SV=3	1.235	0.092
Leucine--tRNA ligase, cytoplasmic OS=Mus musculus OX=10090 GN=Lars PE=1 SV=2	0.819	-0.087
Heat shock 70 kDa protein 1A OS=Mus musculus OX=10090 GN=Hspa1a PE=1 SV=2	1.234	0.091
DNA ligase 1 OS=Mus musculus OX=10090 GN=Lig1 PE=1 SV=2	0.782	-0.107
Cytochrome P450 1B1 OS=Mus musculus OX=10090 GN=Cyp1b1 PE=1 SV=3	1.296	0.113
Phospholipase D3 OS=Mus musculus OX=10090 GN=Pld3 PE=1 SV=1	1.155	0.063
Protein FAM98B OS=Mus musculus OX=10090 GN=Fam98b PE=1 SV=1	0.875	-0.058
DnaJ homolog subfamily C member 1 OS=Mus musculus OX=10090 GN=Dnajc1 PE=1 SV=1	1.443	0.159

Table M.1. continued

Golgi integral membrane protein 4 OS=Mus musculus OX=10090 GN=Golim4 PE=1 SV=1	1.350	0.130
Proteasome assembly chaperone 1 OS=Mus musculus OX=10090 GN=Psmg1 PE=1 SV=1	0.478	-0.321
Tubulin beta-5 chain OS=Mus musculus OX=10090 GN=Tubb5 PE=1 SV=1	0.913	-0.039
ADP-ribosylation factor-binding protein GGA1 OS=Mus musculus OX=10090 GN=Gga1 PE=1 SV=1	0.402	-0.396
Complement C3 OS=Mus musculus OX=10090 GN=C3 PE=1 SV=3	0.818	-0.087
UDP-N-acetylhexosamine pyrophosphorylase-like protein 1 OS=Mus musculus OX=10090 GN=Uap1l1 PE=1 SV=1	1.283	0.108
P2X purinoceptor 4 OS=Mus musculus OX=10090 GN=P2rx4 PE=1 SV=1	1.139	0.057
Unconventional myosin-Ic OS=Mus musculus OX=10090 GN=Myo1c PE=1 SV=2	0.887	-0.052
SAP domain-containing ribonucleoprotein OS=Mus musculus OX=10090 GN=Sarnp PE=1 SV=3	0.910	-0.041
NADH dehydrogenase [ubiquinone] 1 subunit C2 OS=Mus musculus OX=10090 GN=Ndufc2 PE=1 SV=1	1.433	0.156
Myosin light polypeptide 6 OS=Mus musculus OX=10090 GN=Myl6 PE=1 SV=3	0.770	-0.113
Platelet-derived growth factor receptor beta OS=Mus musculus OX=10090 GN=Pdgfrb PE=1 SV=1	1.361	0.134
Ephrin type-B receptor 3 OS=Mus musculus OX=10090 GN=Ephb3 PE=1 SV=2	1.557	0.192
V-type proton ATPase 116 kDa subunit a isoform 2 OS=Mus musculus OX=10090 GN=Atp6v0a2 PE=1 SV=2	1.384	0.141
Pyridoxal kinase OS=Mus musculus OX=10090 GN=Pdxk PE=1 SV=1	0.765	-0.117
Elongation factor 1-gamma OS=Mus musculus OX=10090 GN=Eef1g PE=1 SV=3	0.736	-0.133

Table M.1. continued

Adenylosuccinate synthetase isozyme 2 OS=Mus musculus OX=10090 GN=Adss PE=1 SV=2	0.887	-0.052
Vacuolar protein sorting-associated protein 35 OS=Mus musculus OX=10090 GN=Vps35 PE=1 SV=1	0.941	-0.026
Calcium-regulated heat stable protein 1 OS=Mus musculus OX=10090 GN=Carhsp1 PE=1 SV=1	2.992	0.476
Histone H3.2 OS=Mus musculus OX=10090 GN=Hist1h3b PE=1 SV=2	1.601	0.204
Cysteine-rich with EGF-like domain protein 2 OS=Mus musculus OX=10090 GN=Creld2 PE=1 SV=1	1.233	0.091
Peptidyl-prolyl cis-trans isomerase B OS=Mus musculus OX=10090 GN=Ppib PE=1 SV=2	1.209	0.082
Prostaglandin reductase 2 OS=Mus musculus OX=10090 GN=Ptgr2 PE=1 SV=2	1.436	0.157
Probable glutathione peroxidase 8 OS=Mus musculus OX=10090 GN=Gpx8 PE=1 SV=1	1.151	0.061
Mitochondrial import inner membrane translocase subunit Tim8 A OS=Mus musculus OX=10090 GN=Timm8a1 PE=1 SV=1	0.835	-0.078
T-complex protein 1 subunit zeta OS=Mus musculus OX=10090 GN=Cct6a PE=1 SV=3	0.856	-0.068
Eukaryotic translation initiation factor 2 subunit 2 OS=Mus musculus OX=10090 GN=Eif2s2 PE=1 SV=1	0.837	-0.077
Ras-related protein Ral-B OS=Mus musculus OX=10090 GN=Ralb PE=1 SV=1	0.683	-0.165
Procollagen C-endopeptidase enhancer 1 OS=Mus musculus OX=10090 GN=Pcolce PE=1 SV=2	1.221	0.087
Phospholipid phosphatase 3 OS=Mus musculus OX=10090 GN=Plpp3 PE=1 SV=1	1.293	0.112
Torsin-1A-interacting protein 1 OS=Mus musculus OX=10090 GN=Tor1aip1 PE=1 SV=3	0.802	-0.096

Table M.1. continued

RING-type E3 ubiquitin-protein ligase PPIL2 OS=Mus musculus OX=10090 GN=Ppil2 PE=1 SV=2	1.359	0.133
Phosphatidylinositol transfer protein alpha isoform OS=Mus musculus OX=10090 GN=Pitpna PE=1 SV=2	0.267	-0.573
Mannose-1-phosphate guanyltransferase beta OS=Mus musculus OX=10090 GN=Gmppb PE=1 SV=1	1.202	0.080
N-acylethanolamine-hydrolyzing acid amidase OS=Mus musculus OX=10090 GN=Naaa PE=1 SV=2	1.278	0.106
AP-1 complex subunit beta-1 OS=Mus musculus OX=10090 GN=Ap1b1 PE=1 SV=2	0.876	-0.058
Neurabin-2 OS=Mus musculus OX=10090 GN=Ppp1r9b PE=1 SV=1	1.268	0.103
Acidic leucine-rich nuclear phosphoprotein 32 family member A OS=Mus musculus OX=10090 GN=Anp32a PE=1 SV=1	0.874	-0.058
Oxysterol-binding protein 1 OS=Mus musculus OX=10090 GN=Osbp PE=1 SV=3	0.616	-0.210
Diphosphoinositol polyphosphate phosphohydrolase 1 OS=Mus musculus OX=10090 GN=Nudt3 PE=1 SV=1	0.800	-0.097
116 kDa U5 small nuclear ribonucleoprotein component OS=Mus musculus OX=10090 GN=Eftud2 PE=1 SV=1	0.796	-0.099
Regulator of nonsense transcripts 1 OS=Mus musculus OX=10090 GN=Upf1 PE=1 SV=2	1.299	0.114
Thioredoxin OS=Mus musculus OX=10090 GN=Txn PE=1 SV=3	0.878	-0.056
Aspartyl aminopeptidase OS=Mus musculus OX=10090 GN=Dnpep PE=1 SV=2	0.765	-0.116
LIM and SH3 domain protein 1 OS=Mus musculus OX=10090 GN=Lasp1 PE=1 SV=1	0.891	-0.050
GTP:AMP phosphotransferase AK3, mitochondrial OS=Mus musculus OX=10090 GN=Ak3 PE=1 SV=3	1.246	0.095
Vesicle transport through interaction with t-SNAREs homolog 1B OS=Mus musculus OX=10090 GN=Vti1b PE=1 SV=1	1.253	0.098

Table M.1. continued

BAG family molecular chaperone regulator 5 OS=Mus musculus OX=10090 GN=Bag5 PE=1 SV=1	1.403	0.147
Translation initiation factor eIF-2B subunit epsilon OS=Mus musculus OX=10090 GN=Eif2b5 PE=1 SV=1	0.828	-0.082
Synaptic vesicle membrane protein VAT-1 homolog OS=Mus musculus OX=10090 GN=Vat1 PE=1 SV=3	1.132	0.054
Hsc70-interacting protein OS=Mus musculus OX=10090 GN=St13 PE=1 SV=1	0.886	-0.052
Nucleolin OS=Mus musculus OX=10090 GN=Ncl PE=1 SV=2	0.917	-0.038
Dynein light chain roadblock-type 1 OS=Mus musculus OX=10090 GN=Dynlrb1 PE=1 SV=3	1.279	0.107
Long-chain-fatty-acid--CoA ligase 5 OS=Mus musculus OX=10090 GN=Acsl5 PE=1 SV=1	0.427	-0.370
Coiled-coil-helix-coiled-coil-helix domain-containing protein 2 OS=Mus musculus OX=10090 GN=Chchd2 PE=2 SV=1	1.137	0.056
Elongation factor G, mitochondrial OS=Mus musculus OX=10090 GN=Gfm1 PE=1 SV=1	0.860	-0.066
Activated RNA polymerase II transcriptional coactivator p15 OS=Mus musculus OX=10090 GN=Sub1 PE=1 SV=3	0.762	-0.118
Collagen alpha-2(I) chain OS=Mus musculus OX=10090 GN=Col1a2 PE=1 SV=2	1.247	0.096
COP9 signalosome complex subunit 8 OS=Mus musculus OX=10090 GN=Cops8 PE=1 SV=1	1.109	0.045
GATOR complex protein WDR59 OS=Mus musculus OX=10090 GN=Wdr59 PE=1 SV=2	1.298	0.113
EH domain-binding protein 1-like protein 1 OS=Mus musculus OX=10090 GN=Ehbp1l1 PE=1 SV=1	0.794	-0.100
1-phosphatidylinositol 4,5-bisphosphate phosphodiesterase beta-3 OS=Mus musculus OX=10090 GN=Plcb3 PE=1 SV=2	0.864	-0.063
Heat shock protein HSP 90-beta OS=Mus musculus OX=10090 GN=Hsp90ab1 PE=1 SV=3	0.898	-0.047

Table M.1. continued

Cytosolic non-specific dipeptidase OS=Mus musculus OX=10090 GN=Cndp2 PE=1 SV=1	0.929	-0.032
Uncharacterized protein CXorf38 homolog OS=Mus musculus OX=10090 PE=1 SV=1	0.501	-0.300
Isoleucine--tRNA ligase, mitochondrial OS=Mus musculus OX=10090 GN=Iars2 PE=1 SV=1	0.828	-0.082
Selenoprotein F OS=Mus musculus OX=10090 GN=Selenof PE=1 SV=3	0.887	-0.052
Probable RNA polymerase II nuclear localization protein SLC7A6OS OS=Mus musculus OX=10090 GN=Slc7a6os PE=1 SV=1	1.206	0.081
Peroxisomal multifunctional enzyme type 2 OS=Mus musculus OX=10090 GN=Hsd17b4 PE=1 SV=3	1.264	0.102
Phosphoglycerate kinase 1 OS=Mus musculus OX=10090 GN=Pgk1 PE=1 SV=4	0.906	-0.043
Myeloid-associated differentiation marker OS=Mus musculus OX=10090 GN=Myadm PE=1 SV=2	1.226	0.088
Solute carrier family 41 member 3 OS=Mus musculus OX=10090 GN=Slc41a3 PE=1 SV=1	1.395	0.144
Gamma-adducin OS=Mus musculus OX=10090 GN=Add3 PE=1 SV=2	1.421	0.153
Putative phospholipase B-like 2 OS=Mus musculus OX=10090 GN=Plbd2 PE=1 SV=2	1.151	0.061
Slit homolog 2 protein OS=Mus musculus OX=10090 GN=Slit2 PE=2 SV=2	1.950	0.290
Fibronectin type III domain-containing protein 3B OS=Mus musculus OX=10090 GN=Fndc3b PE=1 SV=1	1.585	0.200
Tubulin-specific chaperone C OS=Mus musculus OX=10090 GN=Tbcc PE=1 SV=1	1.630	0.212
Coiled-coil domain-containing protein 58 OS=Mus musculus OX=10090 GN=Ccdc58 PE=1 SV=1	0.843	-0.074

Table M.1. continued

39S ribosomal protein L12, mitochondrial OS=Mus musculus OX=10090 GN=Mrpl12 PE=1 SV=2	0.722	-0.141
Glyoxylate reductase/hydroxypyruvate reductase OS=Mus musculus OX=10090 GN=Grhpr PE=1 SV=1	0.635	-0.197
Sequestosome-1 OS=Mus musculus OX=10090 GN=Sqstm1 PE=1 SV=1	1.556	0.192
Nicotinamide phosphoribosyltransferase OS=Mus musculus OX=10090 GN=Nampt PE=1 SV=1	0.914	-0.039
Leucine-rich repeat flightless-interacting protein 1 OS=Mus musculus OX=10090 GN=Lrrfip1 PE=1 SV=2	1.327	0.123
Ras-related protein Rab-21 OS=Mus musculus OX=10090 GN=Rab21 PE=1 SV=4	1.152	0.062
Early endosome antigen 1 OS=Mus musculus OX=10090 GN=Eea1 PE=1 SV=2	1.391	0.143
Probable ATP-dependent RNA helicase DDX46 OS=Mus musculus OX=10090 GN=Ddx46 PE=1 SV=2	0.804	-0.095
Transducin beta-like protein 2 OS=Mus musculus OX=10090 GN=Tbl2 PE=1 SV=2	2.052	0.312
Ras-related protein Rab-7a OS=Mus musculus OX=10090 GN=Rab7a PE=1 SV=2	1.118	0.049
60S ribosomal protein L13 OS=Mus musculus OX=10090 GN=Rpl13 PE=1 SV=3	0.937	-0.028
Prostaglandin G/H synthase 1 OS=Mus musculus OX=10090 GN=Ptgs1 PE=1 SV=1	0.834	-0.079
Arf-GAP with GTPase, ANK repeat and PH domain-containing protein 3 OS=Mus musculus OX=10090 GN=Agap3 PE=1 SV=1	1.516	0.181
Jupiter microtubule associated homolog 1 OS=Mus musculus OX=10090 GN=Jpt1 PE=1 SV=3	0.514	-0.289
ER membrane protein complex subunit 4 OS=Mus musculus OX=10090 GN=Emc4 PE=1 SV=1	1.170	0.068

Table M.1. continued

Catenin alpha-1 OS=Mus musculus OX=10090 GN=Ctnna1 PE=1 SV=1	1.140	0.057
39S ribosomal protein L1, mitochondrial OS=Mus musculus OX=10090 GN=Mrpl1 PE=1 SV=2	0.675	-0.171
Myeloid differentiation primary response protein MyD88 OS=Mus musculus OX=10090 GN=Myd88 PE=1 SV=3	0.586	-0.232
Protein BUD31 homolog OS=Mus musculus OX=10090 GN=Bud31 PE=1 SV=2	0.908	-0.042
Transportin-3 OS=Mus musculus OX=10090 GN=Tnpo3 PE=1 SV=1	1.655	0.219
ATP-dependent 6-phosphofructokinase, platelet type OS=Mus musculus OX=10090 GN=Pfkp PE=1 SV=1	0.651	-0.186
CD63 antigen OS=Mus musculus OX=10090 GN=Cd63 PE=1 SV=2	1.254	0.098
28S ribosomal protein S22, mitochondrial OS=Mus musculus OX=10090 GN=Mrps22 PE=1 SV=1	0.729	-0.137
E3 UFM1-protein ligase 1 OS=Mus musculus OX=10090 GN=Ufl1 PE=1 SV=2	0.809	-0.092
Histone H2A type 2-A OS=Mus musculus OX=10090 GN=Hist2h2aa1 PE=1 SV=3	1.201	0.079
Catenin delta-1 OS=Mus musculus OX=10090 GN=Ctnnd1 PE=1 SV=2	0.938	-0.028
ER membrane protein complex subunit 3 OS=Mus musculus OX=10090 GN=Emc3 PE=1 SV=3	0.828	-0.082
Protein WWC2 OS=Mus musculus OX=10090 GN=Wwc2 PE=1 SV=1	1.633	0.213
Protein phosphatase 1A OS=Mus musculus OX=10090 GN=Ppm1a PE=1 SV=1	1.641	0.215
Mannosyl-oligosaccharide 1,2-alpha-mannosidase IB OS=Mus musculus OX=10090 GN=Man1a2 PE=1 SV=1	1.207	0.082
Epidermal growth factor receptor OS=Mus musculus OX=10090 GN=Egfr PE=1 SV=1	1.341	0.127

Table M.1. continued

Ribosomal protein S6 kinase alpha-4 OS=Mus musculus OX=10090 GN=Rps6ka4 PE=1 SV=2	1.469	0.167
GTP-binding protein Rheb OS=Mus musculus OX=10090 GN=Rheb PE=1 SV=1	2.025	0.306
Long-chain specific acyl-CoA dehydrogenase, mitochondrial OS=Mus musculus OX=10090 GN=Acadl PE=1 SV=2	0.811	-0.091
Electron transfer flavoprotein subunit beta OS=Mus musculus OX=10090 GN=Etfb PE=1 SV=3	1.059	0.025
Heme oxygenase 1 OS=Mus musculus OX=10090 GN=Hmox1 PE=1 SV=1	1.172	0.069
Calponin-2 OS=Mus musculus OX=10090 GN=Cnn2 PE=1 SV=1	0.826	-0.083
Ribose-phosphate pyrophosphokinase 1 OS=Mus musculus OX=10090 GN=Prps1 PE=1 SV=4	0.714	-0.146
Heterogeneous nuclear ribonucleoproteins A2/B1 OS=Mus musculus OX=10090 GN=Hnrnpa2b1 PE=1 SV=2	0.857	-0.067
EH domain-binding protein 1 OS=Mus musculus OX=10090 GN=Ehbp1 PE=1 SV=3	1.441	0.159
Supervillin OS=Mus musculus OX=10090 GN=Svil PE=1 SV=1	1.773	0.249
Uveal autoantigen with coiled-coil domains and ankyrin repeats OS=Mus musculus OX=10090 GN=Uaca PE=1 SV=2	0.373	-0.428
Fatty acid-binding protein, adipocyte OS=Mus musculus OX=10090 GN=Fabp4 PE=1 SV=3	0.896	-0.047
Coiled-coil domain-containing protein 47 OS=Mus musculus OX=10090 GN=Ccdc47 PE=1 SV=2	1.638	0.214
Peroxiredoxin-6 OS=Mus musculus OX=10090 GN=Prdx6 PE=1 SV=3	0.881	-0.055
3-hydroxyisobutyryl-CoA hydrolase, mitochondrial OS=Mus musculus OX=10090 GN=Hibch PE=1 SV=1	1.271	0.104
Mevalonate kinase OS=Mus musculus OX=10090 GN=Mvk PE=1 SV=1	1.302	0.115

Table M.1. continued

BRISC and BRCA1-A complex member 1 OS=Mus musculus OX=10090 GN=Babam1 PE=1 SV=1	1.352	0.131
RNA cytidine acetyltransferase OS=Mus musculus OX=10090 GN=Nat10 PE=1 SV=1	0.694	-0.159
Bifunctional 3'-phosphoadenosine 5'-phosphosulfate synthase 1 OS=Mus musculus OX=10090 GN=Papss1 PE=1 SV=1	0.901	-0.045
Vesicle-associated membrane protein-associated protein B OS=Mus musculus OX=10090 GN=Vapb PE=1 SV=3	1.252	0.097
28S ribosomal protein S23, mitochondrial OS=Mus musculus OX=10090 GN=Mrps23 PE=1 SV=1	0.811	-0.091
m7GpppX diphosphatase OS=Mus musculus OX=10090 GN=Dcps PE=1 SV=1	0.848	-0.072
Glutathione S-transferase Mu 1 OS=Mus musculus OX=10090 GN=Gstm1 PE=1 SV=2	1.100	0.041
ATP synthase F(0) complex subunit B1, mitochondrial OS=Mus musculus OX=10090 GN=Atp5pb PE=1 SV=1	0.836	-0.078
Elongator complex protein 2 OS=Mus musculus OX=10090 GN=Elp2 PE=1 SV=1	0.505	-0.297
Propionyl-CoA carboxylase alpha chain, mitochondrial OS=Mus musculus OX=10090 GN=Pcca PE=1 SV=2	1.210	0.083
Golgin subfamily A member 5 OS=Mus musculus OX=10090 GN=Golga5 PE=1 SV=2	1.505	0.178
Proteasome subunit beta type-7 OS=Mus musculus OX=10090 GN=Psmb7 PE=1 SV=1	1.366	0.135
Protein MEMO1 OS=Mus musculus OX=10090 GN=Memo1 PE=1 SV=1	0.736	-0.133
Signal recognition particle 54 kDa protein OS=Mus musculus OX=10090 GN=Srp54 PE=1 SV=2	0.797	-0.098
Perilipin-4 OS=Mus musculus OX=10090 GN=Plin4 PE=1 SV=2	1.679	0.225
Exopolyphosphatase PRUNE1 OS=Mus musculus OX=10090 GN=Prune1 PE=1 SV=1	0.794	-0.100

Table M.1. continued

Protein arginine N-methyltransferase 3 OS=Mus musculus OX=10090 GN=Prmt3 PE=1 SV=2	0.568	-0.246
Ataxin-2 OS=Mus musculus OX=10090 GN=Atxn2 PE=1 SV=1	1.495	0.175
Ephrin-B1 OS=Mus musculus OX=10090 GN=Efnb1 PE=1 SV=1	0.820	-0.086
Alpha-actinin-4 OS=Mus musculus OX=10090 GN=Actn4 PE=1 SV=1	0.938	-0.028
ADP-ribosylation factor GTPase-activating protein 3 OS=Mus musculus OX=10090 GN=Arfgap3 PE=1 SV=2	1.284	0.108
Inactive tyrosine-protein kinase 7 OS=Mus musculus OX=10090 GN=Ptk7 PE=1 SV=1	0.902	-0.045
Anoctamin-6 OS=Mus musculus OX=10090 GN=Ano6 PE=1 SV=1	1.210	0.083
Obscurin-like protein 1 OS=Mus musculus OX=10090 GN=Obsl1 PE=1 SV=1	0.894	-0.049
Prefoldin subunit 3 OS=Mus musculus OX=10090 GN=Vbp1 PE=1 SV=2	0.848	-0.071
DNA primase large subunit OS=Mus musculus OX=10090 GN=Prim2 PE=1 SV=1	0.714	-0.146
Probable ATP-dependent RNA helicase DDX5 OS=Mus musculus OX=10090 GN=Ddx5 PE=1 SV=2	0.875	-0.058
Sorting nexin-5 OS=Mus musculus OX=10090 GN=Snx5 PE=1 SV=1	0.891	-0.050
Spermidine synthase OS=Mus musculus OX=10090 GN=Srm PE=1 SV=1	0.859	-0.066
Vesicle transport protein USE1 OS=Mus musculus OX=10090 GN=Use1 PE=1 SV=1	1.554	0.191
Delta(24)-sterol reductase OS=Mus musculus OX=10090 GN=Dhcr24 PE=1 SV=1	1.528	0.184
Coatomer subunit zeta-1 OS=Mus musculus OX=10090 GN=Copz1 PE=1 SV=1	0.946	-0.024

Table M.1. continued

ATP-dependent 6-phosphofructokinase, muscle type OS=Mus musculus OX=10090 GN=Pfkm PE=1 SV=3	0.867	-0.062
Thioredoxin reductase 1, cytoplasmic OS=Mus musculus OX=10090 GN=Txnrd1 PE=1 SV=3	0.860	-0.066
Nucleoporin Nup43 OS=Mus musculus OX=10090 GN=Nup43 PE=1 SV=2	1.442	0.159
Echinoderm microtubule-associated protein-like 2 OS=Mus musculus OX=10090 GN=Eml2 PE=1 SV=1	0.631	-0.200
Reticulon-4 OS=Mus musculus OX=10090 GN=Rtn4 PE=1 SV=2	1.066	0.028
CCR4-NOT transcription complex subunit 4 OS=Mus musculus OX=10090 GN=Cnot4 PE=1 SV=2	1.258	0.100
Ubiquitin carboxyl-terminal hydrolase 4 OS=Mus musculus OX=10090 GN=Usp4 PE=1 SV=3	0.841	-0.075
Retinal rod rhodopsin-sensitive cGMP 3',5'-cyclic phosphodiesterase subunit delta OS=Mus musculus OX=10090 GN=Pde6d PE=1 SV=1	0.849	-0.071
GDP-fucose protein O-fucosyltransferase 2 OS=Mus musculus OX=10090 GN=Pofut2 PE=1 SV=1	1.120	0.049
N-alpha-acetyltransferase 50 OS=Mus musculus OX=10090 GN=Naa50 PE=1 SV=1	0.928	-0.033
Endoplasmic reticulum junction formation protein lunapark OS=Mus musculus OX=10090 GN=Lnpk PE=1 SV=1	1.474	0.168
Calpain small subunit 1 OS=Mus musculus OX=10090 GN=Capns1 PE=1 SV=1	1.192	0.076
SNARE-associated protein Snapin OS=Mus musculus OX=10090 GN=Snapin PE=1 SV=1	1.187	0.074
Cytochrome c oxidase subunit 3 OS=Mus musculus OX=10090 GN=mt-Co3 PE=1 SV=2	1.632	0.213
Solute carrier family 12 member 4 OS=Mus musculus OX=10090 GN=Slc12a4 PE=1 SV=2	1.585	0.200
Cytochrome b-c1 complex subunit 2, mitochondrial OS=Mus musculus OX=10090 GN=Uqcrc2 PE=1 SV=1	1.221	0.087

Table M.1. continued

72 kDa type IV collagenase OS=Mus musculus OX=10090 GN=Mmp2 PE=1 SV=1	1.226	0.088
Zinc finger protein ZPR1 OS=Mus musculus OX=10090 GN=Zpr1 PE=1 SV=1	1.445	0.160
Transportin-2 OS=Mus musculus OX=10090 GN=Tnpo2 PE=1 SV=1	0.897	-0.047
Integrin alpha-V OS=Mus musculus OX=10090 GN=Itgav PE=1 SV=2	1.273	0.105
Collagen alpha-1(XI) chain OS=Mus musculus OX=10090 GN=Col11a1 PE=1 SV=2	1.802	0.256
Ubiquitin-40S ribosomal protein S27a OS=Mus musculus OX=10090 GN=Rps27a PE=1 SV=2	1.364	0.135
Solute carrier family 12 member 9 OS=Mus musculus OX=10090 GN=Slc12a9 PE=1 SV=2	0.478	-0.320
Triosephosphate isomerase OS=Mus musculus OX=10090 GN=Tpi1 PE=1 SV=4	1.082	0.034
Pre-mRNA-processing-splicing factor 8 OS=Mus musculus OX=10090 GN=Prpf8 PE=1 SV=2	0.869	-0.061
Peptidyl-prolyl cis-trans isomerase FKBP9 OS=Mus musculus OX=10090 GN=Fkbp9 PE=1 SV=1	1.107	0.044
Rho guanine nucleotide exchange factor 7 OS=Mus musculus OX=10090 GN=Arhgef7 PE=1 SV=2	1.130	0.053
E3 ubiquitin-protein ligase RNF149 OS=Mus musculus OX=10090 GN=Rnf149 PE=1 SV=3	1.573	0.197
Sorbitol dehydrogenase OS=Mus musculus OX=10090 GN=Sord PE=1 SV=3	1.268	0.103
Glutaredoxin-1 OS=Mus musculus OX=10090 GN=Glrx PE=1 SV=3	0.857	-0.067
Maspardin OS=Mus musculus OX=10090 GN=Spg21 PE=1 SV=1	1.281	0.107
Methionine aminopeptidase 1 OS=Mus musculus OX=10090 GN=Metap1 PE=1 SV=1	0.825	-0.084

Table M.1. continued

Ras-related protein Rab-34 OS=Mus musculus OX=10090 GN=Rab34 PE=1 SV=2	1.168	0.068
Fatty acid synthase OS=Mus musculus OX=10090 GN=Fasn PE=1 SV=2	1.132	0.054
F-box/WD repeat-containing protein 8 OS=Mus musculus OX=10090 GN=Fbxw8 PE=1 SV=2	0.862	-0.065
Prolyl-tRNA synthetase associated domain-containing protein 1 OS=Mus musculus OX=10090 GN=Prorsd1 PE=1 SV=1	1.763	0.246
DnaJ homolog subfamily C member 8 OS=Mus musculus OX=10090 GN=Dnajc8 PE=1 SV=2	1.817	0.259
Endoplasmic reticulum metallopeptidase 1 OS=Mus musculus OX=10090 GN=Ermp1 PE=1 SV=2	1.616	0.209
Macrophage-capping protein OS=Mus musculus OX=10090 GN=Capg PE=1 SV=2	1.952	0.290
60S ribosomal protein L18a OS=Mus musculus OX=10090 GN=Rpl18a PE=1 SV=1	0.914	-0.039
Lysosome membrane protein 2 OS=Mus musculus OX=10090 GN=Scarb2 PE=1 SV=3	0.838	-0.077
Endoplasmic reticulum-Golgi intermediate compartment protein 1 OS=Mus musculus OX=10090 GN=Ergic1 PE=1 SV=1	1.141	0.057
26S proteasome non-ATPase regulatory subunit 14 OS=Mus musculus OX=10090 GN=Psmd14 PE=1 SV=2	0.843	-0.074
Serine protease inhibitor A3F OS=Mus musculus OX=10090 GN=Serpina3f PE=1 SV=3	0.818	-0.087
Serine/threonine-protein kinase MRCK beta OS=Mus musculus OX=10090 GN=Cdc42bpb PE=1 SV=2	0.850	-0.071
Delta-1-pyrroline-5-carboxylate dehydrogenase, mitochondrial OS=Mus musculus OX=10090 GN=Aldh4a1 PE=1 SV=3	0.663	-0.178
Dynactin subunit 6 OS=Mus musculus OX=10090 GN=Dctn6 PE=1 SV=1	1.814	0.259

Table M.1. continued

Keratin, type II cytoskeletal 1 OS=Mus musculus OX=10090 GN=Krt1 PE=1 SV=4	1.795	0.254
Histone-lysine N-methyltransferase NSD3 OS=Mus musculus OX=10090 GN=Nsd3 PE=1 SV=2	1.628	0.212
Cleavage stimulation factor subunit 1 OS=Mus musculus OX=10090 GN=Cstf1 PE=1 SV=1	0.764	-0.117
Trans-L-3-hydroxyproline dehydratase OS=Mus musculus OX=10090 GN=L3hypdh PE=1 SV=1	1.099	0.041
Annexin A11 OS=Mus musculus OX=10090 GN=Anxa11 PE=1 SV=2	1.551	0.191
Actin-related protein 2/3 complex subunit 4 OS=Mus musculus OX=10090 GN=Arpc4 PE=1 SV=3	0.852	-0.070
ELAV-like protein 1 OS=Mus musculus OX=10090 GN=Elavl1 PE=1 SV=2	0.863	-0.064
SUN domain-containing protein 1 OS=Mus musculus OX=10090 GN=Sun1 PE=1 SV=2	1.406	0.148
U6 snRNA-associated Sm-like protein LSm3 OS=Mus musculus OX=10090 GN=Lsm3 PE=1 SV=2	0.840	-0.075
Major facilitator superfamily domain-containing protein 1 OS=Mus musculus OX=10090 GN=Mfsd1 PE=1 SV=1	1.690	0.228
60 kDa heat shock protein, mitochondrial OS=Mus musculus OX=10090 GN=Hspd1 PE=1 SV=1	1.321	0.121
Acyl-CoA 6-desaturase OS=Mus musculus OX=10090 GN=Fads2 PE=1 SV=1	2.453	0.390
Phenylalanine--tRNA ligase alpha subunit OS=Mus musculus OX=10090 GN=Farsa PE=1 SV=1	1.548	0.190
Translocator protein OS=Mus musculus OX=10090 GN=Tspo PE=1 SV=1	0.751	-0.125
Protein transport protein Sec23A OS=Mus musculus OX=10090 GN=Sec23a PE=1 SV=2	0.863	-0.064
Splicing factor 1 OS=Mus musculus OX=10090 GN=Sf1 PE=1 SV=6	1.118	0.049

Table M.1. continued

SAM and SH3 domain-containing protein 1 OS=Mus musculus OX=10090 GN=Sash1 PE=1 SV=1	1.567	0.195
RNA transcription, translation and transport factor protein OS=Mus musculus OX=10090 GN=RTRAF PE=1 SV=1	0.862	-0.064
Netrin-1 OS=Mus musculus OX=10090 GN=Ntn1 PE=1 SV=3	1.300	0.114
Nucleolar protein 56 OS=Mus musculus OX=10090 GN=Nop56 PE=1 SV=2	0.854	-0.069
Chromobox protein homolog 6 OS=Mus musculus OX=10090 GN=Cbx6 PE=1 SV=2	1.311	0.118
tRNA (cytosine(34)-C(5))-methyltransferase OS=Mus musculus OX=10090 GN=Nsun2 PE=1 SV=2	0.902	-0.045
Protein C19orf12 homolog OS=Mus musculus OX=10090 PE=1 SV=1	0.788	-0.103
Growth arrest-specific protein 2 OS=Mus musculus OX=10090 GN=Gas2 PE=1 SV=1	1.089	0.037
Polyadenylate-binding protein 1 OS=Mus musculus OX=10090 GN=Pabpc1 PE=1 SV=2	0.875	-0.058
Superoxide dismutase [Mn], mitochondrial OS=Mus musculus OX=10090 GN=Sod2 PE=1 SV=3	1.139	0.056
Ras GTPase-activating protein-binding protein 2 OS=Mus musculus OX=10090 GN=G3bp2 PE=1 SV=2	1.424	0.153
Coatomer subunit zeta-2 OS=Mus musculus OX=10090 GN=Copz2 PE=1 SV=1	1.167	0.067
Acyl-CoA dehydrogenase family member 9, mitochondrial OS=Mus musculus OX=10090 GN=Acad9 PE=1 SV=2	1.174	0.070
Sister chromatid cohesion protein PDS5 homolog B OS=Mus musculus OX=10090 GN=Pds5b PE=1 SV=1	0.622	-0.206
Centrosomal protein of 170 kDa OS=Mus musculus OX=10090 GN=Cep170 PE=1 SV=2	1.248	0.096
Serine/arginine repetitive matrix protein 2 OS=Mus musculus OX=10090 GN=Srrm2 PE=1 SV=3	2.404	0.381

Table M.1. continued

Serine/arginine-rich splicing factor 10 OS=Mus musculus OX=10090 GN=Srsf10 PE=1 SV=2	0.895	-0.048
Arf-GAP with coiled-coil, ANK repeat and PH domain-containing protein 2 OS=Mus musculus OX=10090 GN=Acap2 PE=1 SV=2	1.510	0.179
Glutathione peroxidase 7 OS=Mus musculus OX=10090 GN=Gpx7 PE=1 SV=1	1.267	0.103
F-box only protein 2 OS=Mus musculus OX=10090 GN=Fbxo2 PE=1 SV=1	0.872	-0.059
Calcium-binding mitochondrial carrier protein SCaMC-1 OS=Mus musculus OX=10090 GN=Slc25a24 PE=1 SV=1	0.866	-0.063
Monofunctional C1-tetrahydrofolate synthase, mitochondrial OS=Mus musculus OX=10090 GN=Mthfd1l PE=1 SV=2	0.768	-0.114
Breast cancer anti-estrogen resistance protein 1 OS=Mus musculus OX=10090 GN=Bcar1 PE=1 SV=2	0.843	-0.074
N-alpha-acetyltransferase 20 OS=Mus musculus OX=10090 GN=Naa20 PE=1 SV=1	0.799	-0.097
Double-strand-break repair protein rad21 homolog OS=Mus musculus OX=10090 GN=Rad21 PE=1 SV=3	0.883	-0.054
ER lumen protein-retaining receptor 2 OS=Mus musculus OX=10090 GN=Kdelr2 PE=1 SV=1	4.894	0.690
E3 ubiquitin-protein ligase RNF181 OS=Mus musculus OX=10090 GN=Rnf181 PE=1 SV=1	1.641	0.215
DnaJ homolog subfamily A member 3, mitochondrial OS=Mus musculus OX=10090 GN=Dnaja3 PE=1 SV=1	0.887	-0.052
Abl interactor 1 OS=Mus musculus OX=10090 GN=Abi1 PE=1 SV=3	0.846	-0.073
Ubiquitin-protein ligase E3C OS=Mus musculus OX=10090 GN=Ube3c PE=1 SV=2	2.111	0.325
Pyroglutamyl-peptidase 1 OS=Mus musculus OX=10090 GN=Pgpep1 PE=1 SV=1	0.707	-0.151

Table M.1. continued

Spectrin alpha chain, non-erythrocytic 1 OS=Mus musculus OX=10090 GN=Sptan1 PE=1 SV=4	1.068	0.029
Na(+)/H(+) exchange regulatory cofactor NHE-RF2 OS=Mus musculus OX=10090 GN=Slc9a3r2 PE=1 SV=2	1.312	0.118
Pleckstrin homology-like domain family B member 2 OS=Mus musculus OX=10090 GN=Phldb2 PE=1 SV=2	1.181	0.072
N-acylneuraminate cytidylyltransferase OS=Mus musculus OX=10090 GN=Cmas PE=1 SV=2	0.308	-0.512
Nucleoprotein TPR OS=Mus musculus OX=10090 GN=Tpr PE=1 SV=1	0.663	-0.178
Flotillin-2 OS=Mus musculus OX=10090 GN=Flot2 PE=1 SV=2	1.193	0.077
Keratin, type II cytoskeletal 2 epidermal OS=Mus musculus OX=10090 GN=Krt2 PE=1 SV=1	1.993	0.300
Phenylalanine--tRNA ligase beta subunit OS=Mus musculus OX=10090 GN=Farsb PE=1 SV=2	0.920	-0.036
Neurolysin, mitochondrial OS=Mus musculus OX=10090 GN=Nln PE=1 SV=1	0.753	-0.123
OTU domain-containing protein 7B OS=Mus musculus OX=10090 GN=Otud7b PE=1 SV=1	1.196	0.078
Prolactin-8A6 OS=Mus musculus OX=10090 GN=Prl8a6 PE=2 SV=1	0.509	-0.294
Minor histocompatibility antigen H13 OS=Mus musculus OX=10090 GN=Hm13 PE=1 SV=1	0.778	-0.109
Tapasin OS=Mus musculus OX=10090 GN=Tapbp PE=1 SV=2	0.531	-0.275
Protein IMPACT OS=Mus musculus OX=10090 GN=Impact PE=1 SV=2	1.223	0.087
Flotillin-1 OS=Mus musculus OX=10090 GN=Flot1 PE=1 SV=1	1.348	0.130
Hemoglobin subunit alpha OS=Mus musculus OX=10090 GN=Hba PE=1 SV=2	0.788	-0.103

Table M.1. continued

PDZ and LIM domain protein 5 OS=Mus musculus OX=10090 GN=Pdlim5 PE=1 SV=4	0.912	-0.040
Ubiquitin-like modifier-activating enzyme ATG7 OS=Mus musculus OX=10090 GN=Atg7 PE=1 SV=1	0.859	-0.066
DNA-directed RNA polymerase II subunit RPB2 OS=Mus musculus OX=10090 GN=Polr2b PE=1 SV=2	0.729	-0.137
Protein phosphatase 1 regulatory subunit 12B OS=Mus musculus OX=10090 GN=Ppp1r12b PE=1 SV=2	1.091	0.038
Pyruvate dehydrogenase E1 component subunit beta, mitochondrial OS=Mus musculus OX=10090 GN=Pdhb PE=1 SV=1	1.145	0.059
Prolyl 3-hydroxylase 3 OS=Mus musculus OX=10090 GN=P3h3 PE=1 SV=1	0.596	-0.224
Kinesin-like protein KIF1C OS=Mus musculus OX=10090 GN=Kif1c PE=1 SV=2	1.248	0.096
Raftlin-2 OS=Mus musculus OX=10090 GN=Rftn2 PE=1 SV=3	1.210	0.083
Phostensin OS=Mus musculus OX=10090 GN=Ppp1r18 PE=1 SV=1	0.893	-0.049
H(+)/Cl(-) exchange transporter 7 OS=Mus musculus OX=10090 GN=Clcn7 PE=1 SV=1	1.403	0.147
ATP-dependent Clp protease proteolytic subunit, mitochondrial OS=Mus musculus OX=10090 GN=Clpp PE=1 SV=1	1.507	0.178
Splicing factor U2AF 65 kDa subunit OS=Mus musculus OX=10090 GN=U2af2 PE=1 SV=3	0.902	-0.045
Transmembrane protein 33 OS=Mus musculus OX=10090 GN=Tmem33 PE=1 SV=1	1.784	0.251
Septin-7 OS=Mus musculus OX=10090 GN=Sept7 PE=1 SV=1	1.255	0.099
Signal peptide peptidase-like 2A OS=Mus musculus OX=10090 GN=Sppl2a PE=1 SV=2	0.674	-0.172
Ribosomal protein S6 kinase alpha-3 OS=Mus musculus OX=10090 GN=Rps6ka3 PE=1 SV=2	0.714	-0.146

Table M.1. continued

40S ribosomal protein S28 OS=Mus musculus OX=10090 GN=Rps28 PE=1 SV=1	1.357	0.133
ATP-dependent RNA helicase DDX42 OS=Mus musculus OX=10090 GN=Ddx42 PE=1 SV=3	2.368	0.374
Neogenin OS=Mus musculus OX=10090 GN=Neo1 PE=1 SV=1	1.707	0.232
Apoptotic chromatin condensation inducer in the nucleus OS=Mus musculus OX=10090 GN=Acin1 PE=1 SV=3	1.175	0.070
Engulfment and cell motility protein 1 OS=Mus musculus OX=10090 GN=Elmo1 PE=1 SV=2	1.368	0.136
Glypican-4 OS=Mus musculus OX=10090 GN=Gpc4 PE=1 SV=2	0.896	-0.048
Plasminogen activator inhibitor 1 OS=Mus musculus OX=10090 GN=Serpine1 PE=1 SV=1	1.446	0.160
X-ray repair cross-complementing protein 5 OS=Mus musculus OX=10090 GN=Xrcc5 PE=1 SV=4	0.691	-0.160
Short-chain specific acyl-CoA dehydrogenase, mitochondrial OS=Mus musculus OX=10090 GN=Acads PE=1 SV=2	1.205	0.081
Acyl-coenzyme A thioesterase 13 OS=Mus musculus OX=10090 GN=Acot13 PE=1 SV=1	1.117	0.048
Cell division cycle and apoptosis regulator protein 1 OS=Mus musculus OX=10090 GN=Ccar1 PE=1 SV=1	1.295	0.112
Septin-8 OS=Mus musculus OX=10090 GN=Sept8 PE=1 SV=4	1.238	0.093
Heparan-alpha-glucosaminide N-acetyltransferase OS=Mus musculus OX=10090 GN=Hgsnat PE=1 SV=2	1.161	0.065
Nuclear transcription factor Y subunit gamma OS=Mus musculus OX=10090 GN=Nfyc PE=1 SV=2	1.145	0.059
BTB/POZ domain-containing adapter for CUL3-mediated RhoA degradation protein 3 OS=Mus musculus OX=10090 GN=Kctd10 PE=1 SV=1	1.717	0.235
Proliferating cell nuclear antigen OS=Mus musculus OX=10090 GN=Pcna PE=1 SV=2	0.932	-0.031

Table M.1. continued

Cytochrome c oxidase assembly protein COX14 OS=Mus musculus OX=10090 GN=Cox14 PE=3 SV=1	2.130	0.328
Brain acid soluble protein 1 OS=Mus musculus OX=10090 GN=Basp1 PE=1 SV=3	1.152	0.062
U4/U6.U5 tri-snRNP-associated protein 2 OS=Mus musculus OX=10090 GN=Usp39 PE=1 SV=2	0.813	-0.090
Microtubule-associated protein 4 OS=Mus musculus OX=10090 GN=Map4 PE=1 SV=3	1.185	0.074
Serine--tRNA ligase, cytoplasmic OS=Mus musculus OX=10090 GN=Sars PE=1 SV=3	0.879	-0.056
Ubiquitin carboxyl-terminal hydrolase 5 OS=Mus musculus OX=10090 GN=Usp5 PE=1 SV=1	0.879	-0.056
Inosine triphosphate pyrophosphatase OS=Mus musculus OX=10090 GN=Itpa PE=1 SV=2	1.227	0.089
Zinc transporter SLC39A7 OS=Mus musculus OX=10090 GN=Slc39a7 PE=1 SV=2	1.212	0.083
Paralemmin-1 OS=Mus musculus OX=10090 GN=Palm PE=1 SV=1	1.258	0.100
Prostaglandin E synthase 3 OS=Mus musculus OX=10090 GN=Ptges3 PE=1 SV=1	0.911	-0.041
Tyrosine-protein kinase JAK1 OS=Mus musculus OX=10090 GN=Jak1 PE=1 SV=1	1.170	0.068
Ankyrin repeat domain-containing protein 17 OS=Mus musculus OX=10090 GN=Ankrd17 PE=1 SV=2	1.331	0.124
Ras-related protein Rab-5B OS=Mus musculus OX=10090 GN=Rab5b PE=1 SV=1	1.207	0.082
Poly [ADP-ribose] polymerase 12 OS=Mus musculus OX=10090 GN=Parp12 PE=1 SV=3	0.866	-0.062
A-kinase anchor protein 8 OS=Mus musculus OX=10090 GN=Akap8 PE=1 SV=1	6.827	0.834
ADP-ribosylation factor-like protein 3 OS=Mus musculus OX=10090 GN=Arl3 PE=1 SV=1	0.863	-0.064

Table M.1. continued

Protein enabled homolog OS=Mus musculus OX=10090 GN=Enah PE=1 SV=2	1.264	0.102
Ribosomal L1 domain-containing protein 1 OS=Mus musculus OX=10090 GN=Rsl1d1 PE=1 SV=1	1.402	0.147
Coatomer subunit beta OS=Mus musculus OX=10090 GN=Copb1 PE=1 SV=1	0.831	-0.080
UDP-glucose 6-dehydrogenase OS=Mus musculus OX=10090 GN=Ugdh PE=1 SV=1	0.938	-0.028
Dynamin-2 OS=Mus musculus OX=10090 GN=Dnm2 PE=1 SV=2	0.717	-0.144
DNA replication licensing factor MCM5 OS=Mus musculus OX=10090 GN=Mcm5 PE=1 SV=1	0.894	-0.049
Niban-like protein 1 OS=Mus musculus OX=10090 GN=Fam129b PE=1 SV=2	1.081	0.034
Pyruvate dehydrogenase E1 component subunit alpha, somatic form, mitochondrial OS=Mus musculus OX=10090 GN=Pdha1 PE=1 SV=1	0.945	-0.025
Serine/threonine-protein phosphatase 6 regulatory subunit 3 OS=Mus musculus OX=10090 GN=Ppp6r3 PE=1 SV=1	1.443	0.159
NADH dehydrogenase [ubiquinone] 1 alpha subcomplex subunit 7 OS=Mus musculus OX=10090 GN=Ndufa7 PE=1 SV=3	0.542	-0.266
Trifunctional enzyme subunit beta, mitochondrial OS=Mus musculus OX=10090 GN=Hadhb PE=1 SV=1	1.251	0.097
Myosin phosphatase Rho-interacting protein OS=Mus musculus OX=10090 GN=Mprip PE=1 SV=2	1.107	0.044
DNA-directed RNA polymerase II subunit RPB1 OS=Mus musculus OX=10090 GN=Polr2a PE=1 SV=3	0.860	-0.065
Oxidation resistance protein 1 OS=Mus musculus OX=10090 GN=Oxr1 PE=1 SV=3	1.265	0.102
E3 ubiquitin-protein ligase NEDD4 OS=Mus musculus OX=10090 GN=Nedd4 PE=1 SV=3	1.110	0.045
Endoplasmic reticulum lectin 1 OS=Mus musculus OX=10090 GN=Erlec1 PE=1 SV=1	0.754	-0.123

Table M.1. continued

Axin interactor, dorsalization-associated protein OS=Mus musculus OX=10090 GN=Aida PE=1 SV=1	1.162	0.065
Alpha-soluble NSF attachment protein OS=Mus musculus OX=10090 GN=Napa PE=1 SV=1	1.109	0.045
Heterogeneous nuclear ribonucleoprotein U-like protein 1 OS=Mus musculus OX=10090 GN=Hnrnpul1 PE=1 SV=1	1.850	0.267
Ras-related protein Rab-1A OS=Mus musculus OX=10090 GN=Rab1A PE=1 SV=3	1.207	0.082
ATPase family AAA domain-containing protein 3 OS=Mus musculus OX=10090 GN=Atad3 PE=1 SV=1	0.744	-0.128
Sarcoplasmic/endoplasmic reticulum calcium ATPase 2 OS=Mus musculus OX=10090 GN=Atp2a2 PE=1 SV=2	1.265	0.102
RNA polymerase II-associated protein 3 OS=Mus musculus OX=10090 GN=Rpap3 PE=1 SV=1	1.197	0.078
ATPase family protein 2 homolog OS=Mus musculus OX=10090 GN=Spata5 PE=1 SV=2	0.738	-0.132
Nuclear pore complex protein Nup214 OS=Mus musculus OX=10090 GN=Nup214 PE=1 SV=2	4.813	0.682
Dynactin subunit 2 OS=Mus musculus OX=10090 GN=Dctn2 PE=1 SV=3	0.898	-0.047
Phosphatidylinositide phosphatase SAC1 OS=Mus musculus OX=10090 GN=Sacm1l PE=1 SV=1	1.223	0.087
Pyrroline-5-carboxylate reductase 1, mitochondrial OS=Mus musculus OX=10090 GN=Pycr1 PE=1 SV=1	1.348	0.130
Bone marrow stromal antigen 2 OS=Mus musculus OX=10090 GN=Bst2 PE=1 SV=1	3.913	0.592
Arf-GAP domain and FG repeat-containing protein 1 OS=Mus musculus OX=10090 GN=Agfg1 PE=1 SV=2	1.230	0.090
Trimethyllysine dioxygenase, mitochondrial OS=Mus musculus OX=10090 GN=Tmlhe PE=1 SV=2	0.674	-0.171

Table M.1. continued

AP-1 complex subunit gamma-like 2 OS=Mus musculus OX=10090 GN=Ap1g2 PE=1 SV=2	2.152	0.333
Cleavage and polyadenylation specificity factor subunit 5 OS=Mus musculus OX=10090 GN=Nudt21 PE=1 SV=1	0.888	-0.052
Syntenin-1 OS=Mus musculus OX=10090 GN=Sdcbp PE=1 SV=1	0.487	-0.313
Cytoskeleton-associated protein 5 OS=Mus musculus OX=10090 GN=Ckap5 PE=1 SV=1	1.140	0.057
Protein LBH OS=Mus musculus OX=10090 GN=Lbh PE=1 SV=1	1.340	0.127
Golgi resident protein GCP60 OS=Mus musculus OX=10090 GN=Acbd3 PE=1 SV=3	1.165	0.066
Acylphosphatase-2 OS=Mus musculus OX=10090 GN=Acyp2 PE=1 SV=2	0.760	-0.119
Geranylgeranyl transferase type-2 subunit alpha OS=Mus musculus OX=10090 GN=Rabggta PE=1 SV=1	0.640	-0.194
Sodium- and chloride-dependent taurine transporter OS=Mus musculus OX=10090 GN=Slc6a6 PE=1 SV=2	0.339	-0.469
Fatty aldehyde dehydrogenase OS=Mus musculus OX=10090 GN=Aldh3a2 PE=1 SV=2	0.821	-0.086
UBX domain-containing protein 1 OS=Mus musculus OX=10090 GN=Ubxn1 PE=1 SV=1	1.281	0.108
Pyrroline-5-carboxylate reductase 3 OS=Mus musculus OX=10090 GN=Pycr3 PE=1 SV=2	1.082	0.034
Catechol O-methyltransferase OS=Mus musculus OX=10090 GN=Comt PE=1 SV=2	1.245	0.095
Sorting nexin-1 OS=Mus musculus OX=10090 GN=Snx1 PE=1 SV=1	0.885	-0.053
Sialic acid synthase OS=Mus musculus OX=10090 GN=Nans PE=1 SV=1	0.908	-0.042
Deubiquitinating protein VCIP135 OS=Mus musculus OX=10090 GN=Vcpip1 PE=1 SV=1	0.812	-0.090

Table M.1. continued

Alpha-enolase OS=Mus musculus OX=10090 GN=Eno1 PE=1 SV=3	0.875	-0.058
Aspartyl/asparaginyl beta-hydroxylase OS=Mus musculus OX=10090 GN=Asph PE=1 SV=1	1.152	0.061
Homeobox protein Nkx-2.5 OS=Mus musculus OX=10090 GN=Nkx2-5 PE=1 SV=1	1.720	0.235
Insulin-degrading enzyme OS=Mus musculus OX=10090 GN=Ide PE=1 SV=1	0.912	-0.040
Amyloid-beta A4 precursor protein-binding family B member 2 OS=Mus musculus OX=10090 GN=Apbb2 PE=1 SV=2	1.437	0.157
DnaJ homolog subfamily C member 2 OS=Mus musculus OX=10090 GN=Dnajc2 PE=1 SV=2	1.408	0.148
Heterogeneous nuclear ribonucleoprotein U-like protein 2 OS=Mus musculus OX=10090 GN=Hnrnpul2 PE=1 SV=2	1.169	0.068
Protein transport protein Sec24A OS=Mus musculus OX=10090 GN=Sec24a PE=1 SV=1	1.299	0.114
Integrin beta-1 OS=Mus musculus OX=10090 GN=Itgb1 PE=1 SV=1	1.142	0.058
Serine/threonine-protein kinase 3 OS=Mus musculus OX=10090 GN=Stk3 PE=1 SV=1	1.264	0.102
Complement component 1 Q subcomponent-binding protein, mitochondrial OS=Mus musculus OX=10090 GN=C1qbp PE=1 SV=1	1.287	0.110
NADH dehydrogenase [ubiquinone] iron-sulfur protein 3, mitochondrial OS=Mus musculus OX=10090 GN=Ndufs3 PE=1 SV=2	0.762	-0.118
Malectin OS=Mus musculus OX=10090 GN=Mlec PE=1 SV=2	2.905	0.463
Programmed cell death protein 5 OS=Mus musculus OX=10090 GN=Pdcd5 PE=1 SV=3	1.320	0.121
Prefoldin subunit 2 OS=Mus musculus OX=10090 GN=Pfdn2 PE=1 SV=2	0.929	-0.032
Non-histone chromosomal protein HMG-17 OS=Mus musculus OX=10090 GN=Hmgn2 PE=1 SV=2	1.216	0.085

Table M.1. continued

Astrocytic phosphoprotein PEA-15 OS=Mus musculus OX=10090 GN=Pea15 PE=1 SV=1	1.387	0.142
ATP-dependent (S)-NAD(P)H-hydrate dehydratase OS=Mus musculus OX=10090 GN=Naxd PE=1 SV=1	0.809	-0.092
Signal peptidase complex subunit 3 OS=Mus musculus OX=10090 GN=Spcs3 PE=1 SV=1	0.871	-0.060
Basement membrane-specific heparan sulfate proteoglycan core protein OS=Mus musculus OX=10090 GN=Hspg2 PE=1 SV=1	1.712	0.234
Mitochondrial import inner membrane translocase subunit TIM50 OS=Mus musculus OX=10090 GN=Timm50 PE=1 SV=1	0.799	-0.097
Mitochondrial glutamate carrier 1 OS=Mus musculus OX=10090 GN=Slc25a22 PE=1 SV=1	0.560	-0.252
GMP synthase [glutamine-hydrolyzing] OS=Mus musculus OX=10090 GN=Gmps PE=1 SV=2	0.777	-0.110
Septin-6 OS=Mus musculus OX=10090 GN=Sept6 PE=1 SV=4	1.084	0.035
3-mercaptopyruvate sulfurtransferase OS=Mus musculus OX=10090 GN=Mpst PE=1 SV=4	3.747	0.574
Proteasome activator complex subunit 1 OS=Mus musculus OX=10090 GN=Psme1 PE=1 SV=2	0.758	-0.120
Reticulophagy regulator 2 OS=Mus musculus OX=10090 GN=Retreg2 PE=1 SV=2	0.383	-0.416
Extended synaptotagmin-1 OS=Mus musculus OX=10090 GN=Esyt1 PE=1 SV=2	0.922	-0.035
E3 ubiquitin-protein ligase PPP1R11 OS=Mus musculus OX=10090 GN=Ppp1r11 PE=1 SV=1	4.433	0.647
Importin subunit alpha-4 OS=Mus musculus OX=10090 GN=Kpna3 PE=1 SV=1	1.094	0.039
COP9 signalosome complex subunit 7b OS=Mus musculus OX=10090 GN=Cops7b PE=1 SV=1	1.836	0.264
Nucleophosmin OS=Mus musculus OX=10090 GN=Npm1 PE=1 SV=1	1.918	0.283

Table M.1. continued

Syntaxin-12 OS=Mus musculus OX=10090 GN=Stx12 PE=1 SV=1	1.639	0.215
CTP synthase 1 OS=Mus musculus OX=10090 GN=Ctps1 PE=1 SV=2	0.836	-0.078
RNA binding protein fox-1 homolog 2 OS=Mus musculus OX=10090 GN=Rbfox2 PE=1 SV=2	0.867	-0.062
Calcium/calmodulin-dependent protein kinase type II subunit delta OS=Mus musculus OX=10090 GN=Camk2d PE=1 SV=1	1.326	0.122
Cytochrome c oxidase subunit 7A2, mitochondrial OS=Mus musculus OX=10090 GN=Cox7a2 PE=1 SV=2	1.084	0.035
Adipocyte enhancer-binding protein 1 OS=Mus musculus OX=10090 GN=Aebp1 PE=1 SV=1	1.979	0.296
Cytoplasmic dynein 1 light intermediate chain 2 OS=Mus musculus OX=10090 GN=Dync1li2 PE=1 SV=2	1.067	0.028
N-acetylgalactosamine kinase OS=Mus musculus OX=10090 GN=Galk2 PE=1 SV=1	0.845	-0.073
Metallothionein-2 OS=Mus musculus OX=10090 GN=Mt2 PE=1 SV=2	39.177	1.593
Beta-glucuronidase OS=Mus musculus OX=10090 GN=Gusb PE=1 SV=2	1.108	0.045
Protein OS-9 OS=Mus musculus OX=10090 GN=Os9 PE=1 SV=2	1.256	0.099
Lon protease homolog, mitochondrial OS=Mus musculus OX=10090 GN=Lonp1 PE=1 SV=2	0.797	-0.098
Dynamin-1 OS=Mus musculus OX=10090 GN=Dnm1 PE=1 SV=2	1.207	0.082
V-type proton ATPase subunit F OS=Mus musculus OX=10090 GN=Atp6v1f PE=1 SV=2	0.810	-0.092
2-oxoglutarate dehydrogenase, mitochondrial OS=Mus musculus OX=10090 GN=Ogdh PE=1 SV=3	1.076	0.032
Transcription intermediary factor 1-beta OS=Mus musculus OX=10090 GN=Trim28 PE=1 SV=3	0.916	-0.038

Table M.1. continued

Eukaryotic translation initiation factor 3 subunit J-B OS=Mus musculus OX=10090 GN=Eif3j2 PE=1 SV=1	0.929	-0.032
Stonin-1 OS=Mus musculus OX=10090 GN=Ston1 PE=1 SV=2	1.355	0.132
Caspase-3 OS=Mus musculus OX=10090 GN=Casp3 PE=1 SV=1	0.869	-0.061
Lysosomal alpha-mannosidase OS=Mus musculus OX=10090 GN=Man2b1 PE=1 SV=4	0.882	-0.054
NEDD8 OS=Mus musculus OX=10090 GN=Nedd8 PE=1 SV=2	0.869	-0.061
Tetratricopeptide repeat protein 38 OS=Mus musculus OX=10090 GN=Ttc38 PE=1 SV=2	0.874	-0.059
Arylsulfatase B OS=Mus musculus OX=10090 GN=Arsb PE=1 SV=3	1.384	0.141
Secretory carrier-associated membrane protein 2 OS=Mus musculus OX=10090 GN=Scamp2 PE=1 SV=1	1.392	0.144
Secernin-1 OS=Mus musculus OX=10090 GN=Scrn1 PE=1 SV=1	1.111	0.046
Metaxin-2 OS=Mus musculus OX=10090 GN=Mtx2 PE=1 SV=1	4.303	0.634
Cytochrome c oxidase subunit 2 OS=Mus musculus OX=10090 GN=Mtco2 PE=1 SV=1	0.493	-0.307
Ubiquitin-fold modifier-conjugating enzyme 1 OS=Mus musculus OX=10090 GN=Ufc1 PE=1 SV=1	0.824	-0.084
Coiled-coil domain-containing protein 124 OS=Mus musculus OX=10090 GN=Ccdc124 PE=1 SV=1	5.156	0.712
Nischarin OS=Mus musculus OX=10090 GN=Nisch PE=1 SV=2	0.815	-0.089
MOB kinase activator 1A OS=Mus musculus OX=10090 GN=Mob1a PE=2 SV=3	1.376	0.139
BRI3-binding protein OS=Mus musculus OX=10090 GN=Bri3bp PE=1 SV=1	1.862	0.270
Casein kinase I isoform alpha OS=Mus musculus OX=10090 GN=Csnk1a1 PE=1 SV=2	0.662	-0.179
Elongin-C OS=Mus musculus OX=10090 GN=Eloc PE=1 SV=1	0.796	-0.099

Table M.1. continued

Polynucleotide 5'-hydroxyl-kinase NOL9 OS=Mus musculus OX=10090 GN=Nol9 PE=1 SV=1	2.962	0.472
La-related protein 1 OS=Mus musculus OX=10090 GN=Larp1 PE=1 SV=3	0.821	-0.086
Conserved oligomeric Golgi complex subunit 1 OS=Mus musculus OX=10090 GN=Cog1 PE=1 SV=3	0.678	-0.169
Enhancer of rudimentary homolog OS=Mus musculus OX=10090 GN=Erh PE=1 SV=1	0.789	-0.103
Serine/threonine-protein phosphatase 2A 65 kDa regulatory subunit A beta isoform OS=Mus musculus OX=10090 GN=Ppp2r1b PE=1 SV=2	0.772	-0.113
Probable 28S rRNA (cytosine-C(5))-methyltransferase OS=Mus musculus OX=10090 GN=Nop2 PE=1 SV=1	0.888	-0.051
Dedicator of cytokinesis protein 1 OS=Mus musculus OX=10090 GN=Dock1 PE=1 SV=3	3.433	0.536
Anaphase-promoting complex subunit 5 OS=Mus musculus OX=10090 GN=Anapc5 PE=1 SV=1	0.434	-0.362
Cell cycle control protein 50A OS=Mus musculus OX=10090 GN=Tmem30a PE=1 SV=1	1.119	0.049
A disintegrin and metalloproteinase with thrombospondin motifs 1 OS=Mus musculus OX=10090 GN=Adamts1 PE=1 SV=4	1.129	0.053
Protein CDV3 OS=Mus musculus OX=10090 GN=Cdv3 PE=1 SV=2	1.129	0.053
Serine/threonine-protein phosphatase 2A catalytic subunit alpha isoform OS=Mus musculus OX=10090 GN=Ppp2ca PE=1 SV=1	0.655	-0.183
Mitogen-activated protein kinase 3 OS=Mus musculus OX=10090 GN=Mapk3 PE=1 SV=5	1.126	0.051
3'(2'),5'-bisphosphate nucleotidase 1 OS=Mus musculus OX=10090 GN=Bpnt1 PE=1 SV=2	1.113	0.047
Mitochondrial fission 1 protein OS=Mus musculus OX=10090 GN=Fis1 PE=1 SV=1	1.265	0.102

Table M.1. continued

Nucleoporin SEH1 OS=Mus musculus OX=10090 GN=Seh1l PE=2 SV=1	0.686	-0.164
40S ribosomal protein S13 OS=Mus musculus OX=10090 GN=Rps13 PE=1 SV=2	0.816	-0.088
Constitutive coactivator of PPAR-gamma-like protein 1 OS=Mus musculus OX=10090 GN=FAM120A PE=1 SV=2	1.325	0.122
Twisted gastrulation protein homolog 1 OS=Mus musculus OX=10090 GN=Twsg1 PE=1 SV=1	0.921	-0.036
Flavin reductase (NADPH) OS=Mus musculus OX=10090 GN=Blvrb PE=1 SV=3	0.726	-0.139
Acylamino-acid-releasing enzyme OS=Mus musculus OX=10090 GN=Apeh PE=1 SV=3	1.082	0.034
NADH dehydrogenase [ubiquinone] 1 alpha subcomplex subunit 5 OS=Mus musculus OX=10090 GN=Ndufa5 PE=1 SV=3	1.071	0.030
Cystatin-C OS=Mus musculus OX=10090 GN=Cst3 PE=1 SV=2	1.323	0.121
Scaffold attachment factor B1 OS=Mus musculus OX=10090 GN=Safb PE=1 SV=2	0.808	-0.093
NAD(P) transhydrogenase, mitochondrial OS=Mus musculus OX=10090 GN=Nnt PE=1 SV=2	1.137	0.056
Kelch-like protein 22 OS=Mus musculus OX=10090 GN=Klhl22 PE=1 SV=1	0.724	-0.141
Disintegrin and metalloproteinase domain-containing protein 23 OS=Mus musculus OX=10090 GN=Adam23 PE=1 SV=1	2.070	0.316
Eukaryotic peptide chain release factor GTP-binding subunit ERF3A OS=Mus musculus OX=10090 GN=Gspt1 PE=1 SV=2	1.361	0.134
60S ribosomal protein L12 OS=Mus musculus OX=10090 GN=Rpl12 PE=1 SV=2	1.058	0.025
Protein ABHD14B OS=Mus musculus OX=10090 GN=Abhd14b PE=1 SV=1	0.876	-0.057
Dihydropyrimidinase-related protein 2 OS=Mus musculus OX=10090 GN=Dpysl2 PE=1 SV=2	1.097	0.040

Table M.1. continued

High mobility group protein HMGI-C OS=Mus musculus OX=10090 GN=Hmga2 PE=1 SV=1	0.857	-0.067
Syntaxin-7 OS=Mus musculus OX=10090 GN=Stx7 PE=1 SV=3	1.124	0.051
RNA-binding protein 39 OS=Mus musculus OX=10090 GN=Rbm39 PE=1 SV=2	0.891	-0.050
Reticulocalbin-2 OS=Mus musculus OX=10090 GN=Rcn2 PE=1 SV=1	1.116	0.047
26S proteasome regulatory subunit 7 OS=Mus musculus OX=10090 GN=Psmc2 PE=1 SV=5	1.284	0.108
Annexin A6 OS=Mus musculus OX=10090 GN=Anxa6 PE=1 SV=3	0.782	-0.107
Calcium-binding mitochondrial carrier protein Aralar1 OS=Mus musculus OX=10090 GN=Slc25a12 PE=1 SV=1	1.150	0.061
Bis(5'-nucleosyl)-tetraphosphatase [asymmetrical] OS=Mus musculus OX=10090 GN=Nudt2 PE=1 SV=3	0.479	-0.319
Latexin OS=Mus musculus OX=10090 GN=Lxn PE=1 SV=2	0.699	-0.156
mRNA cap guanine-N7 methyltransferase OS=Mus musculus OX=10090 GN=Rnmt PE=1 SV=1	1.459	0.164
Gamma-soluble NSF attachment protein OS=Mus musculus OX=10090 GN=Napg PE=1 SV=1	1.426	0.154
Peptidyl-prolyl cis-trans isomerase FKBP11 OS=Mus musculus OX=10090 GN=Fkbp11 PE=1 SV=1	1.330	0.124
EGF-containing fibulin-like extracellular matrix protein 2 OS=Mus musculus OX=10090 GN=Efemp2 PE=1 SV=1	1.093	0.039
Bifunctional epoxide hydrolase 2 OS=Mus musculus OX=10090 GN=Ephx2 PE=1 SV=2	2.028	0.307
E3 ubiquitin-protein ligase RNF126 OS=Mus musculus OX=10090 GN=Rnf126 PE=1 SV=1	1.696	0.230
Dynactin subunit 4 OS=Mus musculus OX=10090 GN=Dctn4 PE=1 SV=1	0.932	-0.031

Table M.1. continued

Dihydrolipoyl dehydrogenase, mitochondrial OS=Mus musculus OX=10090 GN=Dld PE=1 SV=2	1.235	0.092
Ena/VASP-like protein OS=Mus musculus OX=10090 GN=Evl PE=1 SV=2	1.920	0.283
G protein-regulated inducer of neurite outgrowth 3 OS=Mus musculus OX=10090 GN=Gprin3 PE=1 SV=1	1.399	0.146
Aldehyde dehydrogenase, mitochondrial OS=Mus musculus OX=10090 GN=Aldh2 PE=1 SV=1	1.109	0.045
Histone H1.0 OS=Mus musculus OX=10090 GN=H1f0 PE=2 SV=4	1.223	0.088
Unconventional myosin-Va OS=Mus musculus OX=10090 GN=Myo5a PE=1 SV=2	1.144	0.059
GRB10-interacting GYF protein 2 OS=Mus musculus OX=10090 GN=Gigyf2 PE=1 SV=2	1.324	0.122
Glutamine amidotransferase-like class 1 domain-containing protein 3A, mitochondrial OS=Mus musculus OX=10090 GN=Gatd3a PE=1 SV=1	1.190	0.075
Glutaredoxin-3 OS=Mus musculus OX=10090 GN=Glrx3 PE=1 SV=1	0.901	-0.045
Cullin-3 OS=Mus musculus OX=10090 GN=Cul3 PE=1 SV=1	0.895	-0.048
Transportin-1 OS=Mus musculus OX=10090 GN=Tnpo1 PE=1 SV=2	1.215	0.085
Inter alpha-trypsin inhibitor, heavy chain 4 OS=Mus musculus OX=10090 GN=Itih4 PE=1 SV=2	4.255	0.629
Glycine--tRNA ligase OS=Mus musculus OX=10090 GN=Gars PE=1 SV=1	0.787	-0.104
Eukaryotic translation initiation factor 1b OS=Mus musculus OX=10090 GN=Eif1b PE=1 SV=2	0.812	-0.091
Structural maintenance of chromosomes protein 4 OS=Mus musculus OX=10090 GN=Smc4 PE=1 SV=1	1.394	0.144
60S ribosomal protein L27a OS=Mus musculus OX=10090 GN=Rpl27a PE=1 SV=5	0.866	-0.062

Table M.1. continued

Protocadherin beta-6 OS=Mus musculus OX=10090 GN=Pcdhb6 PE=1 SV=1	1.623	0.210
MICOS complex subunit Mic25 OS=Mus musculus OX=10090 GN=Chchd6 PE=1 SV=2	2.459	0.391
Protein YIPF5 OS=Mus musculus OX=10090 GN=Yipf5 PE=1 SV=1	1.143	0.058
Prothymosin alpha OS=Mus musculus OX=10090 GN=Ptma PE=1 SV=2	1.718	0.235
Glutaminase kidney isoform, mitochondrial OS=Mus musculus OX=10090 GN=Gls PE=1 SV=1	1.116	0.048
Cell division control protein 42 homolog OS=Mus musculus OX=10090 GN=Cdc42 PE=1 SV=2	1.135	0.055
RNA-binding protein EWS OS=Mus musculus OX=10090 GN=Ewsr1 PE=1 SV=2	0.955	-0.020
Heat shock 70 kDa protein 13 OS=Mus musculus OX=10090 GN=Hspa13 PE=1 SV=1	1.331	0.124
Sorting nexin-3 OS=Mus musculus OX=10090 GN=Snx3 PE=1 SV=3	1.103	0.042
Tyrosine-protein phosphatase non-receptor type 1 OS=Mus musculus OX=10090 GN=Ptpn1 PE=1 SV=2	1.282	0.108
60S ribosomal protein L32 OS=Mus musculus OX=10090 GN=Rpl32 PE=1 SV=2	0.855	-0.068
Myeloid-derived growth factor OS=Mus musculus OX=10090 GN=Mydgf PE=1 SV=1	0.944	-0.025
AP-2 complex subunit mu OS=Mus musculus OX=10090 GN=Ap2m1 PE=1 SV=1	0.740	-0.131
Poly [ADP-ribose] polymerase 1 OS=Mus musculus OX=10090 GN=Parp1 PE=1 SV=3	0.895	-0.048
C-1-tetrahydrofolate synthase, cytoplasmic OS=Mus musculus OX=10090 GN=Mthfd1 PE=1 SV=4	1.209	0.082
V-type proton ATPase subunit B, brain isoform OS=Mus musculus OX=10090 GN=Atp6v1b2 PE=1 SV=1	0.925	-0.034

Table M.1. continued

Structural maintenance of chromosomes protein 3 OS=Mus musculus OX=10090 GN=Smc3 PE=1 SV=2	0.917	-0.038
Collectin-12 OS=Mus musculus OX=10090 GN=Colec12 PE=1 SV=1	1.191	0.076
Programmed cell death protein 10 OS=Mus musculus OX=10090 GN=Pdcd10 PE=1 SV=1	0.926	-0.033
Ras-related GTP-binding protein A OS=Mus musculus OX=10090 GN=Rraga PE=1 SV=1	0.819	-0.087
TSC22 domain family protein 3 OS=Mus musculus OX=10090 GN=Tsc22d3 PE=1 SV=2	0.565	-0.248
Enoyl-CoA hydratase domain-containing protein 3, mitochondrial OS=Mus musculus OX=10090 GN=Echdc3 PE=1 SV=1	2.004	0.302
Thioredoxin domain-containing protein 17 OS=Mus musculus OX=10090 GN=Txndc17 PE=1 SV=1	0.874	-0.058
WASH complex subunit 5 OS=Mus musculus OX=10090 GN=Washc5 PE=1 SV=2	0.598	-0.223
DNA-directed RNA polymerase II subunit RPB4 OS=Mus musculus OX=10090 GN=Polr2d PE=1 SV=2	2.568	0.410
Eukaryotic initiation factor 4A-III OS=Mus musculus OX=10090 GN=Eif4a3 PE=1 SV=3	1.294	0.112
Collagen alpha-1(I) chain OS=Mus musculus OX=10090 GN=Col1a1 PE=1 SV=4	1.297	0.113
Epoxide hydrolase 1 OS=Mus musculus OX=10090 GN=Ephx1 PE=1 SV=2	1.293	0.112
RNA-binding protein Raly OS=Mus musculus OX=10090 GN=Raly PE=1 SV=3	1.388	0.142
Coatomer subunit gamma-2 OS=Mus musculus OX=10090 GN=Copg2 PE=1 SV=1	0.886	-0.052
DNA-(apurinic or apyrimidinic site) lyase OS=Mus musculus OX=10090 GN=Apex1 PE=1 SV=2	0.879	-0.056

Table M.1. continued

Protein transport protein Sec61 subunit alpha isoform 2 OS=Mus musculus OX=10090 GN=Sec61a2 PE=2 SV=3	0.886	-0.053
Nipped-B-like protein OS=Mus musculus OX=10090 GN=Nipbl PE=1 SV=1	1.705	0.232
Carbonyl reductase [NADPH] 1 OS=Mus musculus OX=10090 GN=Cbr1 PE=1 SV=3	0.926	-0.033
Ras GTPase-activating-like protein IQGAP1 OS=Mus musculus OX=10090 GN=Iqgap1 PE=1 SV=2	0.381	-0.419
Ras-related protein Rab-31 OS=Mus musculus OX=10090 GN=Rab31 PE=1 SV=1	1.185	0.074
Eukaryotic translation initiation factor 1A, X-chromosomal OS=Mus musculus OX=10090 GN=Eif1ax PE=2 SV=3	0.902	-0.045
Aldose 1-epimerase OS=Mus musculus OX=10090 GN=Galm PE=1 SV=1	0.946	-0.024
Vascular endothelial growth factor D OS=Mus musculus OX=10090 GN=Vegfd PE=2 SV=1	1.468	0.167
Hexokinase-1 OS=Mus musculus OX=10090 GN=Hk1 PE=1 SV=3	0.916	-0.038
Glia maturation factor beta OS=Mus musculus OX=10090 GN=Gmfb PE=1 SV=3	1.257	0.099
Choline-phosphate cytidylyltransferase A OS=Mus musculus OX=10090 GN=Pcyt1a PE=1 SV=1	0.762	-0.118
L-lactate dehydrogenase B chain OS=Mus musculus OX=10090 GN=Ldhb PE=1 SV=2	1.265	0.102
Serine/threonine-protein phosphatase 4 catalytic subunit OS=Mus musculus OX=10090 GN=Ppp4c PE=1 SV=2	1.316	0.119
Mitogen-activated protein kinase kinase kinase 20 OS=Mus musculus OX=10090 GN=Map3k20 PE=1 SV=1	0.830	-0.081
Major facilitator superfamily domain-containing protein 10 OS=Mus musculus OX=10090 GN=Mfsd10 PE=1 SV=1	1.216	0.085
Endophilin-A2 OS=Mus musculus OX=10090 GN=Sh3gl1 PE=1 SV=1	1.274	0.105

Table M.1. continued

Inositol 1,4,5-trisphosphate receptor type 1 OS=Mus musculus OX=10090 GN=Itpr1 PE=1 SV=2	1.795	0.254
Platelet-activating factor acetylhydrolase IB subunit beta OS=Mus musculus OX=10090 GN=Pafah1b2 PE=1 SV=2	0.476	-0.322
Protein phosphatase methylesterase 1 OS=Mus musculus OX=10090 GN=Ppme1 PE=1 SV=5	0.825	-0.083
TBC1 domain family member 9B OS=Mus musculus OX=10090 GN=Tbc1d9b PE=1 SV=1	0.591	-0.229
IQ motif and SEC7 domain-containing protein 1 OS=Mus musculus OX=10090 GN=Iqsec1 PE=1 SV=2	1.154	0.062
Inorganic pyrophosphatase 2, mitochondrial OS=Mus musculus OX=10090 GN=Ppa2 PE=1 SV=1	0.895	-0.048
Protein FAM160B1 OS=Mus musculus OX=10090 GN=Fam160b1 PE=1 SV=2	0.779	-0.109
Tyrosine-protein kinase BAZ1B OS=Mus musculus OX=10090 GN=Baz1b PE=1 SV=2	0.700	-0.155
REVERSED Monofunctional C1-tetrahydrofolate synthase, mitochondrial OS=Mus musculus OX=10090 GN=Mthfd1l PE=1 SV=2	1.512	0.180
MARCKS-related protein OS=Mus musculus OX=10090 GN=Marcksl1 PE=1 SV=2	1.415	0.151
Glycogen [starch] synthase, muscle OS=Mus musculus OX=10090 GN=Gys1 PE=1 SV=2	0.504	-0.297
Collagen alpha-1(III) chain OS=Mus musculus OX=10090 GN=Col3a1 PE=1 SV=4	1.212	0.083
Peptidyl-prolyl cis-trans isomerase FKBP2 OS=Mus musculus OX=10090 GN=Fkbp2 PE=1 SV=1	0.863	-0.064
Sorting nexin-12 OS=Mus musculus OX=10090 GN=Snx12 PE=1 SV=1	1.102	0.042
Histone H1.5 OS=Mus musculus OX=10090 GN=Hist1h1b PE=1 SV=2	1.069	0.029

Table M.1. continued

Transcriptional activator protein Pur-alpha OS=Mus musculus OX=10090 GN=Pura PE=1 SV=1	0.296	-0.529
5'-3' exoribonuclease 2 OS=Mus musculus OX=10090 GN=Xrn2 PE=1 SV=1	0.564	-0.249

BIOGRAPHY OF THE AUTHOR

Matthew Edmund Siviski was born and raised in Lewiston, Maine. He is the son of Peter and Janet, and has a younger sister, Anya. Matt is a graduate of Phillips Exeter Academy and Fordham University. He concentrated in chemistry while an undergraduate at Fordham College at Rose Hill. Matt is a candidate for the Doctor of Philosophy degree in Biomedical Science from the University of Maine in December 2023.